

GEORGIA INSTITUTE OF TECHNOLOGY
Engineering Experiment Station

PROJECT INITIATION

Date July 17, 1964

Project Title: An Analytical and Experimental Study of Bed Ripples Under Water Waves

Project No.: A-798

Project Director: M. R. Carstens

Sponsor: Department of the Army, Coastal Engineering Research Center

Effective: 7-1-64 Estimated to run until: 6-30-65

Type agreement: Contract No. DA-49-055-CIVENG-65-1

Amount: \$14,030.00

Reports: Quarterly due within 30 days following the end of each quarter
Final due June 30, 1965

Contact person: ^{Corps} ~~Sergeant~~ of Engineers, U. S. Army
Coastal Engineering Research Center
5201 Little Falls Road, N. W.
Washington, D. C. 20016

Attention: Mr. E. E. Guinder, Contracting Officer

Assigned to Mechanical Sciences Division

COPIES TO:

- | | |
|--|--|
| <input type="checkbox"/> Project Director | <input type="checkbox"/> Technical Information Section |
| <input type="checkbox"/> Director | <input type="checkbox"/> Photographic Laboratory |
| <input type="checkbox"/> Associate Director | <input type="checkbox"/> Shop |
| <input type="checkbox"/> Assistant Director(s) | <input checked="" type="checkbox"/> Security Officer |
| <input type="checkbox"/> Division Chiefs | <input type="checkbox"/> Accounting |
| <input type="checkbox"/> Branch Head | <input type="checkbox"/> Purchasing |
| <input type="checkbox"/> General Office Services | <input type="checkbox"/> Report Section |
| <input type="checkbox"/> Rich Electronic Computer Center | <input type="checkbox"/> Library |
| <input type="checkbox"/> Engineering Design Services | <u>Dr. E. W. Schutz</u> |

GEORGIA INSTITUTE OF TECHNOLOGY
Engineering Experiment Station

PROJECT TERMINATION

Date November 15, 1967

PROJECT TITLE: An Analytical and Experimental Study of Bed Ripples Under Water Waves

PROJECT NO: A-798

PROJECT DIRECTOR: M. R. Carstens

SPONSOR: Dept. of the Army, Coastal Engineering Research Center

TERMINATION EFFECTIVE: 11-13-67

CHARGES SHOULD CLEAR ACCOUNTING BY: 11-30-67

Costs in excess of contract to be transferred to Division "E" Accounts.

Mechanical Sciences

COPIES TO:

Project Director
Director
Associate Director
Assistant Directors
Division Chief
Branch Head
Accounting
Engineering Design Services

REPORTS
300. A-798

General Office Services
Photographic Laboratory
Purchasing
Shop
Technical Information Section
Security

QUARTERLY REPORT 1

PROJECT A-798

AN ANALYTICAL AND EXPERIMENTAL STUDY
OF BED RIPPLES UNDER WATER WAVES

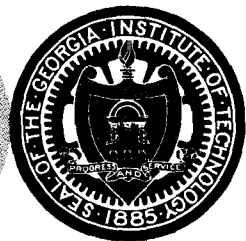
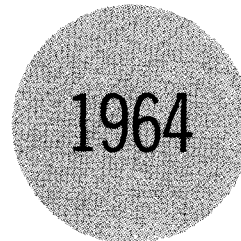
M. R. CARSTENS



Contract No. DA-49-055-CIVENG-65-1

1 July to 30 September 1964

Prepared for
Department of the Army
Coastal Engineering Research Center
Washington, D. C.



Engineering Experiment Station
GEORGIA INSTITUTE OF TECHNOLOGY
Atlanta, Georgia

REVIEW
PATENT 11-3 1964 BY *[Signature]*
FORMAT 11-3 1964 BY *[Signature]*

GEORGIA INSTITUTE OF TECHNOLOGY
School of Civil Engineering
Atlanta, Georgia

QUARTERLY REPORT 1

PROJECT A-798

AN ANALYTICAL AND EXPERIMENTAL STUDY
OF BED RIPPLES UNDER WATER WAVES

By

M. R. CARSTENS

CONTRACT NO. DA-49-055-CIVENG-65-1

1 JULY to 30 SEPTEMBER 1964

Prepared for
DEPARTMENT OF THE ARMY
COASTAL ENGINEERING RESEARCH CENTER
WASHINGTON, D. C.

TABLE OF CONTENTS

	Page
TABLE OF CONTENTS.	ii
LIST OF FIGURES.	iii
LIST OF TABLES	iv
FOREWORD	v
INTRODUCTION	1
EXPERIMENTAL PROGRAM	2
Experimental Set-up.	2
Experimental Procedure	9
Experimental Results	13
SUMMARY.	29

LIST OF FIGURES

	Page
1. Side Elevation and Cross Section of U-Tube.	3
2. Photograph of U-Tube.	6
3. Calibration of Float-Position Measuring System (Run 23)	11
4. Calibration of Pressure Measuring System (Run 23)	12
5. Water-Motion Amplitude (Run 23)	14
6. Progress of Leading Ripple Crest (Run 23)	16
7. Rate of Ripple Propagation.	17
8. Ripple Photograph (Run 23).	18
9. Ripple Wave Length.	19
10. Ripple Amplitude.	20
11. Ratio of Wave Length to Amplitude	21
12. Work-Input Data (Run 23).	25
13. Work-Input (All Runs)	28

LIST OF TABLES

	Page
1. Rate of Ripple Propagation.	22
2. Geometric Characteristics of Ripples.	22
3. Work Input	26

INTRODUCTION

This report includes the results of the experimental study (through September 20, 1964) of ripples performed in the Georgia Tech water tunnel.

The experiments are being performed in a water tunnel in which water is oscillated in a simple-harmonic manner through the test section. Two-dimensional ripples are formed in the sand bed by means of a two-dimensional disturbance element placed in the horizontal test section. Data are being taken from which the rate of formation, the amplitude, the wave length, and the rate of energy dissipation of a ripple system can be determined. The independent flow variables are amplitude of the water motion, frequency of oscillation, size of the disturbance element from which the ripples originate, and characteristics of the bed material. Preliminary tests for the purpose of determining the energy dissipation per cycle as a function of water-motion amplitude with a plane-bed are completed. The results of 37 plane-bed tests with water-motion amplitudes ranging from 3.5 in to 36 in are reported. The results of four tests with a rippled bed are also reported.

EXPERIMENTAL PROGRAM

In order to study ripples on the sea bed resulting from wave action, the decision was made to model only the mass of the water adjacent to the bed. The water motion at a fixed point close to the bed under a first-order Stokian wave is simple harmonic and is parallel to the bed. A large U-tube with forced oscillation of the water was designed in order to model the water motion under a wave.

Experimental Set-up

Description of U-tube - The description of this large U-tube is facilitated by referring to Figure 1. The vertical legs of the U-tube are in two rectangular steel tanks (A) at the ends of the horizontal leg which is the test section (B). Forced oscillation of the water mass is achieved by blowing air into the West vertical leg as the water surface is falling and then exhausting this air as the water surface is rising.

The vertical legs of the U-tube are formed within the rectangular steel tanks which are 3 ft by 4 ft in cross section, by streamlined inserts (C). The water passage in each vertical leg is 1 ft by 4 ft in cross section inasmuch as the water surface is never allowed to fall to the curved section of the upper insert (C). In all tests the equilibrium water level was established 48-1/2 in above the top of the test section (B).

The horizontal leg of the U-tube is the test section which is 1 ft (vertical) by 4 ft (horizontal) in cross section and which is 10 ft long. The central portion of the floor is depressed in order to form a container for the erodible bed material. The erodible bed (D) is 6 ft long by 4 ft wide by 4 in deep. The walls of the test section are fabricated of 1/2 in

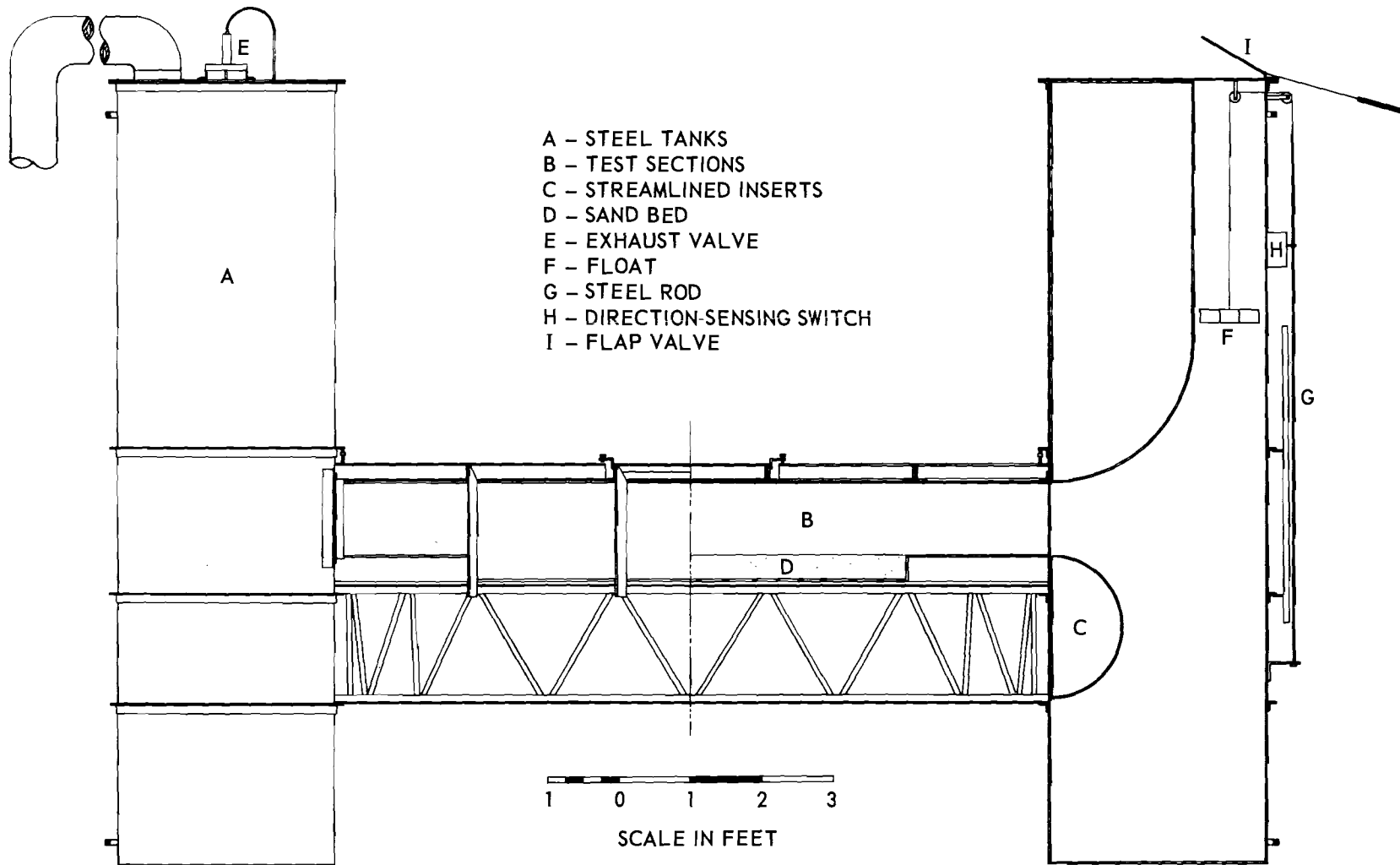


Figure 1. Side Elevation and Cross Section of U-Tube.

clear plastic and are framed on the exterior with steel angles and channels. The test section rests upon three prefabricated steel trusses which span from steel tank (A) to steel tank. A 3 ft square flush-mounted door is located in the center of the roof in order to be able to place the bed material and models.

The water in the U-tube is made to oscillate at the resonant frequency. The output of a centrifugal blower is discharged continuously into the air space above the water surface of the West vertical leg. Two 7 in diameter, pneumatically powered, exhaust valves (E) in the top of West vertical leg are open except for a time during which the water level is falling in the West leg.

The feedback mechanism by which the exhaust valve is sequence-operated at the resonant frequency is as follows. The float (F) in the East vertical leg is attached by a light flexible cable to a steel rod (G) which moves vertically past the direction-sensing switch (H). The direction-sensing switch (H) is a lever-operated microswitch. A permanent magnet on the end of the microswitch operating lever is in contact with the steel rod (G) which, in turn, follows the motion of the float (F). Whenever the steel rod (G) is falling the switch (H) is closed and whenever the steel rod (G) is rising the switch (H) is open. When the steel rod (G) changes direction and starts to fall, a circuit is closed which, in turn, actuates a single-cycle timer. This timer makes one revolution in 2 seconds and then stops. A second microswitch is contained within the timer. By means of an adjustable cam this second microswitch can be made to open or close at any time within the two-second interval. Solenoid valves which operate the pneumatic pistons on the exhaust valves are in the circuit with the timer

microswitch. The timer microswitch is set such that the exhaust valves close when the timer starts and such that the exhaust valves remain closed during one quarter of a cycle. The feedback mechanism described above insures that the water is oscillated at resonant frequency with the result that the frequency of oscillation cannot be controlled.

The amplitude of the oscillation is controlled by means of valves placed in the air-input system. Valve 1 is a cone valve placed on the intake of the centrifugal blower. The cone is attached to a threaded rod in such a manner that the valve opening is adjustable and reproducible. Valve 1 positioning is denoted herein by the number of revolutions from the completely throttled position. In addition, a bleed-off valve, valve 2, is placed in the air duct leading from the blower to the West tank of the U-tube. Valve 2 is simply a rectangular opening in the air duct which is covered by a circumscribing sleeve. The bleed-off opening is adjustable by positioning of the circumscribing sleeve. Valve 2 opening is completely closed at a scale position of 0.18 ft. Major amplitude changes are accomplished by means of valve 1 and minor amplitude changes are accomplished by means of valve 2.

The photograph, Figure 2, shows the South wall of the test section.

Instrumentation - Instrumentation consists of devices for measuring water temperatures elapsed time, amplitude of water motion, float-displacement as a function of time, air pressure in the West tank as a function of time, and ripple characteristics.

Water temperature is measured by means of a completely immersed thermometer which is taped to the interior of the South wall of the test section. Temperatures can be determined to an accuracy of ± 0.5 degree Fahrenheit.

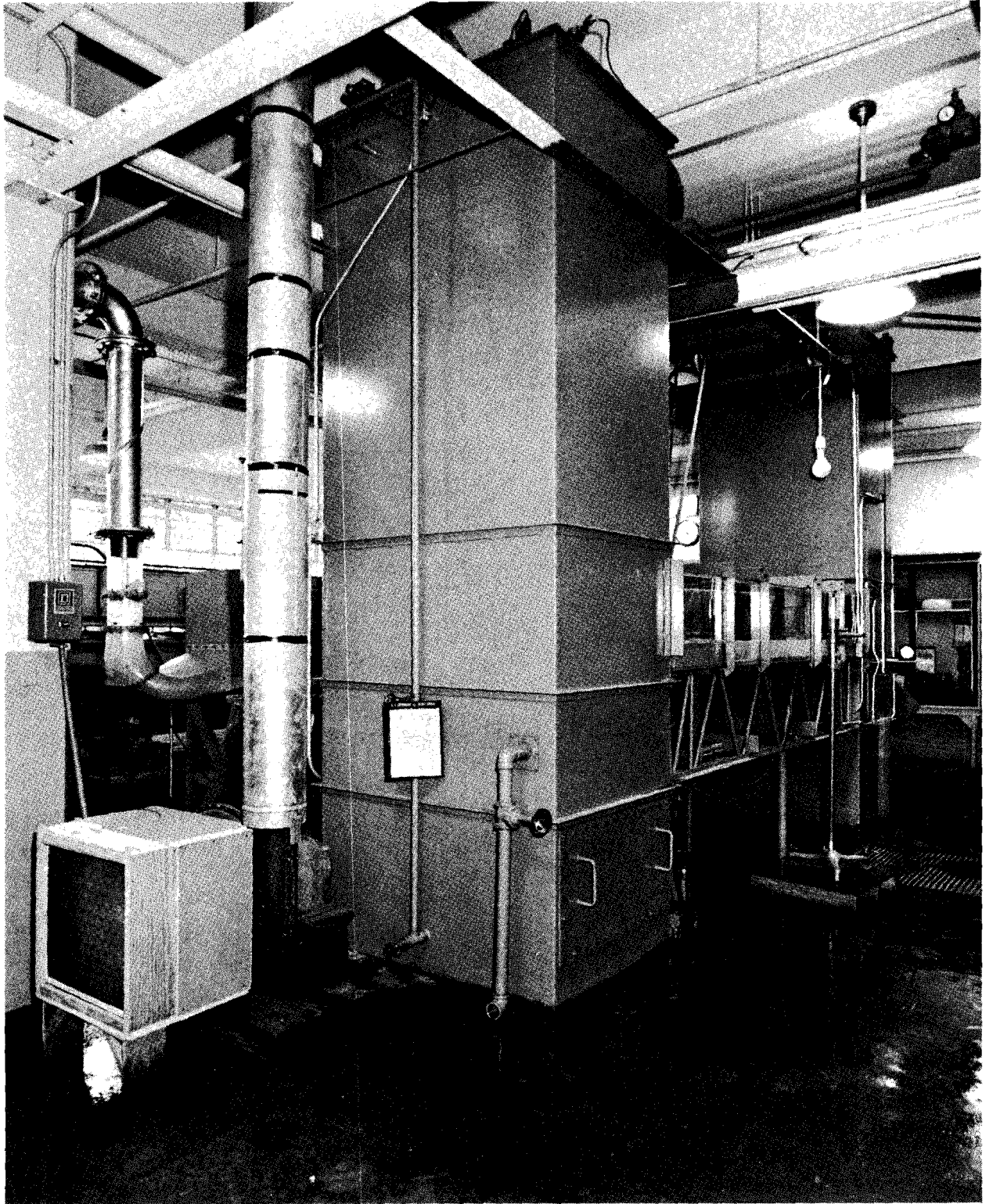


Figure 2. Photograph of U-Tube.

Elapsed time is digitally portrayed on an electronic counter. The counter is placed in the circuit containing the direction-sensing switch (H), Figure 1. Thus the counter is a meter of elapsed dimensionless time, that is, number of cycles from the beginning of a run.

Amplitude of the water motion is determined from the maximum and minimum positions of the steel rod (G), Figure 1, which is mechanically attached to the float (F). A pointer on the steel rod passes over the face of a fixed scale which is aligned parallel to the oscillating steel rod. Maximum and minimum float positions are determined by direct visual observation. Since float (F) rides on the water surface of the East tank, which has the same cross section as the test section, the float amplitude is equivalent to the water-motion amplitude in the test section.

Float-displacement as a function of time is recorded by means of an electronic measuring system. A three-wire stainless-steel cable (model-airplane guide wire) is attached to the float. This cable is looped around a 6 in diameter plastic idler pulley placed in the bottom of the East tank and is looped around an accurately machined 6 in diameter aluminum pulley placed on top of the East tank. The cable forms an endless belt which is attached to the float at one point. With this arrangement, vertical movement of the float is directly proportional to angular displacement of the upper aluminum pulley. The axle of a three-turn, 10-ohm, precision potentiometer is fixed to the axle of the upper pulley. The potentiometer forms a corner junction of a Wheatstone Bridge. Two legs of the Wheatstone Bridge consist of external 250-ohm resistors and the other two legs are internal within the Sanborn 64, strain gage, amplifying and recording system. With this arrangement, the stylus

deflection of the recorder is directly proportional to float displacement. In addition the recorder contains a 1-sec timing marker. The float-displacement-versus-time record is used to determine the period of the motion and to determine the phase relationship between the air pressure force applied to the water surface in the West tank and the water motion.

Air pressure on the space above the water surface in the West tank is measured and recorded as a function of time in order to determine the work-input to the oscillating water mass during a cycle. The pressure transducer is an unbonded strain-gage type (Statham Instruments, Inc., ± 0.15 psi differential). The output of the pressure transducer is the input to the previously mentioned Sanborn 64, strain-gage, amplifying and recording system. The recorder is a two-channel recorder plus the 1-sec timing pulse. One channel is used to record the pressure in the air space in the West tank and the other channel is used to record the float displacement. The piezometer in the top of the West tank is connected to the pressure transducer by means of a piece of 1/4 in ID Tygon tubing approximately 18 in long. The pressure transducer is placed on a mount suspended from the ceiling thereby isolating the transducer from mechanical vibrations of the water tunnel. A tee is placed in the tubing from the piezometer to the transducer. This junction, in turn, is connected to a precision constant-displacement manometer. By means of a pinch clamp the pressure transducer can be connected either to the piezometer on the West tank or to the manometer. With this arrangement, in-place calibration of the pressure-recording system is readily accomplished.

Ripple characteristics are determined by means of photographs of the transparent South wall of the test section. Thus the ripple configuration

adjacent to the wall is recorded on a photograph. Lines marked at 0.1 ft intervals on the wall form a grid from which ripple dimensions can be determined from the photographs. The 4 in x 5 in press camera is mounted on a tripod which, in turn, is located at a fixed position. Fixation of the camera permits fixing the shutter speed, lighting, and lens opening. Polaroid cut film is used in order to obtain a rapidly developed positive print.

Bed of the test section - In order to determine the drag force exerted by the rippled bed, two series of runs are being made - one with a plane bed and one with a rippled bed.

The majority of the plane bed tests were performed with a 20-gage aluminum sheet placed over the bottom of the test section. The aluminum sheet was held in position with waterproof duct tape placed on the surface of the aluminum and the wall of the test section.

The rippled bed tests have been made with a bed of glass beads. The pertinent characteristics of this bed material are as follows:

mean diameter, $d = 0.297$ mm,

geometric standard deviation, $\sigma_{gd} = 1.06$, and

specific gravity, $s = 2.47$

Disturbance element - In order to obtain a regular two-dimensional ripple system, a flow disturber is placed on the bed of the test section. The disturbance element used in Runs 21-24, inclusive is a half-round brass bar. The bar is 4 ft long and is semicircular in cross section having a radius of 1/4 in.

Experimental Procedure

Experimental procedure will be related in chronological order.

Preparation for a run consists of preparing a plane bed and of placing the disturbance element. The saturated bed material is planed with a 2 in x 2 in wooden screed which is sufficiently long to bridge the depressed section of the bed of the test section, Figure 1. Leveling is accomplished by a slight oscillatory motion of the screed as the screed is moved from wall to wall. Bed material is added, if needed. After the bed is leveled, the disturbance element is carefully lowered to the bed with the flat surface resting on the bed material. Next the cover of the test section is replaced and the tunnel is refilled with water.

Immediately prior to a run, the float-displacement and West tank pressure measuring and recording systems are calibrated. First the bridge circuits are balanced with the float clamped such that the amplitude scale reading is zero and with the pressure sensor exposed to atmospheric pressure on both sides of the diaphragm. Next the amplifiers are switched to the position which will give the desired amplification. The float is then moved and clamped in successive positions both above and below the zero position. In each position a short record of stylus deflection is made. Next the pressure is altered in increments in the tubing connecting the pressure transducer and the manometer. A short record of stylus deflection is made. The corresponding manometer reading is recorded. The calibration curves of Run 23 are shown in Figure 3 and Figure 4.

The run commences as the blower is started. The float-displacement recorder is operated on low speed in order to record the transient buildup of the oscillation and in order to obtain an amplitude record prior to the first direct reading of the amplitude gage on the steel rod (G), Figure 1.

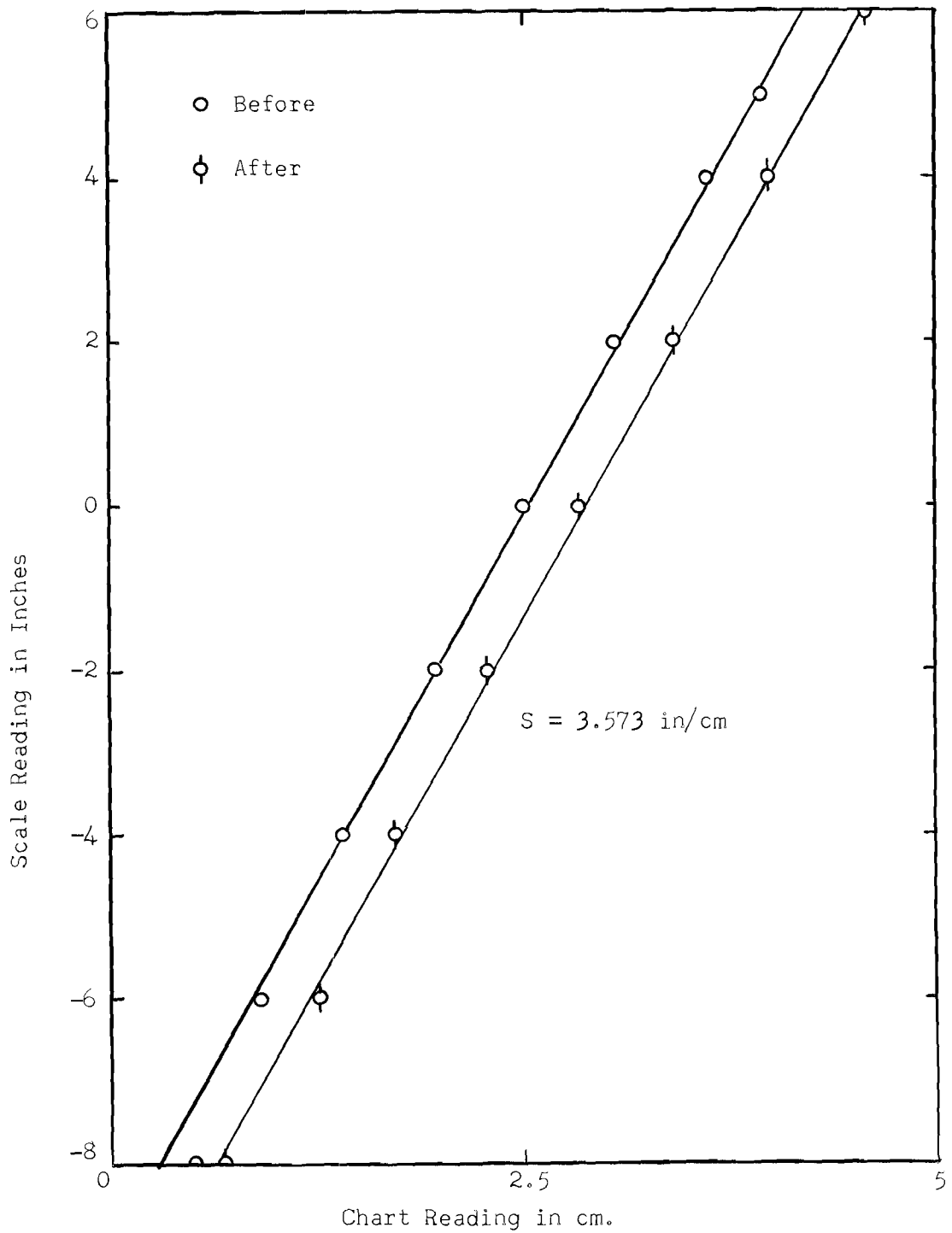


Figure 3. Calibration of Float-Position Measuring System (Run 23)

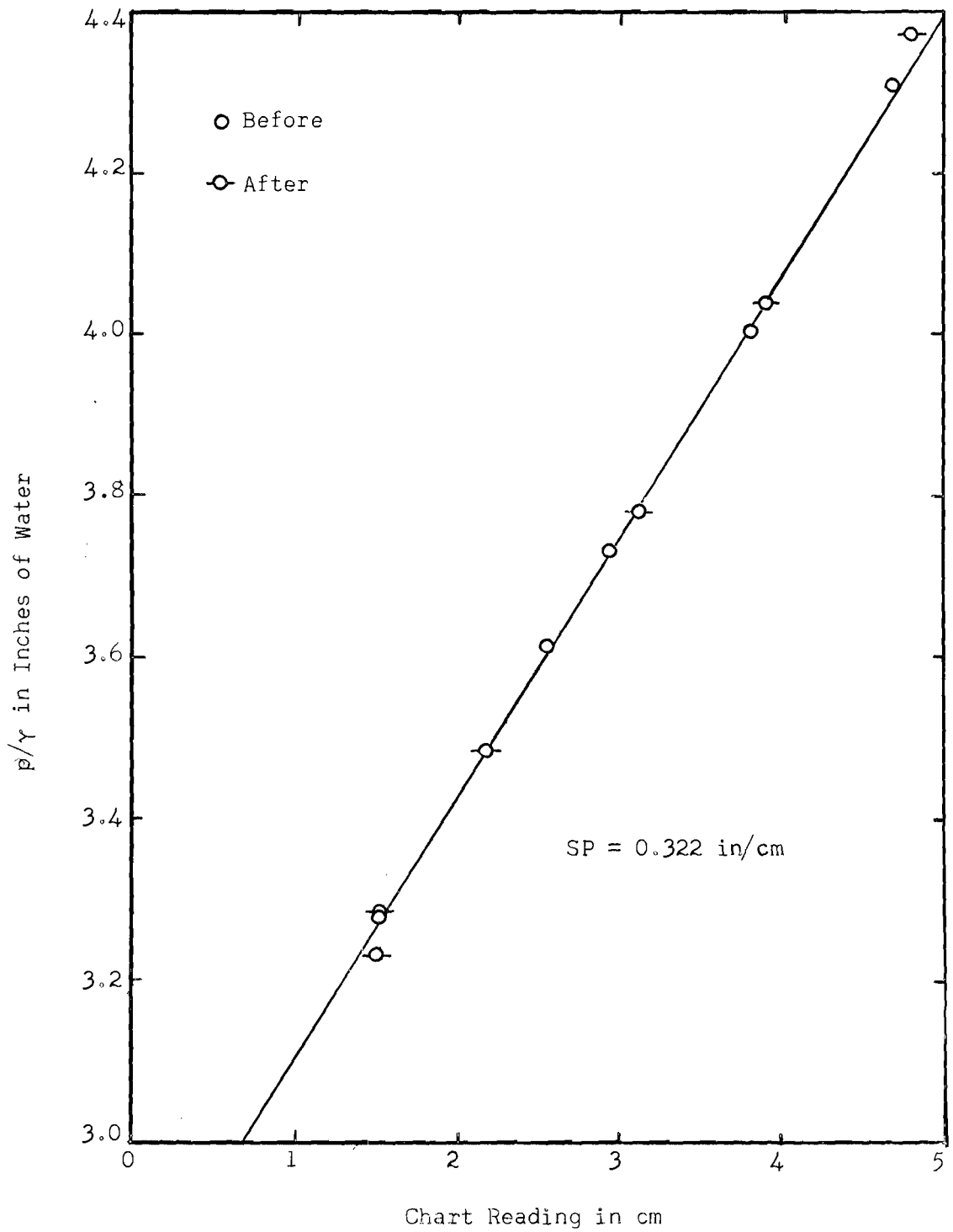


Figure 4. Calibration of Pressure Measuring System (Run 23)

During the early part of a run one observer reads and records the position of the crest of the leading ripple. Simultaneously a second observer reads and records the dimensionless time. From these data the rate of propagation of a ripple system over a plane bed can be determined.

As soon as the ripple system has propagated to the ends of movable bed section, the observers are free to perform other tasks. One of these tasks is to read and record repeatedly the amplitude of the motion as a function of time. Another task is to read and record the water temperature. As the ripple system continues to develop toward equilibrium, photographs are made. Just prior to the cessation of a run, when equilibrium is attained, a pressure record of the air pressure in the West tank is obtained.

Immediately following a run, calibration procedures are repeated in order to obtain float displacement versus recorder stylus deflection and to obtain West-tank pressure versus recorder stylus deflection.

The procedure described above is followed during a run with a rippled bed; however, the procedure during a plane-bed run is the same except that ripple propagation data and ripple photographs are not required.

Experimental Results

General - The general features of a run involving ripple formation is illustrated by the plot of amplitude (total water-motion amplitude) versus time for Run 23 as shown in Figure 5. The transient at the beginning of Run 23 exists for about 15 cycles. However, even after the initial transient, the oscillatory motion is not steady but exhibits a slight decay as the ripple system develops. The reason for the decay is simply that the work-input per cycle is essentially constant whereas

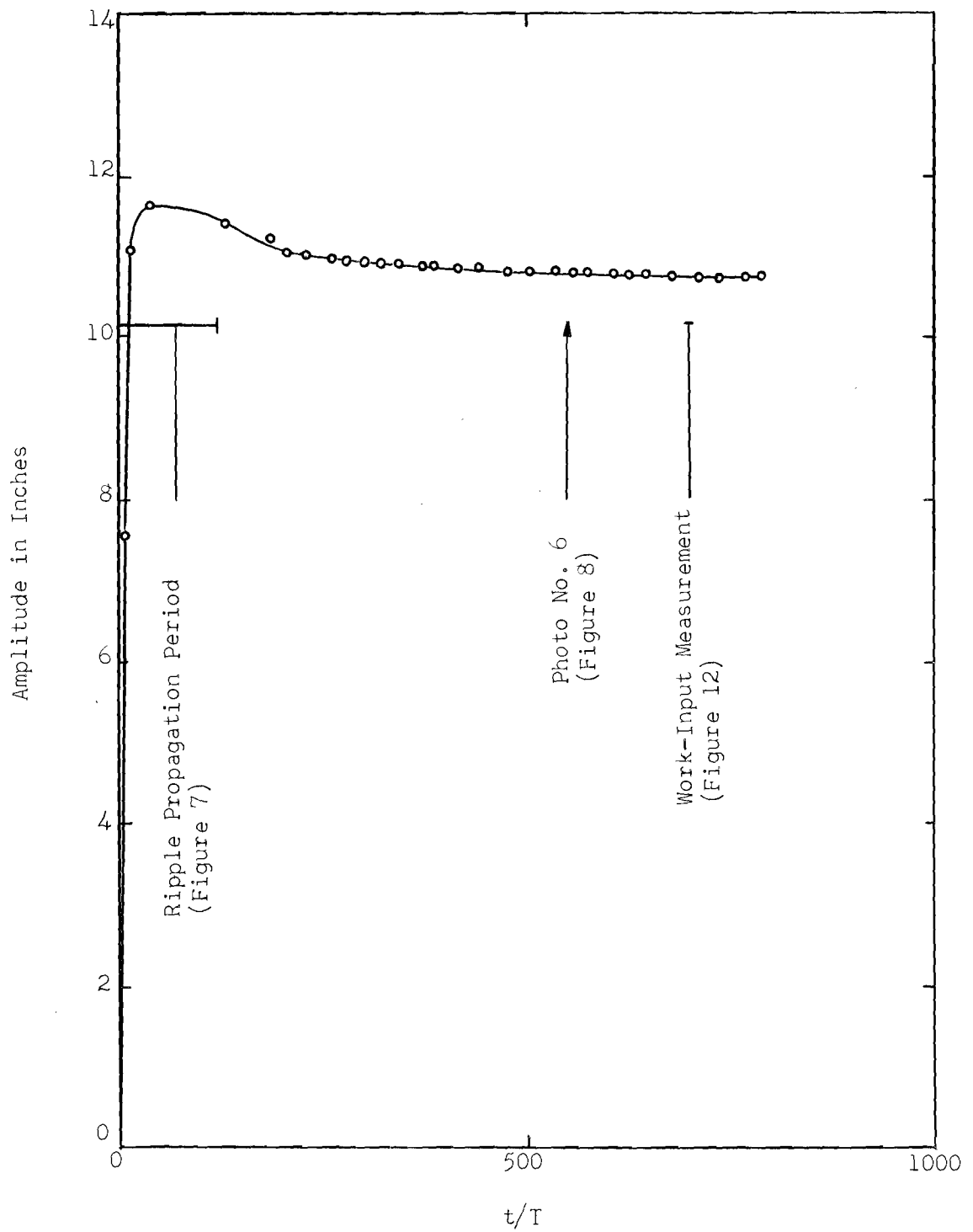


Figure 5. Water-Motion Amplitude (Run 23)

the resistance to motion increases as the ripple system develops. Obviously, the energy dissipation per cycle must equal the work-input per cycle. This equality is maintained by a decay in amplitude as the ripple system develops (resistance force increases).

Ripple propagation - Two-dimensional ripples propagate away from the disturbance with the ripple crests being parallel to the disturbance element. Propagation is accomplished by forming a new crest one wave length beyond the previously formed crest. The limiting crest is essentially a ripple of zero height. The position of the limiting ripple can be determined by the oscillatory motion of the bed particles. The extension of the ripple system over the bed during Run 23 as a function of time is shown in Figure 6. As shown in Figure 6, the ripple system spread over the entire length of the bed (6 ft) in an elapsed time of 123 cycles. The rates of propagation of ripples are presented in Figure 7 and Table 1. The four experimental points were obtained from plots similar to Figure 6 based upon data of Runs 21, 22, 23, and 24. The trend of the experimentally determined points, Figure 7, is indicative that the rate of propagation is infinite with a total water-motion amplitude of about 14 in. The wave length of the ripples which propagate during the initial stages of a run is less than one half the wave length of the equilibrium ripple system shown in Figure 8. The photograph, Figure 8, was taken at an elapsed time of 548 cycles.

Equilibrium ripples - Photographs, such as Figure 8, were taken in order to determine the geometric characteristics of the ripples. The outstanding characteristics, that is, wave length and amplitude, are presented in Table 2 and Figures 9, 10, and 11.

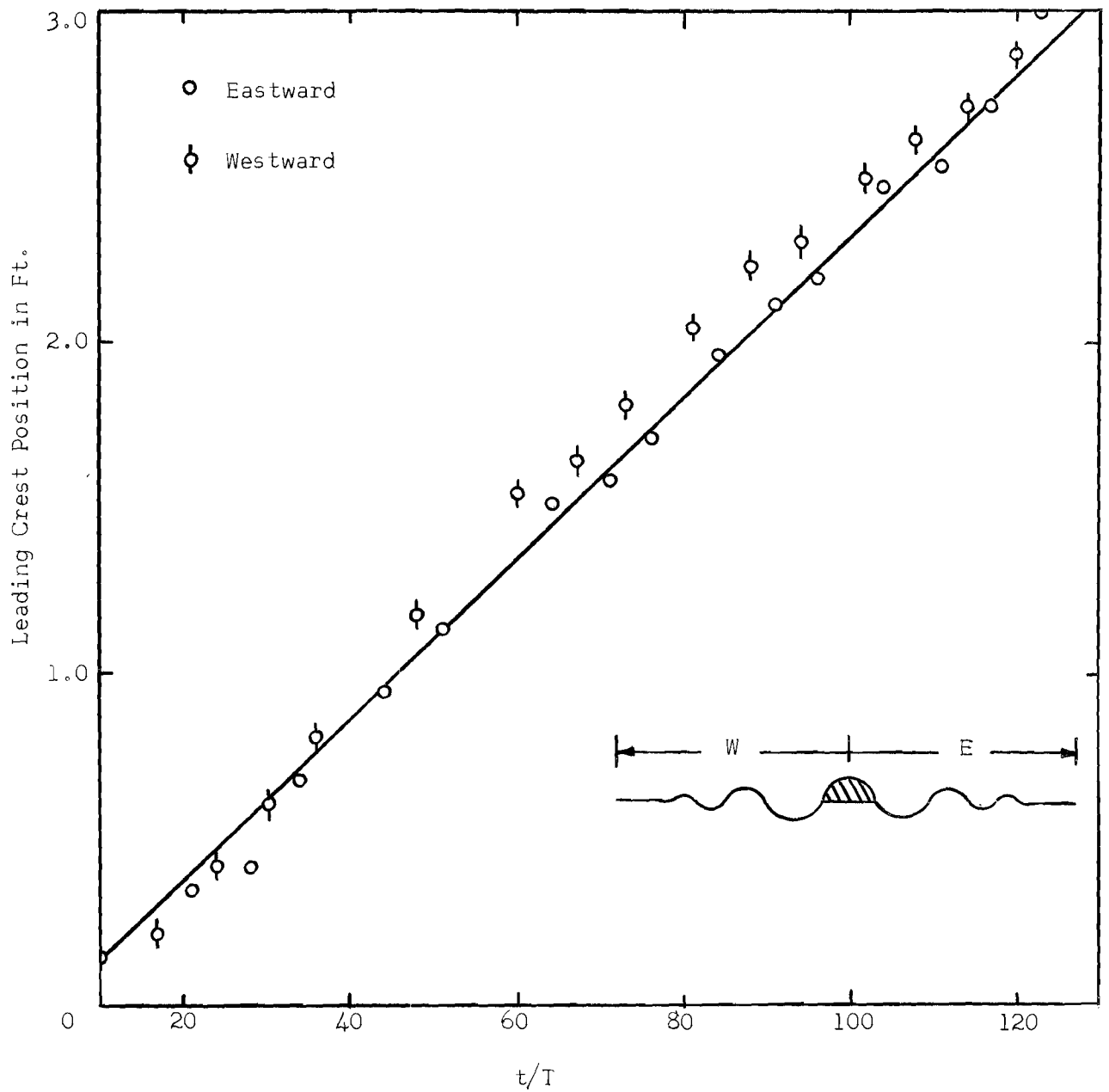


Figure 6. Progress of Leading Ripple Crest (Run 23)

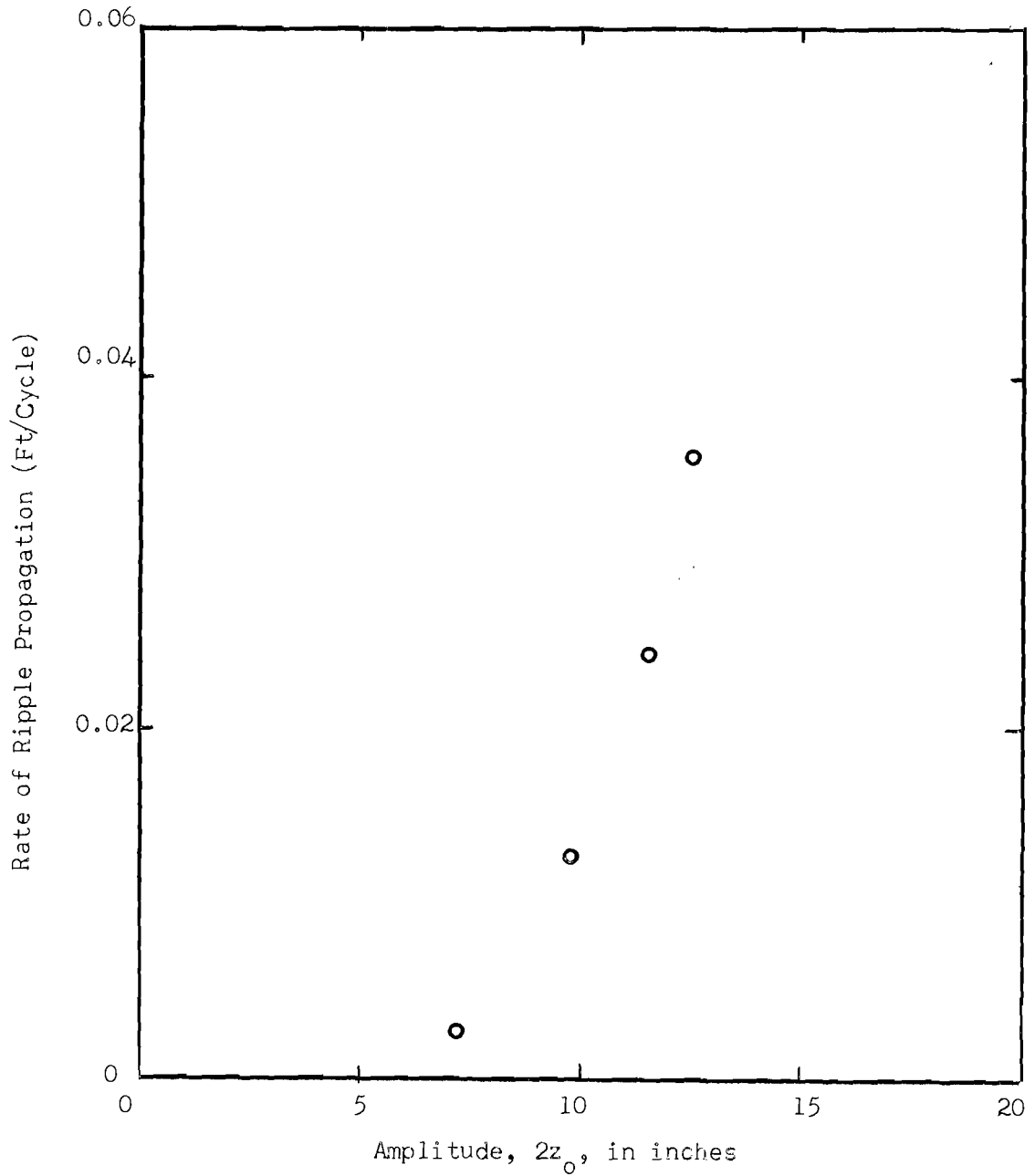


Figure 7. Rate of Ripple Propagation



Figure 8. Ripple Photograph (Run 23).

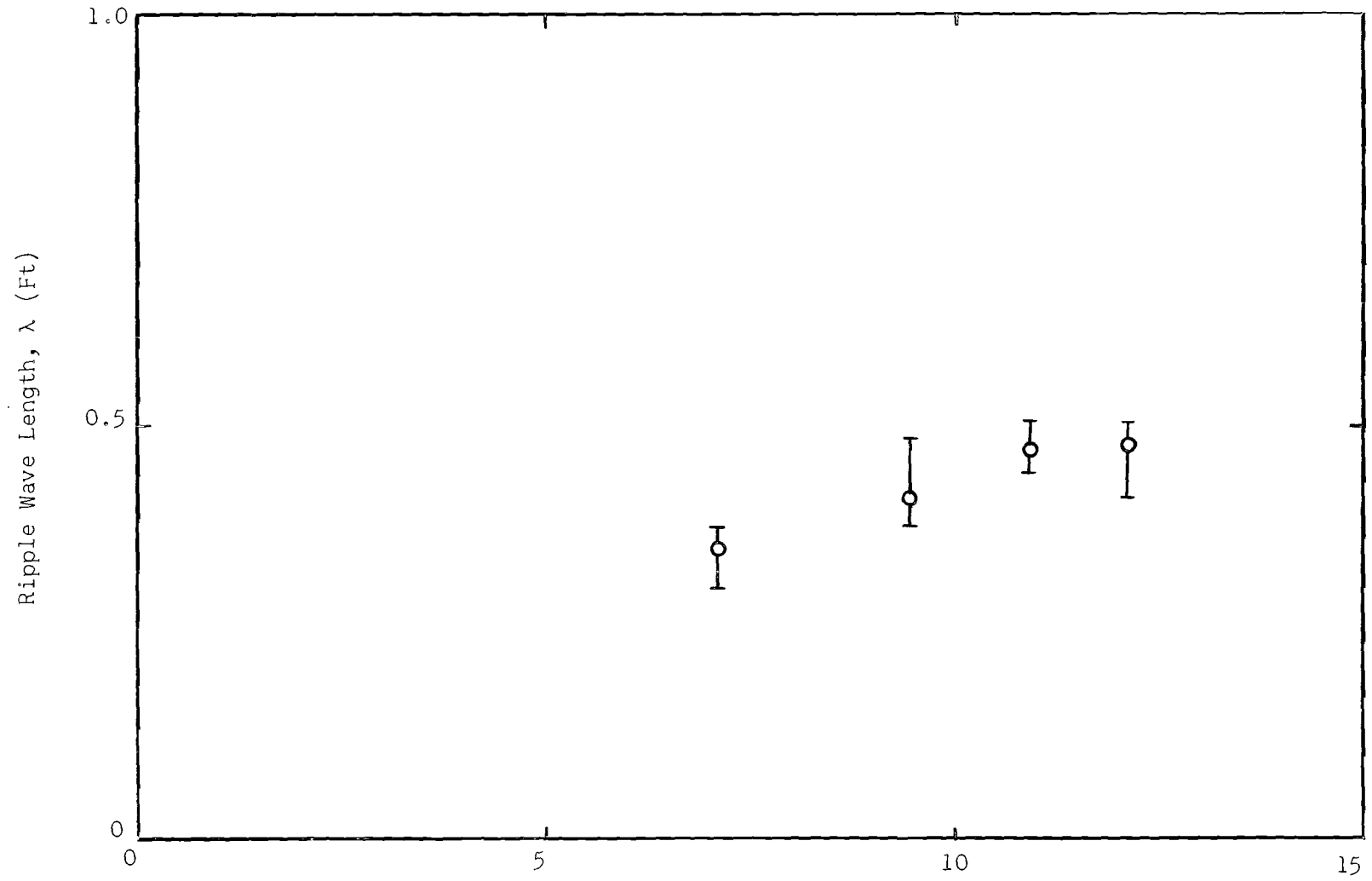


Figure 9. Ripple Wave Length

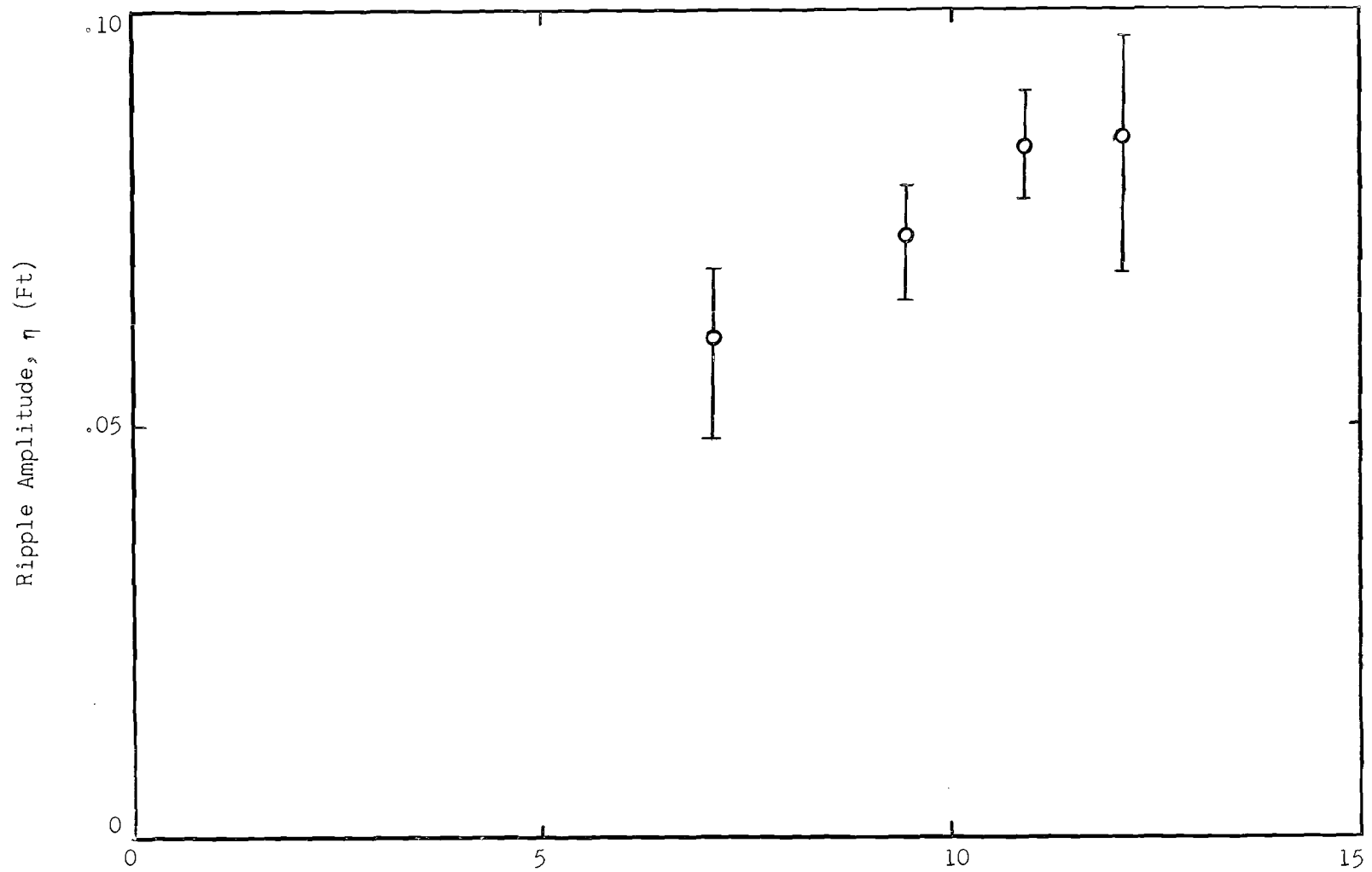


Figure 10. Ripple Amplitude

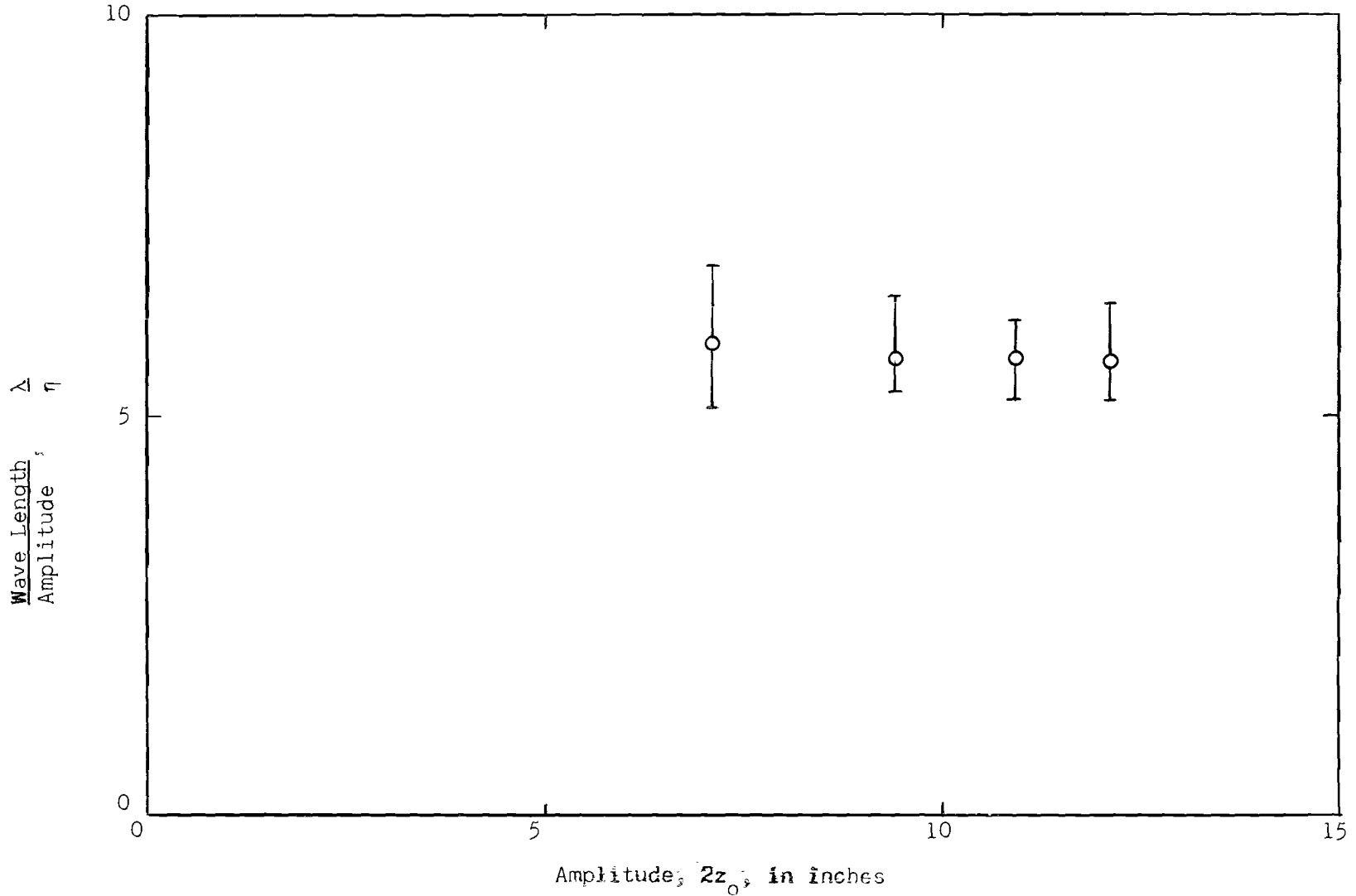


Figure 11: Ratio of Wave Length to Amplitude

TABLE 1
RATE OF RIPPLE PROPAGATION

Run No.	Period, T (sec.)	Amplitude $2z_0$ (in)	Rate of propagation ft./cycle
21	3.56	7.20	0.00282
22	3.56	9.87	0.0127
23	3.55	11.52	0.0243
24	3.55	12.58	0.0356

TABLE 2
GEOMETRIC CHARACTERISTICS OF RIPPLES

Run	t/T	Amplitude (in)	$\lambda, \eta, \lambda/\eta$ of Ripples East, West of Center						
			W3	W2	W1	E1	E2	E3	E4
21	2440	7.10	0.366	0.376	0.344	0.380	0.334	0.328	
			0.0560	0.0691	0.0675	0.0583	0.0482	0.0584	
			6.5	5.4	5.1	6.5	6.9	5.6	
21	2750	7.11	0.372	0.384			0.306	0.346	0.372
			0.0673	0.0639			0.0513	0.0641	0.0641
			5.5	6.0			6.0	5.4	5.8
22	653	9.42		0.41	0.40	0.41	0.415		
				0.075	0.066	0.073	0.079		
				5.5	6.1	5.6	5.3		
22	1219	9.44		0.49	0.43	0.41	0.40	0.38	
				0.075	0.075	0.077	0.070	0.065	
				6.5	5.7	5.3	5.7	5.8	
23	312	10.93		0.461	0.444	0.509	0.496		
				0.0784	0.0771	0.0823	0.0907		
				5.9	5.8	6.2	5.5		
23	527	10.83		0.498	0.468	0.453	0.484		
				0.0885	0.0835	0.0864	0.0819		
				5.6	5.6	5.2	5.9		
24	257	12.19		0.480	0.460	0.465	0.470		
				0.0915	0.0763	0.0770	0.0880		
				5.3	6.0	6.0	5.4		
24	377	12.12		0.507	0.478	0.446	0.507		
				0.0970	0.0834	0.0787	0.0875		
				5.2	5.7	5.7	5.8		
24	516	12.00		0.532	0.500	0.417	0.494		
				0.0935	0.0935	0.0648	0.0864		
				5.7	5.4	6.4	5.7		

Work-input - After considering several schemes to determine the energy dissipation and/or drag force of a ripple system, the decision was made to measure the work input necessary to maintain the oscillation at a given amplitude. Obviously, the work input per cycle is equal to the energy dissipation per cycle of a steady cyclic motion. Thus the difference between the work-input per cycle with a rippled bed and the work input per cycle with a plane bed at the same amplitude is equal to the difference in energy dissipation between the two bed states in a bed area of 4 ft by 6 ft. This subtraction eliminates the need for consideration of energy dissipation in any element of the U-tube other than the movable-bed section. Of course, the principal disadvantage is the loss of significant figures.

The work-input is evaluated as being the work input on the water surface in the West tank of the U-tube. Power is defined as the time rate of doing work.

$$P = dW/dt \quad (1)$$

in which P is power, W is work, and t is time. From equation (1), the work input per cycle is

$$W = \int_0^T P dt \quad (2)$$

in which T is the period of the motion. By definition,

$$P = F v \quad (3)$$

in which F is force on the water surface and v is the velocity of the water surface. The force is simply the product of the pressure, p, and the water surface area, A. The water surface motion is simple harmonic. Thus

$$\dot{W} = Az_0 \int_0^{2\pi} p \cos \omega t d(\omega t) \quad (4)$$

in which $2z_0$ is the total amplitude of the water motion and ω is the circular frequency of the motion, $2\pi/T$.

Work-input per cycle, equation (4), is numerically evaluated from data taken during each run. Typical data are shown in Figure 12 which is a reproduction of Run 23 data. The method of establishing the phase relationship between pressure and water-surface motion is clearly shown in Figure 12. Values of work input are presented in Table 3 and in Figure 13. The slopes shown in Figure 13 are obtained by analysis. The two-to-one slope results from assuming oscillatory laminar flow over a flat plate. The three-to-one slope results from assuming oscillatory turbulent flow with the boundary shear stress being 180 degrees out of phase with the velocity and with the coefficient of drag being constant.

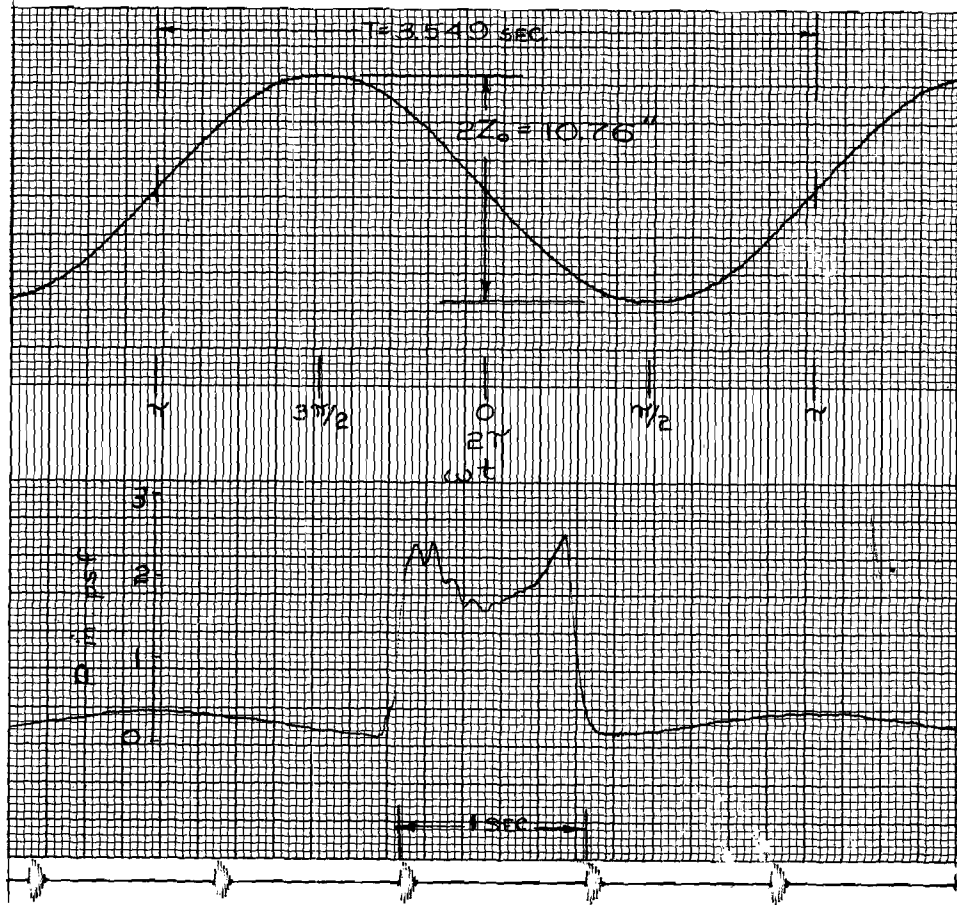


Figure 12. Work-Input Data (Run 23).

TABLE 3
WORK INPUT

Run No.	Period, T (sec.)	Amplitude, $2z_o$ (in)	Work Input (ft-lb/cycle)
13*	3.565	6.21	2.047
	3.552	8.05	3.242
	3.550	11.12	5.339
	3.549	12.97	7.704
	3.549	15.31	10.401
14*	3.555	5.52	1.772
	3.562	6.28	2.431
	3.564	7.29	3.148
	3.554	8.92	3.991
	3.557	10.61	5.375
15*	3.538	8.99	5.000
	3.553	10.48	6.534
	3.557	13.28	9.342
	3.558	14.87	11.439
16*	3.551	12.86	9.718
	3.553	16.32	13.315
	3.552	19.92	19.954
	3.548	22.72	24.109
	3.548	21.23	21.458
17*	3.550	12.17	7.151
	3.553	16.34	12.312
	3.551	22.33	23.968
	3.548	26.33	35.915
	3.540	28.78	47.172
18*	3.550	18.78	18.672
	3.546	26.35	38.251
	3.539	32.00	61.963
	3.534	36.16	88.017
19*	3.555	3.60	0.678
	3.559	4.94	0.970
	3.560	5.87	1.566
20**	3.555	3.41	0.720
	3.552	4.62	1.149
	3.555	6.71	2.366
	3.547	8.31	3.329
	3.549	9.49	4.234
	3.548	10.51	5.215
21***	3.558	7.49	3.571
	3.545	7.30	3.489
	3.556	7.12	3.538
	3.558	7.04	3.471
	3.557	7.02	3.527
	3.560	7.10	3.520

(Continued)

TABLE 3 (Continued)

Run No.	Period, T (sec.)	Amplitude, $2z_0$ (in)	Work Input (ft-lb/cycle)
22***	3.555	9.44	5.986
23***	3.549	10.76	7.779
24***	3.551	12.10	10.071

* Plane bed - aluminum-sheet bed.

** Plane bed - 0.297-mm, glass beads.

*** Rippled bed - 0.297-mm, glass beads.

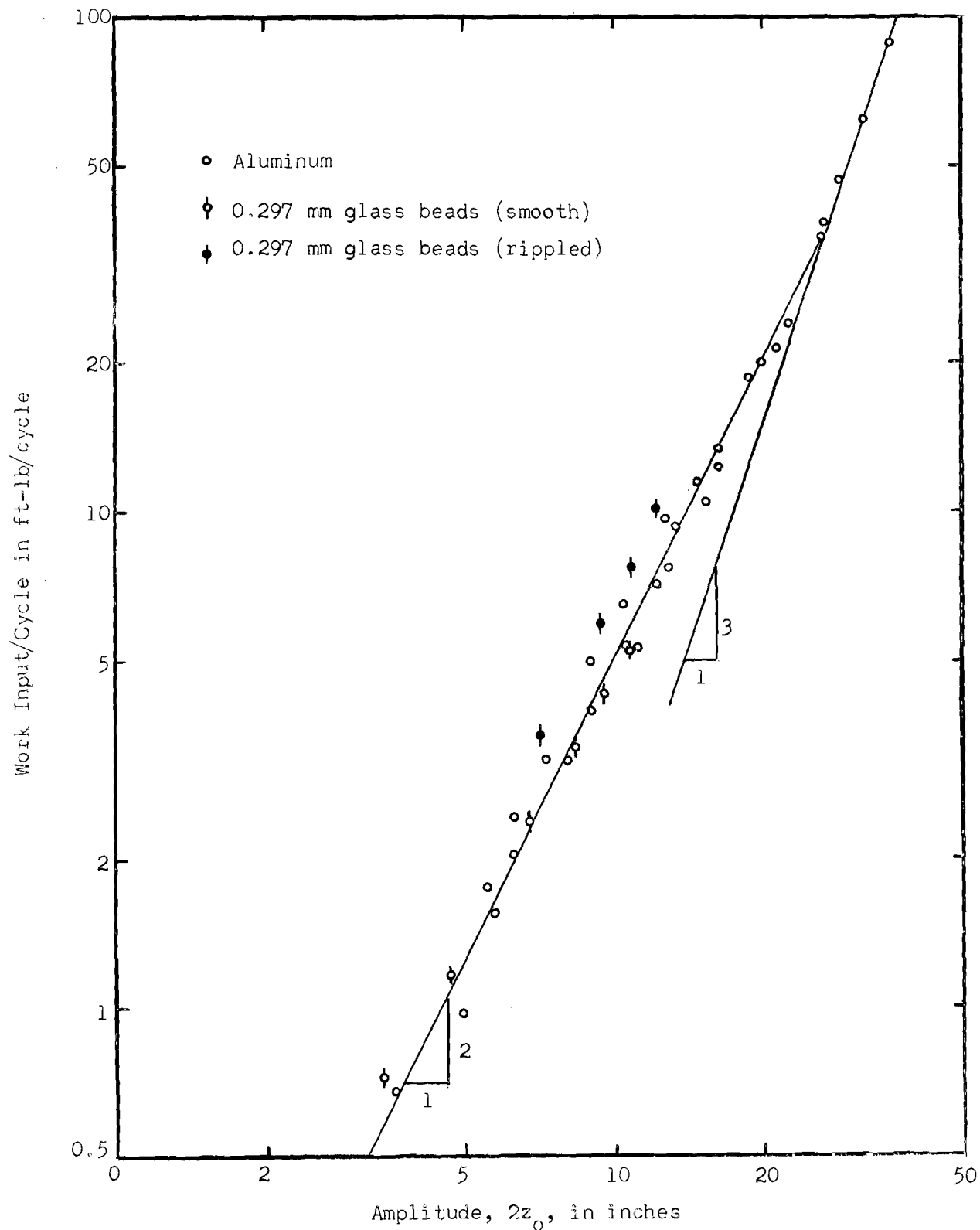


Figure 13. Work Input (All Runs)

SUMMARY

This first quarterly progress report is indicative of the nature of the experimental program. Obviously, many additional experiments must still be accomplished. At this stage in the program very little analysis of results or theoretical analysis has been accomplished.

QUARTERLY REPORT 2

PROJECT A-798



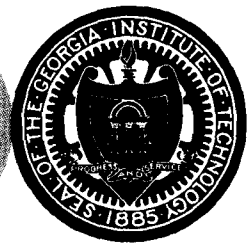
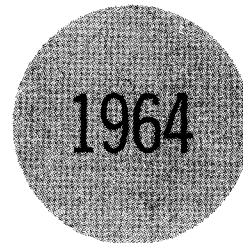
AN ANALYTICAL AND EXPERIMENTAL STUDY
OF BED RIPPLES UNDER WATER WAVES

M. R. CARSTENS AND F. M. NEILSON

Contract No. DA-49-055-CIVENG-65-1

1 October to 31 December 1964

Prepared for
Department of the Army
Coastal Engineering Research Center
Washington, D. C.



Engineering Experiment Station
GEORGIA INSTITUTE OF TECHNOLOGY
Atlanta, Georgia

GEORGIA INSTITUTE OF TECHNOLOGY
School of Civil Engineering
Atlanta, Georgia

QUARTERLY REPORT 2

PROJECT A-798

AN ANALYTICAL AND EXPERIMENTAL STUDY
OF BED RIPPLES UNDER WATER WAVES

By

M. R. CARSTENS
and
F. M. NEILSON

CONTRACT NO. DA-49-055-CIVENG-65-1

1 OCTOBER to 31 DECEMBER 1964

Prepared for
DEPARTMENT OF THE ARMY
COASTAL ENGINEERING RESEARCH CENTER
WASHINGTON, D. C.

LIST OF FIGURES

<u>Figure No.</u>	<u>Title</u>	<u>Page</u>
1	History of Dune Development - Run 49	6
2	Velocity of Propagation of Ripples	7
3	Dune Wave Length	9
4	Dune Amplitude	10
5	Topographic Map of Dunes - Run 50	11
6	Work Input into West Tank	12
7	Theoretical Model	15
8	Comparison of Model with the Geometry of Observed Dunes	17
9	Ratio of Amplitude to Wave Length of Dunes	18
10	Energy Dissipation per Unit Area per Cycle (Dunes)	23
11	Values of $f(\chi)$	27

TABLE OF CONTENTS

	Page
INTRODUCTION	1
Experimental Set-Up	2
Description of U-Tube	2
Instrumentation	2
Bed of the test section	3
Disturbance element	4
Experimental Procedure	4
Experimental Results	4
General	4
Transients in the development of a duned bed	5
Equilibrium bed form (dunes)	8
ANALYSIS OF RESULTS	13
Ripples	13
Dunes	14
Theoretical model	14
Dune geometry	16
Dissipation of energy	19
Incipient Motion	29
Boundary-Layer Transition	29
SUMMARY	31
NOMENCLATURE	32
REFERENCES	34
APPENDIX	35

INTRODUCTION

This report includes the results of the experimental study (through December 31, 1964) of ripple and dune characteristics which are formed on the sea bed by the action of first-order Stokian waves.

The experiments are being performed in a water tunnel in which water is oscillated in a simple-harmonic manner through the test section. Ripples and dunes are formed in the sand bed. Data are being taken from which the rate of formation of ripples, the geometric characteristics of dunes, and the rate of energy dissipation resulting from a system of dunes can be determined. The independent flow variables are amplitude of the water motion, frequency of oscillation, size of the disturbance element from which the ripples originate, and characteristics of the bed material. The status of the experimental program is summarized in TABLE 1 in the APPENDIX.

EXPERIMENTAL PROGRAM

In order to study ripples and dunes on the sea bed resulting from wave action, the decision was made to model only the mass of the water adjacent to the bed. The water motion at a fixed point close to the bed under a first-order Stokian wave is simple harmonic and is parallel to the bed. A large U-tube with forced oscillation of the water was designed in order to model the water motion under a wave.

Experimental Set-up

Description of U-tube - The description of this large U-tube was presented in QUARTERLY REPORT 1 to which the reader is referred.

One change was made in the water tunnel in order to eliminate the transient during either the buildup or decay of the oscillation to an equilibrium condition. An 8-in. diameter circular opening was cut in the cover plate at the top of the East tank through which all transfer of air into or out of the East tank would have to occur. Over this opening is mounted a 10-in. diameter rubber-covered steel plate. The cover plate in turn is driven vertically by a pneumatically operated piston. The pneumatic piston, in turn, is controlled by an electrically operated valve in order that the opening can be closed during starting and stopping and that the opening will remain open during operation of the tunnel. The circuitry is arranged such that by switching to the "blowdown" position the cover plate closes the opening and simultaneously a solenoid valve opens allowing compressed air to be forced into the East tank. The excess air pressure in the East tank forces the water surface downward. When the equilibrium amplitude is attained the switch is moved to the "run" position. Upon switching to the "run" position, the cover plate is withdrawn from the opening and control of the tunnel is switched to the pulsed air drive in the West tank with feedback control. In order to stop the oscillation the control switch is moved to the "stop" position at which time the cover plate covers the opening in the East tank and feedback control of the air in the West tank is cut out. The oscillation stops very quickly since air transfer into and out of the East tank is prevented.

Instrumentation - Likewise the instrumentation has been described in QUARTERLY REPORT 1 with the following additions.

A point gage traverse was made at the end of Run 48 and Run 50 in order to measure the geometric characteristics of the dunes. Upon completion of these runs, the point-gage carriage was mounted over the door opening in the roof of the test section with the point gage protruding vertically downward to the duned bed. The point gage could be positioned in the vertical and could be read to within ± 0.0005 ft. Horizontal positioning of the gage was determined to within ± 0.005 ft. by direct observation of a gaging mark on a scale mounted on the point gage carriage.

In order to observe flow patterns near the bed - in particular, boundary-layer transition - a movable dye injector was installed in the bed material. A 1/8-in. diameter brass tube with a 20 ga. hypodermic needle fastened to the top was inserted through a packing gland in the bottom of the test section. During observations the tip of the hypodermic needle was moved close to the surface of the bed. A valved gravity feed allowed the dye to be injected into the bed surface at a controlled rate.

During Run 47, 16mm color motion pictures were made in order to determine paths of the suspended particles above the bed. A high-intensity collimated light source was placed directly above the test section so as to illuminate the crests of three dunes and the two intervening troughs. The cross section of the light beam was approximately 12 in by 3 in for some photographs and 12 by 1 for others. Photographs were taken with frame speeds of 12, 16 and 24 frames per second corresponding to shutter speed 1/25, 1/34, and 1/50 of a second.

Bed of the test section - In order to determine the drag force exerted by the duned bed, two series of runs are being made - one with a plane bed and one with a duned bed.

The majority of the plane bed tests were performed with a 20-gage aluminum sheet placed over the bottom of the test section. The aluminum sheet was held in position with waterproof duct tape placed on the surface of the aluminum and the wall of the test section. Other plane bed tests (TABLE 1, APPENDIX) were performed with a bed of glass beads.

The duned bed tests have been made with a bed of glass beads. The pertinent characteristics of this bed material are as follows:

mean diameter, $d = 0.297$ mm,
geometric standard deviation, $\sigma_{gd} = 1.06$, and
specific gravity, $s = 2.47$

Disturbance element - In order to induce ripples and then dunes to form on the bed at water-motion amplitudes less than about 18 in., a half-round brass bar was inserted in the test section forming the initial dune crest. In all runs in which the disturbance element was used, the bar was 4 ft. long with a radius of 1/4 in. except in Run 49 for which a bar having a radius of 1/2 in. was used.

Experimental Procedure

The experimental procedure during a typical run was presented in QUARTERLY REPORT 1.

The principal change in the procedure was to blow down the water surface in the East tank to the predetermined equilibrium amplitude. Upon release of the compressed air over the East tank water surface, the water would oscillate at the equilibrium amplitude thereby eliminating the transient buildup. Operating in this manner, meaningful data on work input with a plane bed could be obtained by measuring the air pressure in the West tank. In other words, by eliminating the transient, a nearly equilibrium condition of oscillation prevailed before the bed had time to become duned. This procedure was employed for Runs 28-50, inclusive. The decrease in amplitude shown in TABLE I, APPENDIX, for Runs 28, 30, 31, and 32, is the consequence of increasing resistance forces as the dune system develops.

During Runs 37 through 41, 45 and 46 dye was injected into the plane bed and seeped into the moving water adjacent to the plane bed. Qualitative observation of the dye configurations were made.

During Runs 39, 42, 43, 45, and 46, the condition at which an appreciable percentage of the surface grain were rolling was observed in order to determine the condition called incipient motion.

Experimental Results

General - Runs 29-50, inclusive, were performed utilizing the "blowdown" system to eliminate the initial transient with the result that the oscillatory motion of the water in the test section started oscillating at zero time at essentially equilibrium amplitude. The elimination of the initial transient

in the fluid oscillation does not eliminate the initial transient in the development of an equilibrium duned bed. The general observations related in the following pertain to this starting condition. Inasmuch as the transient condition, during the development of an equilibrium duned bed, is a function of history, the transitory phenomena observed in the development of the equilibrium duned bed may be applicable only to these particular starting conditions.

Transients in the development of a duned bed - The predominant feature during the development of a duned bed is the early appearance of bed features of short wave length. The writers hereafter refer to these wavelets as ripples in contrast to the fully developed dunes which have a much greater wave length. The ripples were observed to appear all over the bed after a few oscillations during Runs 25-29, inclusive. During Runs 21, 22, 23, 24, 48, and 49, the ripple system propagated outward by forming successive crests parallel to the disturbance element. No ripples were observed during Runs 30, 31, 32, and 50. Referring to TABLE I, APPENDIX, the ripple systems can be classified by total amplitude, $2z_0$ of water motion as follows: (a) If $2z_0$ is less than 1.2 ft., the ripples propagated outward with each new ripple being formed in the disturbance created by the next oldest ripple; (b) If $2z_0$ is greater than 1.2 ft., but less than 2.3 ft., the ripples apparently form simultaneously all over the bed in a remarkably homogeneous pattern of two-dimensional ripples; and (c) If $2z_0$ is greater than 2.3 ft., no ripple system was observed.

The only ripple data obtained was the position of the ripple crests as a function of time. The position of the leading crest was observed during Runs 21-24, inclusive. The position of all of the crests as a function of time was observed during Runs 48 and 49. This data for the westward moving system of Run 49 is shown in Figure 1. The velocity of propagation of the ripple system computed from the displacement-time data is shown in Figure 2.

The ripple system was displaced by the equilibrium system of dunes in two different ways. During Runs 48 and 49 the ripple troughs were excavated and the crest were shifted further from the disturbance element by a continuous and orderly process until equilibrium or duned condition was achieved. The orderly transformation to dunes is shown clearly in Figure 1. On the other hand, for all other runs the ripple system was simply erased by the dune system with mixed systems of ripples and dunes prevailing at stages of the development.

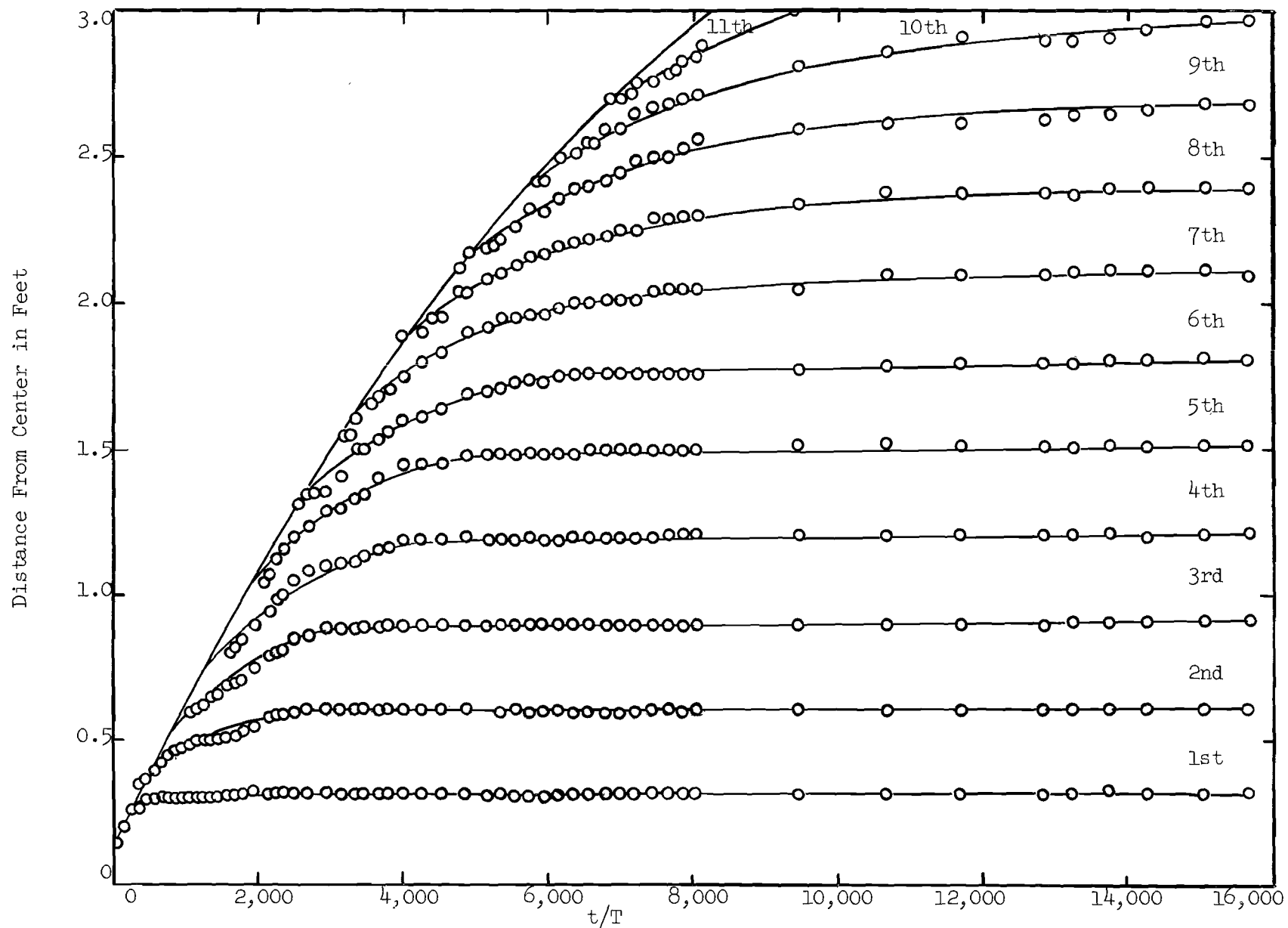


Figure 1. History of Dune Development - Run 49

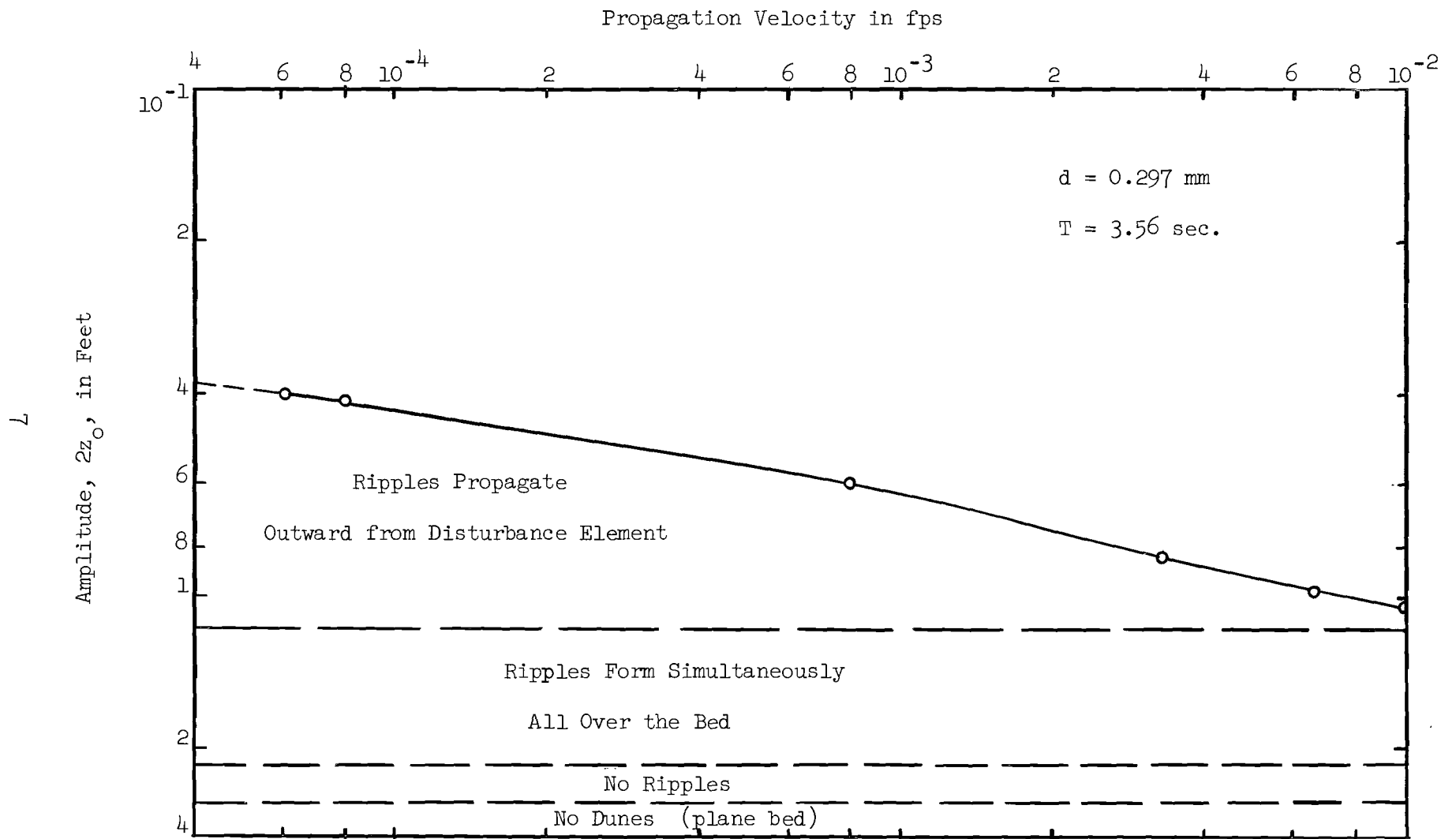


Figure 2. Velocity of Propagation of Ripples

Equilibrium bed form (dunes) - Runs 21-27, 29-32, 36, and 47-50, were continued until the equilibrium bed forms, dunes, were achieved over the bed of the test section in order to determine the geometric characteristics of dunes and to determine the fluid-energy dissipation resulting from flow over the duned bed.

The geometric characteristics of the dunes was primarily determined from photographs through a sidewall of the test section as explained in QUARTERLY REPORT 1. Dune wave length, λ , and dune amplitude, η , as a function of total water-motion amplitude, $2z_0$, are shown on Figure 3 and Figure 4. The dune pattern was two-dimensional with parallel, level, unbroken crests up to a water-motion amplitude of about 1.5 ft. At higher amplitudes the dune crests were no longer parallel, level, or unbroken. The bed characteristics of Run 50 for which $2z_0$ was 2.55 ft. are shown on the topographic map of the bed, Figure 5, with the basic data being determined by means of a point-gage traverse. The definition and determination of wave length, λ , and wave amplitude, η , for such a system of sand hills was necessarily arbitrary. The wave lengths shown in Figure 3 were measured from the photographs through the sidewall of the test section even though successive crests might differ appreciably in elevation. The amplitudes of the dunes shown in Figure 4 were obtained by averaging the crest elevation of two successive crests and subtracting the elevation of the intervening trough.

The process for determining the fluid-energy dissipation resulting from flow over a duned bed is based upon the difference of work input required to maintain a given water-motion amplitude between the duned bed and the plane bed. The method of measurement and calculation of work input are given in QUARTERLY REPORT 1. The computed results from experimental data are shown in Figure 6.

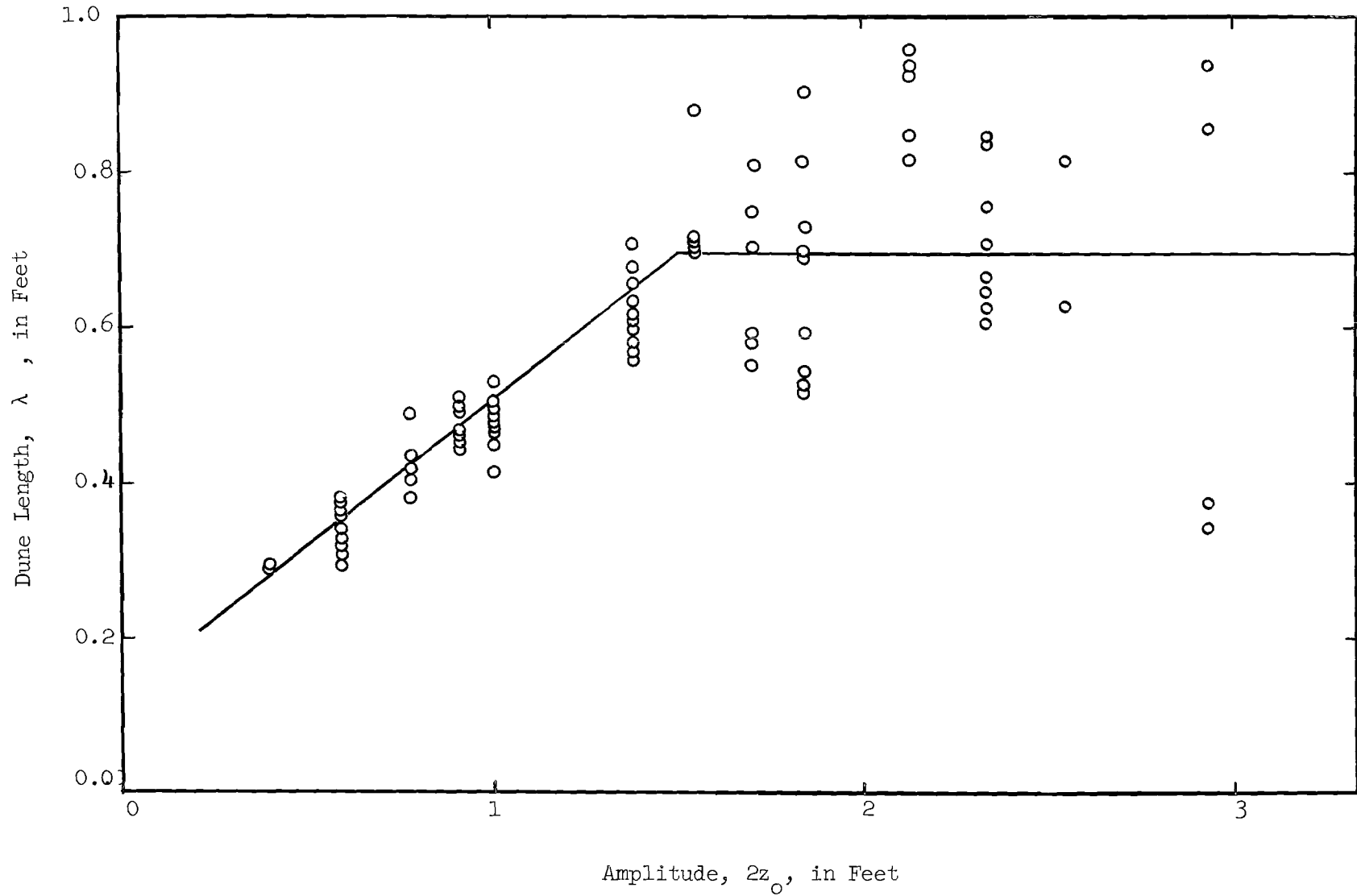
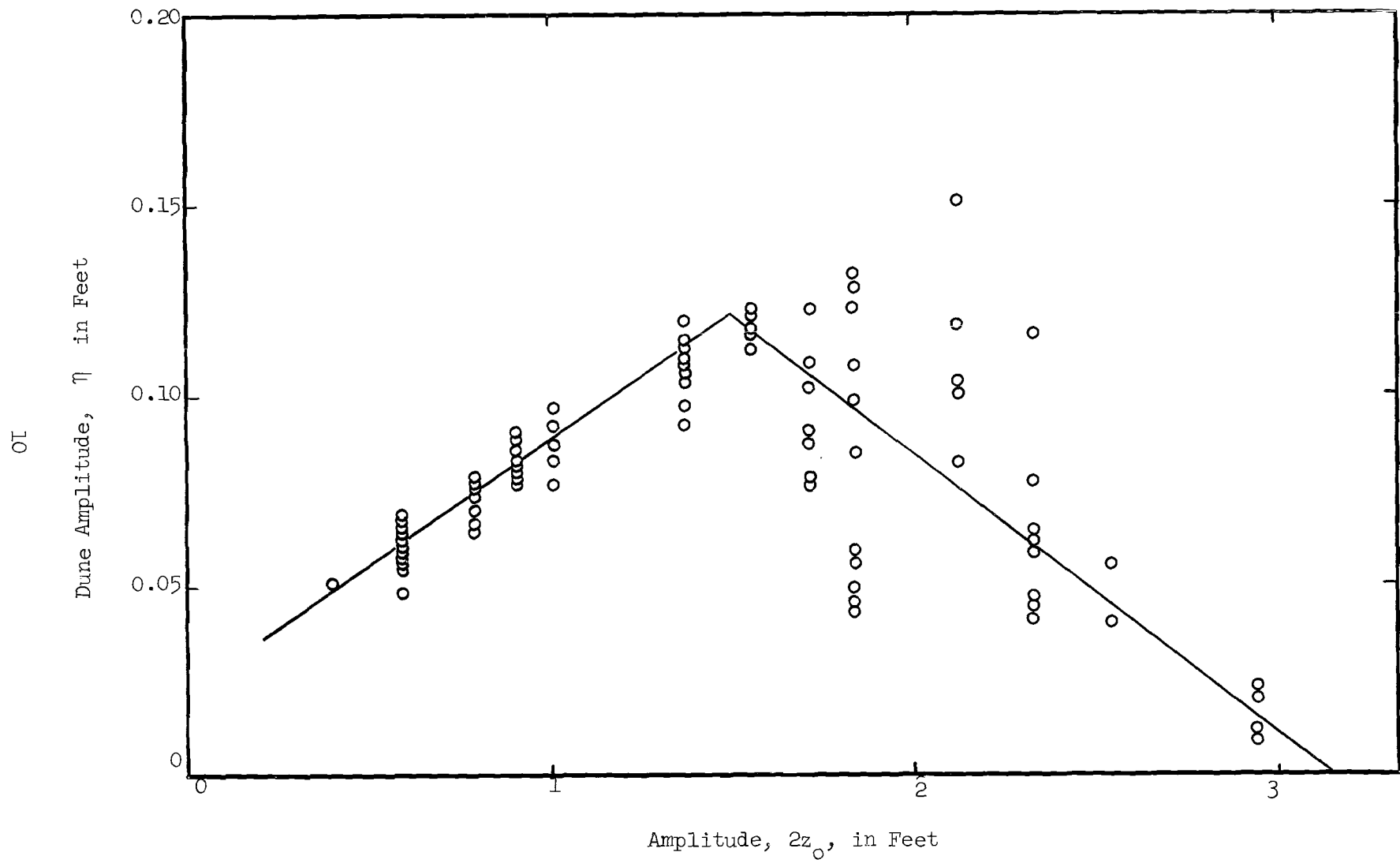


Figure 3. Dune Wave Length



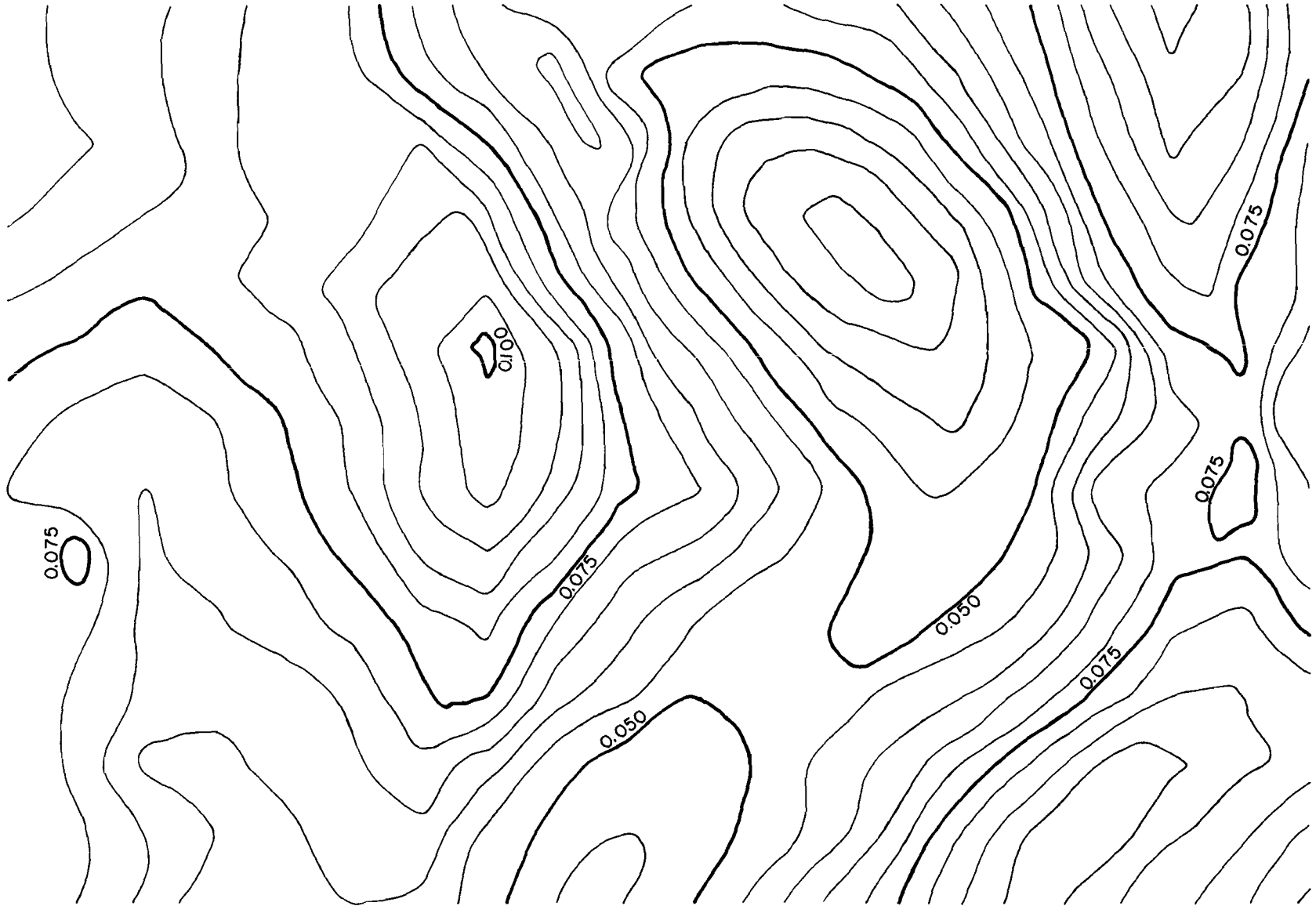


Figure 5. Topographic Map of Dunes - Run 50.

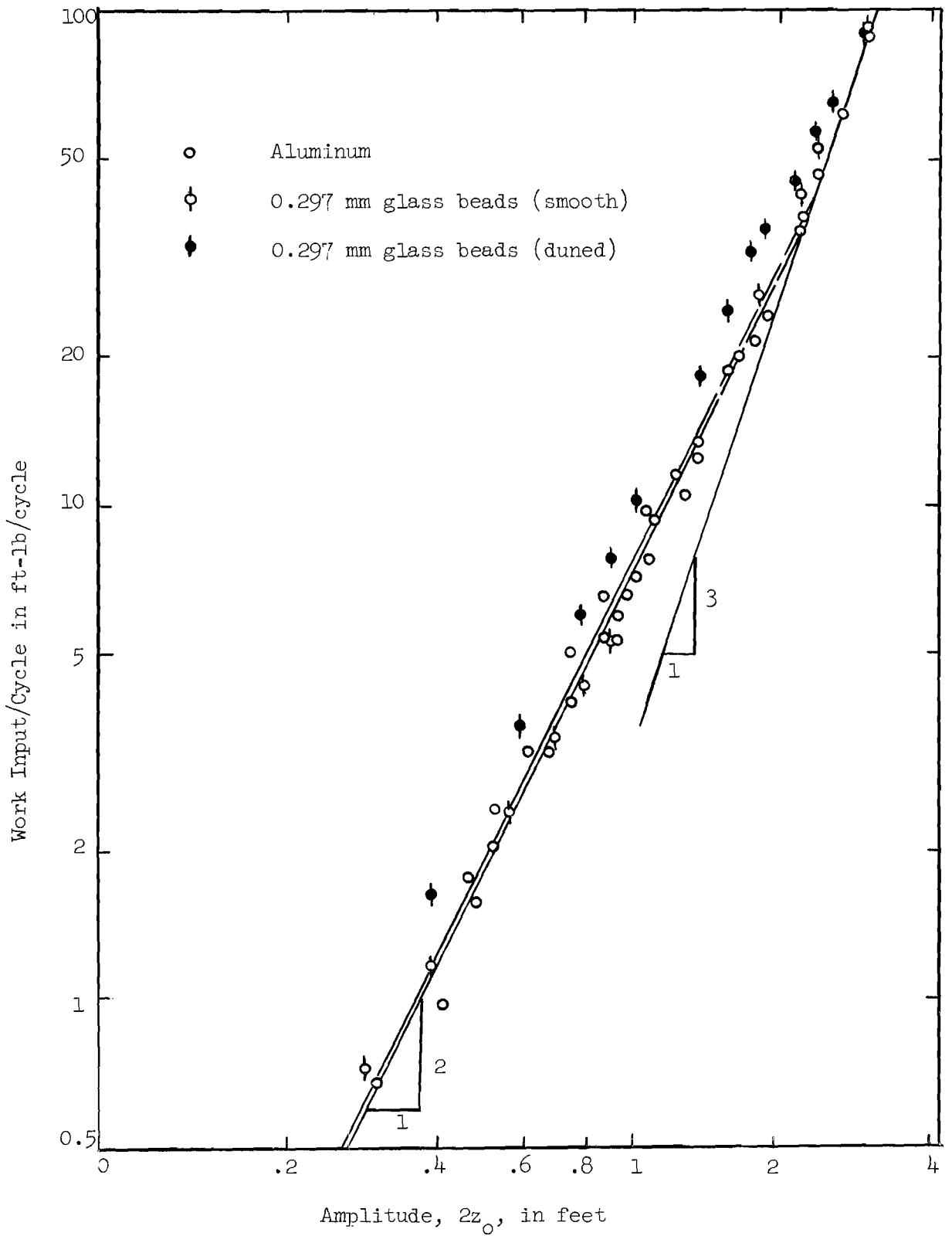


Figure 6. Work Input into West Tank

ANALYSIS OF RESULTS

The analysis presented in the following is preliminary inasmuch as the experimental results have been obtained from experiments involving a single size of bed particle and a single frequency of oscillation.

Ripples

After observing numerous experimental runs, the writers have observed the early appearance of bed features, ripples, which were obliterated in the development of the equilibrium bed features, dunes. The following characteristics of ripples have been observed:

(a) The principal characteristic of ripples is the short wave length as compared to dunes.

(b) With a total water-motion amplitude, $2z_0$, of less than 1.2 ft. the ripple system would propagate away from a disturbance placed in the bed by forming new crests beyond the last crest. The velocity of propagation is very sensitive to the magnitude of $2z_0$ as shown in Figure 2. For example the rate of propagation during Run 24 in which $2z_0$ was 1.05 ft. is 165 times the rate of propagation during Run 49 in which $2z_0$ was 0.40 ft. The rate of propagation appears to be infinite (spontaneous appearance) when $2z_0$ is about 1.2 ft.

(c) Ripples appeared spontaneously all over the bed in the range $1.2 \text{ ft} < 2z_0 < 2.3 \text{ ft}$.

(d) In all cases the ripple system was two-dimensional with parallel crests which were oriented perpendicular to the direction of flow.

(e) No ripples were observed when $2z_0 > 2.3 \text{ ft}$.

The accepted practice in discussion of bed forms in uni-directional flow is to differentiate between ripples and dunes (1), (2), whereas in discussion of bed forms in oscillatory flow (3), (4), (5), the bed forms are all called ripples. Based upon the current studies, the bed forms studied by Manohar (5) would be classified as ripples and the bed forms studied by Bagnold (4) and Inman (3) would be classified as dunes. Inasmuch as the experiments of Manohar and Bagnold were very similar, the writers surmise that Manohar stopped his experiments as soon as the ripple system developed thereby precluding the development of the dune system with a greater wave length and much greater amplitude.

The absence of ripples compares reasonably with Manohar's results. A comparison of the two studies in this regard is given below:

<u>Item</u>	<u>Manohar</u>	<u>Current Study</u>
Particle mean diameter	0.280 mm	0.297 mm
Material	Sand	Glass beads
Specific gravity	2.65	2.47
Period of oscillation	3.45 sec.	3.54 sec.
Water temperature	75° F	72° F
Total Amplitude of Motion	2.67 ft.	2.2 ft $< 2z_0 < 2.3$ ft.

Dunes

The experimental results of this study are primarily concerned with the equilibrium or duned bed conditions. From this study, information is being obtained about the geometric characteristics of dunes and about the energy dissipation in the fluid resulting from oscillatory flow over the duned bed.

In order to provide a basis for generalizing the experimentally determined results a mathematical model is being constructed which exhibits the principal flow characteristics that are observed. Obviously any theoretical model of such a complex time-varying flow in which the bed form is responsive to the flow pattern is not likely to be complete. Nevertheless some features of the motion of a simplified theoretical model are reasonable approximations to the observed characteristics. Also further refinements of the theoretical model are anticipated.

Theoretical model - The theoretical model now being considered is irrotational flow of an infinite row of equally spaced, equal strength, two-dimensional vortices (6). The streamline pattern resulting from this system of vortices is shown Figure 7. The flow in the upper portion of Figure 7 is from right to left. This flow is nearly uniform a short distance above the line of vortices as indicated by the nearly uniform spacing of streamlines. Each vortex lies within a closed streamline forming a vortex cell which adjoins the next cell. The lower half of Figure 7 is visualized as being the bed as indicated by the graphical symbols.

The theoretical model is suggested by the observation that vortices are formed in the lee of every two-dimensional dune crest after each flow reversal.

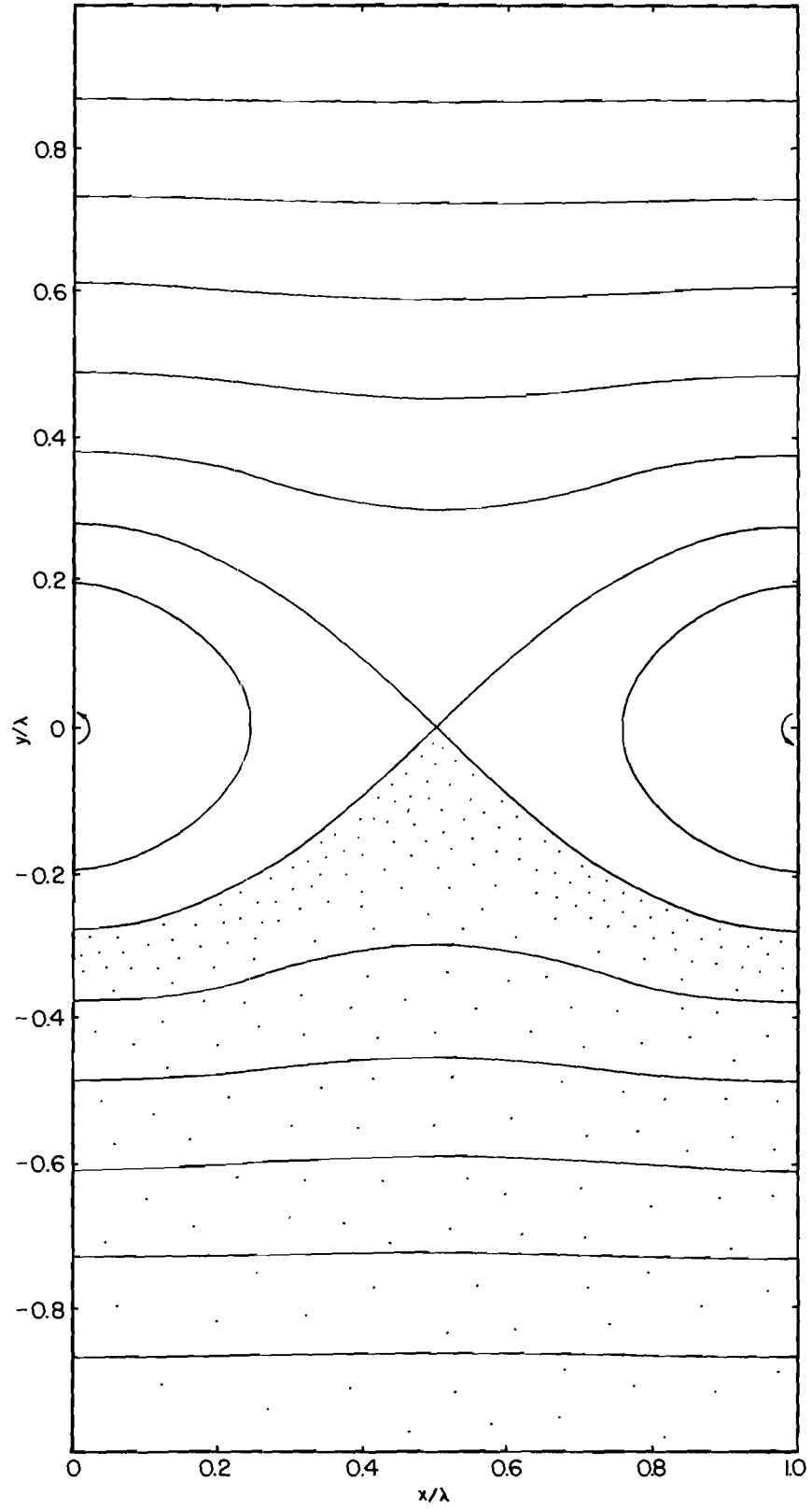


Figure 7. Theoretical Model.

Each vortex appears to grow in size and intensity in phase with the water velocity. If the water velocity some distance above the dunes is

$$u = z_0 \omega \sin \omega t$$

then new vortices are formed when ωt is zero. When ωt is about $7\pi/8$ the vortices begin to move out of the troughs between the crests. Each vortex climbs out or is pushed out of the trough on the lee side of the crest on which formation of that vortex occurred. The ejection of the vortices is complete when ωt is π . The process repeats except that the new vortex system has an opposite sense of rotation to the previous system. The ejected vortices are destroyed in the otherwise nearly uniform flow above the duned bed. Hence the theoretical model can be considered to be an approximation to the observed phenomenon when ωt is approximately $\pi/2$ and $3\pi/2$. Further the theoretical model is limited to a two-dimensional system of dunes or to a value of $2z_0 < 1.5\text{ft.}$ (see Figures 3 and 4) of the experimental program.

Dune Geometry - A comparison of the bed form of the model, Figure 7, is compared with the measured geometry of dunes in Figure 8. Figure 8 is undistorted with the wave length, λ , being used as the reference scale. The theoretical profile compares favorably with the measured profiles in the trough region. Inasmuch as the angle of repose of the 0.297 mm glass beads was determined experimentally to about 24 degrees, the measured profile would not be steeper than 24 degrees. The slope of the theoretical profile exceeds 24 degrees where $x/\lambda > 0.194$ and where $x/\lambda < -0.194$ in which x is measured from the trough. The deviation of the measured profiles is shown in Figure 8 to depart from the theoretical profile at about these points. Thus the deviation of the dune configuration from the theoretical model can be explained solely by considering the angle of repose or slope stability of the bed material.

The ratio of the amplitude to the wave length of dunes, η/λ , is shown in Figure 9. Two-dimensional dunes exhibit a constant value of the ratio of 0.174. This value compares favorably with that determined by Bagnold (3) who determined η/λ to be between 0.20 and 0.22. The values of η/λ found by Manohar (2) were much lower. The two-dimensional dunes begin to break down into three-dimensional bed forms at an amplitude, $2z_0$, of 1.5 ft. The dune

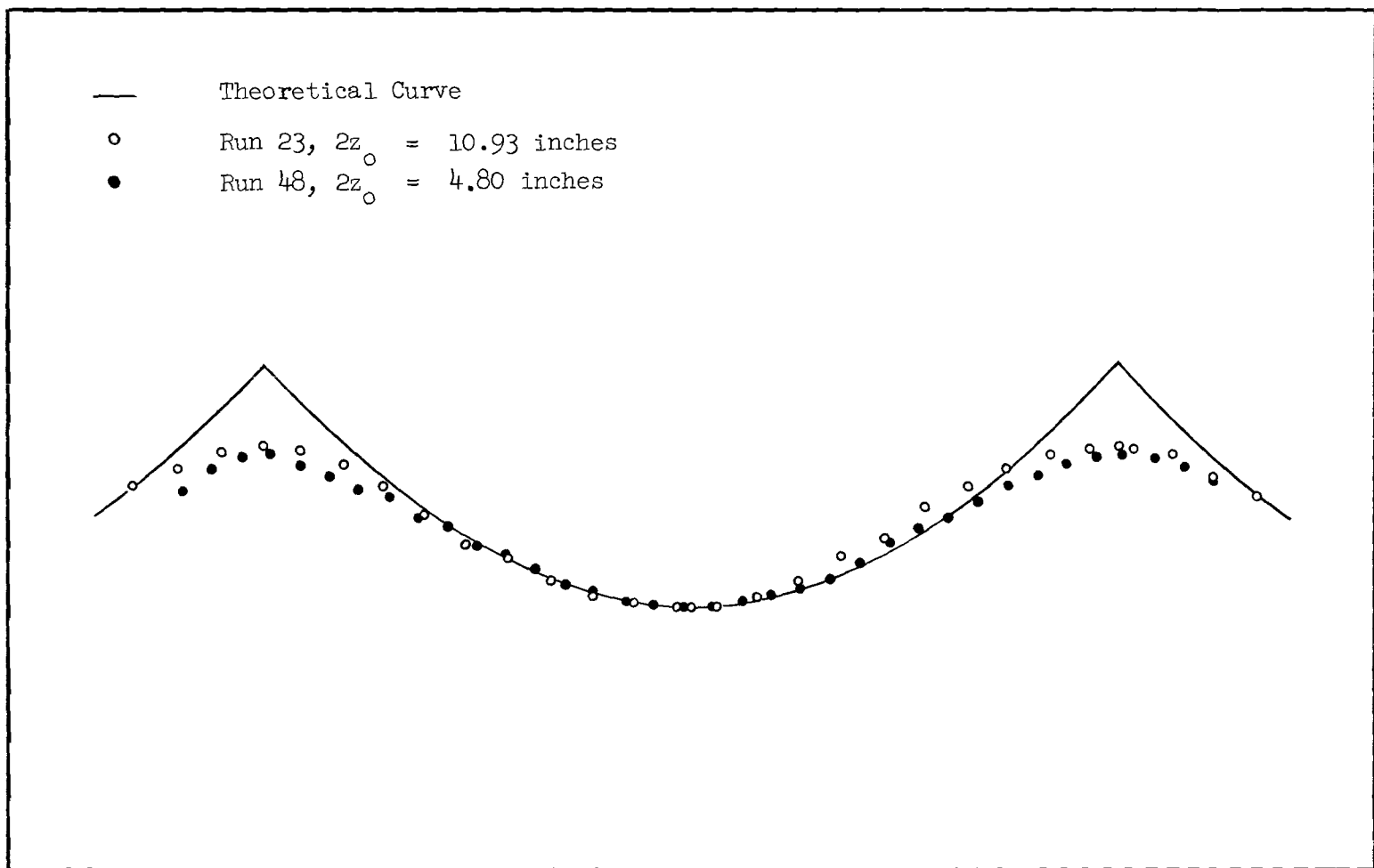


Figure 8. Comparison of Model with the Geometry of Observed Dunes

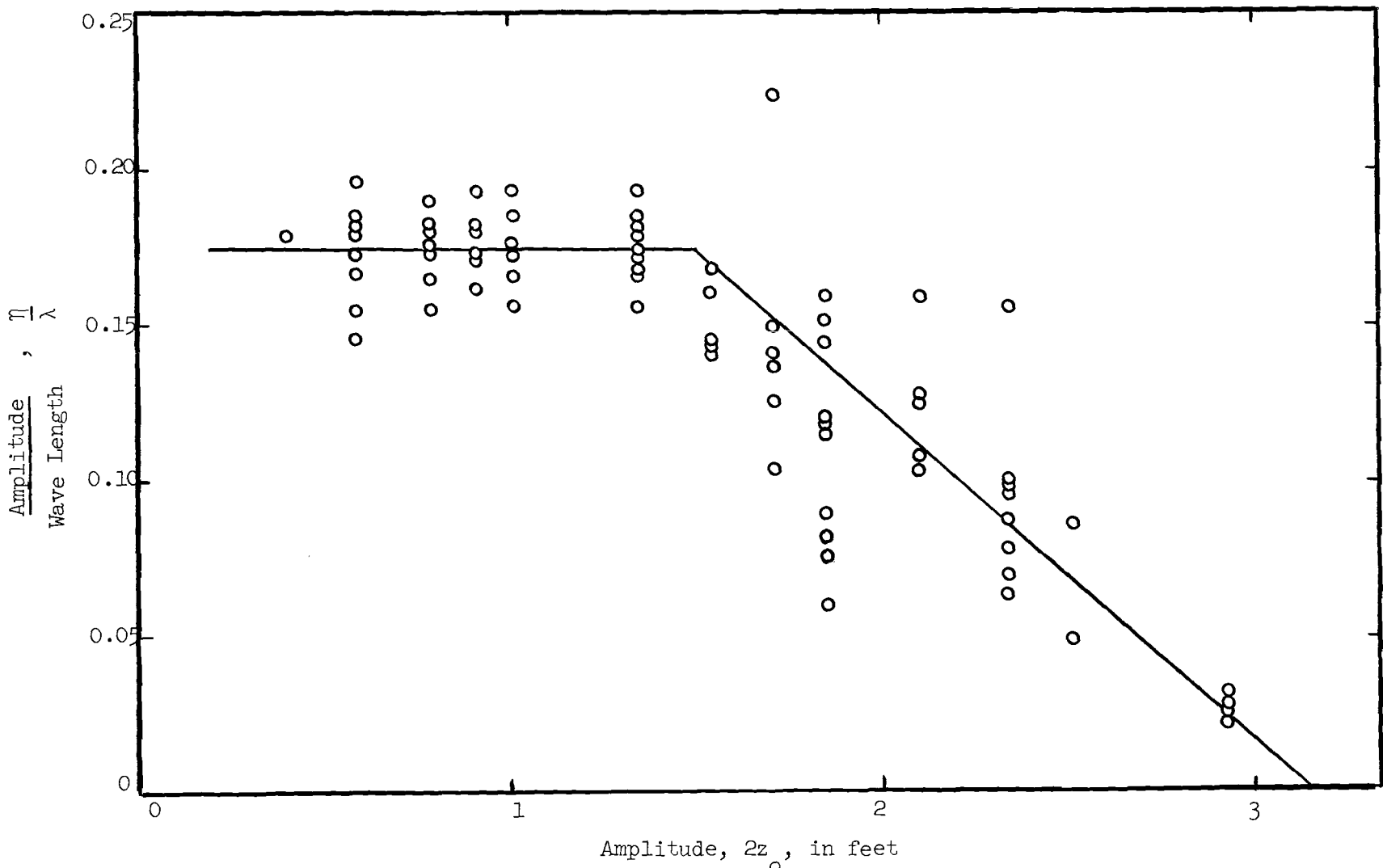


Figure 9. Ratio of Amplitude to Wave Length of Dunes

system is progressively less pronounced with increasing values of $2z_0$. In the limit the bed is plane. In these experiments, the limiting condition was attained at a value of $2z_0$ of about 3.1 or 3.2 ft. At this limit the entire surface of the bed appeared to be in motion.

Dissipation of energy - After considering several schemes to determine the energy dissipation and/or drag force of a ripple system, the decision was made to measure the work input necessary to maintain the oscillation at a given amplitude. Obviously, the work input per cycle is equal to the energy dissipation per cycle of a steady cyclic motion. Thus the difference between the work-input per cycle with a duned bed and the work-input per cycle with a plane bed at the same amplitude is equal to the difference in energy dissipation between the two bed states over a bed area of 4 ft. by 6 ft. This subtraction eliminates the need for consideration of energy dissipation in any element of the U-tube other than the movable-bed section. Of course, the principal disadvantage is the loss of significant figures.

In order to obtain the form of the functions which should represent the experimentally determined results shown in Figure 6, theoretical functions are derived in the following.

The first theoretical derivation is limited to amplitudes for which the boundary layer is laminar adjacent to the walls of the U-tube. Previously Martin (7) had determined that boundary-layer transition occurs with a water-motion total amplitude, $2z_0$, of 1.53 ft. Since the boundary layer is thin and the tunnel walls are large flat expanses, the solution of the Navier-Stokes equations for oscillatory flow over a plane wall (8) can be utilized to predict the form of the energy-dissipation function. The solution for the velocity is

$$u = z_0 \omega \left[\sin \omega t - e^{-\beta} \sin (\omega t - \beta) \right] \quad (1)$$

in which ω is the circular frequency, t is time, and β is $y \sqrt{\omega/2\nu}$ in which ν is the kinematic viscosity and y is the distance from the boundary. The energy dissipation per unit volume of fluid per unit time is $\mu(\partial u/\partial y)^2$. Utilizing equation (1) the energy dissipation per unit volume per unit time is

$$\mu \left(\frac{\partial u}{\partial y} \right)^2 = \rho z_0^2 \omega^3 e^{-2\beta} \sin^2 (\omega t - \beta + \pi/4) \quad (2)$$

in which ρ is the fluid density. Integrating with respect to time in order to obtain the energy dissipation per unit volume per cycle

$$\int_0^T \mu \left(\frac{\partial u}{\partial y} \right)^2 dt = \rho z_0^2 \omega^2 \pi e^{-2\beta} \quad (3)$$

in which T is the period of the oscillation. Integrating equation (3) from the wall where $y = 0$ results in the energy dissipation per unit area of wall per cycle as follows

$$\int_0^\infty \pi \rho z_0^2 \omega^2 e^{-2\beta} dy = \frac{\pi \rho}{\sqrt{2}} \sqrt{\nu} z_0^2 \omega^{3/2} \quad (4)$$

Equation (4) is the desired relationship inasmuch as the total wall area over which the flow passed was constant in all experimental runs. Furthermore the circular frequency ω , density ρ , and kinematic viscosity ν were nearly constant in all the runs. Hence the energy dissipation per cycle which is equal to the work input per cycle should vary with the square of the water-motion amplitude. In other words, the plane-bed data shown in Figure 6 should fall on a line with a slope of two for values of $2z_0$ less than 1.53 ft.

Using the method of least squares, expressions for work input WI as a function of $2z_0$ were derived for the experimentally determined results shown in Figure 6. Expressions were limited to plane-bed results and to results for which $2z_0$ was less than 1.53 ft. The resulting empirical expressions are as follows:

$$WI \text{ (plane bed-glass beads)} = 7.69 (2z_0)^2 \quad (5)$$

and

$$WI \text{ (plane bed-Al sheet)} = 7.36 (2z_0)^2 \quad (6)$$

The units of WI are ft-lb/cycle and of $2z_0$ are ft.

The functional relationship between energy dissipation per unit area of bed per cycle is given by equation (4) for runs in which the boundary layer is laminar over a plane bed. The corresponding analysis for cases in which the boundary layer is turbulent is less satisfactory because of the lack of an analytical solution corresponding to equation (1) and of a more complex energy dissipation function for the turbulent case. Nevertheless, the asymptote of the dissipation function can be formulated by assuming (a) that the boundary shear is π radians out of phase with the velocity and (b) that the boundary-drag coefficient is constant throughout the cycle. Inasmuch as the laminar phase difference is $5\pi/4$ radians, the first assumption tends to be approached in the turbulent case since turbulent diffusion of linear momentum is about three orders of magnitude greater than molecular diffusion of the laminar case. The second assumption tends to become valid as the Reynolds number approaches infinity. Applying the linear momentum equations to a mass of fluid adjacent to the plane boundary and recognizing that the work input to the mass is equivalent to the energy dissipation one obtains the following equation for energy dissipation per unit area of wall per cycle,

$$\frac{\text{WI (plane bed-turbulent)}}{\text{unit area}} = \int_0^T \tau_o u \, dt \quad (7)$$

in which τ_o is the wall shear stress. The wall shear stress τ_o is given by

$$\tau_o = c_f \frac{\rho u^2}{2} \quad (8)$$

in which c_f is the boundary-drag coefficient. Furthermore the velocity u is given by

$$u = z_o \omega \sin \omega t \quad (9)$$

Assuming that c_f is constant, combining equations (8), (9), and (7), and integrating

$$\frac{\text{WI (plane bed-turbulent)}}{\text{unit area}} \propto c_f \rho z_o^3 \omega^2 \quad (10)$$

For oscillatory flow over a plane bed with a highly turbulent boundary layer, equation (10) is indicative that the energy dissipation is proportional to the cube of the water-motion amplitude. Such a function would have a slope of three in Figure 6. Referring to Figure 6, the above analysis appears to be valid if $2z_0$ is greater than 2.16 ft.

The plane-bed analyses applied to the experimental results, Figure 6, are indicative (a) that energy dissipation is proportional to the square of $2z_0$ with a laminar boundary layer ($2z_0 < 1.53$ ft) and (b) that energy dissipation is proportional to the cube of $2z_0$ with a highly turbulent boundary layer ($2z_0 > 2.16$ ft). A transition function is not well defined in the range $1.53 < 2z_0 < 2.16$ ft.

The following procedure was employed in order to determine the energy dissipation per unit area of bed per cycle resulting from the flow over a duned bed. First the work input for a smooth plane bed was calculated using the empirically determined function, equation (6), for the same amplitudes of runs at which work-input determinations had been made for flow over a duned bed. This step was performed for Runs 21-27, 29, 36, and 49 (see TABLE 1, APPENDIX). Second the calculated values of the work input with the plane smooth bed were subtracted from the work input values of the duned bed. This difference is the difference in the energy dissipation resulting from flow over a duned bed and a plane bed which has the dimensions of 6 ft in length by 4 ft in width. Next these values were divided by 24 ft^2 in order to obtain energy-dissipation difference per unit area of bed. Finally the energy dissipation per cycle per unit area of duned bed was determined by adding a calculated value for a plane bed. Equation (4) was utilized in this step. The results of the above calculations from experimentally determined values are shown in Figure (10). Since equation (4) was utilized, this procedure is rational as long as the boundary layer is laminar, that is, $2z_0 < 1.53$ ft.

The theoretical analysis of energy dissipation is predicated on the assumption that the kinetic energy of the vortices which develop twice each cycle is the sole form of energy dissipation. These vortices are developed, are ejected from the dune troughs, and are dissipated in the main stream.

The initial model chosen for the evaluation of the kinetic energy within a finite developing vortex is that of a circular vortex which develops in the fluid contained within a cylinder as the cylinder is suddenly made to rotate

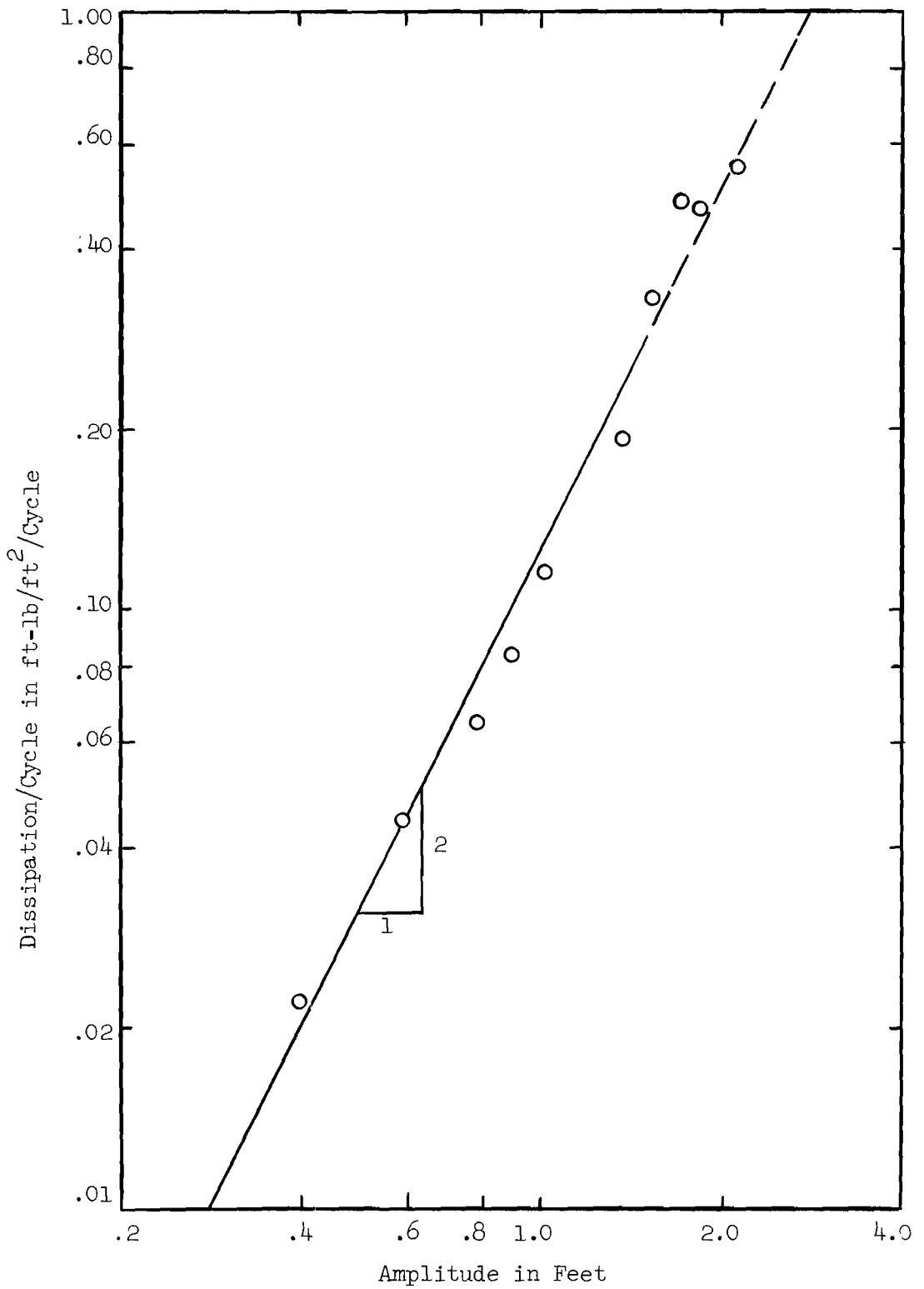


Figure 10. Energy Dissipation per Unit Area per Cycle (Dunes)

with the constant tangential velocity u_m . The radius, a , of the cylinder would be proportional to the wave amplitude, η , of the dunes and the tangential velocity, u_m , would be proportional to the maximum value of the main stream velocity. That is,

$$a \approx \eta \quad (11)$$

and

$$u_m \approx z_0 \dot{\omega} \quad (12)$$

The solution of the Navier-Stokes equations for the fluid velocity within the cylinder is presented by Gray, Mathews, and MacRobert (9) as follows

$$\frac{v}{u_m} = \beta + 2 \sum_{i=1}^{\infty} \frac{J_1(\alpha_i \beta) e^{-\alpha_i^2 (vt/a^2)}}{\alpha_i J_0(\alpha_i)} \quad (13)$$

in which

v is the fluid velocity;

β is r/a in which r is the radial coordinate;

α_i 's are roots of the equation $J_1(\alpha_i) = 0$;

J 's are Bessel functions of the first kind;

ν is the kinematic viscosity; and

t is the time measured from the beginning of rotation of the circumscribing cylinder.

The kinetic energy, KE, of a vortex per unit length of vortex is

$$KE = \int_0^a \left(\frac{\rho v^2}{2} \right) 2 \pi r dr$$

or in dimensionless form

$$\frac{KE}{a^2 \rho u_m^2} = \pi \int_0^1 \left(\frac{v}{u_m} \right)^2 \beta \, d\beta \quad (14)$$

Introducing equation (13) into equation (14) and integrating

$$\frac{KE}{a^2 \rho u_m^2} = \pi \left[\frac{1}{4} - 2 \sum_{i=1}^{\infty} \left(\frac{1}{\alpha_i} \right) \left(2 - e^{-\alpha_i^2 (v t/a^2)} \right) \left(e^{-\alpha_i^2 (v t/a^2)} \right) \right] \quad (15)$$

Designating the RHS of equation (15) as $f(\chi)$ in which χ is $v t/a^2$, the KE per unit length of vortex is

$$KE = f(\chi) a^2 \rho u_m^2 \quad (16)$$

Since two vortices are formed in every cycle

$$\frac{KE}{1 \text{ cycle}} = 2f(\chi) a^2 \rho u_m^2 \quad (17)$$

Introducing equations (11) and (12) into equation (17) results in

$$\frac{KE}{1 \text{ cycle}} = 2f(\chi) \eta^2 \rho z_o^2 \omega^2 \quad (18)$$

The kinetic energy per unit area of duned bed per cycle is

$$\frac{KE}{\lambda \text{ 1 cycle}} = 2f(\chi) \left(\frac{\eta}{\lambda} \right) \eta \rho z_o^2 \omega^2 \quad (19)$$

Values of $f(\chi)$ were numerically evaluated for a range of values of χ . These values are shown in Figure 11. The values of $f(\chi)$ were evaluated on the Burrough B 220 electronic digital computer. The infinite series was terminated either at the hundredth zero root, α_{100} , or when the exponent of e exceeded 112.8. The latter limit is the computer limit. The convergence of the series is rapid at large values the exponent but is slow at small values of the exponent, that is, if $\chi \leq 10^{-4}$.

The numerical solution for $f(\chi)$ as shown in Figure 11 is indicative that the solution is quite simple. If the value of χ is less than 6 (10^{-2})

$$f(\chi) = 2\sqrt{\chi} \quad (20)$$

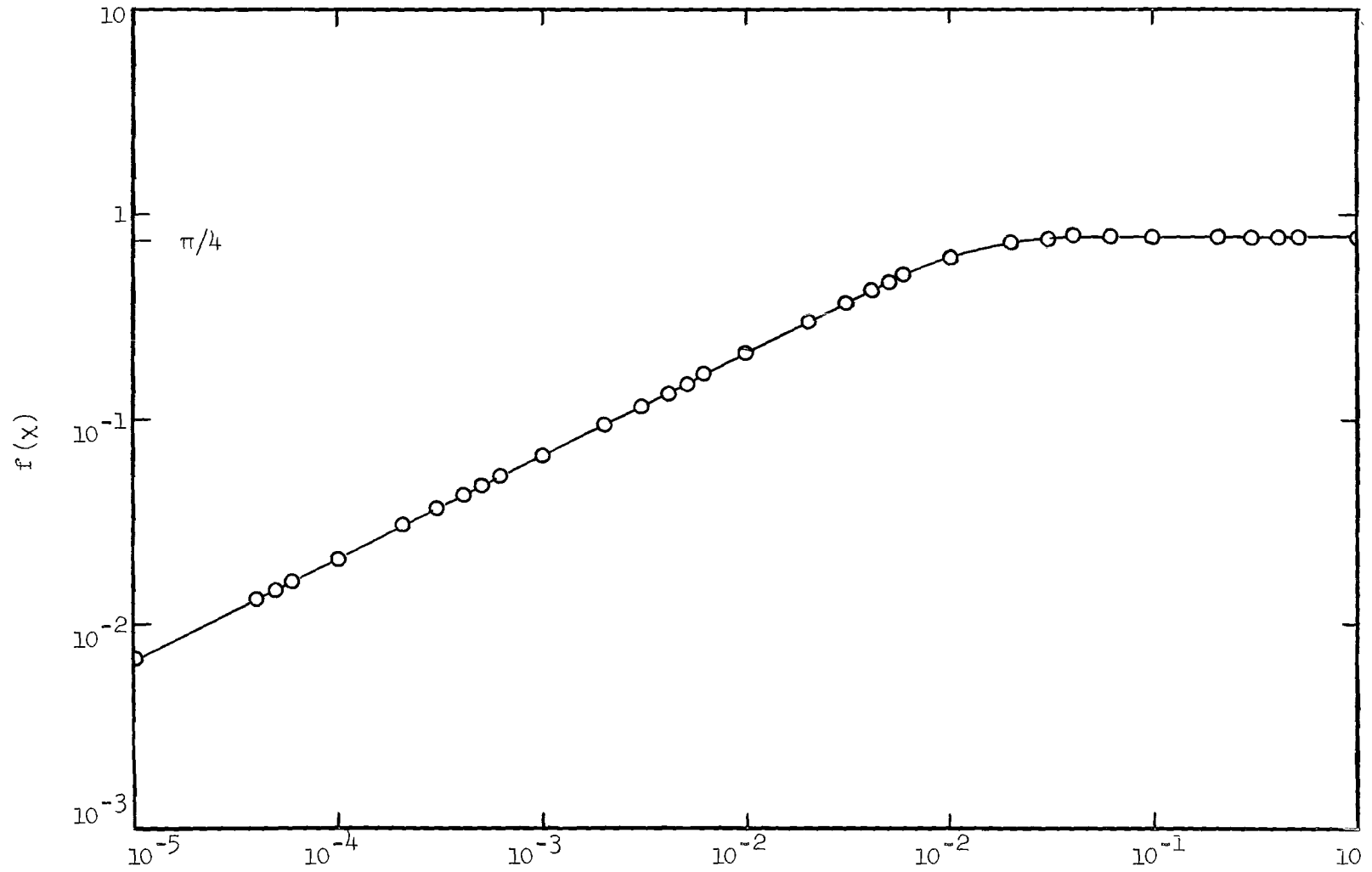
and if χ is greater than $4(10^{-1})$

$$f(\chi) = \pi/4 \quad (21)$$

Equation (21) is the solution for the steady state in which the fluid within the cylinder rotates as a solid body. In other words, if the circumscribing cylinder rotates with the tangential velocity, u_m , for a sufficient time t (such that $vt/a^2 \geq 4(10^{-1})$) the steady state condition will be attained. The simple function, equation (21) for the kinetic energy in a developing vortex undoubtedly could be demonstrated analytically but was not apparent prior to the numerical evaluation of $f(\chi)$. The physical significance of equation (21) is that the kinetic energy of a developing vortex is directly proportional to the square root of the time from the beginning of rotation and is inversely proportional to the linear dimension of the vortex. The maximum value of χ attained in these experiments would be attained in Run 49 in which the dune amplitude, η , was approximately 0.05 ft. Hence

$$\chi_{\max} = \frac{v t}{a^2} \approx \frac{v T}{4 \eta^2} = \frac{(1.05)(10^{-5})(3.56)}{(4)(0.0025)} = 3.7(10^{-3})$$

which is indicative that equation (20) should be used in the interpretation of the experimental results.

Figure 11. Values of $f(\chi)$

Substituting equation (20) into equation (19)

$$\begin{array}{l} \text{energy dissipation} \\ \text{per unit area of duned bed} \\ \text{per cycle} \end{array} = \sqrt{\frac{\pi}{2}} \sqrt{v} \left(\frac{\eta}{\lambda} \right) \rho (2z_0)^2 \omega^{3/2} \quad (22)$$

The surprise in equation (22) is that the energy dissipation anticipated from a duned bed results in exactly the same relationship of variables as the energy dissipation anticipated from laminar oscillatory flow over a plane bed, equation 4, since the ratio η/λ was found to be constant for a two dimensional dune system as shown in Figure 9. In other words both equations (4) and (22) coupled with the experimental finding that η/λ is constant, are indicative that

$$\begin{array}{l} \text{energy dissipation} \\ \text{per unit area of bed} \\ \text{per cycle} \end{array} = K \sqrt{v} \rho (2z_0)^2 \omega^{3/2} \quad (23)$$

for either laminar oscillatory flow over a plane bed or for oscillatory flow over a duned bed (two-dimensional dunes).

The value of K, equation (23), for the oscillatory laminar flow over a plane bed from equation (4) is

$$K_p = \pi/4 \sqrt{2} = 0.555 \quad (24)$$

The value of K in equation (23) for the duned bed can be derived from the straight line function shown in Figure 10. From Figure 10 and equation (23) one finds that

$$K_d \sqrt{v} \rho \omega^{3/2} = 0.127 \quad (25)$$

For Runs 21-27, 29, 36 and 49 (TABLE 1, APPENDIX) the following physical quantities are applicable: (a) temperature (mean value) is 74° F, and (b) period (mean value) is 3.55 sec. From which the following values are determined: (a) v is 1.00 (10^{-5}) ft²/sec, (b) ρ is 1.935 slugs/ft³, and

(c) ω is 1.77 rad/sec. Utilizing these numerical values in equation (25) the value of K_d for oscillatory flow over a duned bed is found to be

$$K_d = 8.82 \quad (26)$$

which is indicative that the energy dissipation per unit area of bed per cycle with a duned bed is about 16 times that with a plane bed with otherwise similar flow conditions.

Incipient Motion

Incipient motion is visualized as being the condition at which the particles on the surface of the plane bed begin to move. The concept is much more understandable than reality because the flow condition which will cause a few particles to oscillate without translation is considerably different from the flow condition which will cause all surface particles to undergo translation. Hence the incipient-motion condition is subject to the judgement of the observer. In Run 45 in which the amplitude of water motion was decreased, an amplitude, $2z_o$, of 0.97 ft was deemed to be the incipient-motion condition. In Run 45 in which the amplitude of water motion was increased, an amplitude, $2z_o$, of 0.93 ft was deemed to be the incipient-motion condition. In Run 39 some particles were observed to tip back and forth at an amplitude, $2z_o$, of 0.84 ft. The incipient-motion condition, that is, $2z_o \approx 0.95$ ft does not seem to be of great significance in this study. For example, dunes would form at much lower values of $2z_o$ when a disturbance element was placed in the bed. Dunes were formed in Runs 42 and 49 with an amplitude $2z_o$ of 0.39 ft. The incipient-motion condition is probably related to the condition at which ripples formed spontaneously over the bed at an amplitude, $2z_o$, of 1.2 ft. The amplitude, $2z_o$, of 1.2 ft is probably the lower limit at which all of the particles on the surface of the plane bed are in motion.

Boundary-Layer Transition

The transition from a laminar to a turbulent boundary layer with oscillatory flow over a plane wall is continuous in the sense that vortices appear in the boundary layer an increasing portion of the time as the amplitude

of the fluid motion is increased. In oscillatory flow over a plane wall with a laminar boundary layer, the fluid close to the boundary reverses direction sooner than in the main stream. In fact, the velocity gradient, $\partial u/\partial y$, at the wall is zero when ωt is $-\pi/4$ and $3\pi/4$ as shown by equation (2) whereas the velocity, u , in the main stream is zero when ωt is 0 and π as shown by equation (1). By means of the dye which was forced to seep upward from the surface of the bed, small vortices were observed to form a small distance above the bed at about the time of flow reversal in Run 39 for which $2z_0$ was 0.723 ft. This layer of vortices was sandwiched between the essentially laminar uniform flow above and below. These vortices decayed very quickly after flow reversal. The axis of these small vortices appeared to be at about $\frac{1}{2}$ in above the bed. The observations were duplicated in Runs 40 and 41. The phenomenon was essentially the same except that the vortices appeared to persist during a slightly greater portion of the cycle. These runs could not be continued inasmuch as the bed particles began to move at slightly greater amplitudes. Martin (7) performed this experiment with a fixed bed in the same water tunnel. He concluded that a layer of vortices persisted through $\frac{1}{2}$ cycle when $2z_0$ was 1.53 ft. The continuous existence of vortices was called the end of transition and the boundary layer was turbulent for greater values of $2z_0$. The boundary-layer transition over a plane bed is of no significance in the current studies since the bed is duned at this value of $2z_0$.

SUMMARY

The experimental studies reported in QUARTERLY REPORTS 1 and 2 are considered to be complete in regard to dunes which formed in the bed composed of 0.297 mm-diameter glass beads. The next experimental studies will be similar except that the bed material will be 0.585 mm-diameter Ottawa sand. The analysis of results presented in this report is quite preliminary. The expectation is that the conceptual models used in the analysis will be improved. Major effort will be devoted to analysis in the immediate future. The emphasis upon analysis is considered to be of prime importance in order to generalize the results since the amplitude of oscillation can be readily varied in the experiments but the frequency cannot. Upon completion of further analysis of dunes and of experiments with the larger sand, the hope is that the transitory bed forms, ripples, can be studied in greater detail.

NOMENCLATURE

Symbol	Definition	Dimensions (F, L, T)
a	radius of a rotating cylinder of fluid	L
C_f	boundary-drag coefficient	none
d	mean diameter of bed particles	L
f (χ)	functional expression	none
J_n	Bessel function of the first kind of order n	none
K	energy dissipation coefficient	none
K_p	energy dissipation coefficient for a plane bed	none
K_d	energy dissipation coefficient for a duned bed	none
KE	kinetic energy	FL
r	radial coordinate	L
s	specific gravity	none
t	time	T
T	period of oscillation	T
u	fluid velocity parallel to bed	LT^{-1}
u_m	maximum fluid velocity	LT^{-1}
v	fluid velocity	LT^{-1}
WI	work input	LF
x	horizontal coordinate	L
y	vertical coordinate	L
z_o	water-motion amplitude	L
α_i	roots of the equation $J_i(\alpha_i) = 0$	none
β	distance parameter; $\beta = r/a$ for a forced vortex; $\beta = y \sqrt{\omega/2\nu}$ for oscillating flow over a plane boundary	none

Symbol	Definition	Dimensions (F, L, T)
η	dune amplitude	L
λ	dune wave length	L
μ	dynamic viscosity of fluid	$F T L^{-2}$
ν	kinematic viscosity of fluid	$L^2 T^{-1}$
ρ	mass density of fluid	$F T^{-2} L^{-3}$
σ'_{gd}	geometric standard deviation of bed particle diameter	none
τ_o	shear stress on the boundary	$F L^{-2}$
$\chi = \nu t/a^2$	time parameter for a forced vortex	none
ω	frequency of simple-harmonic oscillation	T^{-1}

REFERENCES

- (1) D. B. Simons and E. V. Richardson, "Forms of Bed Roughness in Alluvial Channels," Transactions, American Society of Civil Engineers Vol. 128 (1963), pp. 284-323.
- (2) John F. Kennedy, "The Formation of Sediment Ripples in Closed Rectangular Conduits and in the Desert," Journal of Geophysical Research, Vol. 69, No. 8, April 15, 1964, pp. 1517-1524.
- (3) R. A. Bagnold, "Motion of Waves in Shallow Water - Interaction between Waves and Sand Bottoms," Proceedings, Royal Society, A, Vol. 187, Oct. 8, 1946, pp. 1-18.
- (4) Douglas L. Inman, "Wave-Generated Ripples in Nearshore Sand," Tech Memo No. 100, Beach Erosion Board, U. S. Army Corps of Engineers, October 1957, 41 pp.
- (5) Madhav Mamhar, "Mechanics of Bottom Sediment Movement Due to Wave Action," Tech Memo No. 75, Beach Erosion Board, U. S. Army Corps of Engineers, June 1955, 121 pp.
- (6) V. L. Streeter, Fluid Dynamics, McGraw-Hill Publishing Company, New York, 1st edition, 1948, pp.199-200.
- (7) C. S. Martin, "Transition of Oscillatory Boundary-Layer Flow," Tech Rpt. 3 titled "Four Topics Pertinent to Sediment Transport and Scour," Project A-628, Engineering Experiment Station, Georgia Institute of Technology, September 1963, p. 10.
- (8) H. Schlichting, Boundary Layer Theory, J. Kestin translation, published by Pergamon Press, New York, 1955, pp. 67-68, and p. 244.
- (9) A. Gray, G. B. Mathews, and T. M. MacRobert, Bessel Functions, MacMillan and Company, London, 2nd Edition, 1952, example 38, p. 249.

APPENDIX

TABLE I

TABLE I
 COMPLETED EXPERIMENTAL PROGRAM
 (December 31, 1964)

Run No.	Period T (Sec)	Amplitude $2z_0$ (in)	Water Temp °F	Conditions (See key at the end of TABLE I)	Purpose
13 A	3.565	6.21	79	1, 13, 24	53
13 B	3.552	8.05	79	1, 13, 24	53
13 C	3.550	11.12	79	1, 13, 24	53
13 D	3.549	12.97	79	1, 13, 24	53
13 E	3.549	15.31	79	1, 13, 24	53
14 A	3.554	5.52	80	1, 13, 24	53
14 B	3.562	6.28	80	1, 13, 24	53
14 C	3.564	7.29	80	1, 13, 24	53
14 D	3.554	8.92	80	1, 13, 24	53
14 E	3.557	10.61	80	1, 13, 24	53
15 A	3.538	8.99	80	1, 13, 24	53
15 B	3.553	10.48	80	1, 13, 24	53
15 C	3.557	13.28	80	1, 13, 24	53
15 D	3.558	14.87	80	1, 13, 24	53
16 A	3.551	12.86	79	1, 13, 24	53
16 B	3.553	16.32	79	1, 13, 24	53
16 C	3.552	19.92	79	1, 13, 24	53
16 D	3.551	24.40	79	1, 13, 24	53
16 E	3.548	22.72	79	1, 13, 24	53
16 F	3.548	21.23	79	1, 13, 24	53
17 A	3.55	12.17	80	1, 13, 24	53
17 B	3.553	16.34	80	1, 13, 24	53
17 C	3.551	23.33	80	1, 13, 24	53
17 D	3.548	26.33	80	1, 13, 24	53
17 E	3.540	28.78	80	1, 13, 24	53
18 A	3.55	18.78	80.2	1, 13, 24	53
18 B	3.546	26.35	80.2	1, 13, 24	53

TABLE I (CONTINUED)

Run	<u>Period</u>	<u>Amplitude</u>	<u>Water</u>	<u>Conditions</u>	<u>Purpose</u>
<u>No.</u>	T (Sec)	2z _o (in)	Temp °F		
18 C	3.539	32.00	80.2	1, 13, 24	53
18 D	3.534	36.16	80.2	1, 13, 24	53
19 A	3.555	3.60	80.2	1, 13, 24	53
19 B	3.559	4.94	80.2	1, 13, 24	53
19 C	3.560	5.87	80.2	1, 13, 24	53
20 A	3.555	3.41	77	1, 11, 24	53
20 B	3.552	4.62	77	1, 11, 24	53
20 C	3.555	6.71	77	1, 11, 24	53
20 D	3.547	8.31	77	1, 11, 24	53
20 E	3.549	9.49	77	1, 11, 24	53
20 F	3.548	10.51	77	1, 11, 24	53
21	3.557	7.02	79	2, 11, 21	51, 53
22	3.555	9.44	76	2, 11, 21	51, 52, 53
23	3.549	10.76	75	2, 11, 21	51, 52, 53
24	3.551	12.10	77	2, 11, 21	51, 52, 53
25	3.552	16.42	73	2, 11, 21	51, 53
26	3.551	18.42	73	2, 11, 21	51, 53
27	3.528	20.56	73	2, 11, 21	51, 53
28	3.510	21.67	69.5	1, 11, 24	53
29	3.537	26.25	72.5	1, 11, 24	53
	3.544	25.50	73	2, 11, 24	51, 53
30	3.525	28.56	72	1, 11, 24	53
	3.522	28.03	72	2, 11, 24	51, 53
31	3.517	35.41	72	1, 11, 24	53
	3.521	35.04	72	2, 11, 24	51, 53
32	3.551	30.90	71.5	1, 11, 24	53
	3.534	30.75	71.5	2, 11, 24	51, 53
33	3.544	12.90	73.5	1, 11, 24	53
34	3.555	11.79	73.5	1, 11, 24	53

TABLE I (CONTINUED)

Run No.	Period T (Sec)	Amplitude $2z_0$ (in)	Water Temp °F	Conditions	Purpose
	3.554	12.41	73.5	1, 11, 24	53
	3.546	12.90	73.5	1, 11, 24	53
35	3.550	15.23	73.5	1, 11, 24	53
36	3.553	22.11	73	2, 11, 24	51, 53
37	3.552	7.42	68.5	1, 11, 24	53, 54
38	3.546	8.67	69	1, 11, 24	53, 54
39	3.548	10.10	69	1, 11, 24	53, 54, 55
40	3.540	10.44	69	1, 11, 24	53, 54
41	3.545	10.85	69	1, 11, 24	53, 54
42	3.55	11.18	69	1, 11, 24	55, 55
43	3.55	11.50	69	1, 11, 24	55, 55
44	3.55	11.59	69	1, 11, 24	55
45	3.550	11.62	67	1, 11, 24	53, 54, 55
46	3.550	11.11	67	1, 11, 24	53, 54, 55
47	3.55	10.90	63.5	2, 11, 21	51, 53, 56
48	3.55	4.70	64.1	2, 11, 21	51, 52
49	3.560	4.70	70	2, 11, 22	51, 52, 53
50	3.550	30.37	65	2, 11, 24	51, 53

KEY

- 1 - plane bed
- 2 - duned bed
- 11 - bed particles, 0.297mm-diameter glass beads
- 12 - bed particles, 0.585mm-diameter Ottawa sand
- 13 - smooth fixed bed, aluminum sheet
- 21 - $\frac{1}{2}$ -in diameter, half-round, disturbance element
- 22 - 1-in diameter, half-round, disturbance element
- 23 - $1\frac{1}{2}$ -in diameter, half-round, disturbance element
- 24 - no disturbance element
- 51 - geometric characteristics of dunes
- 52 - rate of propagation of dunes
- 53 - work input
- 54 - boundary-layer transition
- 55 - incipient motion
- 56 - motion pictures



QUARTERLY REPORT 3

PROJECT A-798

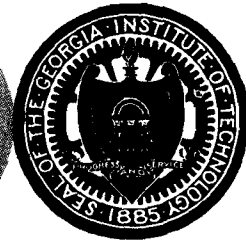
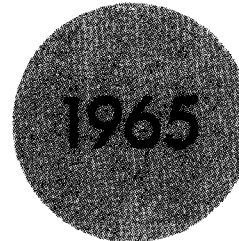
AN ANALYTICAL AND EXPERIMENTAL STUDY
OF BED RIPPLES UNDER WATER WAVES

F. M. Neilson and M. R. Carstens

Contract No. DA-49-055-CIVENG-65-1

1 January to 31 May 1965

Prepared for
Department of the Army
Coastal Engineering Research Center
Washington, D. C.



Engineering Experiment Station
GEORGIA INSTITUTE OF TECHNOLOGY
Atlanta, Georgia

REVIEW
PATENT 10-7 1965 BY DeW
FORMAT 10-7 1965 BY FR

GEORGIA INSTITUTE OF TECHNOLOGY
School of Civil Engineering
Atlanta, Georgia 30332

QUARTERLY REPORT 3

Project A-798

AN ANALYTICAL AND EXPERIMENTAL STUDY
OF BED RIPPLES UNDER WATER WAVES

By

F. M. Neilson and M. R. Carstens

Contract No. DA-49-055-CIVENG-65-1

1 JANUARY to 31 MAY 1965

Prepared for
DEPARTMENT OF THE ARMY
COASTAL ENGINEERING RESEARCH CENTER
WASHINGTON, D. C.

TABLE OF CONTENTS

	Page
INTRODUCTION	1
EXPERIMENTAL PROGRAM	2
Experimental Set-up	2
RESULTS FROM EXPERIMENTAL OBSERVATIONS	6
THEORETICAL ANALYSIS	7
Theoretical Model	7
Velocity Distribution Within the Model	8
Kinetic Energy	10
Work-Input	19
Discussion of the Theoretical Results	26
SUMMARY	28
NOMENCLATURE	29
REFERENCES	31

LIST OF FIGURES

		Page
Figure 1	Ratio of Amplitude to Wave Length of Dunes	4
Figure 2	Amplitude in Feet	5
Figure 3	Velocity Distribution; $M=500$	11
Figure 4	Velocity Distribution; $\omega t = \pi$	12
Figure 5	Convergence of the Steady-State Velocity Coefficients, $M=1000, \beta=0.8$	13
Figure 6	Coefficients for Steady-State Velocity; $M=500$	14
Figure 7	The Transient Velocity Term; $M=500, \beta=0.8$	15
Figure 8	Kinetic Energy of the Developing Vortex	17
Figure 9	Kinetic Energy Remaining at One-half Cycle ($\omega t = \pi$).	18
Figure 10	Analog Computer Results	23
Figure 11	Work-input to the End of Initial Half-cycle ($\omega t = \pi$)	24

FOREWORD

This study, titled AN ANALYTICAL AND EXPERIMENTAL STUDY OF BED RIPPLES UNDER WATER WAVES is being conducted for the U. S. Beach Erosion Board, Corps of Engineers, Washington, D. C. Experimental data is taken from tests conducted in the Hydraulics Laboratory, Georgia Institute of Technology.

This report is concerned primarily with theoretical considerations which are to be guidelines for planning upcoming laboratory tests and for analyzing the previous tests.

INTRODUCTION

This report includes a theoretical investigation (through May 31, 1965) of the energy dissipation for oscillatory flow over a two-dimensionally duned bed.

The analysis of energy dissipation is based on the assumption that the combination of the kinetic energy and the viscous energy dissipation of the vortices is the energy dissipation over the bed. These vortices develop twice each cycle in the dune troughs and are ejected from the troughs into the main stream where they decay.

The analysis is based upon the following model. A circular cylinder filled with fluid is started from rest and made to rotate with a simple-harmonic tangential velocity at its periphery. The energy dissipation is determined by evaluating the work input at the periphery of the cylinder during the first half cycle. In other words, the assumption is made that the energy dissipation consists of the sum of the energy dissipated within the vortex during the development of the vortex and of the kinetic energy remaining in the vortex after one-half of a cycle.

EXPERIMENTAL PROGRAM

In order to study ripples and dunes on the sea bed resulting from wave action, the decision was made to model only the mass of the water adjacent to the bed. The water motion at a fixed point close to the bed under a first order Stokian wave is simple harmonic and parallel to the bed. A large U-tube with forced oscillation of the water was designed in order to model the water motion under a wave.

Experimental Set-up

Description of U-tube - The description of this large U-tube was presented in QUARTERLY REPORTS 1 and 2 to which the reader is referred.

Instrumentation - The instrumentation is also described in QUARTERLY REPORTS 1 and 2.

Experimental Results

The experimental program remains as summarized in APPENDIX, QUARTERLY REPORT 2. The experimental results used for testing the theoretical model are obtained from data given in QUARTERLY REPORT 2.

All test data has been obtained using a bed of glass beads. The pertinent characteristics of this bed material are as follows:

Mean diameter, $d = 0.297$ mm,

Geometric standard deviation, $\sigma_{gd} = 1.06$, and

Specific gravity, $s = 2.47$.

Experimental observations, Figure 1, show that, for oscillations having a total water-motion amplitude of less than about 1.5 feet, the ratio of dune

amplitude to dune wave length is constant. For these amplitudes the dunes were also observed to be two-dimensional and uniform in shape over the bed. During each half-cycle a vortex forms behind the crest of each dune and is ejected from the trough into the main stream at the end of the half-cycle. With total water-motion amplitudes greater than 1.5 feet the dunes were observed to be irregular in shape, both along and across the bed. Also the ratio of dune amplitude to dune wave length was observed to decrease with increasing total water-motion amplitude.

The energy dissipation per cycle per unit area of duned bed calculated from experimental measurements is shown in Figure 2. This figure indicates that the energy dissipation for flow over the duned bed is a function of the square of the total water-motion amplitude.

The effects of the frequency of the oscillations of the main stream flow and of the characteristics of the bed material on both the geometry of the dunes and the energy dissipation have not yet been investigated. Further experiments involving different frequencies and bed materials will be required to generalize the results.

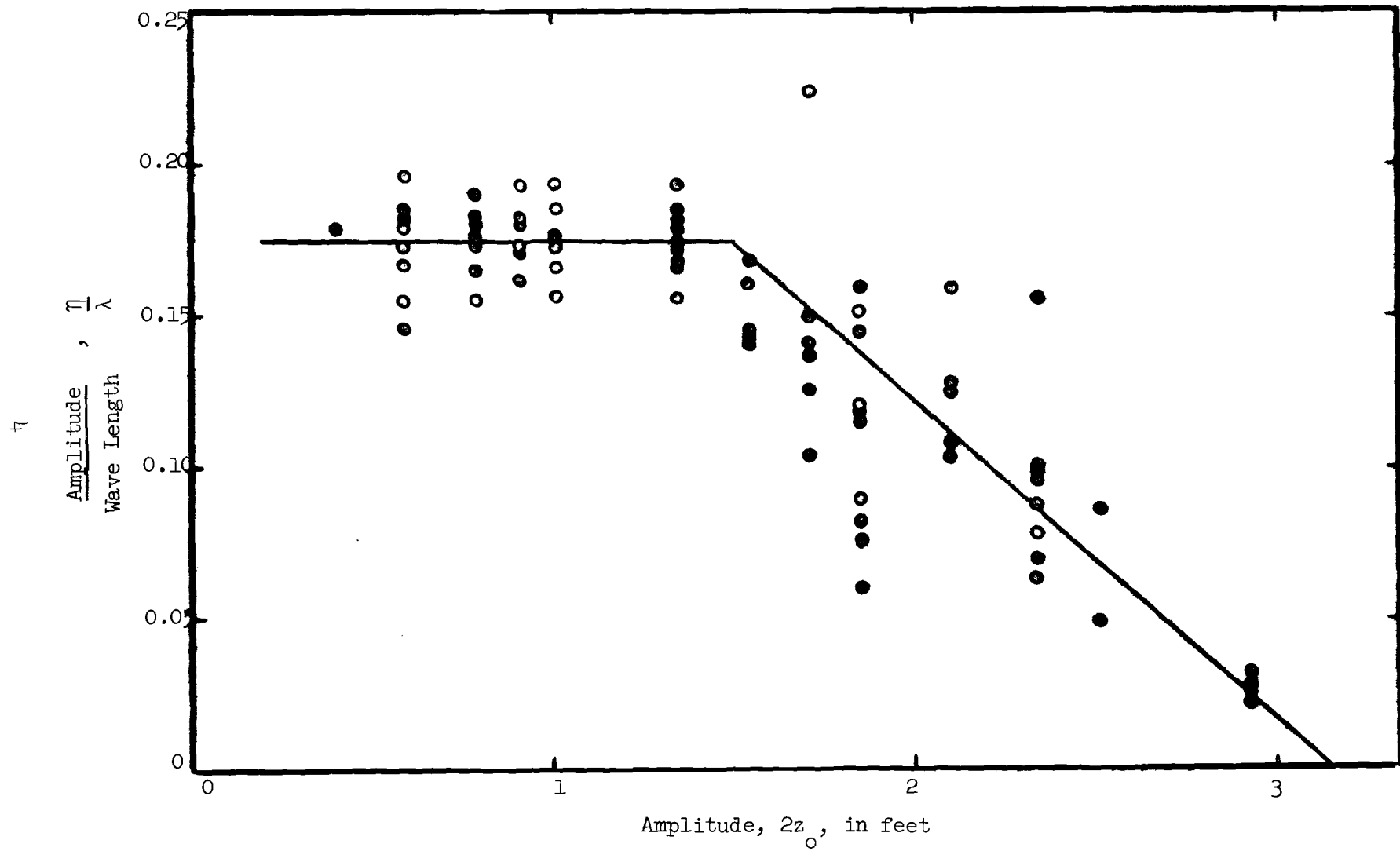


Figure 1. Ratio of Amplitude to Wave Length of Dunes

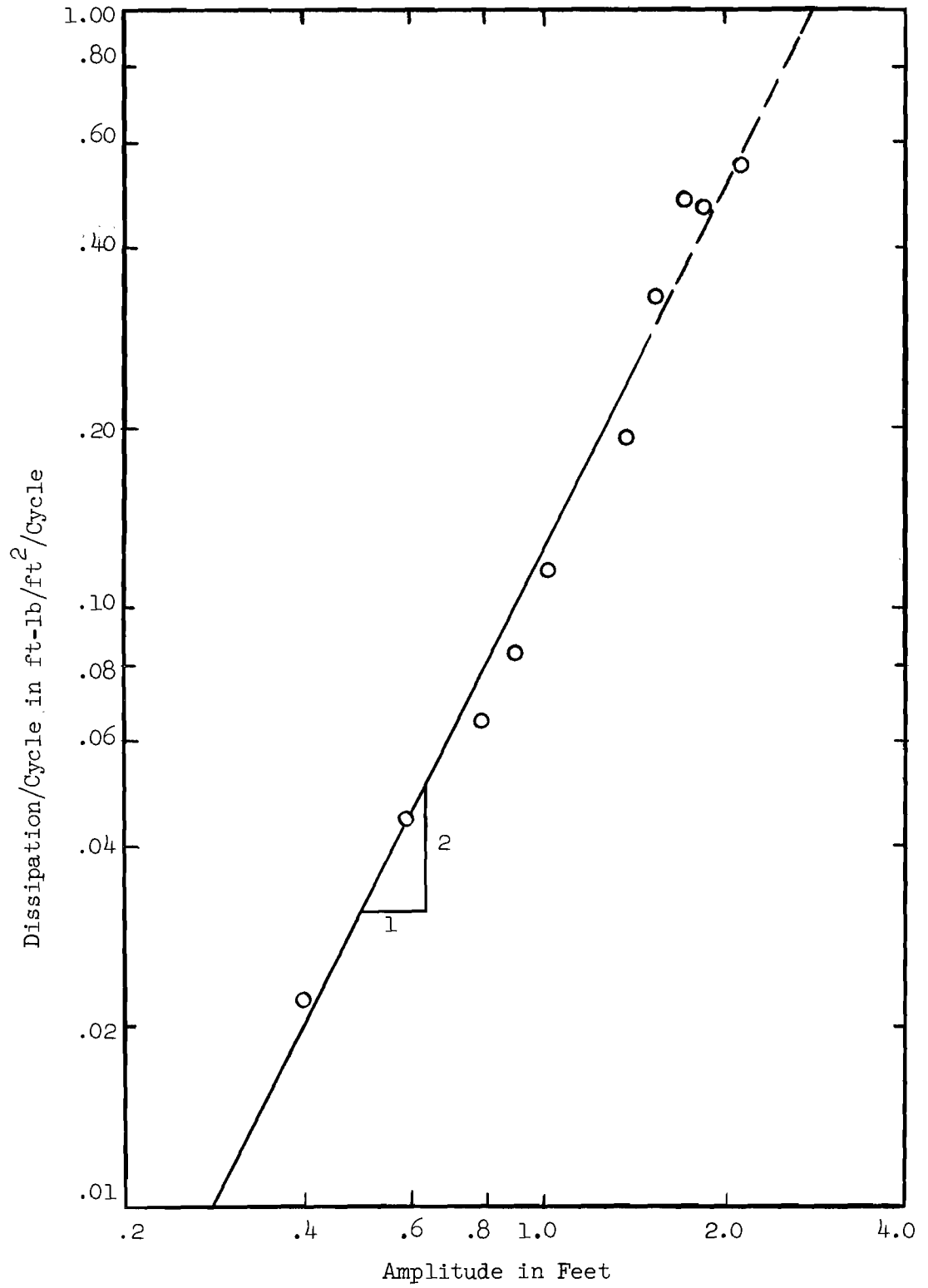


Figure 2. Energy Dissipation per Unit Area per Cycle (Dunes)

RESULTS FROM EXPERIMENTAL OBSERVATIONS

Following QUARTERLY REPORT 2 the energy dissipation for oscillatory flow over a duned, two-dimensional bed is expressed as

energy dissipation

$$\text{per unit area of bed} = K \sqrt{v} \rho (2 z_o)^2 \omega^{3/2} \quad (1)$$

per cycle

Using Figure 2 and equation (1) the following result is obtained.

$$K_d \sqrt{v} \rho \omega^{3/2} = 0.127 \quad (2)$$

Since the temperature (mean value) was 74°F and the period (mean value) was 3.55 sec. for the tests on the two-dimensional dunes the following values are applicable (a) v is $1.00 (10^{-5}) \text{ ft}^2/\text{sec}$, (b) ρ is 1.935 slugs/ft^3 , and (c) ω is 1.77 rad/sec . Using these numerical values and equation (2) the value for K_d for oscillatory flow over a dunes bed is

$$K_d = 8.82 \quad (3)$$

The energy dissipation for oscillatory flow over a plane bed can also be expressed by equation (1). In this case the value of K_p , derived and calculated in QUARTERLY REPORT 2, is

$$K_p = 0.555 \quad (4)$$

Equations (3) and (4) indicate that the energy dissipation per unit area of duned bed per cycle is about 16 times that with a plane bed with otherwise similar flow conditions.

THEORETICAL ANALYSIS

Theoretical Model - The theoretical analysis of energy dissipation is predicated on the assumption that the energy is lost in developing the vortices which form twice each cycle over the bed. The vortices are developed in the dune troughs and are ejected into the main stream where they decay.

The model chosen for the evaluation of the energy dissipation is that of the circular vortex which develops in the fluid in a cylinder as the cylinder is suddenly made to rotate with simple harmonic motion $u_m \sin(\omega t)$. The radius, a , of the cylinder would be proportional to the wave amplitude, η , of the dunes and the maximum tangential velocity, u_m , would be proportional to the maximum value of the main stream velocity. That is,

$$a \approx \eta \quad (5)$$

and

$$u_m \approx z_o \omega \quad (6)$$

in which z_o is the amplitude of the oscillations of the main stream over the bed and ω is the frequency of the simple-harmonic motion of the main stream.

This model will apply only to oscillatory flows over a duned, two-dimensional bed. Consequently the model will apply to the experimental results for runs having a total water-motion amplitude, $2z_o$, of less than about 1.5 feet. For this range of $2z_o$ the ratio of dune wave height to dune wave length is observed to be constant, Figure 1, and the energy

dissipation is observed to vary approximately as the square of the total water-motion amplitude, Figure 2.

Velocity Distribution Within the Model - The solution of the Navier-Stokes equations for the fluid velocity within a circular cylinder made to rotate with an arbitrary peripheral velocity is presented by McLeod₁. The solution of the particular case in which the cylinder is started from rest and made to rotate with the peripheral velocity $u_m \sin(\omega t)$ is

$$\frac{V}{u_m} = -2 \sum_{i=1}^{\infty} \frac{J_1(\alpha_i \beta)}{\alpha_i J_0(\alpha_i)} \left[\frac{\sin(\omega t) - \frac{\omega a^2}{\nu \alpha_i^2} \cos(\omega t) + \frac{\omega a^2}{\nu \alpha_i^2} e^{-\frac{\nu \alpha_i^2 \omega t}{\omega a^2}}}{\left[\frac{\omega a^2}{\nu \alpha_i^2} \right]^2 + 1} \right] \quad (7)$$

in which

- V is the fluid velocity;
- β is r/a in which r is the radial coordinate;
- α_i are the roots of the equation $J_1(\alpha_i) = 0$;
- J 's are the Bessel functions of the first kind;
- ν is the kinematic viscosity; and
- t is the time measured from the beginning of rotation of the circumscribing cylinder.

Equation (3) can be reduced to the simplified form

$$\varphi' = + f_1(\beta, M) \sin(\omega t) - f_2(\beta, M) \cos(\omega t) - 2 \sum_{i=1}^{\infty} \frac{J_1(\alpha_i \beta)}{\alpha_i \beta J_0(\alpha_i)} \left[\frac{M/\alpha_i^2}{\frac{M^2}{\alpha_i^4} + 1} \right] e^{-\frac{\alpha_i^2 \omega t}{M}} \quad (8)$$

in which

$$\varphi' = \frac{V}{\beta u_m};$$

$$M = \frac{\omega a^2}{\nu};$$

$f_1(\beta, M)$ is the coefficient of $\sin(\omega t)$ in equation (7); and

$f_2(\beta, M)$ is the coefficient of $\cos(\omega t)$ in equation (7).

The solution for φ' , equation (8), consists of a steady state solution, the first two terms, and a transient term which dies out as $t \rightarrow \infty$. The values of φ' for M equal 500* during the first one-half cycle are shown in Figure 3. As shown in Figure 3 the angular velocity of the fluid near the core of the vortex, $\beta < 0.8$, is insignificant during the initial half-cycle. The values of φ' for ωt equal to π and for a range of M values are shown in Figure 4. Since φ' is $V/\beta u_m$, the non-zero values of φ' when ωt is π demonstrates that kinetic energy remains in the vortex at the end of one-half cycle.

The values of $f_1(\beta, M)$, $f_2(\beta, M)$ and the transient term were calculated on the B220 digital computer. The infinite series were terminated either at the two-hundredth root, α_{200} , or when the absolute value of the exponent of e exceeded the computer limit, 112.8. The partial sums of the series for

* The minimum value of M attained experimentally was in run 49 in which the dune amplitude, η , was approximately 0.05 ft and the frequency was approximately 1.77 sec^{-1} . Hence

$$M_{\min} = \frac{\omega a^2}{\nu} \approx \frac{\omega a^2}{\nu} = \frac{(1.77)(0.0025)}{(1.05)(10^{-5})} = 421$$

The maximum value of M attained experimentally was in run 26 in which η was approximately 0.12 ft and the frequency was approximately 1.77 sec^{-1} . Hence, as for M_{\min}

$$M_{\max} = 2425$$

$f_1(\beta, M)$ and $f_2(\beta, M)$, terminated at i equal 180, 181, ..., 200 are shown in Figure 5 for M equal 1000 and β equal 0.8. The second coefficient, $f_2(\beta, M)$, has converged to -0.0155. The first coefficient, $f_1(\beta, M)$, is seen to oscillate and converge slowly. The value of $f_1(\beta, M)$, -0.0039, is the mean of the last maximum value and the last minimum value. The transient term converges rapidly because of the exponential term in the denominator.

For M equal 500, the computed values of $f_1(\beta, M)$, $f_2(\beta, M)$ and the transient term are shown in Figures 6 and 7. The two steady state coefficients are shown in Figure 6 for $0.5 \leq \beta \leq 1.0$. The values of the transient term, for M equal 500 and β equal 0.8, are shown in Figure 7 during the period of interest, that is, for ωt equal 0 to ωt equal π .

Kinetic Energy

The kinetic energy, KE, of a vortex per unit length of the vortex tube is

$$KE = \int_0^a \left(\frac{\rho V^2}{2} \right) 2\pi r dr \quad (9)$$

or in dimensionless form

$$\frac{KE}{a^2 \rho u_m^2} = \pi \int_0^1 \left(\frac{V}{u_m} \right)^2 \beta d\beta \quad (10)$$

Introducing equation (7) into equation (10) and integrating

$$\frac{KE}{\rho a^2 u_m^2} = 2\pi \sum_{i=1}^{\infty} \frac{1}{\alpha_i^2} \left[\frac{\sin(\omega t) - \frac{M}{2} \cos(\omega t) + \frac{M}{2} e^{-\frac{\alpha_i^2 \omega t}{M}}}{\left[\frac{M}{2} \right]^2 + 1} \right]^2 \quad (11)$$

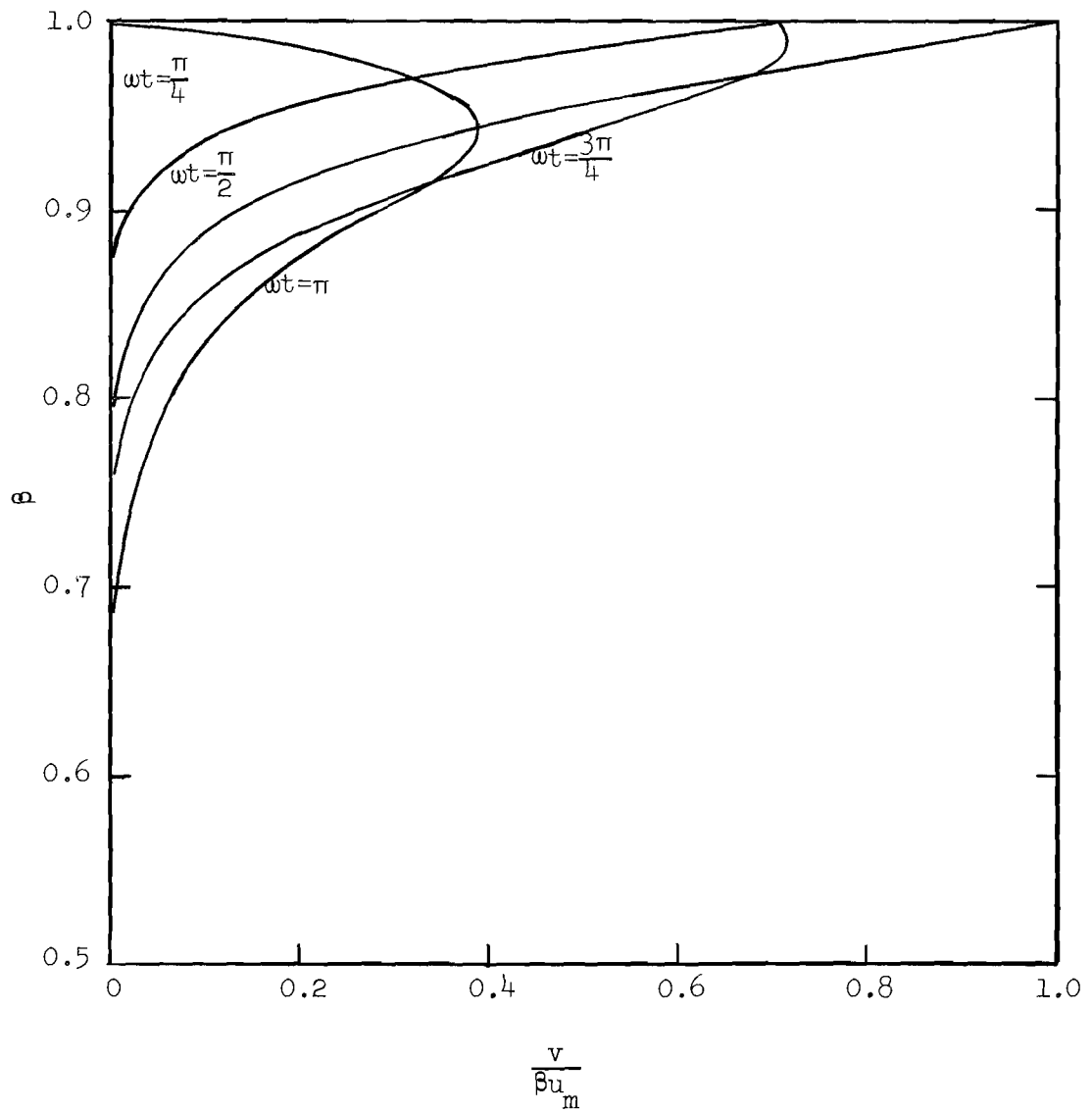


Figure 3. Velocity Distribution; $M = 500$

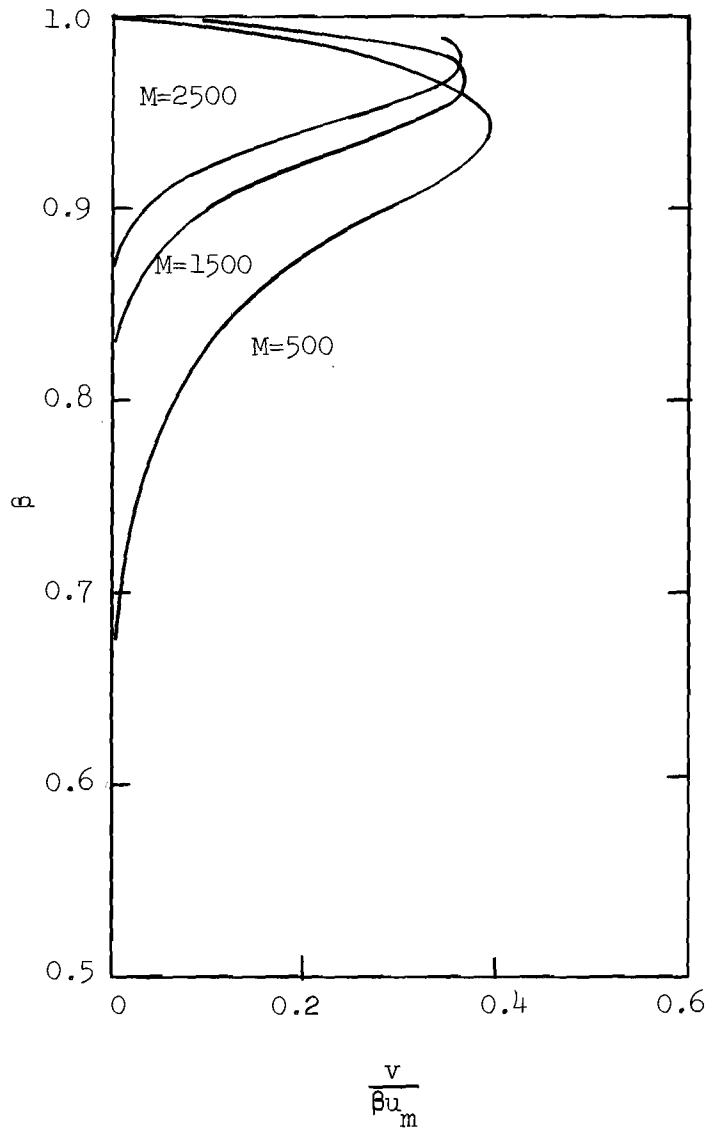


Figure 4. Velocity Distribution; $\omega t = \pi$

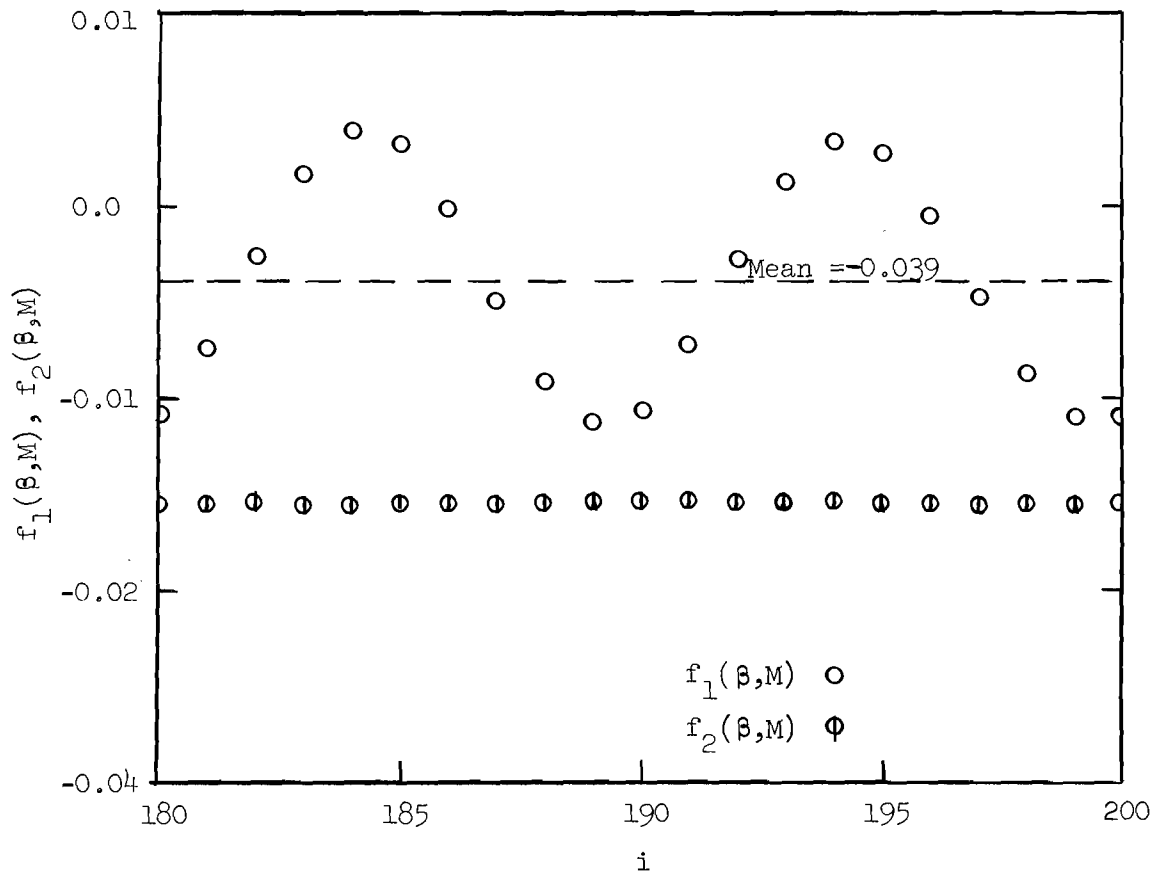


Figure 5. Convergence of the Steady-State Velocity Coefficients, $M = 1000$, $\beta = 0.8$

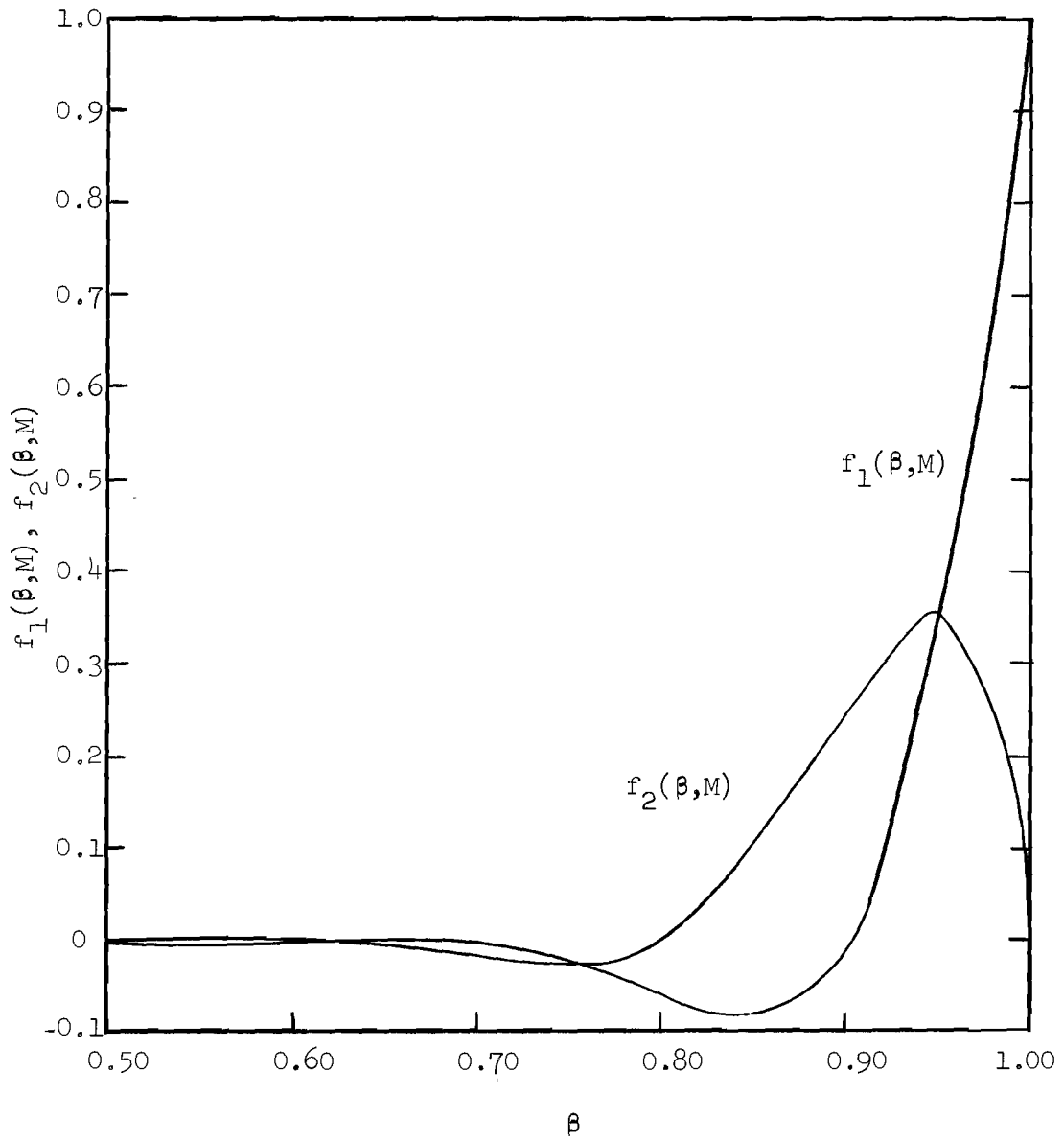


Figure 6. Coefficients for Steady-State Velocity; $M = 500$

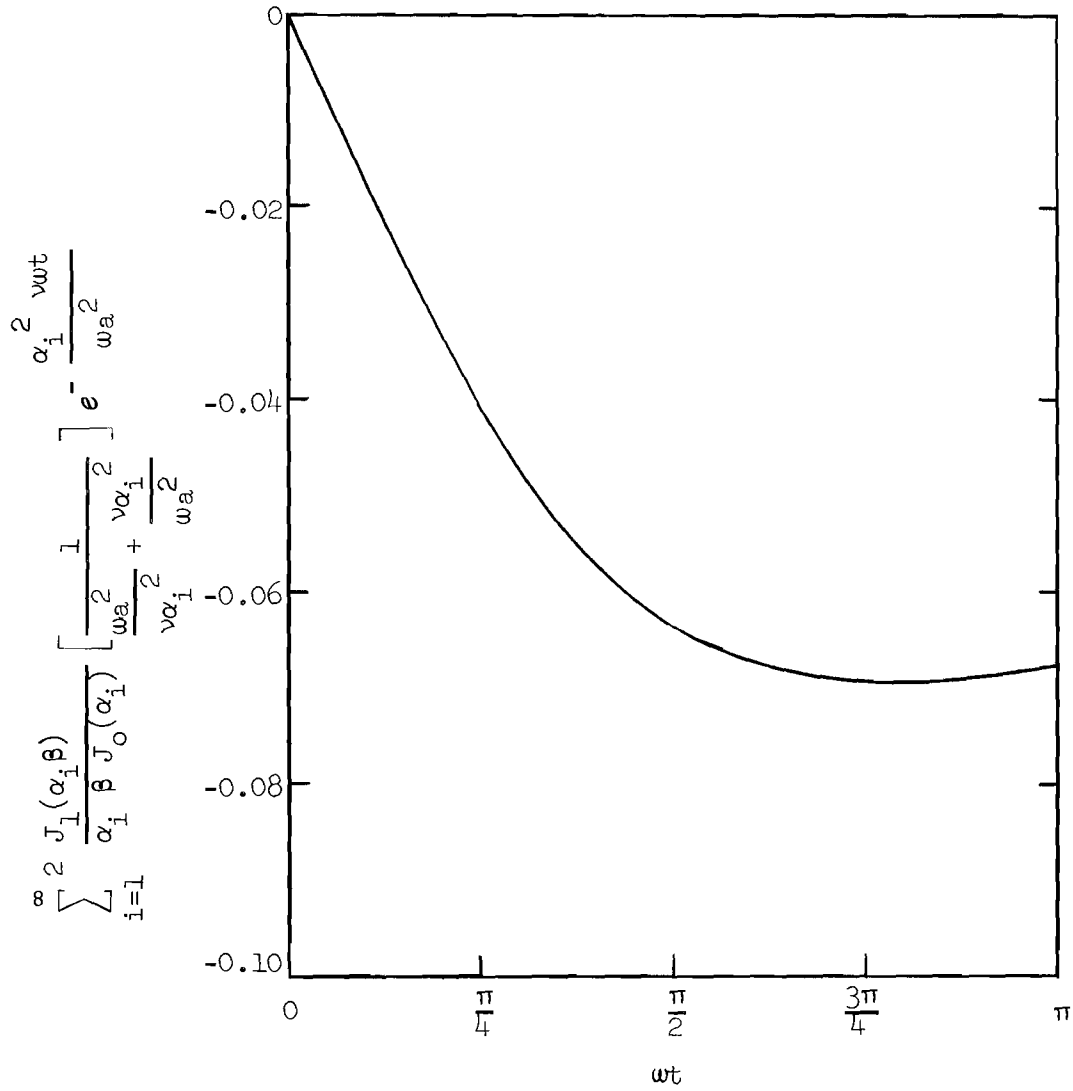


Figure 7. The Transient Velocity Term; $M = 500$, $\beta = 0.8$

Equation (11) has been evaluated on the B220 digital computer. The infinite series was terminated either on the fiftieth root, α_{50} , or when the exponent of e exceeded 112.8. The results are shown in Figure 8 for different M values during the period of interest, that is, $0 < \omega t < \pi$.

Since the vortex in the physical situation is ejected into the main stream at the end of the half-cycle, the kinetic energy still in the vortex at that time is of interest. The kinetic energy remaining in the vortex after one-half cycle is shown in Figure 9. The assumption is made that this kinetic energy is not recovered and, consequently, it is part of the energy dissipated by the flow over the duned bed.

Designating the RHS of equation (11) as $f(M)$, in which M is $\frac{\omega a^2}{\nu}$, the kinetic energy per unit length of vortex remaining at the end of the half cycle is

$$KE = f(M) a^2 \rho u_m^2 \quad (12)$$

Since two vortices are formed every cycle

$$\frac{KE}{\text{one cycle}} = 2 f(M) a^2 \rho u_m^2 \quad (13)$$

Introducing equations (5) and (6) into equation (13) results in

$$\frac{KE}{\text{one cycle}} = 2 f(M) \pi^2 \rho z_o^2 \omega^2 \quad (14)$$

Thus the kinetic energy ejected into the main stream per unit area of duned bed is

$$\frac{KE}{\lambda \text{ one cycle}} = 2 f(M) \left(\frac{\pi}{\lambda} \right) \pi \rho z_o^2 \omega^2 \quad (15)$$

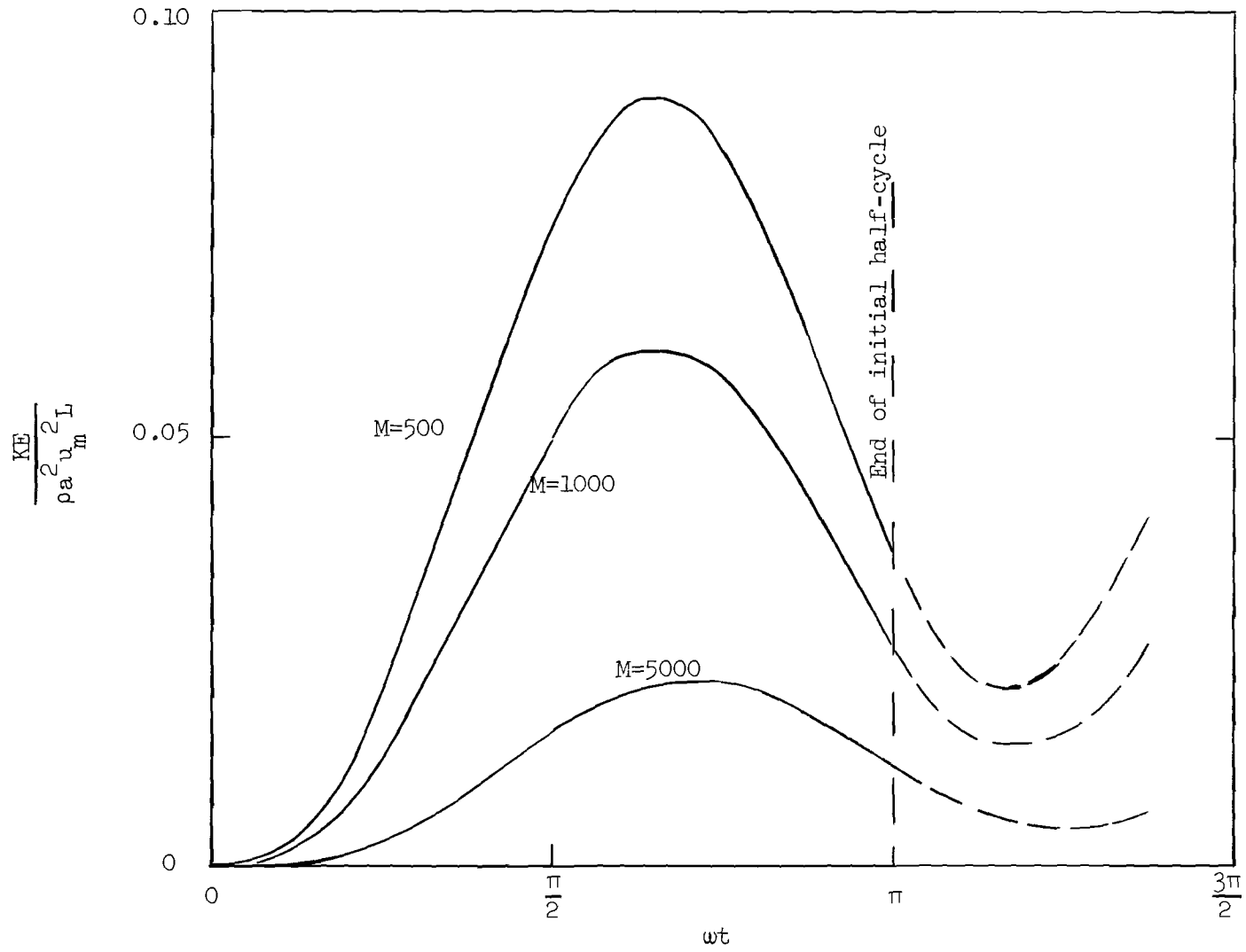


Figure 8. Energy of the Developing Vortex

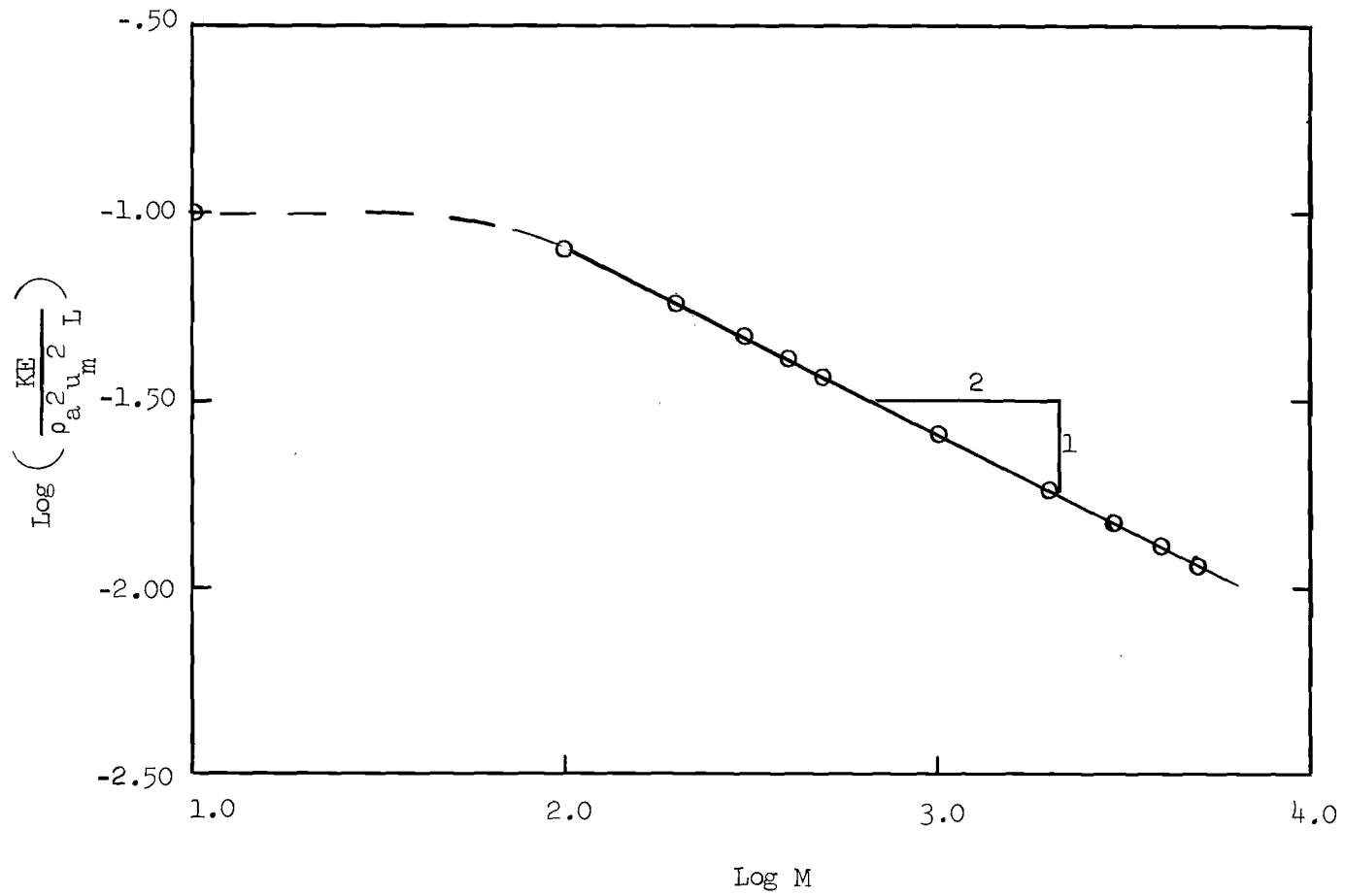


Figure 9. Kinetic Energy Remaining at One-half Cycle ($\omega t = \pi$)

The numerical solution for $f(M)$ shown in figure 9 indicates that, if M is greater than 75, then

$$f(M) = 0.82 M^{-1/2} \quad (16)$$

The physical significance of equation (16) is that the kinetic energy lost in the main stream at the end of the initial half-cycle is inversely proportional to the square root of the frequency of the oscillations in the tank and also inversely proportional to the linear dimension of the vortex. Since the minimum value of M obtained experimentally (see page 8) is 421, equation (16) would apply to the experimental results.

The kinetic energy remaining in the vortex at the end of the initial half-cycle can now be expressed with the same relationship of variables as the expression (see QUARTERLY REPORT 2) for the energy dissipation resulting from oscillatory flow over a plane bed. Introducing equations (5), (6), and (16) into equation (15) yields

$$KE = 0.41 \sqrt{\nu} \frac{\eta}{\lambda} \rho (2z_o)^2 \omega^{3/2} \quad (17)$$

Since the ratio $\frac{\eta}{\lambda}$ was found to be a constant, 0.174, for a two-dimensional dune system equation (17) can be reduced to

$$\begin{array}{l} \text{energy dissipation due} \\ \text{to loss of kinetic energy} \\ \text{per unit area of duned bed} \\ \text{per cycle} \end{array} = 0.0714 \sqrt{\nu} \rho (2z_o)^2 \omega^{3/2} \quad (18)$$

Work-Input

The work-input in developing the vortex has been evaluated by considering the shearing force on the face of the cylinder. Following Schlichting² the tangential shearing stress, $\tau_{r\theta}$, is

$$\tau_{r\theta} = \mu r \frac{\partial}{\partial r} \left(\frac{V}{r} \right) \quad (19)$$

in which μ is the dynamic viscosity. The force, F , on the periphery of a cylinder of length L is

$$F = 2\pi a \tau_{a\theta} L = 2\pi\mu a^2 \frac{\partial}{\partial r} \left(\frac{V}{r} \right) L \quad (20)$$

evaluated at $r = a$. The power, P , at any instant is

$$P = FV = Fu_m \sin(\omega t). \quad (21)$$

Introducing equation (20) into equation (21)

$$P = 2\pi\mu a^2 u_m L \frac{\partial}{\partial r} \left(\frac{V}{r} \right) \Big|_{r=a} \sin(\omega t). \quad (22)$$

The work-input, WI , per unit length of cylinder, is

$$WI = \int_0^t P dt = \frac{1}{\omega} \int_0^{\omega t} P d(\omega t) \quad (23)$$

Introducing equation (8) into equation (22)

$$\frac{WI}{\rho u_m^2 a^2 L} = \frac{2\pi}{M} \int_0^{\pi} \sin(\omega t) \frac{\partial \varphi'}{\partial \beta} d(\omega t) \quad (24)$$

In equation (13) WI is the work-input per half-cycle of rotation and $\frac{\partial \varphi'}{\partial \beta}$ is evaluated at the surface of the cylinder.

Since differentiation of the series solution for φ' , equation (4), results in a divergent series for $\frac{\partial \varphi'}{\partial \beta}$ at the boundary, the solution for the

integral in the RHS of equation (24) was obtained using the analog computer and the following relationships. Following McLeod¹ the Navier-Stokes equation, for a rotating cylinder containing fluid, can be written in the form

$$\frac{\partial^2 \varphi'}{\partial \beta^2} + \frac{3}{\beta} \frac{\partial \varphi'}{\partial \beta} = M \frac{\partial \varphi'}{\partial (\omega t)} \quad (25)$$

For a cylinder starting from rest and oscillating with the peripheral velocity $u_m \sin(\omega t)$ the initial condition is

$$\varphi'(\beta, 0) = 0 \quad (26)$$

and the boundary condition is

$$\varphi'(1, \omega t) = \sin(\omega t) \quad (27)$$

An additional boundary condition, $\varphi'(0.8, \omega t)$, was obtained using the digital computer for the solution of equation (8). Nine equally spaced points ranging from ωt equal 0 to ωt equal π were calculated on the B220 digital computer for β equal 0.8. These values were used as input into the function generator of the analog computer in order to obtain the continuous (with respect to time) boundary condition, $\varphi'(0.8, \omega t)$.

The solution, by means of the analog computer, involved two circuits. In the first circuit the difference equation corresponding to equation (25) was solved on the analog computer. Ten equal, finite increments of β , from β equal 0.8 to β equal 1.0, were used. The boundary conditions were kept continuous with respect to time. In the second circuit the value of $\frac{\partial \varphi'}{\partial \beta}$, evaluated

at the periphery of the cylinder, was used to evaluate the integral in the RHS of equation (24). In this way the complete solution was obtained from the analog computer for each M value. By simply changing the pot settings the integral was evaluated for different M values in the range $50 \leq M \leq 2500$. The values of the integral, for several M values, as evaluated by the analog computer are shown in Figure 10, during the development of the vortex.

The work-input is obtained from the analog-computer results and equation (24). The maximum work-input is observed to occur before the end of the initial half-cycle. The decrease in work-input immediately prior to the end of the half-cycle is due to the recovery of a portion of the kinetic energy.

The values of work-input evaluated at an ωt of π are shown in Figure 12. These values of the work-input are, in effect, the sum of the viscous energy dissipation during the development of the vortex and the kinetic energy remaining in the vortex at the end of the initial half-cycle. The computed values indicate that, for M values larger than about 200, the expression for work-input can be simplified to

$$\frac{WI}{\rho a^2 u_m^2 L} = 5 M^{-1/2} \quad (28)$$

or

$$WI = f(M) a^2 \rho u_m^2 \quad (29)$$

in which $f(M)$ is the RHS of equation (28). Since two vortices are formed every cycle

$$\frac{WI}{\text{one cycle}} = 2 f(M) a^2 \rho u_m^2 \quad (30)$$

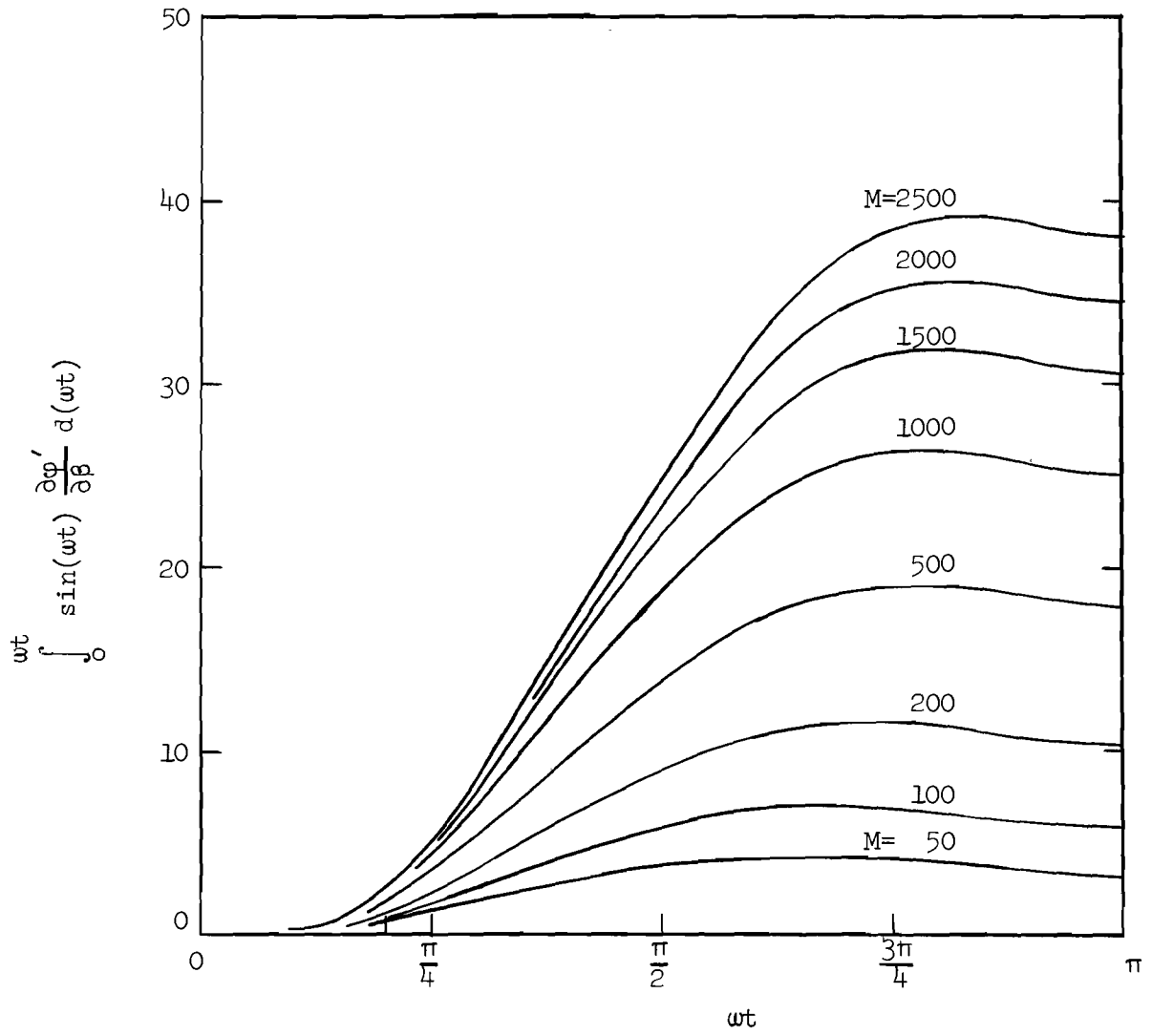


Figure 10. Analog Computer Results

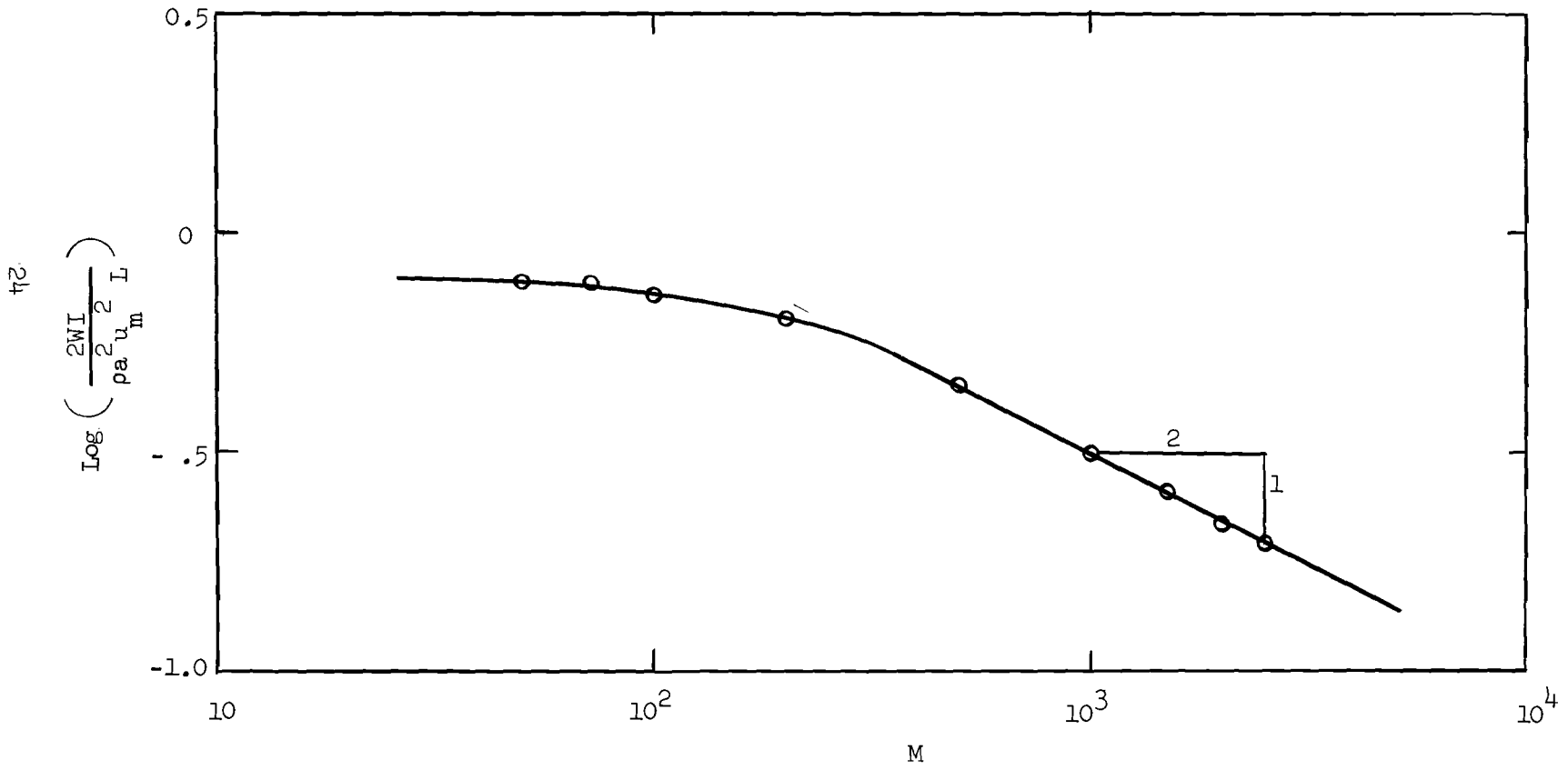


Figure 11. Work-input to the End of Initial Half-cycle ($\omega t = \pi$)

Introducing equations (5) and (6) into equation (30)

$$\frac{WI}{\text{one cycle}} = 2 f(M) \eta^2 \rho z_o^2 \omega^2 \quad (31)$$

Thus the work-input involved in developing the vortices which form across the duned bed per unit area of bed is

$$\frac{WI}{\lambda \text{ one cycle}} = 2 f(M) \left(\frac{\eta}{\lambda} \right) \eta \rho z_o^2 \omega^2 \quad (32)$$

Introducing equation (28) into equation (29) yields

$$WI = \sqrt{\nu} \left(\frac{\eta}{\lambda} \right) \rho (2z_o)^2 \omega^{3/2} \quad (33)$$

for values of M above about 200. Finally, since the ratio $\frac{\eta}{\lambda}$ is constant for the two-dimensional dune system,

$$WI = K_d \sqrt{\nu} \rho (2z_o)^2 \omega^{3/2} \quad (34)$$

Using equation (28) and $\frac{\eta}{\lambda}$ equal 0.174 one finds

$$K_d \approx 0.174(5) = 0.87 \quad (35)$$

Assuming that the energy dissipation of the flow over the two-dimensionally duned bed is equal to the work-input expended in creating the vortices allows equation (34) to be amended to

$$\begin{array}{l} \text{energy dissipation per} \\ \text{unit area of duned bed} = 0.87 \sqrt{\nu} \rho (2z_o)^2 \omega^{3/2} \\ \text{per cycle} \end{array} \quad (36)$$

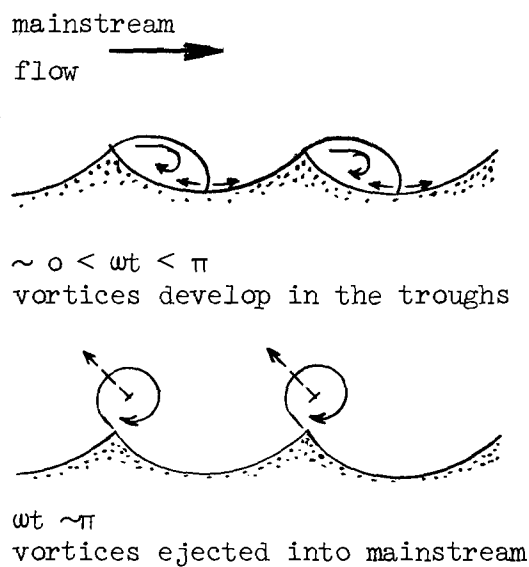
Inspection of equations (1) and (36) shows the same relationship of the variables. The theoretical value of K_d , 0.87, is, however, significantly lower than the corresponding experimentally determined value, 8.82.

Discussion of the Theoretical Results

The theoretical model obviously cannot fully explain the energy dissipation of the flow over the duned bed since the cylindrical vortex does not completely describe the physical situation and since other sources of energy dissipation are present. Energy is dissipated both above the cylinder, viscous dissipation, and below the cylinder, boundary-layer type dissipation, and also along the upstream face of each dune. The effect of the suspended sediment has also not been considered. Another factor not considered is the nature of the diffusion mechanism within the vortex itself. Observations of the actual physical situation indicate a much more rapid increase in vorticity within the vortex than the calculated vorticity profiles indicate. Consequently a more rapid transfer mechanism, turbulent diffusion, is indicated. In other words the parameter, M , would be more correctly evaluated if the turbulent or "eddy" viscosity was used as the coefficient of viscosity. It is interesting to note that a hundred-fold increase in the coefficient of viscosity results in a ten-fold increase in the value of K_d . The dissipation calculated using the new value of K_d would closely agree with the energy dissipation determined experimentally.

The development of the vortices, for a two-dimensionally duned bed, occurs in the manner schematically shown below. The vortex grows in the lee of the dune during the time the mainstream flow is accelerating over the bed. The vortex is shown at ωt equal about $\frac{\pi}{2}$. During the latter half of the initial half-cycle the rapid transfer of vorticity towards the center of the vortex becomes evident. In the second sketch, at about ωt equal π , the vortex has moved back along the crest from which it formed and is being ejected

into the mainstream flow. The nature of the streamlines appear to indicate a geometric solution for the dunes could be found. The sketches also



illustrate the appropriateness of the cylindrical vortex to describe, in part, the complex phenomena associated with oscillating flow over the duned bed.

SUMMARY

The theoretical analysis presented in QUARTERLY REPORT 3 is considered to be complete in regard to two-dimensional dunes. The experimental studies with 0.297 mm-diameter glass beads is also complete with regard to dune formation. Further experimental studies using 0.585 mm-diameter Ottawa sand are to be made. Experimental studies having the frequency of oscillation as an independent variable are under consideration. The analysis has shown that the results would be more generalized if both the frequency and the amplitude of oscillation were varied. The transitory bed forms, ripples, are to be studied in more detail. Due to the time-varying characteristics of the ripples and their transitory nature, the study on ripples will probably include stereo-photography.

NOMENCLATURE

<u>Symbol</u>	<u>Definition</u>	<u>Dimensions</u> <u>F, L, T</u>
a	radius of a rotating cylinder of fluid	L
C_f	boundary-drag coefficient	none
d	mean diameter of bed particles	L
F	force	F
f(x), f(M)	functional expression	none
$f_1(\beta, M), f_2(\beta, M)$	steady state fluid velocity coefficients	
J_n	Bessel function of the first kind of order n	none
K	energy dissipation coefficient	none
K_d	energy dissipation coefficient for a duned bed	none
K_p	energy dissipation coefficient for a plane bed	none
KE	kinetic energy	FL
$M = \frac{\omega a^2}{\nu}$	vortex parameter	none
P	power	FLT^{-1}
Q_f	energy dissipation due to fluid viscosity	none
r	radial coordinate	L
s	specific gravity	none
t	time	T
T	period of oscillation	T
u	fluid velocity parallel to the bed	LT^{-1}
u_m	maximum fluid velocity	LT^{-1}
v	fluid velocity	LT^{-1}

NOMENCLATURE (continued)

<u>Symbol</u>	<u>Definition</u>	<u>Dimensions</u> <u>F, L, T</u>
WI	work input	FL
x	horizontal coordinate	L
y	vertical coordinate	L
z_o	main stream water-motion amplitude	L
α_i	roots of the equation $J_1(\alpha_i) = 0$	none
$\beta = \frac{r}{a}$	distance parameter	none
η	dune amplitude	L
θ	angular coordinate	none
λ	dune wave length	L
μ	dynamic viscosity of fluid	FTL^{-2}
ν	kinematic viscosity of fluid	L^2T^{-1}
ρ	mass density	FT^2L^{-4}
σ_{gd}	geometric standard deviation	none
$\tau_{r\theta}$	tangential shearing stress for rotational flow	FL^{-2}
τ_o	shear stress on the boundary	FL^{-2}
$\varphi' = \frac{V}{\beta u_m}$	fluid velocity parameter	none
$\chi = \frac{\nu t}{a^2}$	time parameter for a forced vortex	none
ω	frequency of simple-harmonic oscillation	T^{-1}

REFERENCES

- (1) A. R. Mcleod, "The Unsteady Motion produced in a Uniformly Rotating Cylinder of Water by a Sudden Change in the Angular Velocity of the Boundary," Philosophical Magazine and Journal of Science, S.6, Vol. 44, No. 259, July 1922, pp. 1-14.
- (2) H. Schlichting, Boundary Layer Theory, J. Kestin translation, published by Pergamon Press, New York, 1955.
- (3) A. Gray, G. B. Mathews, and T. M. MacRobert, Bessel Functions, Macmillan and Company, London, 2nd Edition, 1952, example 38, pp 249.
- (4) Eugene Jahnke and Fritz Emde, Tables of Functions, Dover Publications, New York, 4th Edition, 1945, pp. 166.
- (5) E. A. Christova, Tables of Bessel Functions of the True Argument and of Integrals Derived from Them, published by Pergamon Press, 1959.
- (6) R. A. Bagnold, "Motion of Waves in Shallow Water-Interaction Between Waves and Sand Bottoms," Proceedings, Royal Society, A, Vol. 187, Oct. 8, 1946, pp. 1-18.
- (7) M. R. Carstens and F. M. Neilson, "An Analytical and Experimental Study of Bed Ripples Under Water Waves," Quarterly Report 2, Project A-798, EES, Georgia Institute of Technology, Jan. 1964.

Security Classification

DOCUMENT CONTROL DATA - R&D

(Security classification of title, body of abstract and indexing annotation must be entered when the overall report is classified)

1. ORIGINATING ACTIVITY (Corporate author) Dept. of the Army Coastal Engineering Research Center Washington, D.C.		2a. REPORT SECURITY CLASSIFICATION Unclassified	
		2b. GROUP	
3. REPORT TITLE An Analytical and Experimental Study of Bed Ripples Under Water Waves			
4. DESCRIPTIVE NOTES (Type of report and inclusive dates) Quarterly Report 3, Jan 65-May 65			
5. AUTHOR(S) (Last name, first name, initial) Neilson, F.M. and Carstens, M.R.			
6. REPORT DATE May 65		7a. TOTAL NO. OF PAGES 31	7b. NO. OF REFS 7
8a. CONTRACT OR GRANT NO. DA-49-055-CIVENG-65-1,		8a. ORIGINATOR'S REPORT NUMBER(S) Project A798 Quarterly Report 3	
b. PROJECT NO. A798		8b. OTHER REPORT NO(S) (Any other numbers that may be assigned this report)	
c.			
d.			
10. AVAILABILITY/LIMITATION NOTICES Additional copies available on written request			
11. SUPPLEMENTARY NOTES Theoretical investigation of energy dissipation		12. SPONSORING MILITARY ACTIVITY Dept. of the Army, Coastal Engineering Research Center, Washington, D.C.	
13. ABSTRACT The theoretical investigation of energy dissipation for oscillatory flow over a two-dimensionally duned bed has been extended. The analysis of energy dissipation is based on the assumption that the combination of the kinetic energy and the viscous energy dissipation of the vorticies which develop across the bed is the energy dissipation over the bed. The analysis considers the work-input required to rotate a circular cylinder, filled with fluid, with simple harmonic motion at the periphery. The cylinder is started from rest and the work-input for the initial half-cylce is analysed. The theoretical results are compared with experimental data.			

NOTICE

This document is not to be used by anyone.

Prior to 11-20 1969
without permission of the Research Sponsor
and the Experiment Station Security Office.

QUARTERLY REPORT 4

PROJECT A-798

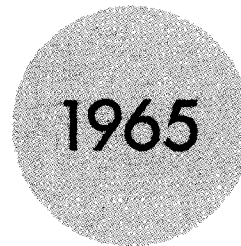
AN ANALYTICAL AND EXPERIMENTAL STUDY
OF BED RIPPLES UNDER WATER WAVES

F. M. NEILSON AND M. R. CARSTENS

Contract No. DA-49-055-CIVENG-65-1

1 June 1965 to 31 July 1965

Prepared for
Department of the Army
Coastal Engineering Research Center
Washington, D. C.



Engineering Experiment Station
GEORGIA INSTITUTE OF TECHNOLOGY
Atlanta, Georgia

REVIEW

PATENT 10-7 1965 BY Law
FORMAT 10-7 1965 BY FSL

GEORGIA INSTITUTE OF TECHNOLOGY
School of Civil Engineering
Atlanta, Georgia

QUARTERLY REPORT 4

PROJECT A-798

AN ANALYTICAL AND EXPERIMENTAL STUDY
OF BED RIPPLES UNDER WATER WAVES

By

F. M. NEILSON AND M. R. CARSTENS

CONTRACT NO. DA-49-055-CIVENG-65-1

1 June 1965 to 31 July 1965

Prepared for
DEPARTMENT OF THE ARMY
COASTAL ENGINEERING RESEARCH CENTER
WASHINGTON, D. C.

TABLE OF CONTENTS

	Page
I. FOREWORD	i
II. INTRODUCTION	1
III.. EXPERIMENTAL PROGRAM	2
A. Experimental Set-up	2
1. Description and Instrumentation	2
2. Bed of the Test Section	2
3. Disturbance Element	3
B. Experimental Procedure	3
1. General	3
2. Runs 51-60	3
3. Run 61	4
IV. RESULTS AND ANALYSIS OF RESULTS	6
A. General	6
B. Development of a Duned Bed	8
C. Ripples	12
1. Geometry of the Ripple System	12
2. Propagation of Ripples	12
D. Dunes	14
1. Geometry of Dunes	14
2. Published Data	16
E. Energy Dissipation	23
1. General	23
2. Published Data	28

TABLE OF CONTENTS (Continued)

	Page
V. RESEARCH PROGRAM	30
VI. NOMENCLATURE	31
VII. REFERENCES	32
VIII. APPENDIX	33

LIST OF TABLES

Table		Page
1	Water-motion Characteristics, Runs 51-60	4
2	Completed Experimental Program	34

LIST OF FIGURES

Figure		Page
1	Period of the Water-motion Oscillations	7
2	Development of the Ripple System, Run 61	10
3	Development of the Bed, Run 51	11
4	Profile of a Ripple System, Run 61	13
5	Rate of Propagation of Ripples	15
6	Dune Wave-length, λ	17
7	Dune Height, η	17
8	Dune Steepness, η/λ	18
9	The Change in λ for Different Periods, Runs 51-55	19
10	The Change in η for Different Periods, Runs 51-55	20
11	The Change in η/λ for Different Periods, Runs 51-55	20
12	Dune Index, λ/η	22
13	Work-input to West-tank, Runs 51-60	24
14	Energy Dissipation, Runs 51-55	25
15	Energy Dissipation as a Function of the Period, Runs 51-55	27

FOREWORD

This study, titled AN ANALYTICAL AND EXPERIMENTAL STUDY OF BED RIPPLES UNDER WATER WAVES, is being conducted for the U. S. Coastal Engineering Research Center, Washington, D. C. Experimental data is taken from tests conducted in the Hydraulics Laboratory, Georgia Institute of Technology.

This report is concerned primarily with experimental data taken to determine the effects of changes in frequency of the water motion on the energy dissipation and on the bed forms. Since the frequency can only be changed a limited amount the results are compared to the results obtained by other investigators.

INTRODUCTION

This report includes the results of the experimental study (through July 15, 1964) of the ripples and dunes which are formed on the sea bed by the action of first-order Stokian waves. Of primary concern is the series of tests, Runs 51-60 inclusive, made to determine the effect on the bed forms and on the energy dissipation caused by a change in frequency of the water motion.

The experiments are being performed in a water tunnel in which water is oscillated in a simple-harmonic manner over an erodible bed. Data are being taken from which the rate of formation of ripples, the geometric characteristics of dunes, and the rate of energy dissipation resulting from a system of dunes can be determined. The independent flow variables are amplitude of the water motion, frequency of oscillation, mean water level in the tank, size of the disturbance element from which the ripples originate, and the characteristics of the bed material. The status of the experimental program is summarized in TABLE 2 in the APPENDIX.

EXPERIMENTAL PROGRAM

In order to study ripples and dunes on the sea bed resulting from wave action, the decision was made to model only the mass of water adjacent to the bed. The water motion at a fixed point adjacent to the bed under a first-order Stokian wave is simple harmonic and is parallel to the bed. A large U-tube with forced oscillation of the water was designed in order to model the water motion under a wave.

The period of oscillation of the water within the U-tube is not controlled by any external mechanism, instead, it is the natural period of the system. Thus a variation in period can be accomplished only by either introducing additional resistances into the system or by varying the mass of water within the tank. For Runs 51-60 inclusive the decision was made to vary the mass of water and, consequently, the period by either raising or lowering the mean water level in the East and West legs of the U-tube. The results of these tests should show whether or not a significant variation in the dune geometry, the rate of ripple propagation or the amount of energy dissipation results from small changes in the period of oscillation.

Experimental Set-up

Description and Instrumentation - The description of the large U-tube water-tunnel and the instrumentation were presented in QUARTERLY REPORTS 1 and 2 to which the reader is referred.

Bed of the Test Section - In order to determine the drag force exerted by the duned bed two series of runs are being made-one with a plane bed and one with a duned bed.

Earlier plane bed tests (TABLE 1, APPENDIX) were performed either with a 20-gage aluminum sheet placed over the bed of the test section or

with a bed of glass beads. The last series of plane bed tests, Runs 56-60 inclusive, were performed with a bed of glass beads.

The duned bed tests have all been made with a bed of glass beads. The pertinent characteristics of this bed material are as follows:

Mean diameter, $d = 0.297$ mm,
geometric standard deviation, $\sigma_{gd} = 1.06$, and
specific gravity, $s = 2.47$

Disturbance Element - In order to initiate the formation of ripples and then dunes on the bed at total water-motion amplitudes of less than about 18 inches, a half-round brass bar was inserted in the test section. This brass bar, or disturbance element, forms the initial dune crest. The size of the disturbance element used for all tests is given in TABLE 2 in the APPENDIX. Runs 51-56 inclusive and Run 61 were performed using a half-round brass bar having a diameter of 1/2 inch and a length of 4 feet.

Experimental Procedure

General - The experimental procedure during a typical run was presented in QUARTERLY REPORTS 1 and 2 to which the reader is referred.

Runs 51-60 - The principal change in the procedure, Runs 51-60, was to change the mean water level in the legs of the U-tube before starting each run. The change in the mean water-level resulted in a change in the mass of the oscillating column of water which, in turn, resulted in a change in the period of the oscillations. The total water-motion amplitude, $2z_o$, for these runs were kept close to a mean value, 6.50 inches, by adjusting the blower valves on the air-input system leading to the West tank.

The drag exerted by the bed of the test section on the oscillating mass of water increases as the bed becomes duned. Since the work-input per cycle is essentially constant during a run the increase in the resistance to motion

results in a decrease in the water-motion amplitude as the bed forms develop. Consequently, the final, steady-state amplitude, which occurs when the bed of the test section is completely covered by the system of equilibrium dunes, differed somewhat from the desired value, $2z_0$ equal 6.5 inches, for each of the five duned bed tests.

The final or equilibrium operating characteristics of the water column oscillations are given in TABLE 1 for Runs 51-60 inclusive. The tabulated values in the second column are of the mean water level in the East tank. An increase in gage reading indicates a decrease in water level. A zero gage reading indicates the mean water level in the East tank is the same as it was for the earlier runs, (i.e. for Runs 13A-50).

WATER-MOTION CHARACTERISTICS, RUNS 51-60

Run No.	Mean Amplitude Gage Reading (East Tank) inches	Total Water Motion Amplitude ($2z_0$) inches	Period (T) seconds	Type of Test
51	-0.08	6.30	3.579	duned bed
52	8.16	6.80	3.430	duned bed
53	15.07	5.79	3.309	duned bed
54	-8.05	7.50	3.681	duned bed
55	-15.96	6.11	3.790	duned bed
56	15.02	6.52	3.295	plane bed
57	8.10	6.52	3.430	plane bed
58	0.21	6.50	3.594	plane bed
59	-7.06	6.53	3.655	plane bed
60	-16.10	6.55	3.764	plane bed

Run 61 - One test, Run 61, was made in order to obtain data on the profile of the advancing ripple system. A strip of sheet metal, on which a reference

grid was inscribed, was placed vertically, parallel to the wall of the test section, in the bed. The grid extended from the disturbance element approximately 2 feet along the test section. The water was made to oscillate in the usual manner. Photographs were taken at regular time intervals showing the profile of the ripples as they formed along the grid. The test was stopped at 1231 cycles when the outermost grain movement was nearly 2 feet from the disturbance element. The sheet metal grid was then removed and placed parallel to its former position and passing through the most fully developed section of the bed. Photographs were again taken of the profile of the ripple system. Since the sheet metal strip hindered the growth of the ripples adjacent to it, the photographs taken during the run serve only to illustrate the order of development, and do not indicate the rate of development, of the bed forms. The photographs taken at the end of the run show the correct profile of the two-dimensional ripple system.

RESULTS AND ANALYSIS OF RESULTS

General

The damped natural period of oscillation, T , of the water-motion is related to the effective mass, M , of the water column approximately by

$$T = \frac{2\pi}{\sqrt{\frac{2\gamma A}{M}}} \quad (1)$$

in which γ is the specific weight of water and A is the cross-sectional areas of the legs of the U-tube. The following average values are applicable to the previous, constant-frequency, tests: (a) T equal 3.56 seconds, (b) γ equal 62.2 lb/ft³, and (c) A equal 4 ft². Using these values and Equation (1), the effective mass, M , is found to be 158 slugs. Now, knowing the effective mass corresponding to a zero float-gage reading and also knowing the areas of the legs of the U-tube, an approximate value for the effective mass at any other gage reading can be calculated merely by considering the change in the mass of water. Using this new value of the effective mass, which results from either a rise or fall of the mean water level, the corresponding, new value of the natural period of oscillation is obtained by again using Equation (1). The resulting curve, showing the period of oscillation versus the float-gage reading, is plotted in figure 1. Also shown in figure 1 is the experimental values of the period and the corresponding float gage readings for Runs 51-60.

The maximum variation in the period of the water-motion oscillations was only about ± 0.24 secs. giving a maximum total change of about 13.5% of the mean period, 3.55 secs. Obviously the small change in the period obtained in the tests is not sufficient to give a comprehensive comparison of ripples and dunes formed by oscillating water-motions with equal amplitudes but with different periods. However, some characteristics of the dune geometry, rate of ripple propagation, and energy dissipation were evident in the tests.

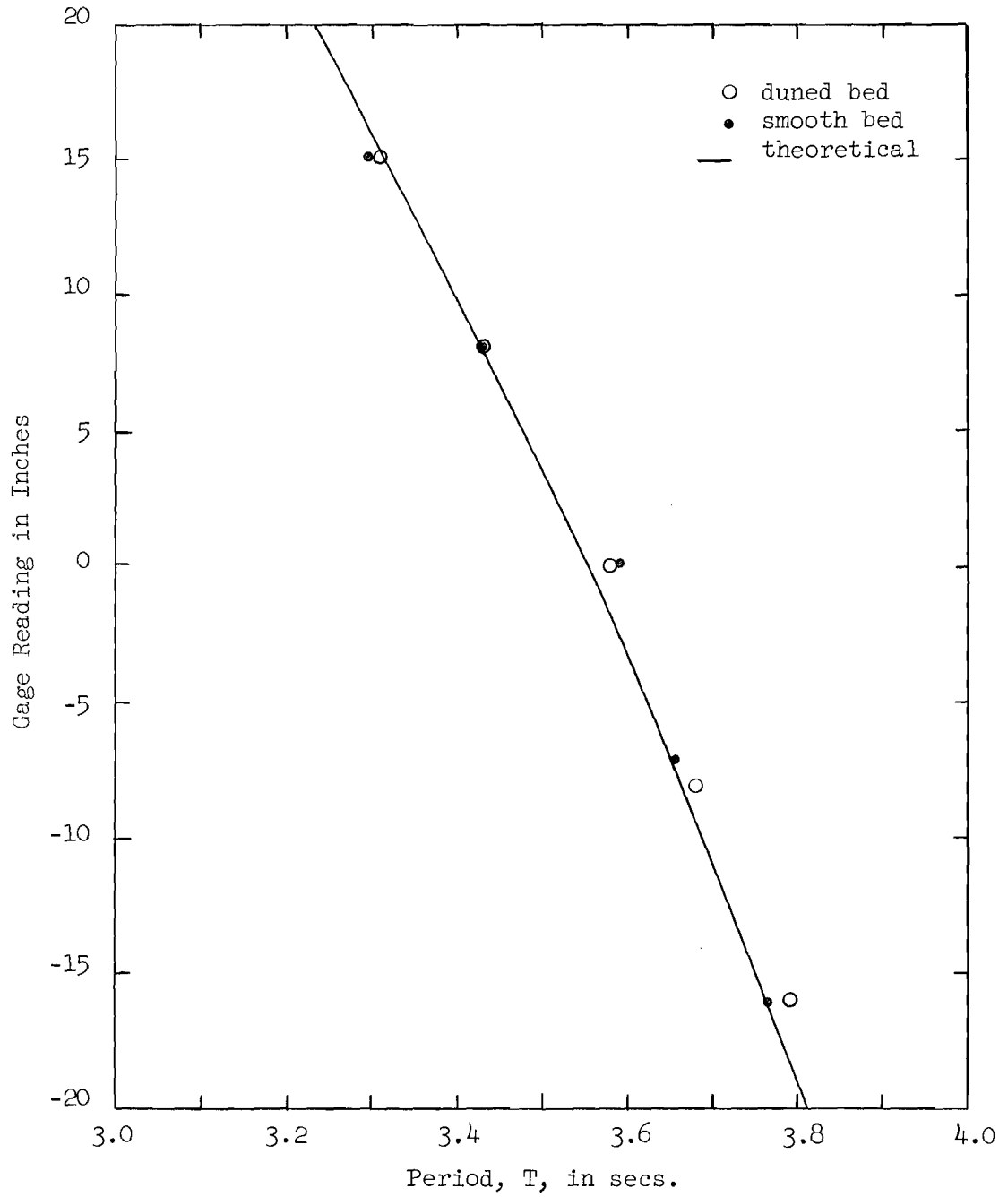


Figure 1. Period of the Water-motion Oscillations

Development of a Duned Bed

The bed of the test section, which, at the start of each run, was a plane surface interrupted only by the disturbance element, developed into a system of two-dimensional, equilibrium dunes, during each of Runs 51-55. The information obtained from the tests indicates that the erodible bed changes form in a systematic process during a run. The flat bed is replaced, in turn, by a transient rippled pattern, an irregular transition pattern, and the final, regular duned pattern. The order in which the bed forms developed was the same in each of the five runs.

The first movement of the bed material occurs during the initial half-cycle of the water-motion. Sediment grains are swept from immediately behind the disturbance to a position a short distance downstream. These grains do not return to their former position during the second half-cycle despite the reversal in flow direction. After a few cycles, during which this scouring process continues, a depression is evident parallel to the disturbance element. The depression forms the trough, and the transplanted grains form the crest, of the first ripple. As the water-motion oscillations continue the ripple height and the ripple wave-length increase. The crest of the forming ripple is not symmetrical in that the side farther from the disturbance element assumes a much steeper slope. The steeper slope is evidently very nearly equal to the angle of repose of the sediment which remains unchanged throughout the cycle. The slope of the side nearer the disturbance, on the other hand, is dependent on the amount of material which has been transferred from the depression to the crest and gradually becomes steeper as the oscillations continue.

When the crest of the forming ripple reaches a height of approximately 10 grain diameters above the bed, grain movement begins on the adjoining flat bed. Thus a second ripple starts to form, being caused, not by the flow over the rod,

but rather by the flow over the existing ripple crest. The second ripple grows in the same manner as the first one until it, too, initiates the formation of another ripple. By this continuing process, the bed forms propagate outward from the disturbance element across the bed of the test section.

The generation of ripples is illustrated in figure 2 for Run 61. The profiles of the developing system of ripples were reproduced from photographs taken of the ripple system as it progressed across the bed adjacent to a sheet metal strip. Although the rate of propagation was hindered by the presence of the metal strip, the order in which the development occurred was the same as the order of the development in undisturbed flow.

As the test continues the oldest ripple, the one adjacent to the rod, grows to a limiting size. By this time the crest of this ripple is symmetrical and, although sediment grains are carried back and forth across the crests during a cycle, the ripple has achieved an essentially stable geometry. A second type of bed form now appears. Starting from the central crest a system of dunes, characterized by a stable, symmetrical geometry, begin to generate outwards from the rod. These dunes, having larger amplitudes and wave lengths than the ripples, cannot replace the smaller ripples evenly which causes an irregular or transition pattern to separate the dunes from the ripples. At this time four regions are evident on the bed. These are:

- (a) The region beyond the limit of ripple propagation in which the bed is still flat and undisturbed,
- (b) the region containing the growing system of ripples,
- (c) the transition region, which separates the dunes from the ripples, containing bed forms which are irregular both in plan and profile, and
- (d) the central region, near the rod, containing a uniform system of stable dunes.

The development of the bed, shown in figure 3, illustrates the progression, during the first 1400 cycles of Run 51, of the developing bed forms. At 1400 cycles

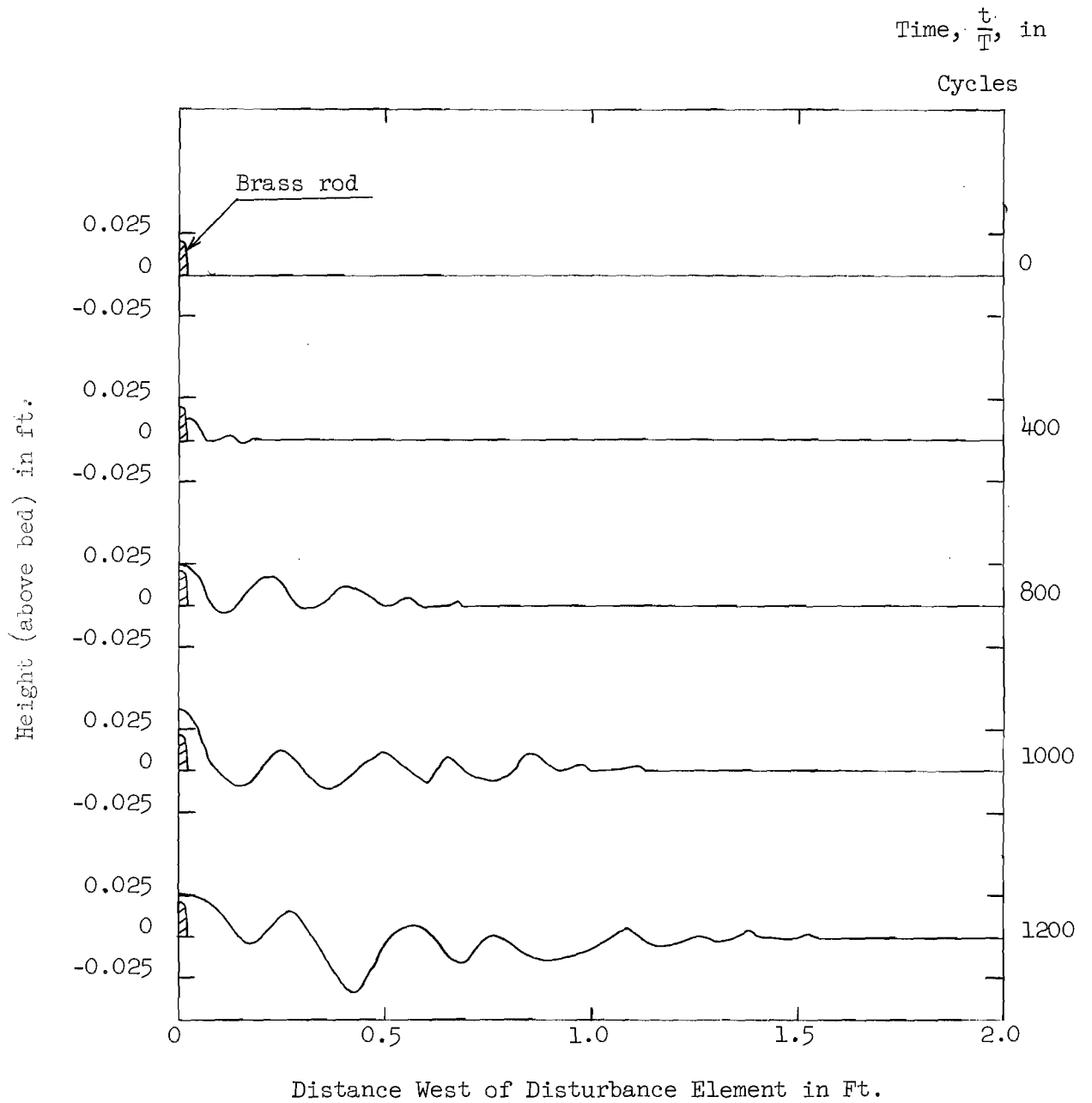
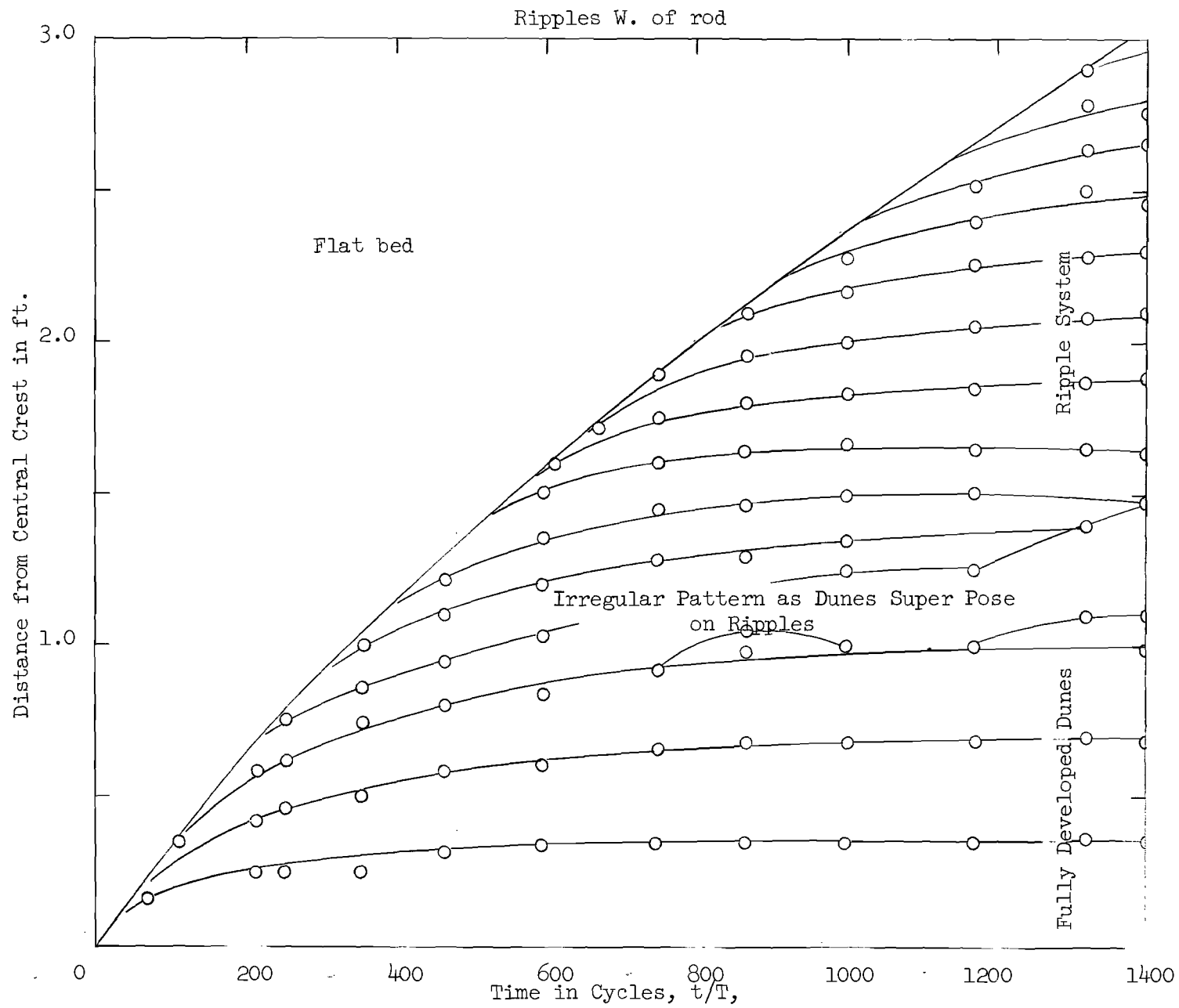


Figure 2. Development of the Ripple System, Run 61



Run 51
 T = 3.58 sec.
 2Z₀ = 6.30 inches

Figure 3. Development of the Bed, Run 51.

the ripples have propagated to the end of the test section (i.e. 3 feet from the central crest) and three dunes have formed.

The bed is fully developed when the equilibrium bed forms, dunes, exist over the entire test section.

Ripples

Geometry of the Ripple System - The profile of the ripple system for Run 61 is shown in figure 4. The photographs, from which the measurements of the ripple profile were taken, were obtained at the end of the run (i.e. at t/T equal 1231 cycles). The cross-section of the crests shown in this figure occurred far enough from both the wall of the test section and the sheet metal grid to preclude end effects. The distinguishing features of the ripple system are the increasing size, and the increasing symmetry, of the individual ripples with increasing time from initiation.

Rate of Propagation of Ripples - The rate of propagation of the ripple system, V_r , is simply expressed by

$$V_r = \frac{dx/d(\frac{t}{T})}{T} \quad (2)$$

where x is the distance from the leading crest to the central crest,

t is the time elapsed since the start of the run,

and T is the period of the water-motion oscillations.

The leading ripple crest separates the flat, undisturbed section from the rippled section of the bed. Thus, the position of the leading crest is given by the continuous curve, which has been shown previously in figure 3 for Run 51, enclosing the rippled section of the bed. The slope of this curve, for a particular run and at a particular stage of development, is the numerator of equation(2).

A convenient non-dimensional parameter describing the rate of ripple propagation is the ratio of rate of ripple propagation to the maximum water-motion velocity, U_m . However, since U_m is equal to $z_0\omega$ and since the water-motion

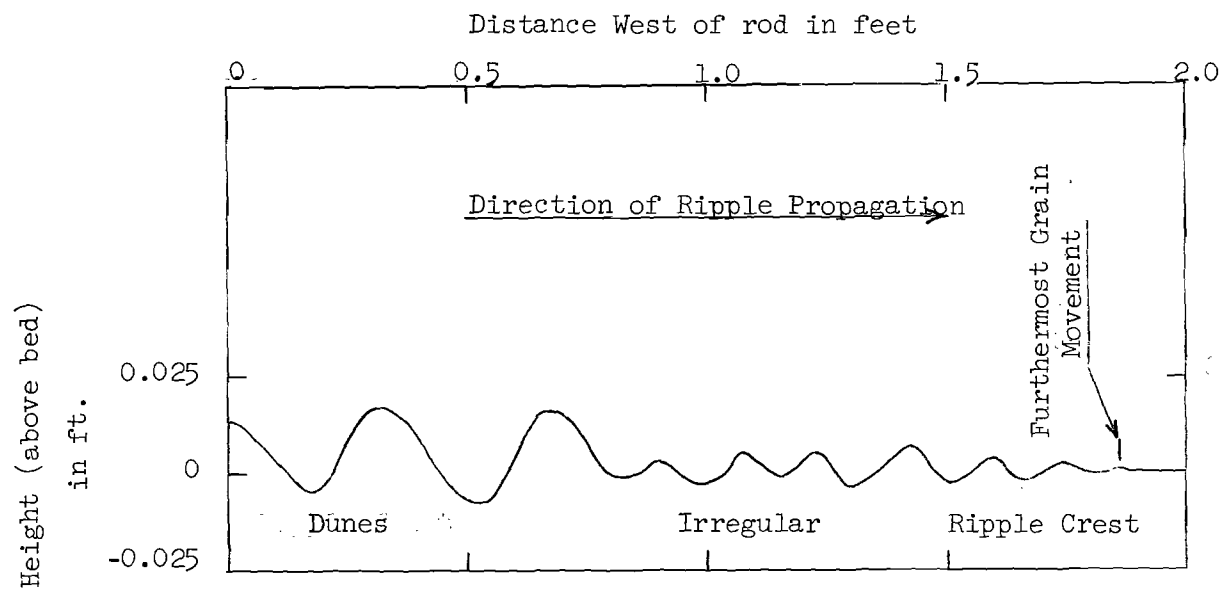


Figure 4. Profile of the Ripple System, Run 61 ($t/T = 1231$ cycles)

amplitude decreases during a run, the value of U_m decreases as the ripples spread across the bed. Consequently, both V_r and U_m must be evaluated for the same cycle. For each of Runs 51-55 and also for Run 49 four values of $\frac{V_r}{U_m}$ have been calculated. These values correspond to the leading ripple crest being 1.0, 1.5, 2.0, and 2.5 feet from the central crest. The rate of ripple propagation for all runs is shown in figure 5. As shown by the straight line in the figure, the results indicate an approximate relationship between the rate of ripple propagation and the maximum water-motion velocity is

$$\frac{V_r}{U_m} \propto U_m^4 \quad (3)$$

or

$$V_r \propto U_m^5 \quad (4)$$

The formation and growth of a ripple system appears to be a recurring process of localized scour. Since scour is known to be highly dependent on local velocity the large power relationship described by Equation (4) is to be expected.

Dunes

Geometry of Dunes - The pertinent geometric characteristics of the dunes are the dune wave-length, dune height and the ratio of dune height to dune wave-length. These characteristics have already been investigated for a bed of glass beads subjected to water-motion oscillations of different amplitudes but of the same period. The investigation of dune geometry for runs having the same period, namely 3.56 seconds, is presented in Quarterly Report 2. The mean values of dune wave-length, λ , dune height, η , and the ratio of dune height to dune wave-length, η/λ , obtained in the earlier, fixed-period runs and given in Quarterly Report 2 are used here as reference values for the analysis of the dune geometry obtained from the tests having different periods of water-motion oscillation (Runs 51-55).

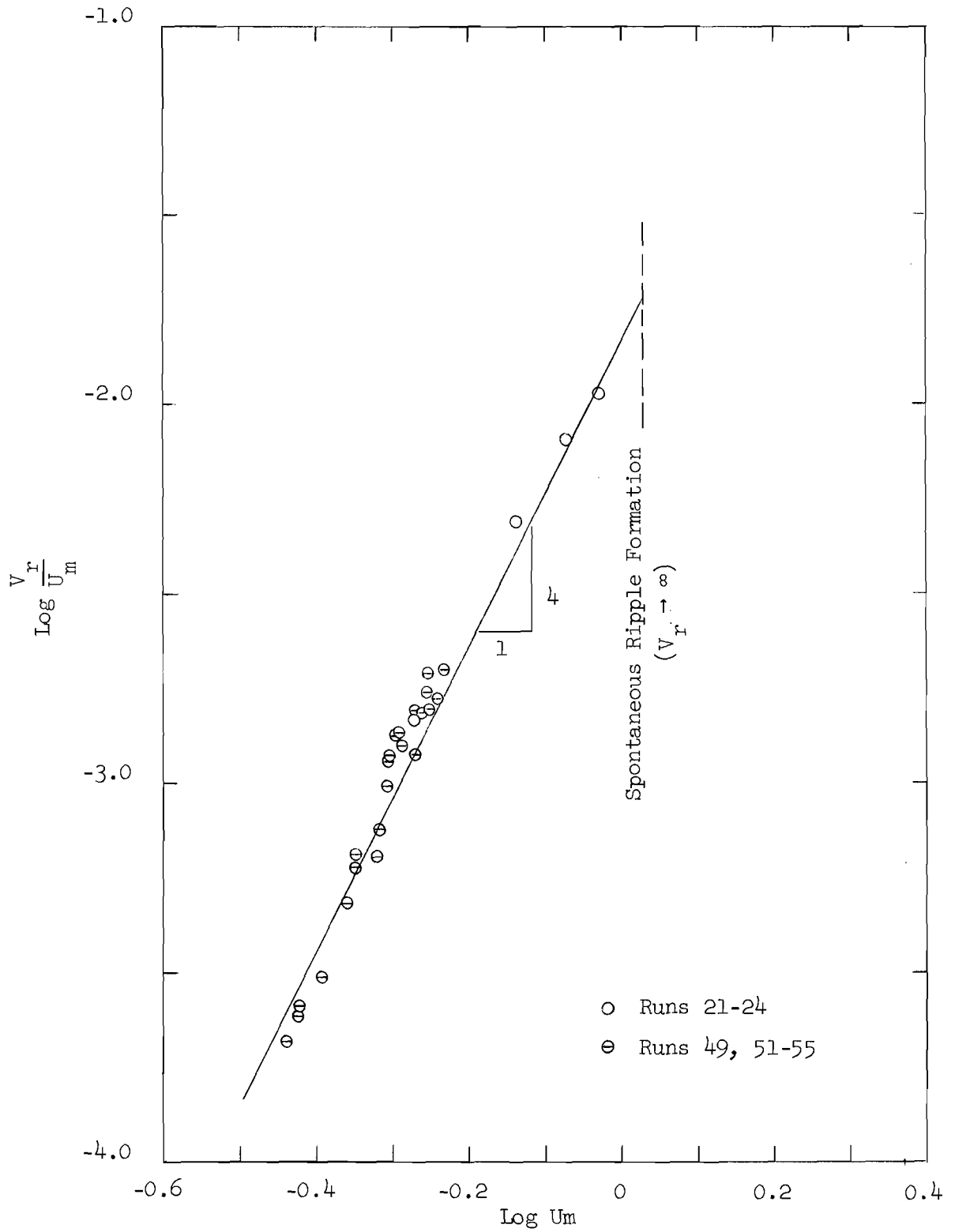


Figure 5. Rate of Propagation of Ripples

In figures 6, 7, and 8, respectively, the mean values of λ , η , and η/λ obtained from the earlier, fixed-period runs are represented as a dashed line. The corresponding characteristics of the dunes obtained in Runs 51-55 are also shown in these figures. The scatter of the data points indicate that the results, regarding the changes in dune geometry with changes in period, are inadequate to allow a complete analysis.

The differences between the dune characteristics obtained in each of Runs 51-55 and the corresponding dune characteristic obtained, for the same amplitude of water-motion oscillation, from the fixed-period runs have been calculated. These differences, $\Delta\lambda$, $\Delta\eta$, and $\Delta(\eta/\lambda)$ are shown in figures 9, 10, and 11, respectively, against the corresponding period of water-motion oscillation. Although the overall change in period is not large enough to provide conclusive information on the behaviour of the dunes, the following features are indicated. For total water-motion amplitudes of about 6.5 inches and increasing periods (ranging from 3.3 to 3.8 seconds) there is

- (a) an apparent increase in λ , as shown in figure 9
- (b) an apparent increase in η , as shown in figure 10
- and (c) no apparent change in η/λ , as shown in figure 11.

The indications, then, are that both the dune wave-length and the dune height increase as the period of the water-motion increases. There is apparently no change in the ratio of the dune height to the dune wave length. However, since the range of periods for the tests was so small, these conclusions are only tentative.

Published Results - An extensive investigation of ripples and dune, in situ, has been presented by D. L. Inman², 1957. Measurements of the bedforms generated by oscillatory wave motion in coastal waters, and of the characteristics of the sediments which form them, were made of the ripples in their natural

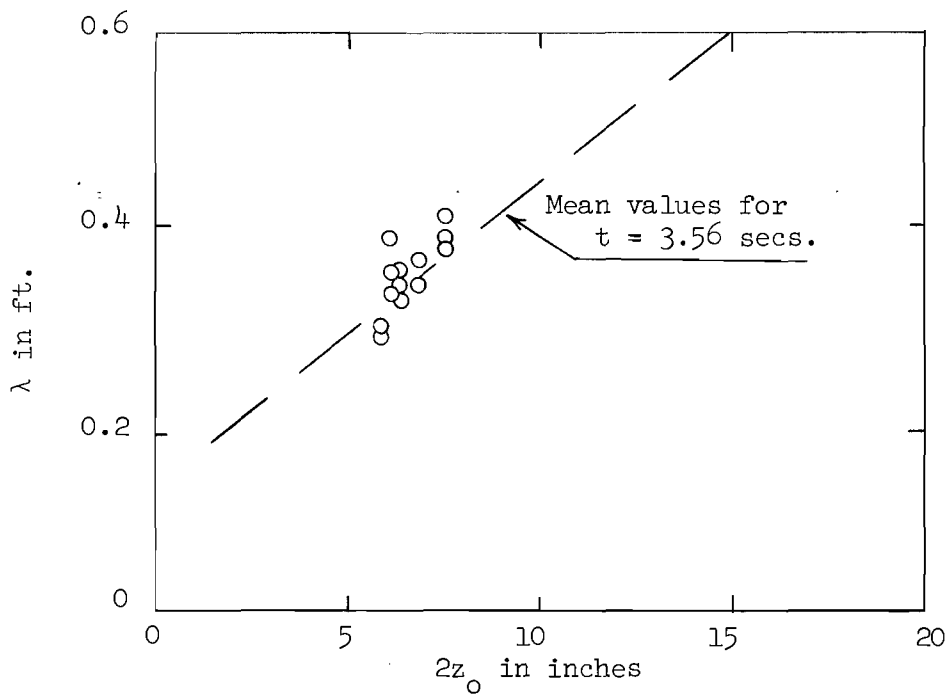


Figure 6. Dune Wave-length, λ

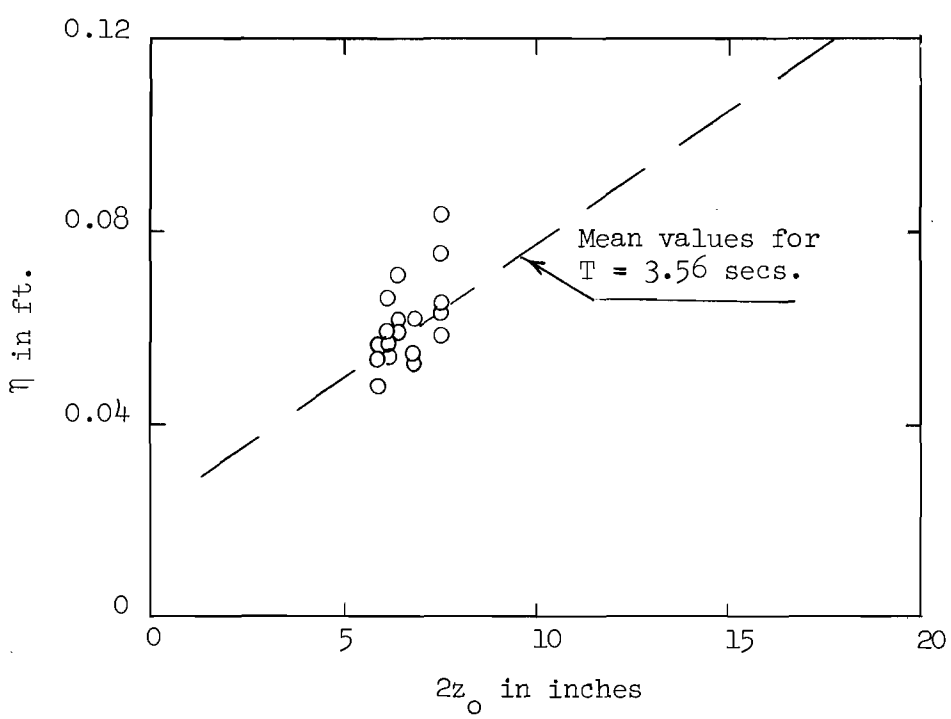


Figure 7. Dune Height, η

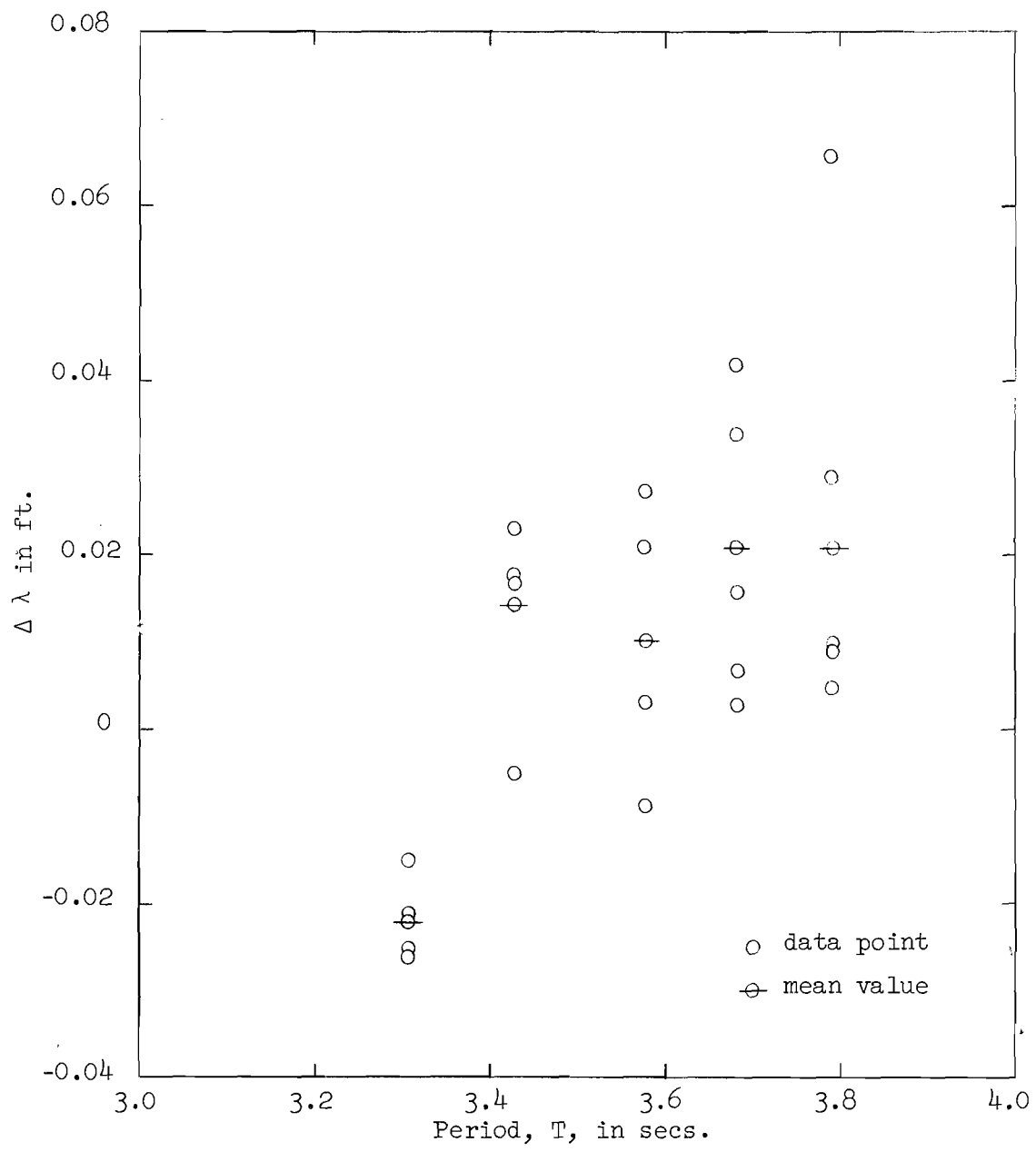


Figure 9. The Change in λ for Different Periods, Runs 51-55

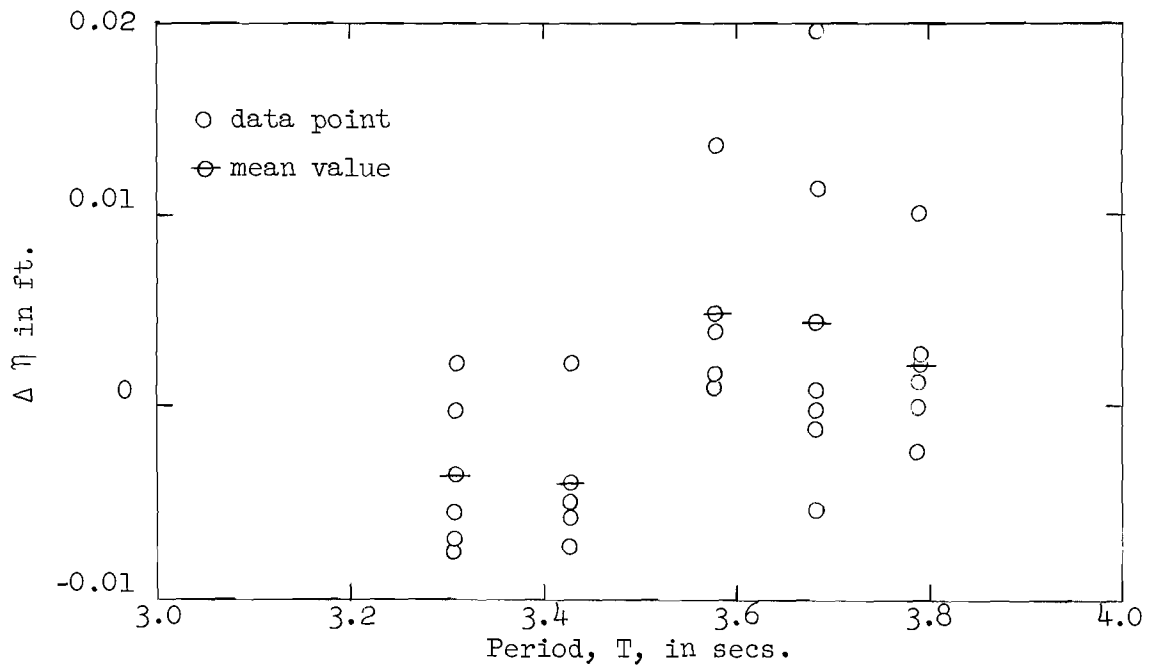


Figure 10. The Change in η for Different Periods, Runs 51-55

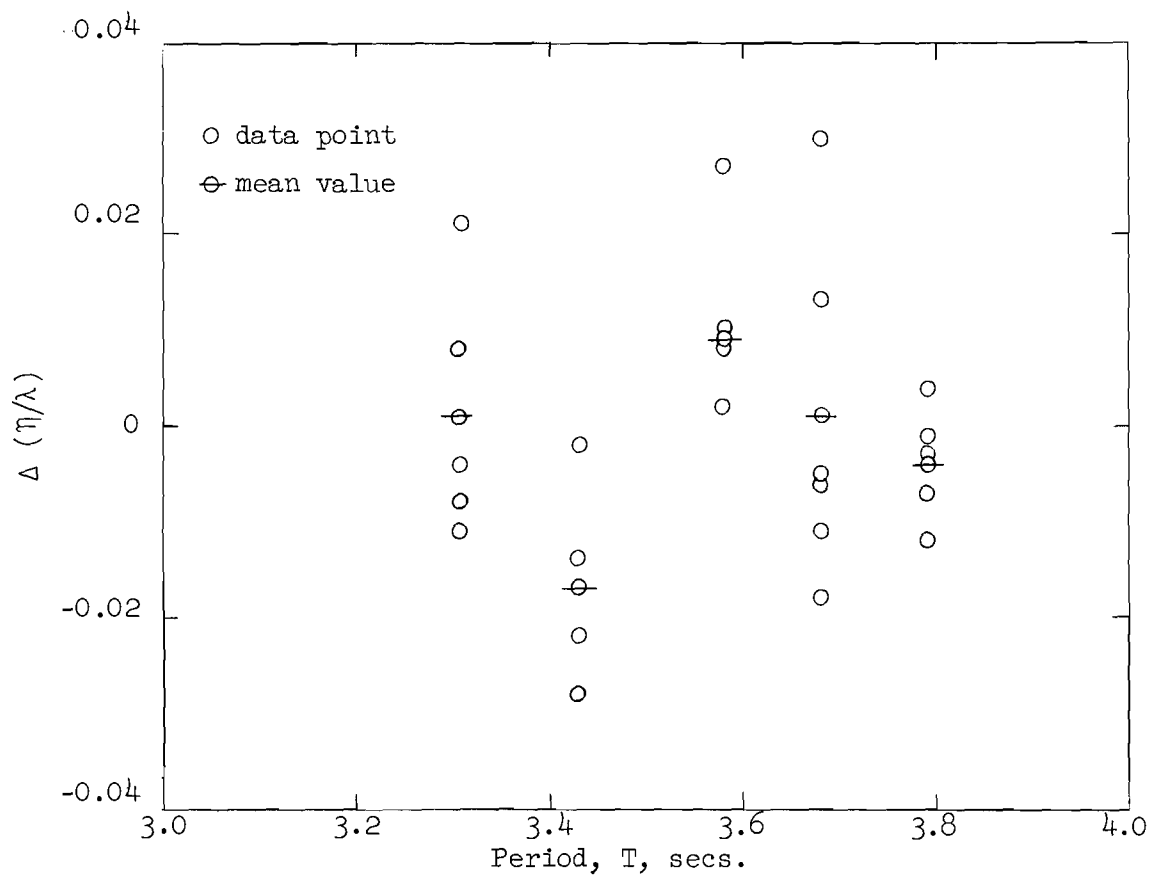


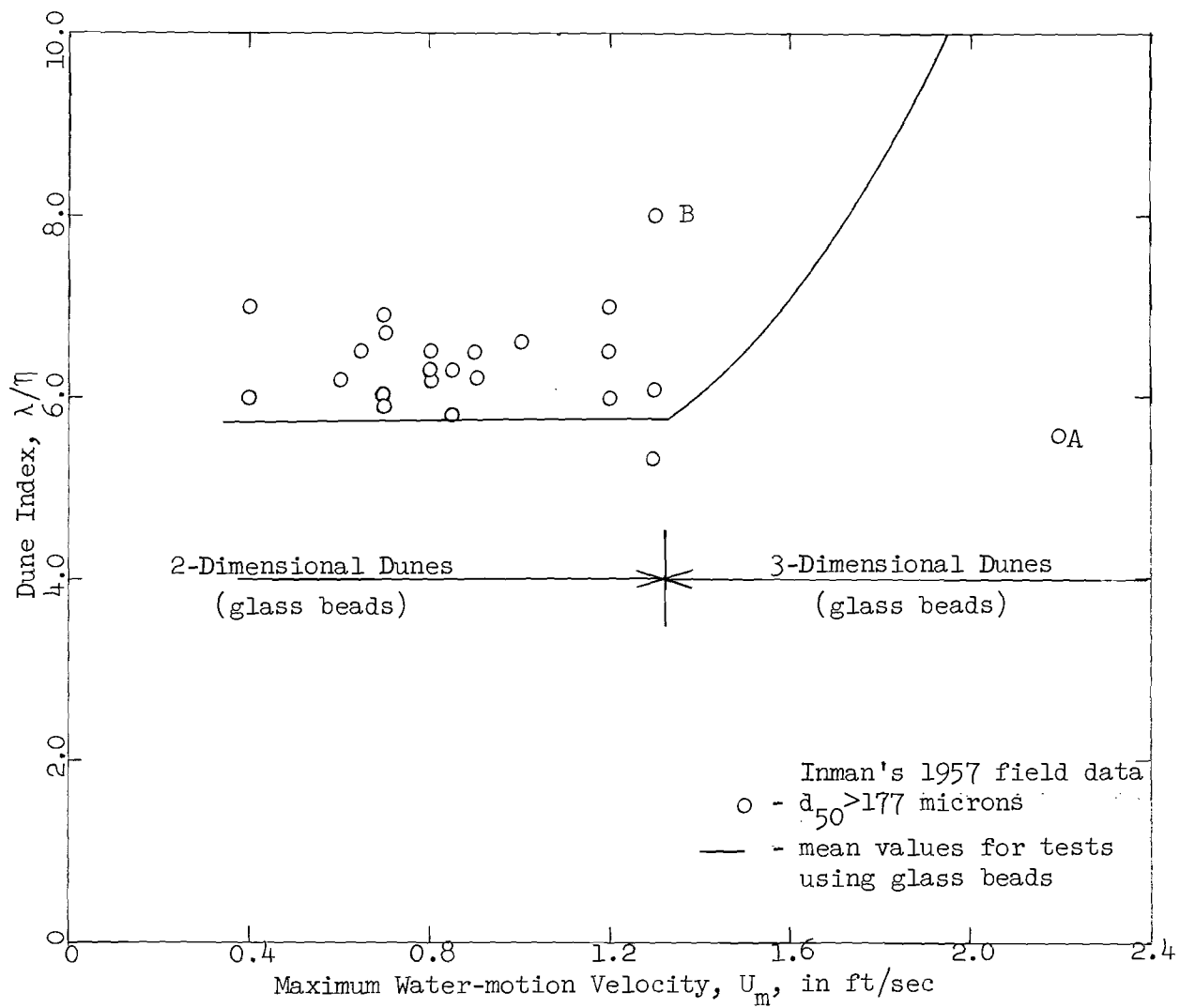
Figure 11. The Change in η/λ for Different Periods, Run 51-55

circumstances. The size of the measured bedforms ranged from 0.14 ft. to over 4 ft. in wave length and from 0.020 ft. to 0.75 ft. in height.

The values of the ratio, λ/η , obtained by Inman for sands coarser than 177 microns in median diameter are plotted in figure 12 against the maximum water-motion velocity occurring at the bed. The solid line in figure 12 is the mean values of λ/η obtained from the duned bed tests for a bed of glass beads. Although the characteristics of the different sediments involved are not included in the parameters used for figure 12 the two sets of data agree very well. The two dunes marked A and B in the figure show the largest variance from the experimental data. It is of interest to comment on the physical properties of the sediment involved in these two special dunes. Dune A, a long crested dune, was composed of sand of median diameter equal 637 microns while dune B, a short-crested dune, was composed of sand of median diameter equal 276 microns. Speculation as to the cause of the variations in the values of λ/η would be that either:

- (a) the dunes had been formed under quite different water-motion than was present at the time of the test and did not have sufficient time to re-form; this does not explain the high value of λ/η for dune B,
- or (b) the water-motion velocity at which transition between two and three-dimensional dunes occurs is influenced by the characteristics of the sediment involved; if this is the case, the size of the sediment alone would explain the large value of λ/η and the short crest of dune B (a three-dimensional dune) and also the low value of λ/η at such a high water-motion velocity and the long crest of dune A (definitely indicating a two-dimensional dune).

Forthcoming tests using a bed of Ottawa sand will give more extensive information on the role of the sediment in the phenomena of dune formation. At this time no definite conclusions can be drawn regarding statements (a) and (b) other than that they are definite possibilities.

Figure 12. Dune Index, λ/η

Energy Dissipation

General - The energy dissipation for a particular run is determined from the test results in the following manner. The work-input required in the smooth-bed runs is subtracted from the work-input required in the duned-bed tests. In taking this difference, the energy dissipation that occurs within the U-tube but which is not dependent on the configuration of the bed is eliminated. The theoretical energy dissipation, resulting from oscillating, laminar flow over a plane wall of the same dimensions as the bed of the test section, is now added to the difference in work-inputs. In other words

$$\begin{aligned}
 & \left(\begin{array}{c} \text{Energy dissipation per} \\ \text{square foot per cycle} \end{array} \right)_{\text{duned bed}} = \left(\begin{array}{c} \text{Work-input per} \\ \text{square foot per cycle} \end{array} \right)_{\text{duned bed}} - \left(\begin{array}{c} \text{Work-input per} \\ \text{square foot per} \\ \text{cycle} \end{array} \right)_{\text{plane bed}} \\
 & + \left(\begin{array}{c} \text{Theoretical energy dissipation} \\ \text{per square foot per cycle} \end{array} \right)_{\text{oscillating laminar flow over}} \\
 & \hspace{10em} \text{a plane wall} \hspace{10em} (5)
 \end{aligned}$$

The work-input to the west tank for each of Runs 51-55, duned bed tests, and also for each of Runs 56-60, plane bed tests, is shown in figure 13. A theoretical expression for the last term in Equation 5 was derived and presented in Quarterly Report 2 to which the reader is referred. The result is given as

$$\begin{aligned}
 & \text{Energy dissipation per square foot per cycle} \\
 & \text{for oscillating laminar flow over a plane wall} = \frac{\pi \rho}{\sqrt{2}} \sqrt{\nu} z_0^2 \omega^{3/2}
 \end{aligned} \hspace{10em} (6)$$

in which ν is the kinematic viscosity,
 ρ is the mass density,
 and ω is the frequency.

The energy dissipation has been evaluated for each of the duned bed tests

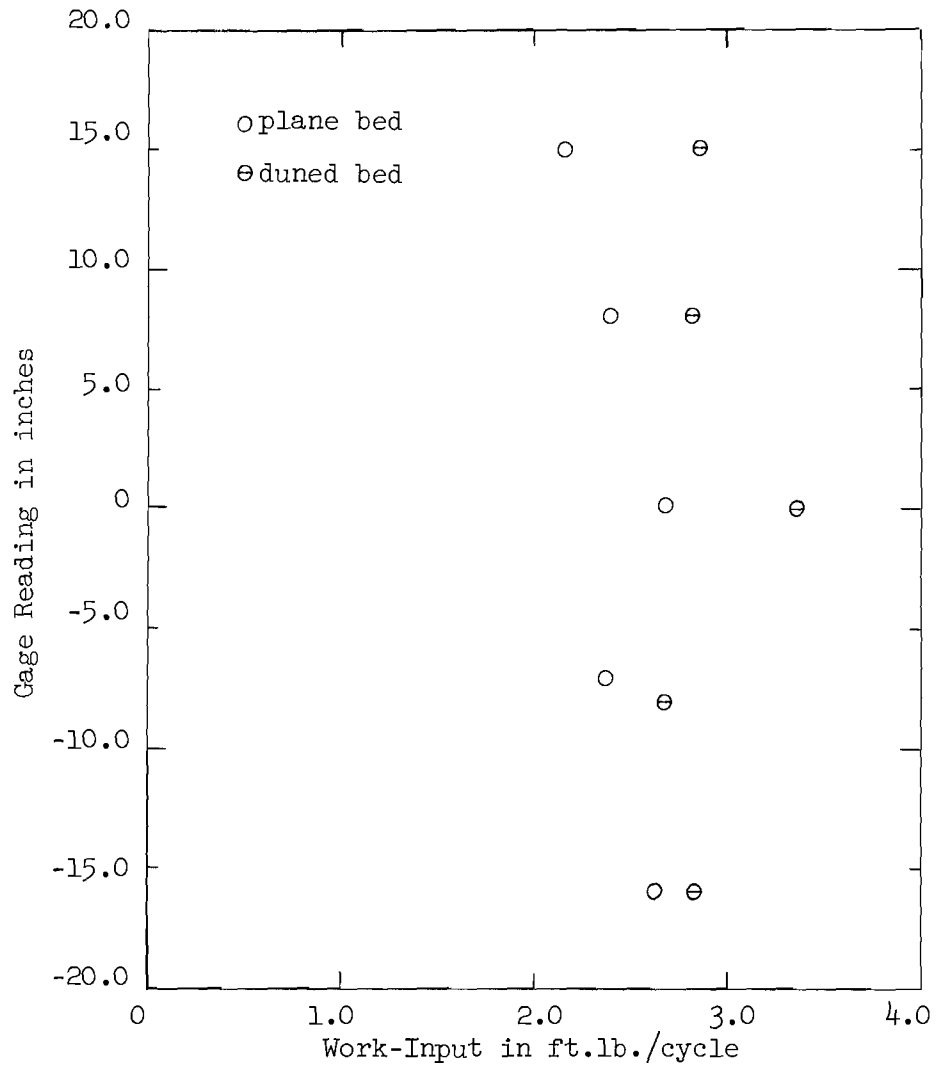


Figure 13. Work-Input to West Tank, Runs 51-60

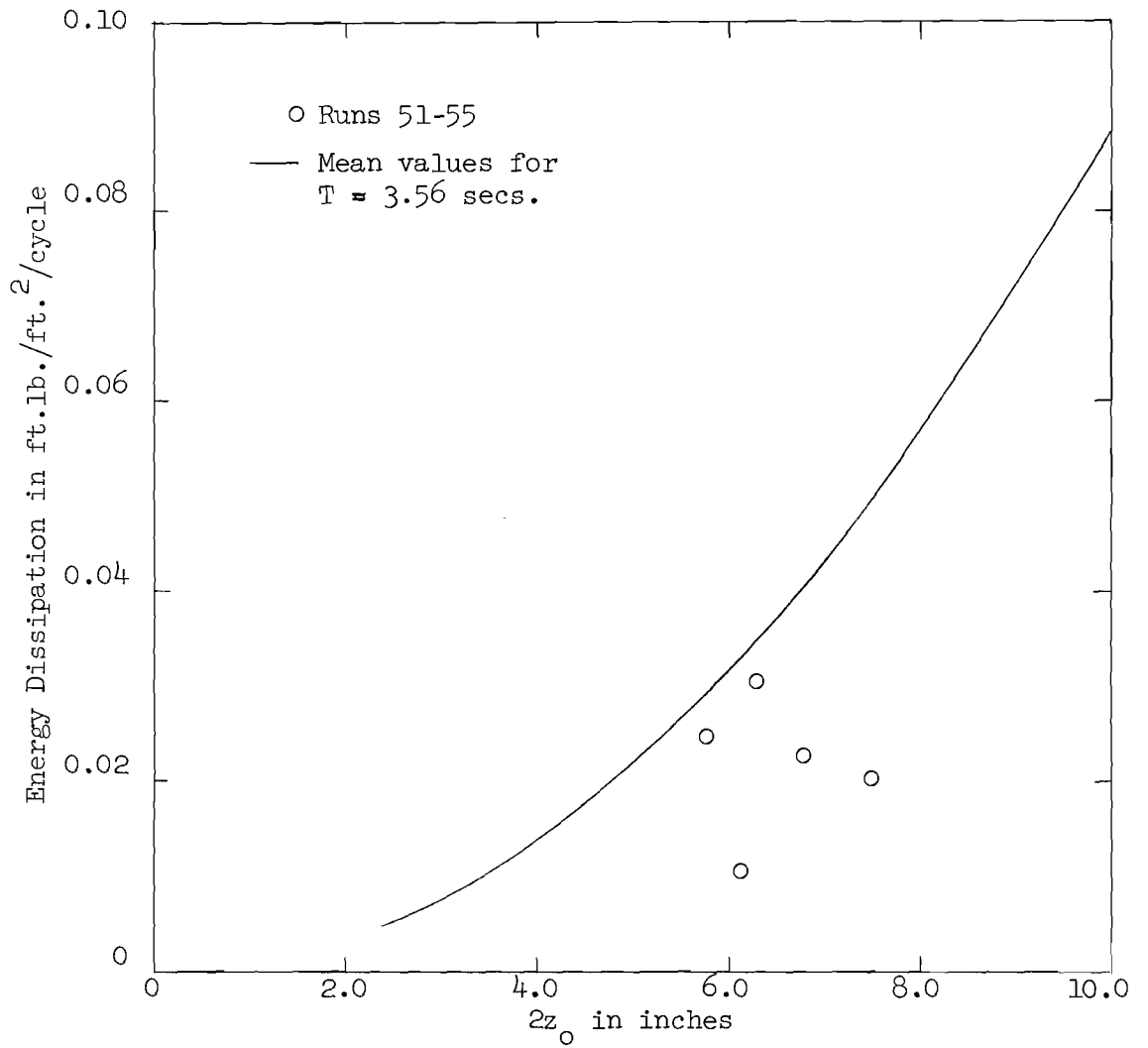


Figure 14. Energy Dissipation, Runs 51-55

according to Equation 5 and the results are shown in figure 14. The solid line is the mean energy dissipation from earlier tests. Two significant differences between Runs 51-60 and the earlier tests are,

- (a) each of the earlier tests had the same period of water-motion oscillation, namely 3.56 seconds, whereas the period for Runs 51-60 ranged from about 3.3 to 3.8 seconds,
- and (b) the earlier smooth bed tests used for the energy dissipation analysis were performed with an aluminum sheet placed over the bed whereas the smooth bed tests (Runs 56-60) were performed with a flat, sediment bed.

In Quarterly Report 3 an expression for the energy dissipation was obtained by considering the energy losses of the vortices which develop in the dune troughs and which are ejected into the mainstream flow twice each cycle. The equation is

$$\left(\begin{array}{l} \text{energy dissipation per} \\ \text{unit area of duned bed} \\ \text{per cycle} \end{array} \right) = K_d \sqrt{v} \rho (2z_0)^2 \omega^{3/2} \quad (7)$$

in which K_d is a constant.

Equation (7) has been substantiated in regard to $2z_0$ by the earlier tests. In order to investigate the role of ω in Equation (7) Runs 51-55 were analyzed in the following manner. The energy dissipation corresponding to a total water-motion amplitude of 6.5 inches was calculated for each test. The required relationship, for constant values of v , ρ , and ω , based on Equation (7), is

$$\left(\begin{array}{l} \text{energy dissipation per} \\ \text{unit area of duned bed} \\ \text{per cycle} \end{array} \right)_{2z_0 \text{ equal } 6.5 \text{ inches}} = \left(\frac{2z_0}{6.5} \right)^2 \left(\begin{array}{l} \text{energy dissipation per} \\ \text{unit area of duned bed} \\ \text{per cycle} \end{array} \right)_{2z_0 \text{ of the test}} \quad (8)$$

The results are plotted in figure 15 against the frequency of the test. The solid line corresponds to a relationship of the form

$$\left(\begin{array}{l} \text{energy dissipation per} \\ \text{unit area of duned bed} \\ \text{per cycle} \end{array} \right) \propto \omega^{3/2} \quad (9)$$

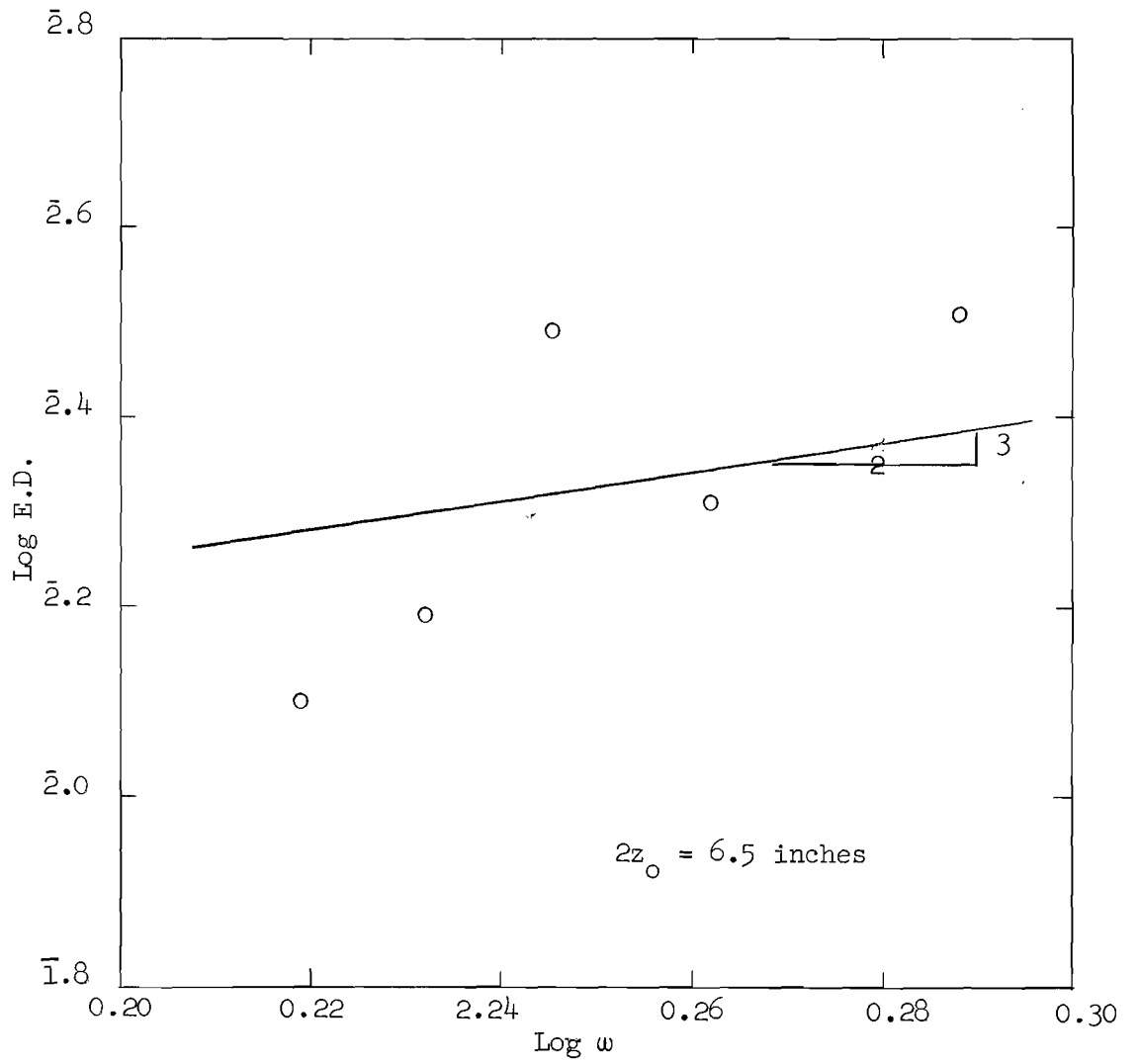


Figure 15. Energy Dissipation as a Function of the Period, Runs 51-55

whereas the results appear to indicate a higher power in the RHS of Equation (9). However, the range in frequencies is so small that the exact relationship could not be expected to show in the results.

Published Results - Bagnold¹ (1946) obtained data on the energy dissipation which resulted when a circular-arc plate, to which fixed imitation ripples were attached, was oscillated through still water. The imitation ripples consisted of circular arcs, meeting at an angle of 120° to form a sharp crest, and having a length to height ratio, λ/η , of 6.7. His results indicate that, for z_0/λ less than 1.0 the coefficient of drag,

$$C_f = \frac{\tau}{\rho \omega^2 z_0^2} \quad (10)$$

is constant, equalling about 0.08. Bagnold also computed the drag coefficient for the upper half of an infinitely long series of flat, independent and widely spaced plates set at right angles to the direction of motion by using values given (for uni-directional flow) in Smithsonian Tables, Washington, 1934. His estimated value for the coefficient of drag for oscillating flows, considering only the upper half of the plates and using the r.m.s. velocity, was 0.15.

For Runs 51-55 inclusive, the value of z_0/λ ranged from 0.745 (Run 55) to 0.832 (Run 53) which, if the results for fixed ripples were strictly applicable to the sediment dunes, would indicate that the drag and, consequently, the energy dissipation would be constant. However, since (a) the length to height ratio of the dunes which formed on the erodible bed had a value of about 5.8 which is considerably less than the value, 6.7, for Bagnold's artificially rippled surface, since (b) the crests of the actual sediment dunes are rounded rather than sharp-crested, and also since (c) the flow pattern for fluid moving over the sediment dunes is not identical to the flow pattern for fluid

RESEARCH PROGRAM

The experimental studies included in Quarterly Reports 1-4 are considered to be complete in regard to dunes which formed in the bed composed of 0.297 mm-diameter glass beads. The next experimental studies will be similar except that the bed material will be 0.585 mm-diameter Ottawa sand. The analysis will also be extended towards incorporating the physical characteristics of the bed material into the conceptual models used in the theoretical analysis of dune geometry and also energy dissipation. The stability of the flow pattern for oscillating flow over the erodible bed must also be considered.

NOMENCLATURE

Symbol	Definition	Dimensions (F,L,T)
A	Cross-sectional area of a leg of the U-tube	L^2
C_f	Coefficient of drag	None
d	Mean diameter of bed particles	L
K_d	Energy dissipation coefficient for a duned bed	None
M	Effective mass of the water within the U-tube	FT^2L^{-1}
S	Specific gravity	None
t	Time	T
T	Period of water-motion oscillations	T
U_m	Maximum water-motion velocity	$L T^{-1}$
V_r	Velocity of ripple propagation	$L T^{-1}$
x	Horizontal coordinate	L
Z_o	Water-motion amplitude	L
γ	Specific weight of water	$F L^{-3}$
η	Dune height	L
λ	Dune wave-length	L
ν	Kinematic viscosity	$L^2 T^{-1}$
ρ	Mass density	FT^2L^{-4}
τ	Shear stress	$F L^{-2}$
ω	Frequency of simple-harmonic oscillations	T^{-1}

REFERENCES

1. R. A. Baghold, "Motion of Waves in Shallow Water-Interaction Between Waves and Sand Bottoms," Proceedings, Royal Society, series A, Vol. 187, 1946, pages 1-18.
2. D. L. Inman, "Wave-Generated Ripples in Nearshore Sand," Tech Memo No. 100, Beach Erosion Board, U. S. Army Corps of Engineers, 1957, 41 pages.
3. Madhav Manohar, "Mechanics of Bottom Sediment Movement Due to Wave Action," Tech Memo No. 75, Beach Erosion Board, U. S. Army Corps of Engineers, 1955, 121 pages.
4. J. F. Kennedy, "The Formation of Sediment Ripples in Closed Rectangular Conduits and in the Desert," Journal of Geophysical Research, Vol. 69, 1964, pages 1517-1524.

APPENDIX

TABLE 2

TABLE 2
 COMPLETED EXPERIMENTAL PROGRAM
 (July 15, 1965)

Run No.	Period T (Sec)	Amplitude $2z_0$ (in)	Water Temp °F	Conditions (See key at the end of TABLE I)	Purpose
13 A	3.565	6.21	79	1, 13, 24	53
13 B	3.552	8.05	79	1, 13, 24	53
13 C	3.550	11.12	79	1, 13, 24	53
13 D	3.549	12.97	79	1, 13, 24	53
13 E	3.549	15.31	79	1, 13, 24	53
14 A	3.554	5.52	80	1, 13, 24	53
14 B	3.562	6.28	80	1, 13, 24	53
14 C	3.564	7.29	80	1, 13, 24	53
14 D	3.554	8.92	80	1, 13, 24	53
14 E	3.557	10.61	80	1, 13, 24	53
15 A	3.538	8.99	80	1, 13, 24	53
15 B	3.553	10.48	80	1, 13, 24	53
15 C	3.557	13.28	80	1, 13, 24	53
15 D	3.558	14.87	80	1, 13, 24	53
16 A	3.551	12.86	79	1, 13, 24	53
16 B	3.553	16.32	79	1, 13, 24	53
16 C	3.552	19.92	79	1, 13, 24	53
16 D	3.551	24.40	79	1, 13, 24	53
16 E	3.548	22.72	79	1, 13, 24	53
16 F	3.548	21.23	79	1, 13, 24	53
17 A	3.55	12.17	80	1, 13, 24	53
17 B	3.553	16.34	80	1, 13, 24	53
17 C	3.551	23.33	80	1, 13, 24	53
17 D	3.548	26.33	80	1, 13, 24	53
17 E	3.540	28.78	80	1, 13, 24	53
18 A	3.55	18.78	80.2	1, 13, 24	53
18 B	3.546	26.35	80.2	1, 13, 24	53

TABLE 2 (Continued)

<u>Run No.</u>	<u>Period T (Sec)</u>	<u>Amplitude $2z_0$ (in)</u>	<u>Water Temp °F</u>	<u>Conditions (See key at the end of TABLE I)</u>	<u>Purpose</u>
18 C	3.539	32.00	80.2	1, 13, 24	53
18 D	3.534	36.16	80.2	1, 13, 24	53
19 A	3.555	3.60	80.2	1, 13, 24	53
19 B	3.559	4.94	80.2	1, 13, 24	53
19 C	3.560	5.87	80.2	1, 13, 24	53
20 A	3.555	3.41	77	1, 11, 24	53
20 B	3.552	4.62	77	1, 11, 24	53
20 C	3.555	6.71	77	1, 11, 24	53
20 D	3.547	8.31	77	1, 11, 24	53
20 E	3.549	9.49	77	1, 11, 24	53
20 F	3.548	10.51	77	1, 11, 24	53
21	3.557	7.02	79	2, 11, 21	51, 53
22	3.555	9.44	76	2, 11, 21	51, 52, 53
23	3.549	10.76	75	2, 11, 21	51, 52, 53
24	3.551	12.10	77	2, 11, 21	51, 52, 53
25	3.552	16.42	73	2, 11, 21	51, 53
26	3.551	18.42	73	2, 11, 21	51, 53
27	3.528	20.56	73	2, 11, 21	51, 53
28	3.510	21.67	69.5	1, 11, 24	53
29	3.537	26.25	72.5	1, 11, 24	53
	3.544	25.50	73	2, 11, 24	51, 53
30	3.525	28.56	72	1, 11, 24	53
	3.522	28.03	72	2, 11, 24	51, 53
31	3.517	35.41	72	1, 11, 24	53
	3.521	35.04	72	2, 11, 24	51, 53
32	3.551	30.90	71.5	1, 11, 24	53
	3.534	30.75	71.5	2, 11, 24	51, 53
33	3.544	12.90	73.5	1, 11, 24	53
34	3.555	11.79	73.5	1, 11, 24	53
	3.554	12.41	73.5	1, 11, 24	53
	3.546	12.90	73.5	1, 11, 24	53

TABLE 2 (Continued)

<u>Run No.</u>	<u>Period</u> T (Sec)	<u>Amplitude</u> 2z ₀ (in)	<u>Water</u> Temp °F	<u>Conditions</u> (See key at the end of TABLE I)	<u>Purpose</u>
35	3.550	15.23	73.5	1, 11, 24	53
36	3.553	22.11	73	2, 11, 24	51, 53
37	3.552	7.42	68.5	1, 11, 24	53, 54
38	3.546	8.67	69	1, 11, 24	53, 54
39	3.548	10.10	69	1, 11, 24	53, 54, 55
40	3.540	10.44	69	1, 11, 24	53, 54
41	3.545	10.85	69	1, 11, 24	53, 54
42	3.55	11.18	69	1, 11, 24	55, 55
43	3.55	11.50	69	1, 11, 24	55, 55
44	3.55	11.59	69	1, 11, 24	55
45	3.550	11.62	67	1, 11, 24	53, 54, 55
46	3.550	11.11	67	1, 11, 24	53, 54, 55
47	3.55	10.90	63.5	2, 11, 21	51, 53, 56
48	3.55	4.70	64.1	2, 11, 21	51, 52
49	3.560	4.70	70	2, 11, 22	51, 52, 53
50	3.550	30.37	65	2, 11, 24	51, 53
51	3.579	6.30	75	2, 11, 21	51, 52, 53
52	3.430	6.80	75	2, 11, 21	51, 52, 53, 57
53	3.309	5.79	74	2, 11, 21	51, 52, 53, 57
54	3.681	7.50	72	2, 11, 21	51, 52, 53, 57
55	3.790	6.11	75	2, 11, 21	51, 52, 53, 57
56	3.295	6.52	76	1, 11, 24	53, 57
57	3.430	6.52	76	1, 11, 24	53, 57
58	3.594	6.50	76	1, 11, 24	53
59	3.655	6.53	75	1, 11, 24	53, 57
60	3.764	6.55	75	1, 11, 24	53, 57
61	3.55	6.46	75	2, 11, 21	52

KEY

- 1 - plane bed
- 2 - duned bed
- 11 - bed particles, 0.297mm-diameter glass beads
- 12 - bed particles, 0.585mm-diameter Ottawa sand
- 13 - smooth fixed bed, aluminum sheet
- 21 - 1/2-in diameter, half-round, disturbance element
- 22 - 1-in diameter, half-round, disturbance element
- 23 - 1-1/2-in diameter, half-round, disturbance element
- 24 - no disturbance element
- 51 - geometric characteristics of dunes
- 52 - rate of propagation of dunes
- 53 - work input
- 54 - boundary-layer transition
- 55 - incipient motion
- 56 - motion pictures
- 57 - small change in frequency

QUARTERLY REPORT 5

PROJECT A-798

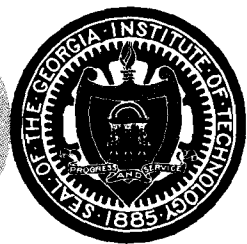
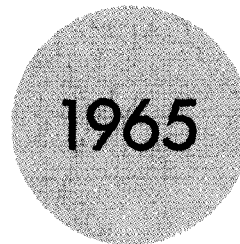
AN ANALYTICAL AND EXPERIMENTAL STUDY
OF BED FORMS UNDER WATER WAVES
(SIMILARITY--LOCALIZED SCOUR)

M. R. Carstens

Contract No. DA-49-055-CIVENG-65-1

October 1965

Prepared for
Corps of Engineers, U. S. Army
Coastal Engineering Research Center
Washington, D. C.



Engineering Experiment Station
GEORGIA INSTITUTE OF TECHNOLOGY
Atlanta, Georgia

QUARTERLY REPORT 5

PROJECT A-798

AN ANALYTICAL AND EXPERIMENTAL STUDY
OF BED FORMS UNDER WATER WAVES
(SIMILARITY--LOCALIZED SCOUR)

M. R. Carstens

Contract No. DA-49-055-CIVENG-65-1

October 1965

Prepared for
Corps of Engineers, U. S. Army
Coastal Engineering Research Center
Washington, D. C.

TABLE OF CONTENTS

	Page
INTRODUCTION	2
A. DEFINED SCOUR HOLE	8
B. SCOUR BY DUNES	11
C. TWO-DIMENSIONAL JET SCOUR	19
D. SCOUR AROUND A VERTICAL CYLINDER	22
E. SCOUR AROUND A HORIZONTAL CYLINDER	28
CONCLUSIONS	32
ACKNOWLEDGMENTS	33
APPENDIX--NOTATION	34

LIST OF FIGURES*

Figure No.	Title	Page Mentioned
1	Defined Scour Hole	8
2	Sediment-Transport Rate (Defined Scour Hole)	9
3	Dune Amplitude (Oscillatory Flow)	14
4	Dune Amplitude (Uni-directional Flow)	15
5	Sediment-Transport Rate (Dunes)	16
6	Scour Hole (Jet)	19
7	Sediment-Transport Rate (Jet)	20
8	Scour Depth versus Time (Jet)	21
9	Sediment-Transport Rate (Vertical Cylinder)	23
10	Scour Depth versus Time (Vertical Cylinder)	24
11	Maximum and Minimum Scour Depths (Vertical Cylinder)	26
12	Sediment-Transport Rate (Horizontal Cylinder)	30
13	Settlement versus Time (Horizontal Cylinder)	31

*The figures are grouped together and are placed immediately following the written portion of the text.

SIMILARITY--LOCALIZED SCOUR

By M. R. Carstens¹, M. ASCE

SYNOPSIS

Similarity criteria are developed for rate of sediment transport and for scour depth of localized scour. The similarity relations are demonstrated for the following localized-scour situations: (A) in a defined scour hole, (B) by two-dimensional dunes, (C) by a two-dimensional jet, (D) around a vertical cylinder, and (E) around a horizontal cylinder.

¹Professor of Civil Engineering, Georgia Institute of Technology, Atlanta, Georgia.

INTRODUCTION

The object of this study is to formulate similarity criteria for localized scour. An intermediate step is to formulate sediment-transport functions of localized scour which are then integrated to obtain scour-depth functions. Inasmuch as localized scour occurs in non-uniform flow regions resulting from obstructions placed in the flow, any sediment-transport function for localized scour will be strongly dependent upon the geometry of the obstruction. Obviously, then, a general sediment-transport function for localized scour is quite unobtainable. Rather the hope would be in analyzing localized-scour experimental results that the fluid, sediment, and flow variables could be grouped separately from the geometric variables. The functional relation between sediment-transport parameter and the geometric parameters would be expected to vary from one scouring situation to another. On the other hand, the functional relation between the sediment-transport parameter and the parameter containing fluid, sediment, and flow variables should be similar from one scouring situation to another.

Localized scour will occur where the water has been accelerated as the water is moved past the obstruction in the stream or where large vortices are generated as the flow separates from the obstruction. In either event the boundary-layer thickness adjacent to the bed where maximum scouring is occurring can be expected to be negligible. The following analysis is predicated upon the assumption that the boundary layer is of negligible thickness in areas of active localized scour. In other words the velocity and velocity distribution in areas of active local scour are assumed to be functions only of the geometry of the obstruction and of the scour hole.

Also the following analysis is based upon the assumption that no sediment is transported into the hole other than the sediment which would slide into the hole down the sides and down the upstream slope. Situations in which sediment is transported into the scour-hole area from upstream are subsequently analyzed by mass-transport continuity assuming that the incoming sediment does not affect the localized scouring process, per se.

The rate of sediment transport can be expected to be a function of the forces on a typical particle on the surface of the bed. The disturbing force on a typical particle is the resultant of the drag and lift forces resulting from the flow around and over the surface particle, that is,

$$\Sigma F_M = C_D K_1 D_g^2 \frac{\rho V^2}{2} + C_L K_1 D_g^2 \frac{\rho V^2}{2} \quad (1)$$

in which

ΣF_M is the disturbing force on the particle;

C_D is the coefficient of drag of the particle;

C_L is the coefficient of lift of the particle;

K_1 is a dimensionless particle-shape factor (projected area);

D_g is the typical grain diameter of the surface particles;

ρ is the density of water; and

V is the fluid velocity adjacent to the bed.

The stabilizing force on a typical particle is the effective weight, that is,

$$\Sigma F_R = (\gamma_s - \gamma) K_2 D_g^3 \quad (2)$$

in which

- ΣF_R is the effective weight of the particle;
- γ_s is the specific weight of the particles;
- γ is the specific weight of water; and
- K_2 is a dimensionless particle-shape factor (volume).

The force ratio is

$$\frac{\Sigma F_M}{\Sigma F_R} = \frac{K_1 \sqrt{C_L^2 + C_D^2}}{K_2} \frac{V^2}{(s - 1) g D_g} \quad (3)$$

The particle shape factors, K_1 and K_2 , are sediment-geometry variables which are independent of the flow situation. The coefficients of lift and drag, C_L and C_D , would, in general, be functions of (a) the particle geometry and geometric arrangement of the surface particles, (b) the Reynolds number, and (c) the velocity distribution in the vicinity of the particle. Since the particles are unstreamlined, since the velocity is large in areas of localized scour, since the fluid (water) has a low viscosity, and since the boundary layer is expected to be of negligible thickness in areas of active scour, a reasonable assumption is that C_L and C_D are also sediment-geometry variables which are independent of the flow situation. In light of these considerations equation (3) is indicative that

$$\frac{\Sigma F_M}{\Sigma F_R} = \left[f \text{ (sediment-grain geometry)} \right] N_s^2 \quad (3a)$$

in which N_s is $V/\sqrt{(s-1)gD_g}$. Hereafter N_s will be referred to as sediment number.

The local rate of scour will vary over the surface of the scour hole. The greatest rate of scour will occur where the fluid velocity is greatest. At this location the scour hole will be the deepest. Since the capacity for pickup and transport will decrease away from the position of greatest depth much of the sediment scoured at the bottom will deposit on the downstream slope of the scour hole. The deposition of the sediment on the downstream slope of the scour hole and the sliding of the sediment down the upstream slope and side of the scour hole results in the wall slope of the scour hole being nearly equal to the angle of repose ϕ of the cohesionless sediment (sediment-grain geometry). The net rate of transport out of the hole Q_s is the transport over the downstream edge. As the scour hole deepens, the lateral limit of the hole is moved further from the flow disturbance. Hence, the rate of transport out of the hole can be expected to decrease drastically as the depth of scour S increases.

Utilizing these geometric concepts as well as the assumption that the sediment transport rate is a function of the force ratio $\Sigma F_M/\Sigma F_R$, equation (3a), a dimensionless form of the sediment-transport function can be hypothesized as follows

$$\frac{Q_s}{VBD_g} = f\left(\left(N_s^2 - N_{sc}^2\right), \frac{S}{L}, \text{disturbance geometry, sediment-grain geometry}\right) \quad (4)$$

in which

- N_{sc} is the lowest value of the sediment number for which scour will occur;
- V is a reference velocity;
- B is the width of the scour hole; and
- L is a pertinent dimension of the obstruction.

In equation (4), the sediment-grain geometry includes not only the variables involving the shape of the bed material but also the gradation. The geometric variable S/L is necessary to establish the stage of the scour-hole development. The reference discharge VBD_g used in the discharge ratio, LHS of equation (4), can be visualized as the approaching water discharge through an area having a width B equal to the scour-hole width and having a height D_g equal to a grain diameter (or some multiple of the grain diameter). The choice of the height D_g rather than the depth of flow is based upon the idea that the pickup and transport of sediment in the active scour area is a function of the flow conditions close to the bed and is essentially independent of the flow conditions in the water some distance above the bed. Of course, this concept is invalid if the water depth is small or if the Froude number is large resulting in appreciable changes in elevation of the water surface which has the effect of changing the flow pattern in addition to the changes resulting from the obstruction and the scour-hole.

If one were to include all of the possible variables upon which the sediment transport rate is dependent, the object of this study would appear hopeless at the outset. Lacking a mathematical model for sediment pickup and transport in non-uniform flow, the writer has been forced to use physical reasoning in order to eliminate many variables having a second-order effect. The validity of the result, equation (4), can only be determined by analyzing the data from different experiments in which the localized scour results from different types of flow obstructions. In the following, localized scour experiments with (A) a defined scour hole, (B) scour associated with dunes, (C) two-dimensional jet scour, (D) scour around a vertical cylinder, and (E) scour around a cylinder lying on the bed, are analyzed in order to formulate sediment-transport functions associated with

localized scour. Subsequent integration involving the sediment-transport functions leads to the relationship of the dependent variables with which to express scour depth as a function of time.

A. DEFINED SCOUR HOLE

In order to study a steady-state localized scour situation, LeFeuvre² studied sediment transport from a scour hole of fixed geometry. The top of the scour hole was the opening formed by the junction of a two-inch diameter transparent plastic pipe with the bottom of the main-flow section which was a three-inch diameter transparent plastic pipe as shown in Figure 1. A machined plastic wedge was fastened inside the vertical two-inch diameter pipe forming a defined scour hole with a sloping (60-degree) upstream wall and with vertical sidewalls. Sediment was forced into the bottom of the scour hole by means of a piston which was moved upward at a uniform rate by means of a system of gears powered by a synchronous motor. By means of various combinations of gears the sediment-feed rate could be varied in finite steps with a total range of 126.5 to 1. During a run, the water discharge through the main-flow section was adjusted by means of a downstream pinch valve until the horizontally oriented vortex within the scour hole could pick up and transport the sediment being forced into the bottom at a uniform rate. In all runs the water discharge was adjusted until the sediment bed was stabilized at the same equilibrium level. A total of 148 runs were made involving variation of sediment-transport rate Q_s^1 and six different sediments.

In LeFeuvre's experiments, the scour depth S and the dimensions of vortex-generating system were fixed with the result that equation (4) is simplified as follows

²LeFeuvre, A. R., "Sediment Transport Functions with Special Emphasis on Localized Scour," Ph.D. Dissertation, Georgia Institute of Technology, Atlanta, Georgia, 1965.

$$\frac{Q_s^1}{VBD_g} = f \left[(N_s^2 - N_{sc}^2), \text{ sediment grain geometry} \right] \quad (4a)$$

The reference velocity V used is the mean velocity in the main flow section since the velocity at a given point within the vortex would be proportional to the velocity of the flow which generates the vortex. The width of the scour hole B is simply the two-inch dimension of the vertical tube.

LeFeuvre determined the zero-transport limit for each of the six sediments. At zero transport the value of N_s is equal to N_{sc} . Values of N_{sc} and sediment properties are listed in TABLE 1.

TABLE 1. PROPERTIES OF SEDIMENTS USED BY LEFEUVRE²

Sediment	Material	Specific Gravity (s)	Diameter D_g (mm)	Standard Deviation σ_g	Angle of Repose ϕ	Porosity P	N_{sc}
1	Nickel	8.75	0.570	1.10	35°	0.501	10.27
2	Sand	2.62	0.585	1.04	47°	0.499	8.70
3	Sand	2.63	0.185	1.24	48°	0.512	8.12
4	Glass	2.47	0.297	1.08	37°	0.513	8.52
5	Glass	2.46	0.106	1.05	40°	0.512	9.64
6	Lucite	1.20	0.250	1.31	40°	0.517	8.81

The experimental results of LeFeuvre's study are presented in Figure 2 in the form of equation (4a). The line shown in Figure 2 is a simple and reasonable approximation of the experimental results for all sediments and for all values of N_s .

$$\frac{Q_s^1}{VBD_g} \propto (N_s^2 - N_{sc}^2)^{5/2} \quad (5)$$

Equation (5) will be utilized in the following sections in analyzing more complicated scouring situations. Reliance upon LeFeuvre's experiment is based upon (a) the absence of free-surface effects, (b) the existence of a steady-state scour hole, (c) the absence of superposed effects such as dunes, and (d) the accuracy with which the variables could be measured (particularly sediment-transport rate). In other scour experiments one or more of the complicating factors listed above occur which makes the task of separating the effect of the sediment number quite difficult.

B. SCOUR BY DUNES

Bed-load transport of sediment by means of a moving dune system is an example of localized scour. Scour occurs on the upstream face of the dune with the scoured material being deposited on the downstream face. The repeating flow pattern of separation at the crest, reattachment in the trough, and contracting flow over the upstream face is a flow situation in which the boundary layer would tend to be of negligible thickness in the area of active scour. Hence a reasonable expectation is that the analysis leading to equation (4a) and that the experimental results leading to equation (5) are likewise applicable to bed-load transport by dunes.

Neither the reason for the existence nor the sequence of development of dunes is well understood at the present time. However, a current study being conducted in the Georgia Tech Hydraulics Laboratory is revealing as to the principal features of the sequence of dune development.

Geometric characteristics and energy dissipation of dunes on a movable bed under oscillatory flow of water are being studied in the Georgia Tech Hydraulics Laboratory. These studies are being conducted in a large U-tube in which the test section is the bottom horizontal leg of the U. The test section is 10 ft. long, 1 ft. high, and 4 ft. wide. The central section of the floor is depressed in order to form a container for the erodible bed material. The erodible bed is 6 ft. long, 4 ft. wide, and 4 in. deep. The sidewalls and top of the test section are transparent plastic in order to permit visual observation of the phenomena occurring within the test section. The vertical legs of the U-tube are also 1 ft. by 4 ft. in dimension. The vertical legs are joined to the horizontal leg so as to form a streamlined flow passage. The free surface of the water in one of the vertical legs serves as a piston. Air is continuously forced into the con-

fined volume above the water. Two large, solenoid-actuated, piston-operated, exhaust valves are used to quickly relieve the excess pressure in the air above the water surface. The exhaust valves are closed for about one-quarter cycle during the time when the water surface is falling in that leg. A float gage in the other vertical leg is joined to a direction-sensing switch which is the first element in a feedback-control system used to close and to open the exhaust valves at the proper time during the cycle. This system oscillates the water in the U-tube with simple harmonic motion at resonant frequency. Equilibrium amplitude can be controlled by adjustment of the air pressure. Air pressure is controlled by means of a bypass valve in the air-supply conduit from the blower. Initial transients are eliminated by means of a separate air system whereby the water levels are initially unbalanced to the desired equilibrium amplitude. Upon release of the initial unbalance, the water oscillates at equilibrium amplitude. The U-tube is also equipped with a mechanism for eliminating the final transient (oscillatory decay) at the end of a run.

As of the present time, the experimental study has been limited to only one bed material, glass beads, having the following properties:

- D_g (geometric mean diameter) - 0.297mm,
- σ_g (geometric standard deviation) - 1.06,
- s (specific gravity) - 2.47, and
- ϕ (angle of repose) - 24° .

Amplitude and period of oscillation are recorded on a direct-writing oscillograph. The float-elevation sensor system consists of an endless, small-diameter, stainless-steel cable which passes over pulleys at the top and bottom in one vertical leg of the U-tube. The endless cable is fastened to a wooden

float. A three-turn potentiometer, which is connected to the axle of the upper pulley, is one leg of a wheatstone bridge. Bridge unbalance is sensed and recorded. The recorder is also equipped with a timing marker which marks pips at one-second intervals on the record. In all runs, the float elevation system is calibrated just before and immediately following a run by making short records at several elevations of the float.

Dune geometry is recorded photographically. After the dune system has attained an equilibrium geometry, a photograph is taken through the transparent sidewall of the test section in order to record the dune configuration of the bed material adjacent to the sidewall.

The traditional concept of incipient motion is of doubtful relevance in relation to the formation of dunes. Incipient-motion condition is normally considered to exist when an appreciable number of particles on the surface of an initially flat bed are moved by the overlying moving fluid. In the oscillatory tests, incipient motion occurred at a sediment number N_s of about 3.9. The maximum velocity is used in computing the sediment number in oscillatory flow. An embryo dune system would spontaneously occur over the entire flat bed when the sediment number attained a value of 4.9. However a dune system would propagate outward from a disturbance placed in the bed when the sediment number was less than 3.9--the incipient motion condition. In fact a dune system was generated during one run in which the sediment number was 1.6. For all runs in which the sediment number was less than 4.9, a half-round bar with a radius of 1/4 in. and a length of 4 ft. was used as the disturbance element. Prior to a run, the disturbance was placed on the bed perpendicular to the direction of the water motion and in the center of the 6 ft. long bed. Inasmuch as all natural stream channels and ocean beds would have disturbance elements on the bed, the conclusion is that

the incipient-motion criterion as determined in the laboratory is probably irrelevant. Generation of the dunes from a disturbance element was noted by Bagnold³. In fact Bagnold also utilized a disturbance element for generating dunes in his experiments. The effect of disturbance elements is mentioned by Simons and Richardson⁴ as being used during one run in an experimental program involving sediment transport in a flume.

The principal features of dunes are shown in Figure 3 in which the dune amplitude η is plotted as a function of the sediment number. The period of the simple harmonic motion was essentially constant, that is $3.52 \text{ sec} < T < 3.56 \text{ sec}$.

If the value of N_s is less than about 6.5 the dune system is two-dimensional. The crests of the dunes are unbroken and are essentially constant in elevation. The crest of the dunes are perpendicular to the direction of the fluid motion. In this range the fluid motion appears to be two-dimensional with line vortices being formed in the lee of the dune crests. Two vortices are formed each cycle in the trough between a pair of adjacent crests. Upon reversal of motion the previously formed vortex is moved back toward the crest upon which it was formed and is ejected into the main flow above the dune system. Being a symmetrical and cyclic motion, the dunes are essentially symmetrical with the crests moving slightly to and fro as scour and deposition occur alternately on each side of the crest. Two-dimensional dunes are geometrically similar as evidenced by the

³Bagnold, R. A., "Motion of Waves in Shallow Water--Interaction between Waves and Sand Bottom," Proceedings, Royal Society, A, Vol. 187, Oct. 8, 1946, pp. 1-18.

⁴Simons, D. B., and E. V. Richardson, "Studies of Flow in Alluvial Channels--Basic Data from Flume Experiments," Colorado State University Report, CER61EVR31, May, 1961, 13 pp. plus 9 figures plus 17 tables.

constancy of the ratio of amplitude to wave length η/λ . For the runs shown in Figure 3 the ratio η/λ was 0.174.

If the value of N_s is greater than 6.5, the flow pattern is no longer two-dimensional. The breakdown of the two-dimensional dune system is progressive. When N_s is about 9 the dunes can be described as sand hills with valleys both across and along the bed. As N_s is increased to greater than 9 the elevation of the peaks of the dunes (sand hills) decrease as shown in Figure 3. At values of N_s greater than 10 the entire surface of the bed is in motion resembling a second fluid under the water. Extrapolation of the measured points shown in Figure 3 is indicative that the flat-bed condition is attained when N_s is about 13.

Similar characteristics between the dunes under oscillatory flow and dunes under uni-directional flow are shown by comparison of Figure 3 with Figure 4. Figure 4 has been prepared from the data of Stein⁵. Stein's experiments were conducted in a 4 ft. wide flume having a length of 100 ft. The bed material was sand having a mean diameter D_g of 0.40 mm and geometric standard deviation σ_g of 1.50. The data shown in Figure 4 are from runs in which the depth of flow was essentially constant, that is, 0.98 ft. $< y < 1.02$ ft. The mean velocity is used in computing the value of the sediment number, N_s . The comparison of the two figures reveals that dune amplitude η increases linearly with increasing values of the sediment number N_s at low values of N_s . In oscillatory flow this region is characterized by two-dimensional dunes with unbroken crests and by geometric similarity. Presumably these key features of the dune system also exist in the dune system generated in uni-directional flow. That two-dimensional

⁵Stein, Richard A., "Laboratory Studies of Total Load and Apparent Bed Loads," Journal of Geophysical Research, Vol. 70, No. 8, April 15, 1965, pp. 1831-1842.

dunes have not been noted by experimenters in uni-directional flow might be the result of the curved crests. In oscillatory flow a new boundary layer forms twice each cycle from the sidewalls. This boundary layer is thin at the maximum stage of development. Consequently the effect of the sidewalls is negligible in oscillatory flow. In contrast, the sidewalls cause a retardation of the flow for an appreciable distance into the main stream of uniform, steady, open-channel flow. In this retarded zone the dune crest would lag behind that in the central zone and the dune amplitude would tend to decrease as the wall is approached. Thus an observer might observe a central region in which the dunes were truly two-dimensional with the crest being curved in plan view as the wall is approached. Simons and Richardson⁴ classify dunes as being ripples and dunes. In reviewing their data, the writer has concluded that the "ripples" of Simons and Richardson are probably equivalent to that "two-dimensional dunes" as designated by the writer.

The preceding observations are indicative that a sediment-transport function could be formulated for transport by dunes which are geometrically similar. Geometric similarity of the scour hole is a requisite condition, that is, two-dimensional dunes. Data of Simons and Richardson⁴ were used in preparing Figure 5. The analogy between Figure 2 for a defined scour hole and Figure 5 for dunes is obvious. In preparing Figure 5 only the runs in which the sediment number N_s was less than 6.5 were used in order to be certain that geometrically similar dunes were being considered. The properties of the eight different sediments are listed in TABLE 2.

TABLE 2. BED MATERIAL USED IN THE COLORADO STATE UNIVERSITY STUDIES

Sediment No.	Material	Mean Diameter D_g (mm)	Geometric Standard Deviation σ_g
1	Sand	0.19	1.30
2	Sand	0.27	1.54
3	Sand	0.28	1.67
4	Sand	0.32	1.57
5	Sand	0.45	1.60
6	Sand	0.47	1.54
7	Sand	0.54	1.52
8	Sand	0.93	1.54

In preparing Figure 5 using the similarity relationship, equation (5), judgement was required in the selection of a value of N_{sc} . The basis of selection is illustrated in TABLE 3. Values of the zero-transport sediment number N_{sc} were selected as being slightly less than the values for which some transport was observed. No attempt was made to explain or to smooth out the somewhat erratic values at N_{sc} as determined from observations.

TABLE 3. SELECTION OF N_{sc}

Sediment	D_g (mm)	Values of the sediment number N_s		N_{sc}
		Lowest Recorded Movement	Lowest Recorded Dunes	
1	0.19	4.03	4.03	3.9
2	0.27	3.66	3.88	3.6
3	0.28	4.00	4.00	3.9
4	0.32	5.25	5.25	3.8 (?)
5	0.45	2.50	2.50	2.4
6	0.47	—	3.91	3.6 (?)
7	0.54	2.90	2.90	2.8
8	0.93	3.28	3.98	3.1

From Figure 5, the sediment-transport rate by dunes (if the sediment number is less than 7 or 8) can be approximated by

$$\frac{Q_s^1}{VBD_g} = 4 (10^{-5}) (N_s^2 - N_{sc}^2)^{5/2} \quad (6)$$

The data are scattered considerably about the function, equation (6), which is shown as a solid line in Figure 5. Considerable scatter of experimental data is to be expected inasmuch as the sediment-transport rate is extremely small. Relative errors of measurement are likely to be large under such conditions. In spite of the scatter, the writer believes that the similarity relationship, equation (5), is shown to be valid for sediment transport by two-dimensional dunes.

C. TWO-DIMENSIONAL JET-SCOUR

Laursen⁶ performed an experiment in which a two-dimensional jet of water was directed over a two-dimensional bed of sand which was initially flat. Laursen observed the development of the scour-hole depth, S , with elapsed time t . The scour-hole geometry remained constant with time. The scour hole had essentially the configuration shown in Figure 6. Three different sizes of quartz sand were used with the properties as listed in TABLE 4.

TABLE 4. SANDS USED IN LAURSEN'S EXPERIMENTS

D_g (mm)	σ_g	ϕ
0.24	1.14	33°
0.69	1.11	33°
1.60	1.25	33°

Each run was executed with a constant value of the jet velocity V .

A study of Laursen's results of scour depth S as a function of time indicates a difference between the early periods and the later periods. The writer's interpretation of this difference is that since the bed was initially flat some material transport (and elapsed time) occurred before the scour-hole geometry was established in the form shown in Figure 6. Only data obtained with established scour-hole geometry are used in the following analysis.

The rate of sediment transport Q_s out of the scour hole shown in Figure 6 is equal to the rate of change of the scour-hole volume V , that is,

$$Q_s = \frac{dV}{dt} \quad (7)$$

⁶Laursen, E. M., "Observations on the Nature of Scour," Proceedings, 5th Hydraulics Conference, University of Iowa Studies in Engineering, Bulletin 34, 1952.

For Laursen's experiment, Figure 6,

$$\frac{Q_s}{B} = \frac{4}{\tan \phi} S \frac{dS}{dt} \quad (8)$$

Using the experimental results of S as a function of t , the sediment-transport rate Q_s out of the scour hole was calculated.

Laursen's results are shown in Figure 7 in the form of equation (4). The reference velocity V is taken to be the velocity of the water issuing from the nozzle. The pertinent dimension L in equation (4) is taken as the thickness of the jet b as shown in Figure 6. The scour-hole width B is simply the channel width since the scour-hole was two-dimensional. Considering the wide range of sediment numbers ($4.6 < N_s < 25.9$) and sediment sizes (D_g of 0.24 mm, 0.69 mm, and 1.6 mm), the similarity relationship, equation (5) appears to apply to the jet-scour study. The function

$$\frac{Q_s}{VBD_g} = 1.9 (10^{-3}) (N_s^2 - 4)^{5/2} \left(\frac{S}{b}\right)^{-4} \quad (9)$$

is a reasonable empirical approximation for the sediment transport rate. The value of N_{sc} was chosen as being two. Since Laursen's jet was directed slightly downward by a lip on the upper flow boundary, the writer felt that the value of N_{sc} would be somewhat lower than for a parallel stream over a flat bed as given in TABLE 3. Detailed study of the 16 individual runs is indicative that equation (9) is a better approximation for the 0.69-mm size than for the smallest and largest sizes. For the 0.24-mm size and for the 1.6-mm size the function appears to be more complex than a simple variation with S^{-4} . In spite of this observation, the similarity criterion of scour, equation (5), appears to be substantiated by the jet-scour experiment.

Finally the scour depth-versus-time function can be formulated. Substituting equation (9) into equation (8),

$$\frac{(S/b)^5}{\tan \phi} \frac{d(S/b)}{d(V_o t/b)} = 4.75 (10^{-4}) (N_s^2 - 4)^{5/2} (D_g/b) \quad (10)$$

Integrating equation (10)

$$\left(\frac{S}{b}\right)^6 = 2.85 (10^{-3}) (N_s^2 - 4)^{5/2} \tan \phi \left(\frac{D_g}{b}\right) \left(\frac{V_o t}{b}\right) + C \quad (11)$$

in which the constant of integration, C, is determined by initial conditions and by the time required for the scour hole to be scoured from the flat bed to the geometry shown in Figure 6. Since the time of adjustment was short this period is ignored and the initial condition that S = 0 when t = 0 is used to determine that C = 0. An example of Laursen's data of scour-depth versus time is shown in Figure 8 for comparison with equation (11).

D. SCOUR AROUND A VERTICAL CYLINDER

As a part of an extensive study of scour around bridge piers, Chabert and Engeldinger⁷ studied scour around single vertical cylinders placed in a recirculating flume. The cylinders were placed at midwidth of a rectangular channel which was 0.8m wide and 21.0m long. The bed of the channel was covered with sand to a depth of 0.3m for a length of 15 m along the channel. Three piles each having a different diameter were placed in the channel during each run with an axial separation of 6.5m along the channel between adjacent cylinders. Runs were made with depths of flow of 100mm, 200mm, and 350mm. The channel slope and discharge were adjusted to obtain uniform flow with the mean velocity ranging from 0.25m/sec to 1.25m/sec. Depths of the scour holes were measured at 15-minute intervals. Tests were made with four different sizes of sands, that is, D_g of 3.08mm, 1.52mm, 0.52mm, and 0.26mm. Measured values of depth of scour S as a function of time t are presented graphically for 75 runs.

Since this analysis is based upon the determination of the sediment-transport rate Q_s out of the scour hole, runs in which bed material was carried into the hole from upstream at an unknown rate could not be utilized. From the data presented only Run 204 could be identified as having no sediment-transport into the hole from upstream.

Study of contour maps of the scour holes is indicative that the scour hole can be closely approximated by an inverted frustum of a right circular cone having a base diameter equal to the pile diameter D and having a side

⁷Chabert, J. and P. Engeldinger, "Etude des Affouillements Autour des Piles de Ponts," Report of the National Hydraulic Laboratory (Chatou, France), Series A, October, 1956.

slope equal to the angle of repose ϕ . The volume V of such a frustum is

$$V = \frac{\pi}{3 \tan \phi} \left(\frac{S^3}{\tan \phi} + \frac{3 DS^2}{2} \right) \quad (12)$$

Differentiating equation (12) and substituting into equation (7)

$$Q_s = \frac{\pi}{\tan \phi} \left(\frac{S}{\tan \phi} + D \right) S \frac{dS}{dt} \quad (13)$$

Using the experimental results of S as a function of t , the sediment-transport rate Q_s was calculated.

The calculated values from Chabert and Engeldinger's results are shown in Figure 9 in the form of equation (4). The reference velocity V is taken as the mean velocity of the approaching flow. The pertinent dimension L in equation (4) is taken as the pile diameter D . The scour-hole width B is $D + (2S/\tan \phi)$. The sediment-transport function as shown in Figure 9 can be represented as

$$\frac{Q_s}{V(D + 2S/\tan \phi) D_g} = 1.3(10^{-5}) (N_s^2 - N_{sc}^2)^{5/2} (S/D)^{-3} \quad (14)$$

Equation (14) is an approximation of the experimentally determined results of Run 204 for D of 50mm and 100mm but not for the pile having a diameter of 150mm. The implication is that free-surface effects are significant if $y/D < 2$.

Scour depth as a function of time can be reconstructed by substituting equation (14) into equation (13).

$$\left(\frac{1}{\tan \phi} \left(\frac{S/D + \tan \phi}{2S/D + \tan \phi} \right) \left(\frac{S}{D} \right)^4 \right) \frac{d(S/D)}{d(Vt/D)} = 4.14 (10^{-6}) (N_s^2 - N_{sc}^2)^{5/2} \left(\frac{D_g}{D} \right) \quad (15)$$

Integrating equation (15) and letting $S = 0$ when $t = 0$

$$\begin{aligned} 4.14 (10^{-6}) (N_s^2 - N_{sc}^2)^{5/2} \left(\frac{D_g}{D} \right) \left(\frac{Vt}{D} \right) &= \frac{(S/D)^5}{\tan \phi} + \frac{(S/D)^4}{16} \\ &- \frac{(\tan \phi)(S/D)^3}{24} + \frac{(\tan \phi)^2(S/D)^2}{32} - \frac{(\tan \phi)^3(S/D)}{32} \\ &+ \frac{(\tan \phi)^4}{64} \ln \left(\frac{2(S/D)}{\tan \phi} + 1 \right) \end{aligned} \quad (16)$$

The integrated scour-depth function, equation (16), as well as the experimentally determined results of Run 204 are shown in Figure 10.

The above analysis, which pertains to a limited range of velocities at which scour occurs around the cylinder but does not occur in the bed material away from the pile, can be extended to include the typical case in which sediment is carried into the scour hole from upstream. The principal assumption is that the incoming sediment does not affect the localized scouring process adjacent to the pile. With sediment inflow into the scour hole equation (7) is modified as follows

$$Q_s(\text{out}) - Q_s(\text{in}) = \frac{dV}{dt} \quad (17)$$

The rate of sediment transport out of the scour hole, $Q_s(\text{out})$, is evaluated from equation (14). The rate of sediment transport into the scour hole, $Q_s(\text{in})$, would have to be evaluated by means of a bed-load transport equation such as equation (6). Substituting equations (6), (12), and (14) into equation (17)

$$1.3 (10^{-5})(N_s^2 - N_{sc1}^2)^{5/2} VD_g \left(\frac{2S}{\tan \phi} + D \right) \left(\frac{S}{D} \right)^{-3} \\ - \frac{4 (10^{-5})(N_s^2 - N_{sc2}^2)^{5/2}}{P} VD_g \left(\frac{2S}{\tan \phi} + D \right) = \frac{\pi}{\tan \phi} \left(\frac{S}{\tan \phi} + D \right) S \frac{dS}{dt} \quad (18)$$

in which P is the porosity of the bed material. In equation (18) the sediment number N_s for the pile and for the bed would be identical. However the zero-transport sediment number N_{sc1} of the pile would be less than N_{sc2} of bed by virtue of higher velocities around the sides of the pile. For irrotational flow, the velocity at the sides of the cylinder is twice the approach velocity. Therefore a reasonable approximation is that

$$N_{sc1} = \frac{N_{sc2}}{2} \quad (19)$$

A further reasonable approximation for use in equation (18) is that $P = 0.5$ for all bed materials.

In order to illustrate the various aspects of scour around a pile with sediment inflow, the following discussion will be restricted to the experiments of Chabert and Engeldinger⁷ with bed material having a mean diameter D_g of 3.08mm. From a study of the data, the value of N_{sc2} appears to be 2.24.

The first topic of discussion is that of terminal scour depth S_T for which the RHS of equation (18) would be zero. In this case and with the previously stated numerical values equation (18) reduces to

$$1.3 (N_s^2 - 1.64)^{5/2} \left(\frac{S_T}{D} \right)^{-3} - 8 (N_s^2 - 5.02)^{5/2} = 0 \quad (20)$$

Solving for the terminal-depth-of-scour ratio

$$\frac{S_T}{D} = 0.546 \left(\frac{N_s^2 - 1.64}{N_s^2 - 5.02} \right)^{5/6} \quad (21)$$

Equation (20) is displayed in Figure 11. Figure 11 is a graph of the depth of scour around vertical cylinder. The maximum and minimum depths were obtained from data. The oscillation of scour depth for sediment numbers greater than 2.24 is undoubtedly the result of dunes moving downstream past the cylinder. As shown in Figure 11, equation (20) appears to bear some relation to the minimum scour depth but not to the maximum. In any event, the oscillating scour depth resulting from dune passage illustrates a major problem of movable-bed model studies. Namely, the magnitude of scour around an object is related to the size of the object whereas the dune amplitude and flow pattern over the dunes are not. Yet the flow pattern over the dunes can result in significant alteration of the flow pattern within the scour hole as illustrated in Figure 11.

The region of localized scour shown in Figure 11 is restricted to the range of sediment numbers between 1.12 and 2.24. In other words, with this bed material, model tests would have to be conducted within a narrow range of sediment numbers in order to avoid the complications introduced by dunes. The other alternative would be to conduct the tests at a high value of the sediment number, say 15, where the bed is again flat. Model testing at a high value of the sediment number would not only involve sediment transport into the hole but may introduce a flow-pattern disturbance resulting from gravity-waves. These difficulties enhance the value of the studies of LeFeuvre² and Laursen⁶ in which neither the problem of incoming sediment, gravity waves, nor passage of dunes through the scour area existed.

A terminal scour depth is unquestioned when sediment is being transported into the scour hole from upstream. In fact an expression for terminal scour was derived, equation (21), by simply equating the transport rate out of the hole by localized scour to the transport rate into the hole by bed-load movement. On the other hand, in the absence of transport into the hole, equation (16) is indicative that no terminal depth exists. The nature of the scour function as shown in Figure 10 is such that scour depth increases at a progressively slower rate as time passes. Run 20⁴ shown in Figure 10 was continued for 40.5 hours yet there is no indication of a terminal condition. The writer is of the opinion that terminal scour depth is too poorly defined to be useful as an experimental variable as has been suggested by some.

E. SCOUR AROUND A HORIZONTAL CYLINDER

Scour around a cylinder lying on a movable bed and in oscillatory flow is being studied in the Georgia Tech Hydraulics Laboratory. These studies are being performed in the large U-tube described previously in B. SCOUR BY DUNES. The cylinders are aluminum with a length-to-diameter ratio of four. Three different cylinders are used having diameters of 8.76 cm, 4.32 cm and 2.54 cm. The bed material is the 0.297-mm diameter glass beads which were described previously.

Scour-hole development is determined by visual observation of the settlement of the cylinder into the scour hole. The telescope of a cathetometer is attached to a traversing mechanism such that an observer can raise or lower the telescope by operating a crank. The telescope is attached to a differential transformer in order that the elevation of the axis of the telescope can be recorded on a direct-writing oscillograph.

The transient data are recorded by means of a two-channel direct-writing oscillograph. One channel is utilized to record the elevation of the telescope of the cathetometer. The other channel is utilized to record the water-surface elevation (actually float elevation) in one of the vertical legs. The recorder is also equipped with a timing marker which marks pips at one-second intervals on the record.

Immediately prior to a run, both the telescope-elevation and water-level-elevation systems were calibrated directly by making short records at several elevations of the telescope and of the float.

During a run, one observer would start the oscillatory motion at the preset equilibrium amplitude while the other observer maintained the crossed hairs of the telescope on the top of the cylinder as seen through the sidewall of the test section.

Immediately following a run the elevation-recording instruments were again calibrated.

The cylinder settles into the scour hole in a stepwise manner. The region of greatest scour is at the ends of the cylinder. The scour hole is enlarged under the cylinder from the ends. This action continues until the central support is insufficient to support the cylinder at which time the cylinder drops suddenly. The process is repetitive. The cylinder axis always remains perpendicular to the direction of water motion.

In order to avoid the effect of dunes upon the flow pattern within the scour hole, settlement runs are made with a high value of the sediment number. Referring to Figure 3, the sediment number should be about 13 in order for the bed to be flat. A sediment number of 13 could not be achieved in these tests by virtue of an equipment limitation which corresponds to a total amplitude of oscillation of about 35 in. Thus the maximum attainable sediment number was about 12. Visual inspection of the scour holes was indicative that the effect of dunes was negligible if N_s was greater than 9. In the following, only runs for which $10.3 < N_s < 11.9$ are utilized in order to avoid the effects of dunes. Since the flow is oscillatory, the net rate of sediment-transport from the area away from the hole into the hole is zero even at the high values of N_s at which the surface layer of the bed material is in motion.

Scour hole geometry was determined from contour maps prepared from point-gage surveys and from pairs of stereophotographs.

The contour maps of the scour holes are indicative that the scour hole can be closely approximated by an inverted frustum of a right circular cone having a base diameter of $\ell + 0.24D$ in which ℓ is the length of the cylinder and D is the diameter and having a side slope equal to the angle of repose ϕ . The volume V of such a frustum is

$$V = \frac{\pi}{3} \left(\frac{S^3}{\tan^2 \phi} + \frac{3D (\ell/D + 0.24) S^2}{2 \tan \phi} + \frac{3D^2}{4} (\ell/D + 0.24)^2 S \right) \quad (22)$$

and

$$\frac{dV}{dt} = Q_s = \pi \left(\frac{S^2}{\tan^2 \phi} + \frac{D (\ell/D + 0.24) S}{\tan \phi} + \frac{D^2}{4} (\ell/D + 0.24)^2 \right) \frac{dS}{dt} \quad (23)$$

Using the experimental results of S as a function of t and equation (23), the sediment-transport rate Q_s out of the scour holes was calculated.

A separate experiment was performed to determine the value of N_{sc} . The cylinder was placed on the flat bed. The amplitude of oscillation was increased until movement was observed at the ends of the cylinder. The corresponding sediment number is the zero-transport sediment number, N_{sc} . The value of N_{sc} was found to be 1.2 for the 0.297 mm glas beads.

The calculated values are shown in Figure 12 in the form of equation (4). The reference velocity V is taken to be the maximum velocity of the uniform stream in the test section. The diameter D of the cylinder is taken as the reference dimension of the obstruction. The scour-hole width B is $\ell + 0.24D + (25/\tan \phi)$. The data having the highest order of accuracy are obtained with the largest cylinder. The smallest cylinder settled out of sight in 15 cycles or in 53 seconds. The briefness of the observation time tends to decrease the accuracy of observation since the observer must follow the settlement with the telescope of the cathetometer. Recognizing the order of accuracy, the empirical function shown as a solid line in Figure 12 was selected by giving greater weight to the data for the runs with the largest cylinder.

$$Q_s = \left(f \left(\frac{S}{d} \right) \right) \left(V (\lambda + 0.24D + 2S/\tan \phi) D_g (N_s^2 - N_{sc}^2)^{5/2} \right) \quad (24)$$

Finally the scour-depth function can be formulated. Introducing equation (24) into equation (23) and integrating

$$\pi \int_0^{(S/D)} \frac{\frac{1}{\tan^2 \phi} \left(\frac{S}{D} \right)^2 + \frac{(\lambda/D + 0.24)}{\tan \phi} \left(\frac{S}{D} \right) + \frac{(\lambda/D + 0.24)^2}{4}}{\left(f \left(\frac{S}{D} \right) \right) \left(\frac{\lambda}{D} + 0.24 + \frac{2(S/D)}{\tan \phi} \right)} d \left(\frac{S}{D} \right) = (N_s^2 - N_{sc}^2)^{5/2} (D_g/D)(Vt/D) \quad (25)$$

Experimental data are shown in Figure 13 in the form indicated by equation (25). Equation (25) is identical in form to the previous examples of jet scour, equation (11), and of scour around a vertical cylinder, equation (16). All of these scouring functions are of the form

$$\frac{S}{L} = f \left((N_s^2 - N_{sc}^2)^{5/2} (D_g/L)(Vt/L) \right) \quad (26)$$

CONCLUSIONS

The object of this study is to develop similarity criteria for sediment-transport rate and for scour depth in localized-scour situations. The principal assumption is that in an area of localized scour the velocity and velocity distribution are the result of the disturbance element around which scour was occurring. For flow situations which are free from (a) gravity waves, (b) sediment inflow from upstream, and (c) extraneous influences on the flow pattern such as dunes passing through the scour hole, the following criteria are presented. For sediment-transport rate

$$\frac{Q_s}{(N_s^2 - N_{sc}^2)^{5/2} VBD_g} = f (\text{disturbance element, } S/L, \text{ sediment-grain geometry}) \quad (27)$$

and for scour depth

$$\frac{S/L}{(N_s^2 - N_{sc}^2)^{5/2} (D_g/L)(Vt/L)} = f (\text{disturbance element, sediment-grain geometry}) \quad (28)$$

In order to apply the similarity relation, equation (27) or equation (28), to a given situation of localized scour a minimum of two model tests is required. The first is an empirical determination of the sediment number with zero transport, N_{sc} . The second model test required is for the empirical determination of the RHS of equation (27) or equation (28). The procedure is demonstrated for the case of a horizontal cylinder settling into the scour hole in oscillatory flow.

ACKNOWLEDGMENTS

The writer wishes to acknowledge that the results obtained in the Georgia Tech Hydraulics Laboratory were obtained, in part, from research projects sponsored by The U. S. Navy Mine Defense Laboratory and by The Coastal Engineering Research Center of the U. S. Army Corps of Engineers. The writer particularly wishes to thank Dr. Jasper and Dr. Hogge of the Mine Defense Laboratory for their initial and continuing encouragement for the investigation of similarity criteria. Based upon their initial encouragement, the writer was able to obtain the necessary funds from Georgia Tech for the construction of the unique water tunnel. The assistance of the following colleagues and students is likewise acknowledged: C. S. Martin, F. M. Neilson, H. Majumdar, and L. DeJarnette.

APPENDIX - NOTATION

The following symbols have been adopted for use in this paper:

- B = width of scour hole;
- b = nozzle breadth in Laursen's experiment;
- C = constant of integration;
- C_D = coefficient of drag of sediment particle on surface of bed;
- C_L = coefficient of drag of sediment particle on surface of bed;
- D = cylinder diameter;
- D_g = mean grain diameter of sediment;
- ΣF_M = resultant disturbing force on particle;
- ΣF_R = resultant stabilizing force on particle;
- f = denotes "function of";
- g = acceleration of gravity;
- K_1 = particle shape factor (projected area);
- K_2 = particle shape factor (volume);
- L = reference dimension to characterize flow pattern;
- l = length of cylinder;
- N_s = sediment number, $V / \sqrt{(s-1)gD_g}$;
- N_{sc} = value of sediment number at limit of zero transport;
- P = porosity
- Q_s = volume rate of sediment transport (solids plus voids);
- Q_s^1 = volume rate of sediment transport (solids);
- S = scour depth and settlement depth;
- S_T = terminal scour depth;
- s = ratio of solids density to fluid density;

T = period of oscillatory motion;
 t = time;
 V = reference velocity;
 ∇ = volume of scour hole;
 γ = specific weight of fluid;
 γ_s = specific weight of sediment;
 η = dune amplitude;
 λ = dune wave length;
 ρ = fluid density;
 σ_g = geometric standard deviation (sediment diameter); and
 ϕ = angle of repose.

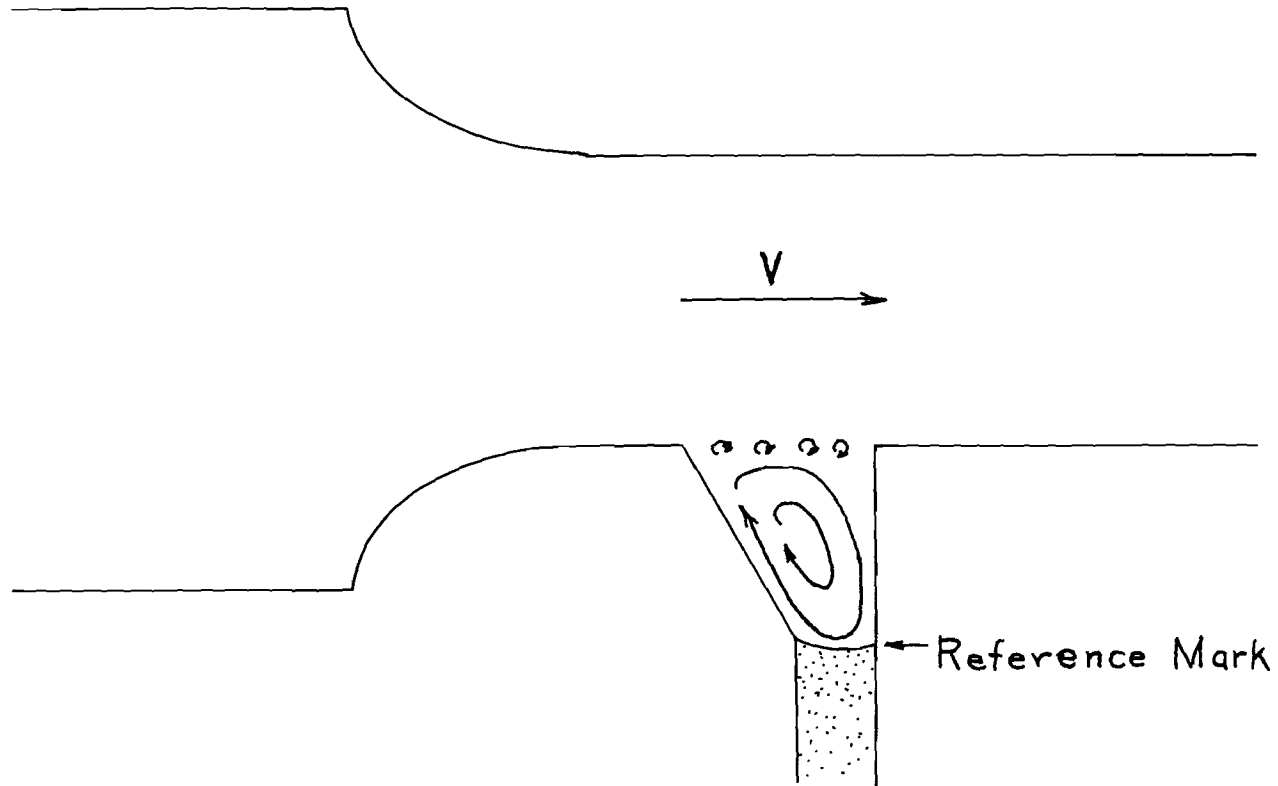


Figure 1. Defined Scour Hole.

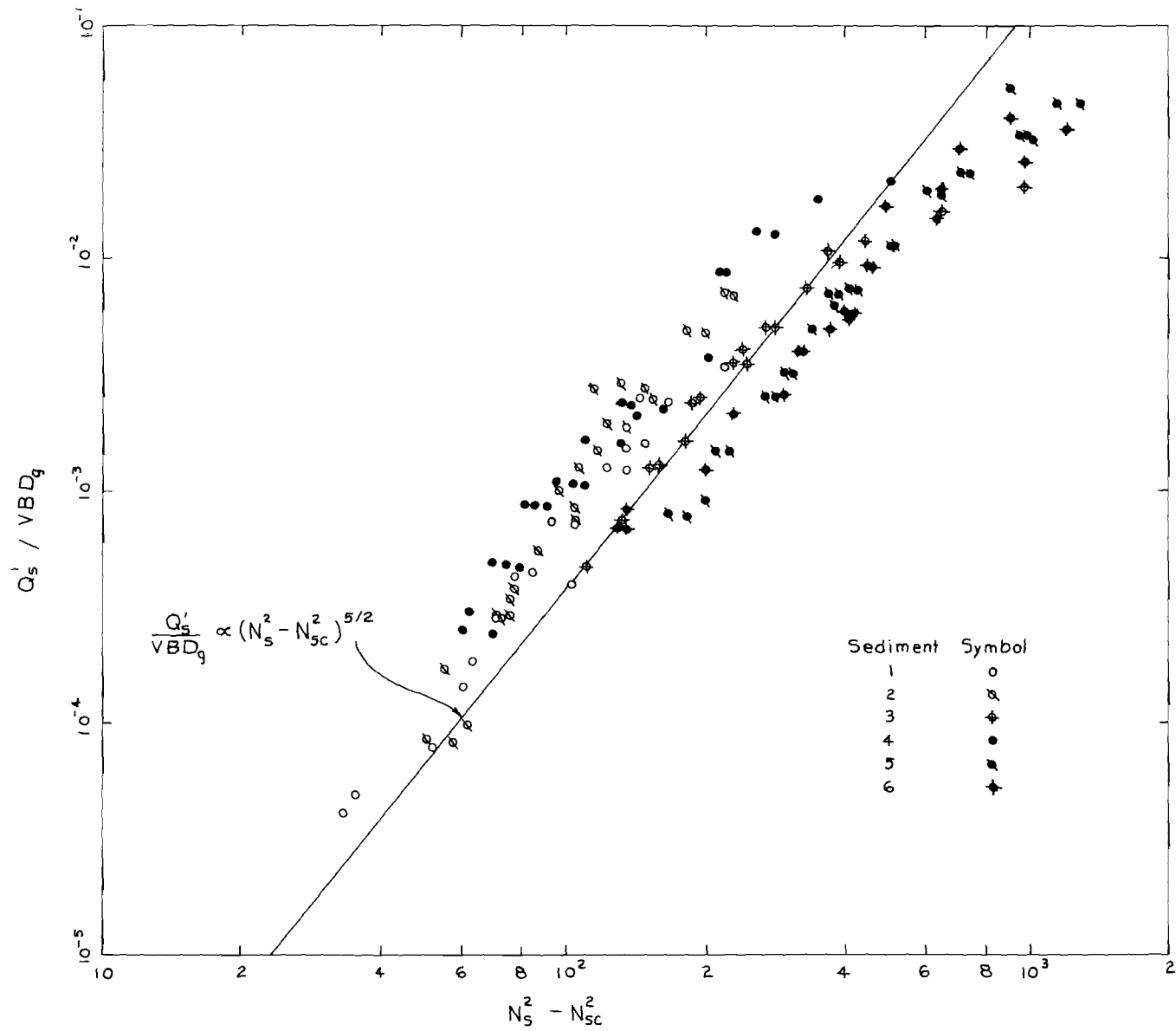


Figure 2. Sediment-Transport Rate (Defined Scour Hole).

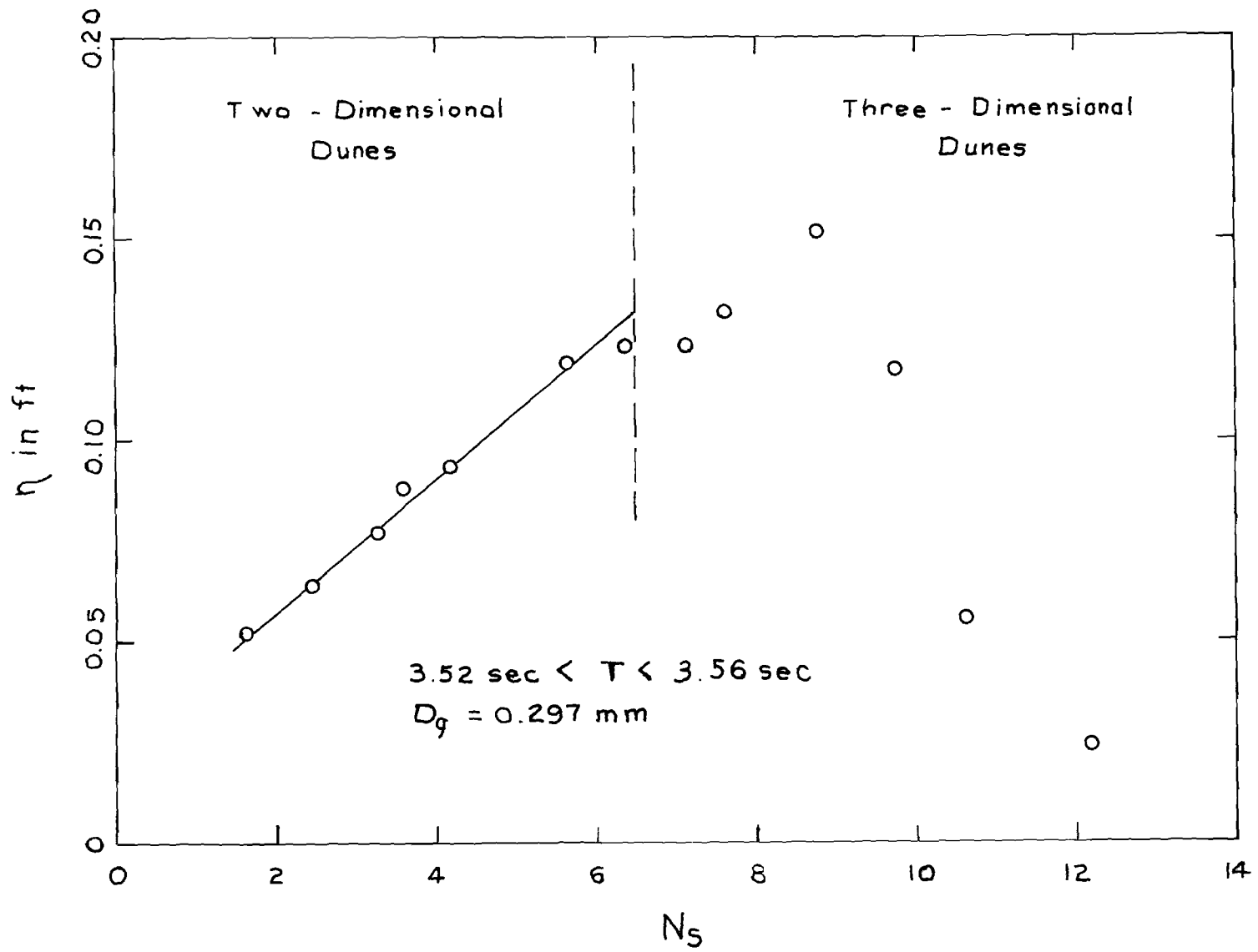


Figure 3. Dune Amplitude (Oscillatory Flow).

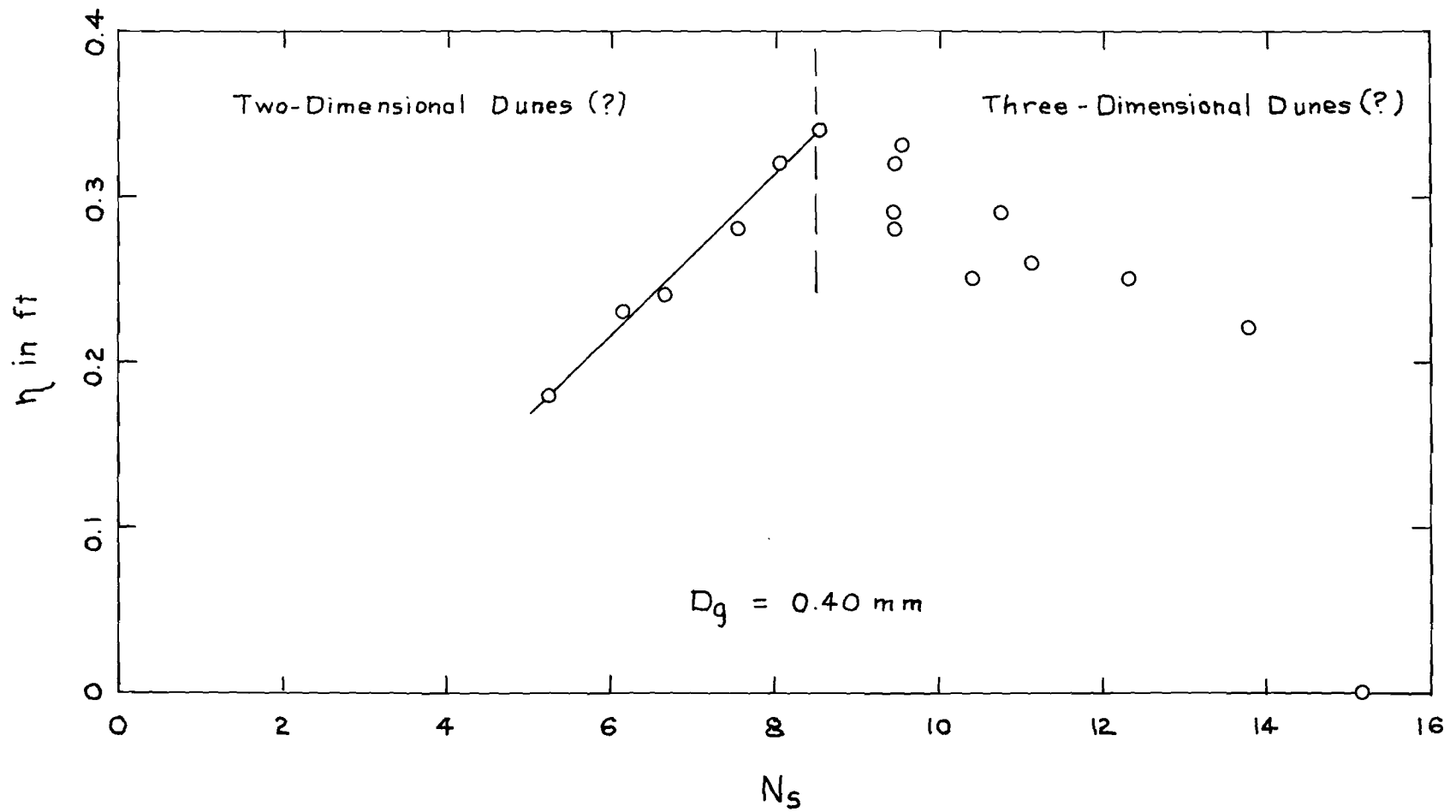


Figure 4. Dune Amplitude (Uni-directional Flow).

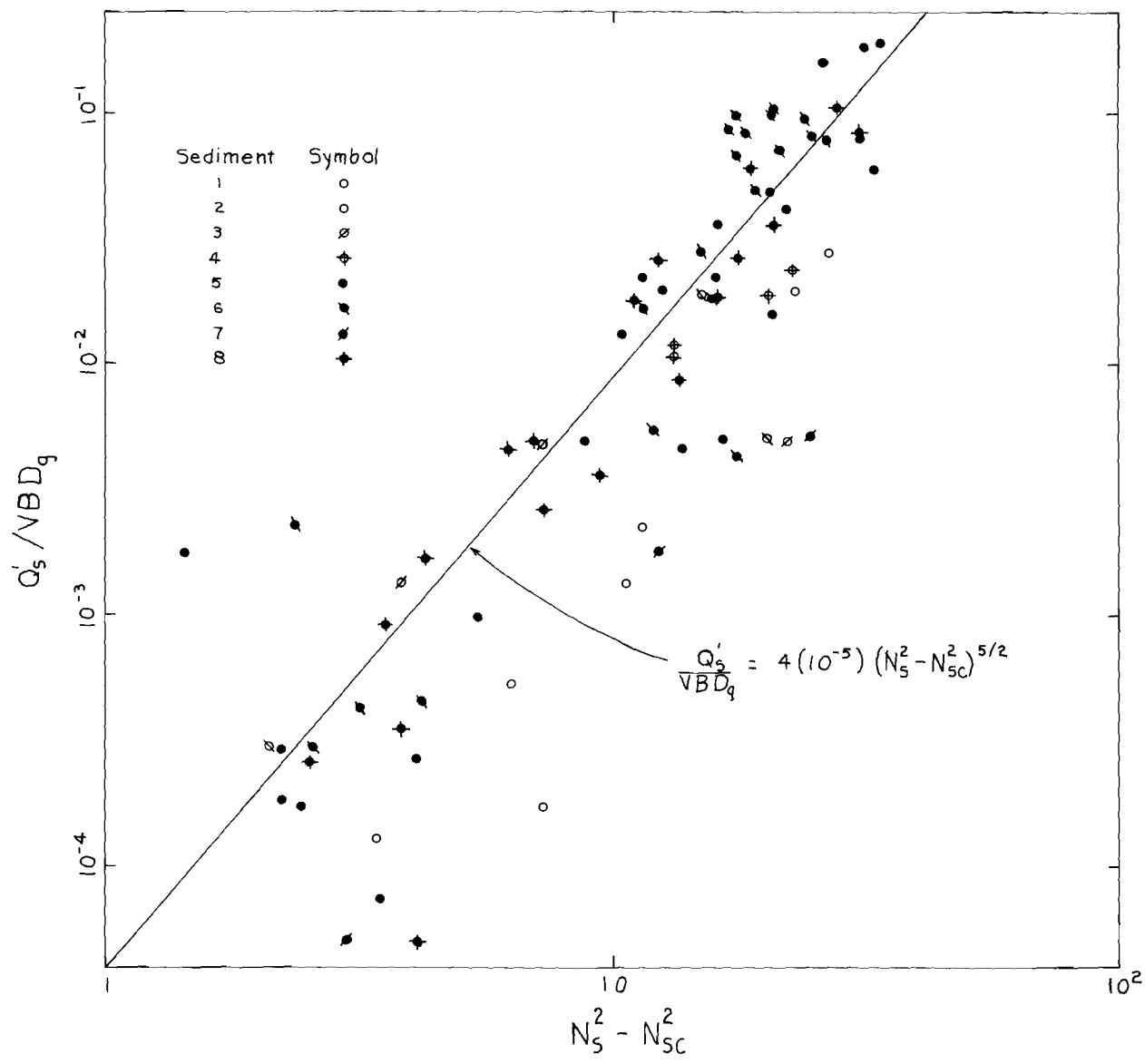


Figure 5. Sediment-Transport Rate (Dunes).

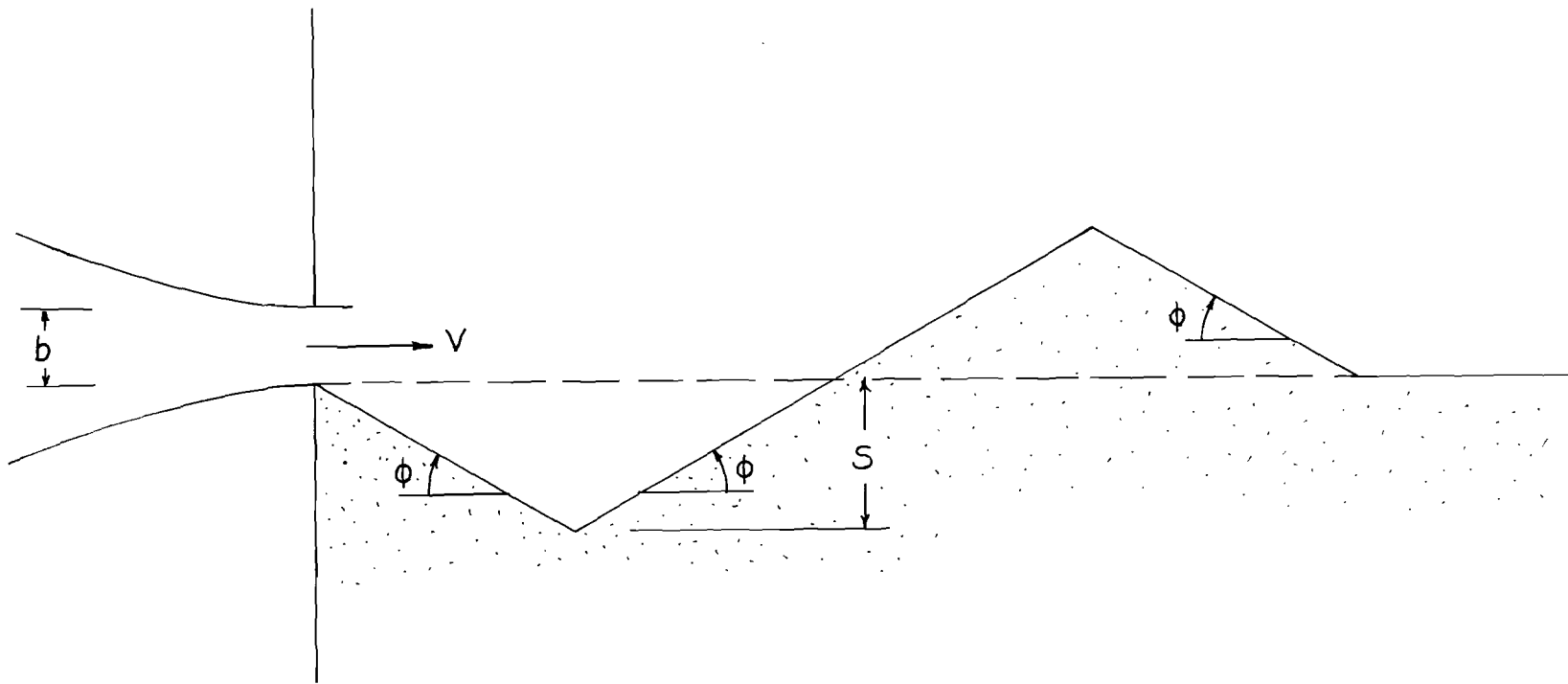


Figure 6. Scour Hole (Jet).

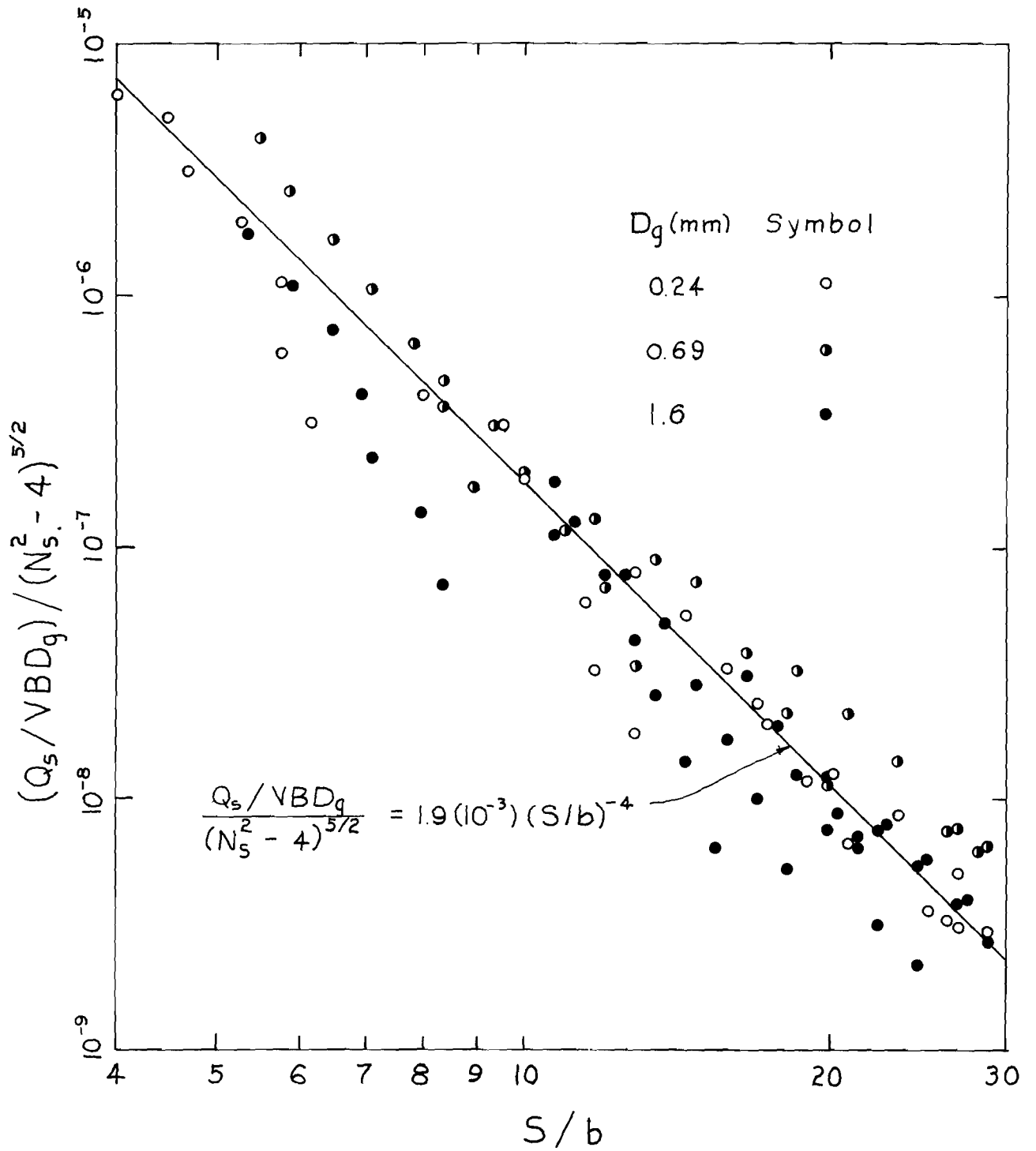


Figure 7. Sediment-Transport Rate (Jet).

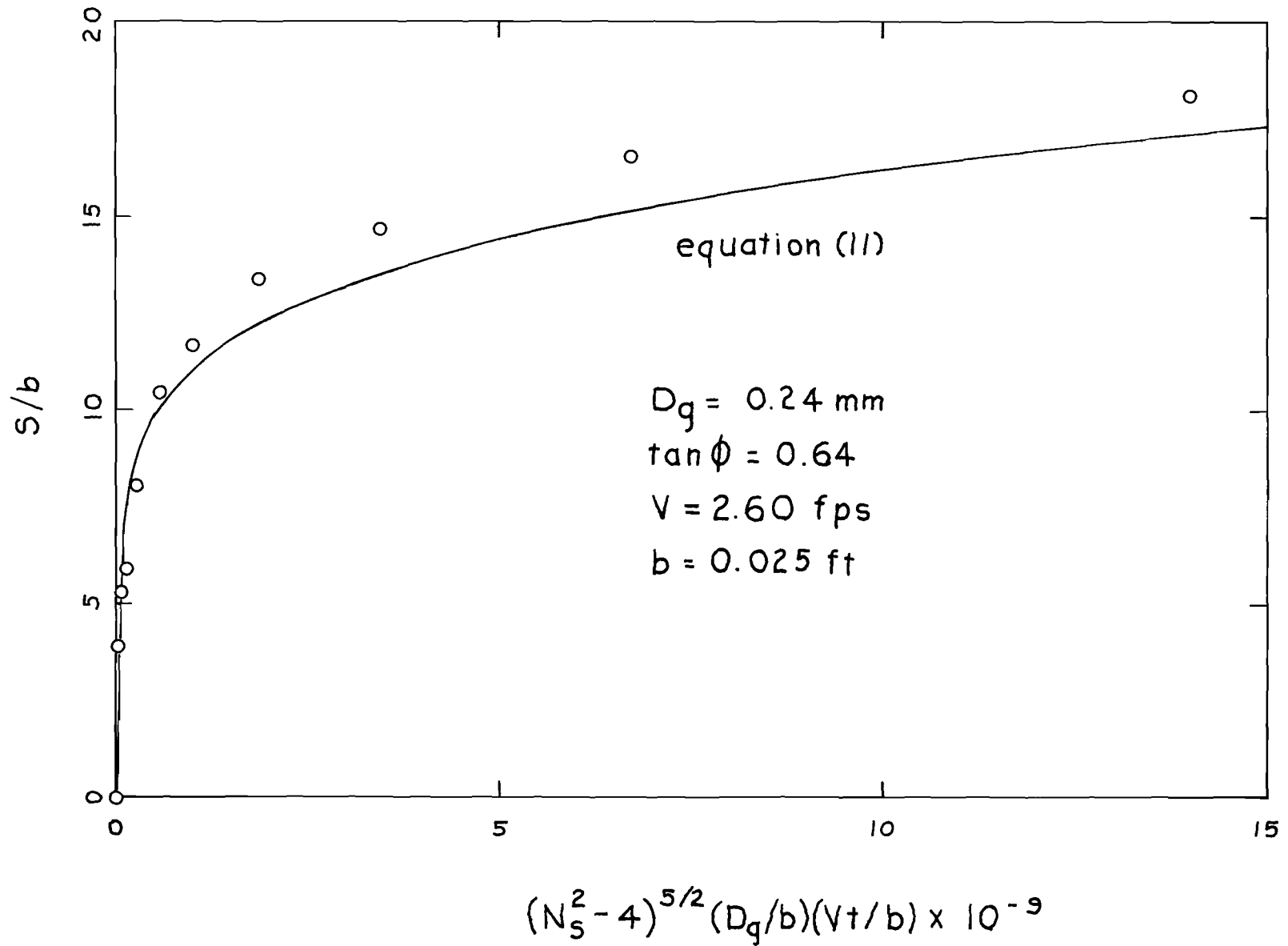


Figure 8. Scour Depth Versus Time (Jet).

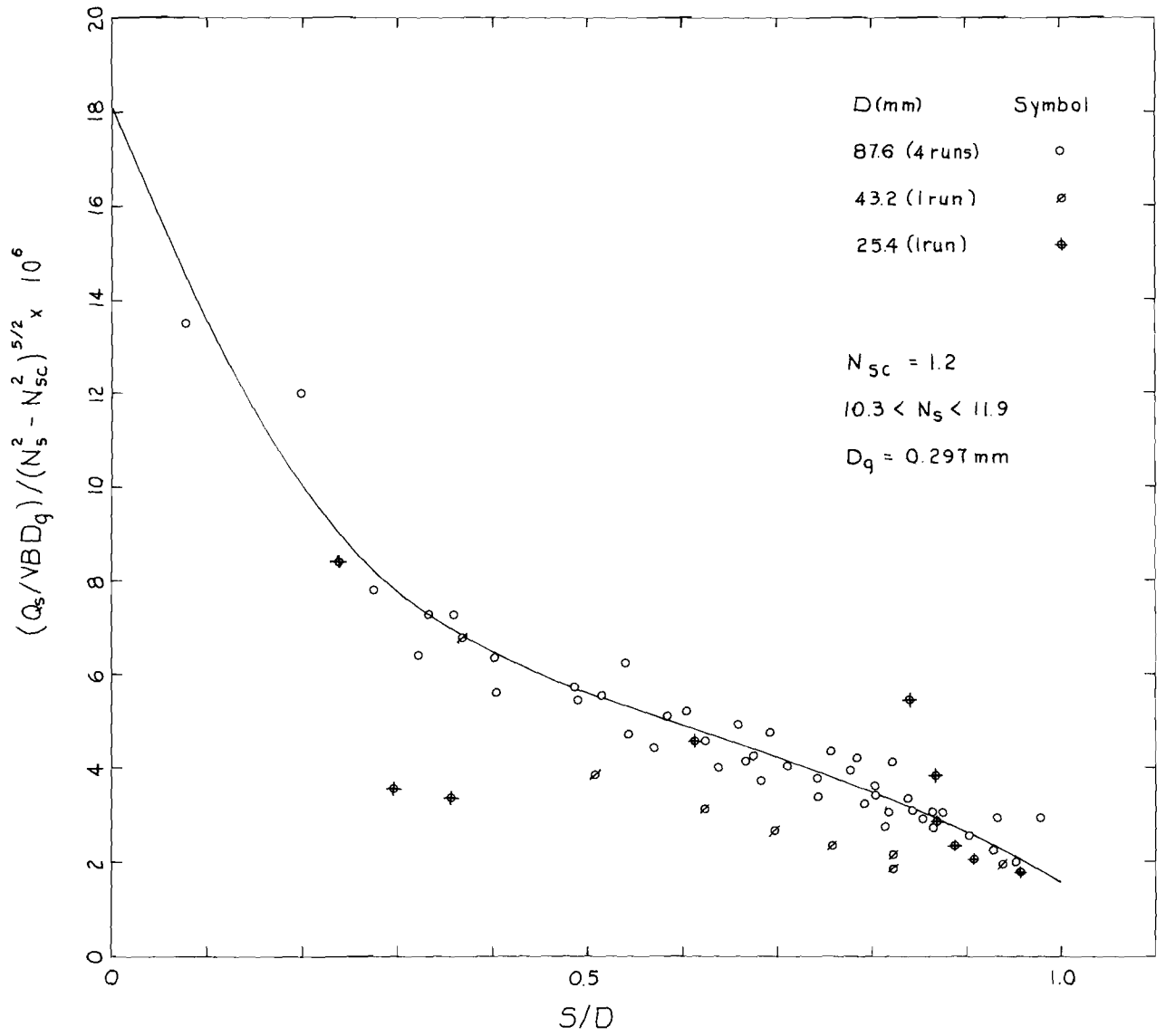


Figure 12. Sediment-Transport Rate(Horizontal Cylinder).

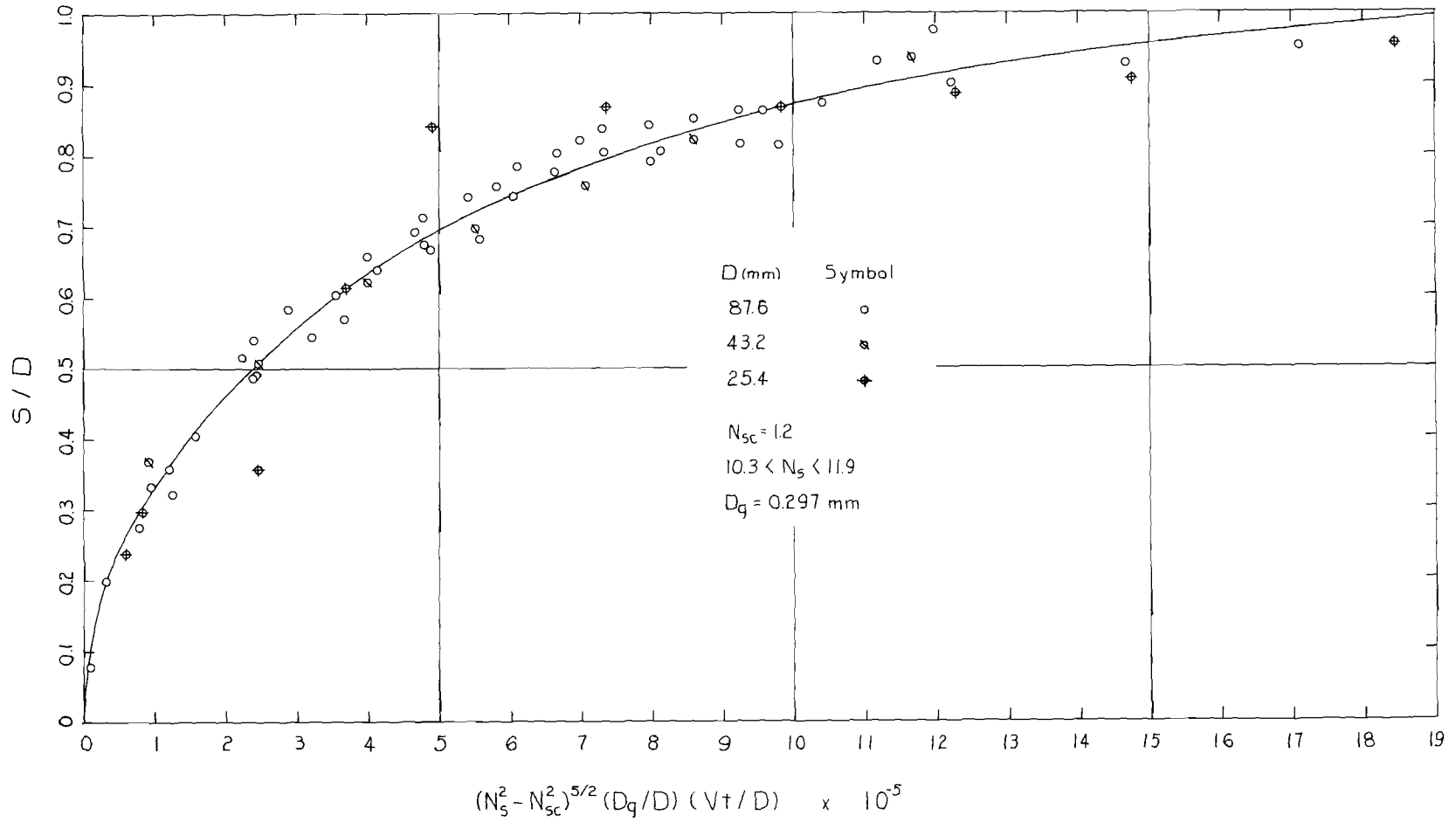


Figure 13. Settlement Versus Time (Horizontal Cylinder).

NOTICE

This document is not to be used by anyone
Prior to ~~12-31~~ 11-20 1967
without permission of the Research Center
and the Experiment Station Staff Office.

QUARTERLY REPORT 6

GEOMETRY OF DUNES

PROJECT A-798

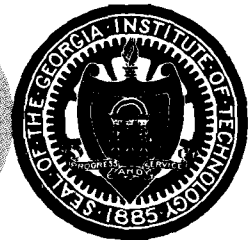
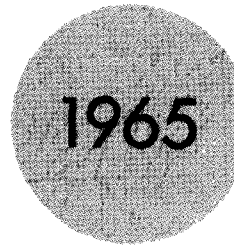
AN ANALYTICAL AND EXPERIMENTAL STUDY
OF BED RIPPLES UNDER WATER WAVES

F. M. NEILSON AND M. R. CARSTENS

Contract No. DA-49-055-CIVENG-65-1.

1 October 1965 to 31 December 1965

Prepared for
Department of the Army
Coastal Engineering Research Center
Washington, D. C.



Engineering Experiment Station
GEORGIA INSTITUTE OF TECHNOLOGY
Atlanta, Georgia

REVIEW

PATENT 2-10 1967 BY *FLL*

FORMAT 2-10 1967 BY *FLL*

GEORGIA INSTITUTE OF TECHNOLOGY
School of Civil Engineering
Atlanta, Georgia

QUARTERLY REPORT 6

GEOMETRY OF DUNES

PROJECT A-798

AN ANALYTICAL AND EXPERIMENTAL STUDY
OF BED RIPPLES UNDER WATER WAVES

By

F. M. NEILSON AND M. R. CARSTENS

CONTRACT NO. DA-49-055-CIVENG-65-1

1 OCTOBER 1965 to 31 DECEMBER 1965

Prepared for
DEPARTMENT OF THE ARMY
COASTAL ENGINEERING RESEARCH CENTER
WASHINGTON, D. C.

ABSTRACT

This report includes the results of the experimental study (through December, 1965) of equilibrium dune characteristics after they have formed on the sea bed by the action of first-order Stokian waves. The experiments at Georgia Tech were performed in a water tunnel in which water is oscillated, in a simple-harmonic manner, through the test section.

Also included in this report are the results obtained by others on dune geometry. Some of these investigations have been conducted in wave channels using surface waves to create water-motion velocities at the bed level. Others have oscillated a tray, on which a sediment bed had been placed, through still water. Data on in situ dunes, for which the dune characteristics were actually measured on the ocean floor, are given by Inman and are also included.

The data on dune geometry are compiled in APPENDIX II.

GEOMETRY OF DUNES

The following qualitative description of dune geometry is expressed in terms of increasing values of the maximum velocity U_m of the oscillatory flow at the bed level.* At some velocity the originally flat bed becomes unstable and a symmetrical two-dimensional system of dunes will cover the bed. At some higher value of the velocity the two-dimensional dune system begins to be transformed into a three-dimensional system in which the dune crests are somewhat irregular in plan and in which the dune crests are uneven in elevation. With an even higher value of the velocity the dune system appears to be a system of sand hills of differing elevations. Finally at an elevated value of the velocity the sand hills (dunes) are completely gone and the bed is again flat.

As of this date no acceptable theory has been presented with which to predict dune geometry as a function of the fluid, flow, and sediment variables. Numerous experimental results are available. However, the range of variables of the various experiments has been quite spotty. Before attempting to present the experimental results which are pertinent to this study, a discussion of the variables and the dimensionless form of these variables will be undertaken in order to explain the manner of presentation of the pertinent experimental results.

The dependent variables of dune geometry are amplitude η and wave length λ . The fluid-property variables are fluid density ρ and the fluid specific weight γ . The fluid specific weight γ is a variable because the stabilizing force of the bed particles is a function of the submerged weight which is proportional to $\gamma_s - \gamma$ or $\Delta\gamma$ in which γ_s is the specific weight of the sediment. The fluid viscosity has been omitted as a variable by virtue of the negligible boundary

*A nomenclature list is included as APPENDIX I.

layer thickness anticipated in the flow occurring over dunes. The fluid flow variables would be any two of the following three variables: the maximum velocity U_m at the bed level, the period T of the oscillatory motion, and the amplitude a of the water motion at bed level. The sediment-property variables are mean diameter D_g , geometric standard deviation σ_g with regard to size, particle shape, and specific weight of the sediment γ_s . The omission of the sediment density ρ_s is founded upon the idea that the inertial reaction of the sediment particles is insignificant in the movement of the bed grains. Since the two specific weights are involved in a known way, that is, by submerged weight, γ and γ_s can be replaced with a single variable $\Delta\gamma$. Thus

$$\eta \text{ or } \lambda = f(U_m, T, \rho, \Delta\gamma, D_g, \sigma_g, \text{particle shape}) \quad (1)$$

or

$$\eta \text{ or } \lambda = f(U_m, a, \rho, \Delta\gamma, D_g, \sigma_g, \text{particle shape}) \quad (2)$$

In dimensionless form the first combination is

$$\frac{\eta}{D_g}, \frac{\lambda}{D_g}, \text{ or } \frac{\eta}{\lambda} = f\left(\frac{T\sqrt{(s-1)g}}{D_g}, \frac{U_m}{\sqrt{(s-1)gD_g}}, \sigma_g, \text{particle shape}\right) \quad (3)$$

and the second is

$$\frac{\eta}{D_g}, \frac{\lambda}{D_g}, \text{ or } \frac{\eta}{\lambda} = f\left(\frac{a}{D_g}, \frac{U_m}{\sqrt{(s-1)gD_g}}, \sigma_g, \text{particle shape}\right) \quad (4)$$

A summary of published data, and also the data obtained in the present investigation, is presented in APPENDIX II according to the parameters shown in equations 3 and 4. A brief description of the various equipment and methods employed by the different authors is included in the following discussion.

1. The purpose of the experiments conducted by Inman and Bowen¹ was to determine the sand transport caused by waves and currents travelling over a horizontal, erodible bed in water 50 cm deep. The experiments were performed in a 94-foot wave channel at the Hydraulics Research Station, Wallingford, England. Water waves were generated, by means of a "paddle-type" wave maker, across a 11 m x 0.61 m sand bed. The waves, thus generated, had a height of 15 cm. The period of the water waves was 1.4 secs for the first series of tests and 2.0 secs for the second series. A steady current of 2, 4, or 6 cm/sec was introduced from the down wave end of the channel to include a drift velocity in the flow phenomena. The bed material used in both series of experiments was a quartz sand which had a median diameter of about 0.2 mm and a specific gravity of 2.65.

2. Kennedy and Falcon² recently investigated the stability of an erodible bed under water waves and also investigated the geometry of the resulting bedforms. Their tests were conducted in a glass-walled channel, 100 ft long, 2.5 ft wide, and 3 ft deep located in the Hydrodynamics Laboratory at M.I.T. Water waves were generated with (a) a "flap-type" wave generator having a range in periods from 0.26 to 3.16 seconds and a maximum wave height of 0.5 ft, and, (b) a "piston-type"

¹Inman, D. L and Bowen, A. J. 1962 Flume experiments on sand transport by waves and currents. Proc. of the Eighth Conf. on Coastal Engineering, Mexico City, Mexico.

²Kennedy, J. F. and Marco Falcon. 1965 Wave-generated sediment ripples, Hydrodynamics Laboratory Report No. 86, M.I.T.

wave generator having a range in periods from 0.6 to 12 seconds and a maximum wave height of one foot. The erodible bed material was placed in a 10 ft reach of the wave tank to a depth of 2.75 inches. Four different types of bed material were used in the tests: these were two different quartz sands and two types of plastic sediments (Opalon and Pelaspan).

The water-wave envelope was observed by means of a resistance-type wave gauge and the ripple amplitude and ripple wave length were obtained by means of a travelling point-gage. The maximum bed velocity and the deviation of a fluid particle from its mean position were computed using the characteristics of the water-wave amplitude-envelope.

For low velocities the sediment ripples were initiated by transverse grooves placed along the test section. The ripples were allowed to grow to an apparent equilibrium size during a run. The values of η and λ given in TABLE 1, APPENDIX, are those of the equilibrium form.

3. The experiments conducted by Yalin and Russell³ were made in a wave channel at the Hydraulics Research Station, Wallingford, England. The purpose of the tests was to investigate a similarity criteria, which was developed using dimensional analysis, for relating ripple height, ripple wave length, and sediment transport in a model situation to the same characteristics in a prototype situation. The dimensions of the bed of the test section were 8.00 m by 0.75 m. The sediment bed was not less than 3 cm deep. Coal, having a mean diameter of 0.355 mm and a specific gravity of 1.48, was used as the sediment in the model whereas perspex, having a mean diameter of 0.480 mm and a specific gravity of 1.19, was used as

³Russell, R. C. H. and Yalin, S. 1962 Similarity in sediment transport due to waves. Proc. of the Eighth Conf. on Coastal Engineering, Mexico City, Mexico.

the sediment in the prototype. The period of the water waves in the model situation was 1.00 seconds and the corresponding period in the prototype situation was 1.82 seconds. The orbit length $2a$ near the bed level was obtained by means of pendulum arrangement consisting of a disc, which was weightless in water, mounted on a spanned steel wire parallel to a ruler. The orbital lengths obtained using this apparatus were used as a calibration relating the orbital length to the height of the generated water waves. The values of η and λ used in preparing TABLE 1 are mean values of a "ripple train" which consisted of at least 20 individual ripples.

4. Inman⁴ investigated the characteristics of the bed forms occurring on the ocean floor located, primarily, in the nearshore area off La Jolla, California. Divers measured the ripple characteristics and photographs were taken of the ripples in situ while the water-wave characteristics were measured on the surface. The Airy theory for waves of small amplitude was used for computing orbital velocities and displacements in regions of deeper water and an adaptation of the solitary wave theory was used for these computations when the waves were near the breaker zone. The observations were taken in depths ranging upwards to 120 feet however ripples were seen, but not measured, at a depth of 170 feet. The sand which comprised the ripples ranged in median diameter from slightly less than 0.1 mm to over 0.6 mm.

5. Bagnold⁵ investigated the characteristics of the forms which develop on an erodible bed as the bed is made to oscillate through still water. The apparatus

⁴Inman, D. L. 1957 Wave-generated ripples in nearshore sands. Beach Erosion Board, Tech. Memo. No. 100.

⁵Bagnold, R. A. 1946b Motion of waves in shallow water. Interaction of waves and sand bottoms. Proc. of the Royal Soc. of London, Vol. 187, series A, pp 1-15.

employed for these series of tests consisted of a cradle, in the shape of an arc, on which the sediment bed was placed. The cradle was made to oscillate through still water and the character of the developing ripples was observed. The tests covered a wide range of amplitudes, ranging from 0.5 to 25 cm, and through a corresponding range of periods. The primary limits governing the speed of oscillation were (a) the minimum speed required for bed forms to develop and (b) the maximum speed allowable before the mass of sediment began slipping over the floor of the cradle. Eight types of sediments were used in these tests; these being two sizes of coal, four sizes of quartz sands, and two sizes of steel sediments. Thus the specific gravity of the sediments covered a significant range; i.e. 7.9 for steel, 2.65 for quartz, and 1.3 for coal. The median diameter of the particles ranged from 0.009 cm to 0.25 cm.

6. The data obtained in the present investigation is also included in APPENDIX II. These experiments were performed in a U-tube water-tunnel in which water-motion oscillations, having a nearly constant period of 3.54 seconds and a variable amplitude, are used to create the bed forms. The sediments used in these tests have been glass beads and also an Ottawa sand. The reader should refer to previous Quarterly Reports for the details of the experimental setup and procedure.

APPENDIX I
NOMENCLATURE

NOMENCLATURE

<u>Symbol</u>	<u>Definition</u>	<u>Dimensions</u> (F, L, T)
a	amplitude of the water-motion near the bed level	L
D_g	median diameter of the bed material	L
f	denotes function of	none
g	acceleration of gravity	LT^{-2}
s	specific gravity	none
T	period of the water-motion oscillations	T
U_m	maximum water-motion velocity at the bed level	LT^{-1}
γ	specific weight of the fluid	FL^{-3}
γ_s	specific weight of the sediment	FL^{-3}
$\Delta\gamma$	submerged specific weight of the sediment	FL^{-3}
η	dune height	L
λ	dune wave length	L
ρ_s	mass density of the sediment	$FT^{-2}L^{-4}$
σ_g	geometric standard deviation of the sediment particle diameter	none

APPENDIX II

TABLE 1

TABLE 1. DUNE GEOMETRY

AUTHOR(S): INMAN AND BOWEN				BED MATERIAL(S): MEDIUM SAND			
D_g MM.	T SEC.	s	η/D_g	λ/D_g	a/ D_g	$U_m/\sqrt{(s-1)g D_g}$	$T\sqrt{(s-1)g/D_g}$
0.290	1.40	2.65	37.9	224.1	169.0	3.21	330.8
0.290	1.40	2.65	34.5	224.1	162.1	3.08	330.8
0.290	1.40	2.65	34.5	224.1	165.5	3.14	330.8
0.290	1.40	2.65	34.5	220.7	165.5	3.14	330.8
0.290	2.00	2.65	51.7	372.4	331.0	4.40	472.5
0.290	2.00	2.65	55.2	351.7	319.0	4.24	472.5
0.290	2.00	2.65	51.7	365.5	320.7	4.26	472.5
0.290	2.00	2.65	55.2	355.2	313.8	4.17	472.5
AUTHOR(S): KENNEDY AND FALCON				BED MATERIAL(S): FINE AND MEDIUM SAND, PELASPAN, OPALUN			
D_g MM.	T SEC.	s	η/D_g	λ/D_g	a/ D_g	$U_m/\sqrt{(s-1)g D_g}$	$T\sqrt{(s-1)g/D_g}$
0.095	1.07	2.67	53.6	320.8	208.5	2.95	444.4
0.095	1.95	2.67	86.6	500.5	625.6	4.85	809.9
0.095	1.95	2.67	117.1	593.5	561.4	4.36	809.9
0.095	2.34	2.67	104.3	574.3	609.6	3.94	971.9
0.095	7.32	2.67	70.6	561.4	3096.0	6.40	3040.4
0.095	7.32	2.67	62.6	532.6	2438.3	5.04	3040.4
0.095	3.86	2.67	179.0	840.6	2694.9	10.56	1603.3
0.320	1.39	2.67	32.6	198.1	152.4	3.04	314.6
0.320	1.57	2.67	36.5	225.7	166.7	2.95	355.3
0.320	1.57	2.67	50.8	267.6	200.0	3.54	355.3
0.320	1.39	2.67	36.5	193.3	147.6	2.95	314.6
0.320	1.57	2.67	39.6	185.7	133.3	2.36	355.3
0.320	1.39	2.67	22.2	143.8	100.0	2.00	314.6
1.000	1.82	1.04	0.0	0.0	24.4	4.54	33.7
1.000	1.82	1.04	0.9	22.2	25.9	4.83	33.7
1.000	1.83	1.04	0.0	0.0	7.6	1.41	33.9
1.000	1.83	1.04	0.0	0.0	16.8	3.11	33.9
1.000	1.83	1.04	1.4	23.0	18.3	3.39	33.9
1.000	2.21	1.04	1.5	30.2	19.8	3.04	41.0
1.000	2.21	1.04	1.8	35.7	22.9	3.51	41.0
1.000	2.24	1.04	0.0	22.2	10.7	1.61	41.5
1.000	2.24	1.04	2.7	30.2	15.2	2.31	41.5

TABLE 1. (CONTINUED)

1.000	2.24	1.04	0.0	0.0	18.3	2.77	41.5
1.000	2.83	1.04	6.7	44.5	29.0	3.47	52.4
1.000	2.93	1.04	3.8	33.4	15.2	1.76	54.3
1.000	1.85	1.04	0.0	0.0	25.9	4.75	34.3
1.000	1.85	1.04	0.0	0.0	38.1	6.98	34.3
1.000	2.35	1.04	1.5	27.7	30.5	4.40	43.6
1.000	2.86	1.04	5.5	42.1	25.9	3.07	53.0
1.000	2.86	1.04	3.7	35.7	36.6	4.34	53.0
0.107	1.11	1.35	0.0	161.2	113.9	3.60	198.9
0.107	1.87	1.35	62.7	326.4	284.8	5.34	335.0
0.107	1.97	1.35	61.8	356.1	242.1	4.31	353.0
0.107	2.39	1.35	0.0	0.0	356.1	5.22	428.2
0.107	2.95	1.35	0.0	0.0	341.8	4.06	528.6
0.107	1.54	1.35	0.0	0.0	199.4	4.54	275.9

AUTHOR(S):
YALIN AND RUSSELL

BED MATERIAL(S):
PERSPEX, CUAL

D_g MM.	T SEC.	s	η/D_g	λ/D_g	a/ D_g	$u_m \sqrt{(s-1)g/D_g}$	$T \sqrt{(s-1)g/D_g}$
0.480	1.82	1.19	19.6	84.0	43.2	2.39	113.4
0.480	1.82	1.19	18.8	97.5	49.9	2.76	113.4
0.480	1.82	1.19	16.6	102.0	63.3	3.51	113.4
0.480	1.82	1.19	16.6	106.0	70.6	3.91	113.4
0.480	1.82	1.19	15.5	110.0	76.4	4.23	113.4
0.480	1.82	1.19	14.3	122.0	88.9	4.92	113.4
0.480	1.82	1.19	12.5	136.0	96.5	5.35	113.4
0.480	1.82	1.19	12.5	143.0	103.5	5.73	113.4
0.480	1.82	1.19	10.4	144.0	105.4	5.84	113.4
0.480	1.82	1.19	8.3	156.0	114.0	6.31	113.4
0.480	1.82	1.19	7.3	158.0	118.4	6.56	113.4
0.480	1.82	1.19	4.2	165.0	126.4	7.00	113.4
0.480	1.82	1.19	2.1	171.0	133.3	7.39	113.4
0.355	1.00	1.48	14.0	61.0	22.2	1.21	115.2
0.355	1.00	1.48	16.7	74.5	28.8	1.57	115.2
0.355	1.00	1.48	19.5	82.5	36.5	1.99	115.2
0.355	1.00	1.48	19.7	87.5	42.0	2.29	115.2
0.355	1.00	1.48	19.3	89.0	47.2	2.58	115.2
0.355	1.00	1.48	19.3	91.5	51.3	2.80	115.2
0.355	1.00	1.48	16.9	101.0	59.5	3.25	115.2
0.355	1.00	1.48	16.8	107.5	69.0	3.77	115.2
0.355	1.00	1.48	15.5	115.0	80.4	4.38	115.2
0.355	1.00	1.48	15.5	117.0	81.6	4.45	115.2
0.355	1.00	1.48	15.3	120.5	83.9	4.58	115.2

TABLE 1. (CONTINUED)

AUTHOR(S): INMAN		BED MATERIAL(S): NATURAL BEACH SANDS					
D_g MM.	T SEC.	s	η/D_g	λ/D_g	a/D_g	$U_m/\sqrt{(s-1)gD_g}$	$T\sqrt{(s-1)g/D_g}$
0.118	10.00	2.65	38.7	490.8	8221.7	13.94	3704.5
0.153	7.00	2.65	65.7	478.1	2663.2	7.35	2277.3
0.145	8.00	2.65	84.1	609.6	2408.7	5.66	2673.5
0.152	10.00	2.65	80.2	521.3	2553.1	4.91	3264.0
0.147	10.00	2.65	41.5	435.4	5609.8	10.62	3319.0
0.157	11.00	2.65	38.8	504.7	5098.0	9.07	3532.7
0.137	10.00	2.65	44.5	556.2	5665.2	10.35	3438.0
0.124	9.20	2.65	73.7	589.9	3958.9	7.48	3324.6
0.117	8.00	2.65	104.2	729.4	5638.5	11.90	2976.2
0.120	6.00	2.65	127.0	762.0	2425.4	6.91	2204.1
0.117	6.20	2.65	156.3	1016.0	1285.3	3.50	2306.6
0.118	8.60	2.65	51.7	568.2	5303.0	10.46	3185.8
0.124	9.70	2.65	73.7	737.4	2656.2	4.76	3505.3
0.129	10.00	2.65	106.3	685.2	2256.2	4.00	3543.0
0.126	10.10	2.65	60.5	604.7	3499.5	6.07	3620.8
0.118	9.50	2.65	51.7	594.1	3124.3	5.58	3519.2
0.114	11.00	2.65	53.5	668.4	7020.9	10.64	4145.8
0.117	13.00	2.65	52.1	599.2	6467.7	8.40	4836.3
0.135	6.00	2.65	169.3	1377.2	1149.8	2.61	2770.7
0.127	5.00	2.65	96.0	744.0	763.9	2.69	1785.4
0.127	5.00	2.65	96.0	744.0	763.9	2.69	1785.4
0.115	8.00	2.65	212.0	1643.2	1349.8	2.83	3002.0
0.106	6.50	2.65	143.8	1121.4	1189.8	2.94	2540.5
0.107	6.00	2.65	170.9	940.0	2176.1	5.86	2334.1
0.102	10.40	2.65	47.8	747.0	5935.1	9.00	4143.8
0.102	8.50	2.65	65.7	776.9	3638.1	6.75	3386.8
0.102	13.00	2.65	89.6	776.9	5564.2	6.75	5179.8
0.103	5.00	2.65	177.5	1094.9	588.7	1.87	1982.5
0.109	13.00	2.65	167.8	1090.5	2892.7	3.63	5010.7
0.106	13.00	2.65	129.4	747.6	4759.3	5.89	5081.1
0.106	10.00	2.65	143.8	1408.9	3203.4	5.15	3908.5
0.109	12.00	2.65	167.8	1146.4	2136.1	2.90	4625.2
0.113	12.00	2.65	134.9	1024.9	2575.7	3.56	4542.6
0.110	9.00	2.65	152.4	914.4	793.8	1.44	3453.1
0.556	9.00	2.65	164.5	1030.6	2434.1	9.96	1535.9
0.484	9.00	2.65	188.9	1114.6	2164.8	8.26	1646.2
0.637	15.00	2.65	239.2	1339.7	2513.0	6.60	2391.6
0.276	9.70	2.65	165.6	1325.2	2216.3	5.93	2349.5

TABLE 1. (CONTINUED)

0.325	10.30	2.65	206.3	1425.5	1076.1	2.94	2299.1
0.457	10.00	2.65	246.8	1553.9	849.2	2.83	1882.4
0.415	13.00	2.65	257.0	1703.9	1063.7	2.60	2567.9
0.432	12.00	2.65	289.3	1883.7	1212.7	3.28	2323.3
0.441	11.00	2.65	304.1	1762.4	1028.5	3.07	2107.9
0.441	11.00	2.65	290.3	1824.6	1028.5	3.07	2107.9
0.514	12.00	2.65	266.8	1571.4	792.7	2.34	2129.9
0.398	8.00	2.65	237.4	1569.9	975.0	3.80	1613.7
0.359	11.00	2.65	339.6	2207.4	1189.1	3.20	2336.2
0.470	9.70	2.65	311.3	1945.4	901.0	3.14	1800.5
0.525	10.30	2.65	276.7	1741.6	571.0	1.98	1808.9
0.432	11.00	2.65	275.2	1785.0	802.9	2.37	2129.7
0.448	12.00	2.65	299.3	1850.5	1039.5	2.86	2281.4
0.913	13.00	2.65	217.0	1151.7	897.9	3.26	1731.3
0.460	10.00	2.65	196.8	1192.6	1265.4	4.24	1876.2
0.457	10.00	2.65	166.7	1167.1	1273.7	4.25	1882.4
0.195	0.70	2.65	31.3	218.8	69.7	2.17	201.7
0.123	0.70	2.65	61.9	371.7	110.4	2.73	254.0
0.344	3.50	2.65	336.7	2037.8	641.6	5.31	759.4
0.595	3.50	2.65	82.0	537.9	342.4	3.73	577.4
0.221	2.12	2.65	75.9	455.1	325.7	3.57	573.9

AUTHOR(S):
BAGNOLD

BED MATERIAL(S):
QUARTZ, STEEL, COAL

D_g MM.	T SEC.	s	η/D_g	λ/D_g	a/D_g	$U_m/\sqrt{(s-1)g D_g}$	$T\sqrt{(s-1)g/D_g}$
0.09		2.65		644.4	3555.6		
0.09		2.65		644.4	2111.1		
0.09		2.65		644.4	1444.4		
0.09		2.65		633.3	733.3		
0.09		2.65		522.2	433.3		
0.09		2.65		355.6	211.1		
0.09		2.65		277.8	165.6		
0.09		2.65		161.1	80.0		
0.16		2.65		506.2	2000.0		
0.16		2.65		500.0	418.6		
0.16		2.65		237.5	118.7		
0.36		2.65		347.2	888.9		
0.36		2.65		347.2	527.6		
0.36		2.65		347.2	413.9		
0.36		2.65		347.2	361.1		
0.36		2.65		333.3	250.0		
0.36		2.65		261.1	183.3		

TABLE 1. (CONTINUED)

D_g MM.	T SEC.	s	η/D_g	λ/D_g	a/D_g	$U_m \sqrt{(s-1)gD_g}$	$T \sqrt{(s-1)g/D_g}$
0.36		2.65		133.3	77.8		
0.36		2.65		97.2	49.2		
0.80		2.65		225.0	400.0		
0.80		2.65		231.3	312.5		
0.80		2.65		225.0	237.5		
0.80		2.65		231.3	186.3		
0.80		2.65		225.0	162.5		
0.80		2.65		221.3	115.0		
0.80		2.65		152.5	82.5		
0.80		2.65		85.0	48.8		
0.36		1.30		305.6	527.8		
0.36		1.30		283.3	250.0		
0.36		1.30		227.8	183.3		
0.36		1.30		180.6	108.3		
0.36		1.30		144.4	75.0		
0.36		1.30		113.9	51.4		
2.50		1.30		82.0	128.0		
2.50		1.30		82.0	76.0		
2.50		1.30		80.0	52.0		
2.50		1.30		64.0	36.4		
2.50		1.30		46.0	26.8		
2.50		1.30		26.4	17.6		
0.36		7.90		291.7	888.9		
0.36		7.90		291.7	527.8		
0.36		7.90		272.2	361.1		
0.36		7.90		230.6	255.6		
0.36		7.90		194.4	183.3		
0.36		7.90		147.2	108.3		
0.36		7.90		77.8	41.4		
0.60		7.90		300.0	316.7		
0.60		7.90		233.3	216.7		

AUTHOR(S):
GEORGIA TECH

BED MATERIAL(S):
GLASS BEADS, UTTAWA SAND

D_g MM.	T SEC.	s	η/D_g	λ/D_g	a/D_g	$U_m \sqrt{(s-1)gD_g}$	$T \sqrt{(s-1)g/D_g}$
0.297	3.56	2.47	57.5	375.6	303.6	2.43	784.6
0.297	3.56	2.47	70.9	385.9	303.6	2.43	784.6
0.297	3.56	2.47	69.3	353.0	303.6	2.43	784.6
0.297	3.56	2.47	59.8	390.0	303.6	2.43	784.6

TABLE 1. (CONTINUED)

D_g MM.	f SEC.	s	η/D_g	λ/D_g	a/D_g	$U_m/\sqrt{(s-1)gD_g}$	$T\sqrt{(s-1)g/D_g}$
0.297	3.56	2.47	49.5	342.8	303.6	2.43	784.6
0.297	3.56	2.47	59.9	336.6	303.6	2.43	784.6
0.297	3.56	2.47	69.1	381.8	304.0	2.43	784.6
0.297	3.56	2.47	65.6	394.1	304.0	2.43	784.6
0.297	3.56	2.47	52.6	314.0	304.0	2.43	784.6
0.297	3.56	2.47	65.8	355.1	304.0	2.43	784.6
0.297	3.56	2.47	65.8	381.8	304.0	2.43	784.6
0.297	3.56	2.47	77.0	420.7	402.8	3.23	784.6
0.297	3.56	2.47	67.7	410.5	402.8	3.23	784.6
0.297	3.56	2.47	74.9	420.7	402.8	3.23	784.6
0.297	3.56	2.47	81.1	425.9	402.8	3.23	784.6
0.297	3.56	2.47	77.0	502.8	403.6	3.23	784.6
0.297	3.56	2.47	77.0	441.3	403.6	3.23	784.6
0.297	3.56	2.47	79.0	420.7	403.6	3.23	784.6
0.297	3.56	2.47	71.8	410.5	403.6	3.23	784.6
0.297	3.56	2.47	66.7	390.0	403.6	3.23	784.6
0.297	3.55	2.47	80.5	473.1	467.4	3.75	782.4
0.297	3.55	2.47	79.1	455.6	467.4	3.75	782.4
0.297	3.55	2.47	84.5	522.3	467.4	3.75	782.4
0.297	3.55	2.47	93.1	509.0	467.4	3.75	782.4
0.297	3.55	2.47	90.8	511.1	463.1	3.72	782.4
0.297	3.55	2.47	85.7	480.3	463.1	3.72	782.4
0.297	3.55	2.47	86.7	464.9	463.1	3.72	782.4
0.297	3.55	2.47	84.0	496.7	463.1	3.72	782.4
0.297	3.55	2.47	95.9	492.6	521.2	4.19	782.4
0.297	3.55	2.47	76.3	472.1	521.2	4.19	782.4
0.297	3.55	2.47	79.0	477.2	521.2	4.19	782.4
0.297	3.55	2.47	90.3	482.3	521.2	4.19	782.4
0.297	3.55	2.47	99.5	520.3	518.2	4.16	782.4
0.297	3.55	2.47	85.6	490.5	518.2	4.16	782.4
0.297	3.55	2.47	80.8	457.7	518.2	4.16	782.4
0.297	3.55	2.47	89.8	520.3	518.2	4.16	782.4
0.297	3.55	2.47	96.0	545.9	513.1	4.12	782.4
0.297	3.55	2.47	96.0	513.1	513.1	4.12	782.4
0.297	3.55	2.47	66.5	427.9	513.1	4.12	782.4
0.297	3.55	2.47	88.7	506.9	513.1	4.12	782.4
0.297	3.55	2.47	122.1	723.5	702.1	5.64	782.4
0.297	3.55	2.47	116.7	670.1	702.1	5.64	782.4
0.297	3.55	2.47	105.4	594.2	702.1	5.64	782.4
0.297	3.55	2.47	108.9	625.0	702.1	5.64	782.4
0.297	3.55	2.47	119.1	715.3	786.8	6.32	782.4

TABLE 1. (CONTINUED)

D_g MM.	I SEC.	s	η/D_g	λ/D_g	a/D_g	$U_m \sqrt{(s-1)g/D_g}$	$T \sqrt{(s-1)g/D_g}$
0.297	3.55	2.47	115.9	722.5	786.8	6.32	782.4
0.297	3.55	2.47	126.1	901.0	787.6	6.33	782.4
0.297	3.55	2.47	120.4	722.5	787.6	6.33	782.4
0.297	3.53	2.47	105.9	721.4	880.0	7.11	778.0
0.297	3.53	2.47	93.0	904.1	880.0	7.11	778.0
0.297	3.53	2.47	125.9	771.7	877.8	7.09	778.0
0.297	3.53	2.47	110.9	904.1	877.8	7.09	778.0
0.297	3.54	2.47	85.2	835.3	1095.9	8.83	780.2
0.297	3.54	2.47	103.6	962.6	1095.9	8.83	780.2
0.297	3.54	2.47	122.1	949.2	1088.2	8.76	780.2
0.297	3.54	2.47	155.0	981.1	1081.8	8.71	780.2
0.297	3.54	2.47	106.7	864.1	1075.4	8.66	780.2
0.297	3.52	2.47	119.6	774.8	1195.1	9.68	775.8
0.297	3.52	2.47	66.4	680.4	1195.1	9.68	775.8
0.297	3.52	2.47	63.1	664.0	1195.1	9.68	775.8
0.297	3.52	2.47	63.0	641.4	1190.8	9.64	775.8
0.297	3.52	2.47	48.0	622.9	1190.8	9.64	775.8
0.297	3.52	2.47	24.0	875.4	1500.8	12.16	775.8
0.297	3.52	2.47	9.6	384.8	1500.8	12.16	775.8
0.297	3.52	2.47	11.2	349.9	1500.8	12.16	775.8
0.297	3.52	2.47	20.8	961.6	1500.8	12.16	775.8
0.297	3.53	2.47	56.2	645.5	1304.1	10.53	778.0
0.297	3.53	2.47	40.2	835.3	1304.1	10.53	778.0
0.297	3.55	2.47	131.4	834.3	945.4	7.59	782.4
0.297	3.55	2.47	60.9	710.1	945.4	7.59	782.4
0.297	3.55	2.47	87.5	608.5	945.4	7.59	782.4
0.297	3.55	2.47	135.5	1180.1	942.4	7.57	782.4
0.297	3.55	2.47	125.7	792.2	942.4	7.57	782.4
0.297	3.58	2.47	63.2	360.2	269.4	2.15	789.0
0.297	3.58	2.47	73.0	366.4	269.4	2.15	789.0
0.297	3.58	2.47	62.9	341.7	269.4	2.15	789.0
0.297	3.58	2.47	60.0	329.4	269.4	2.15	789.0
0.297	3.58	2.47	60.8	348.9	269.4	2.15	789.0
0.297	3.43	2.47	64.0	376.6	290.8	2.42	756.0
0.297	3.43	2.47	56.4	371.5	290.8	2.42	756.0
0.297	3.43	2.47	55.5	347.9	290.8	2.42	756.0
0.297	3.43	2.47	54.1	370.5	290.8	2.42	756.0
0.297	3.31	2.47	47.9	293.5	247.6	2.13	729.5
0.297	3.31	2.47	55.5	304.8	247.6	2.13	729.5
0.297	3.31	2.47	50.2	294.5	247.6	2.13	729.5
0.297	3.31	2.47	48.7	294.5	247.6	2.13	729.5
0.297	3.31	2.47	58.1	298.6	247.6	2.13	729.5

TABLE 1. (CONTINUED)

D_g MM.	T SEC.	s	η/D_g	λ/D_g	a/D_g	$U_m/\sqrt{(s-1)g D_g}$	$T\sqrt{(s-1)g/D_g}$
0.297	3.68	2.47	85.6	419.7	320.7	2.48	811.1
0.297	3.68	2.47	77.0	411.5	320.7	2.48	811.1
0.297	3.68	2.47	66.2	393.0	320.7	2.48	811.1
0.297	3.68	2.47	64.1	379.7	320.7	2.48	811.1
0.297	3.68	2.47	59.7	383.8	320.7	2.48	811.1
0.297	3.68	2.47	64.9	398.2	320.7	2.48	811.1
0.297	3.79	2.47	67.8	397.1	261.3	1.97	835.3
0.297	3.79	2.47	60.2	359.2	261.3	1.97	835.3
0.297	3.79	2.47	58.7	338.7	261.3	1.97	835.3
0.297	3.79	2.47	57.4	339.7	261.3	1.97	835.3
0.297	3.79	2.47	55.0	339.7	261.3	1.97	835.3
0.297	3.79	2.47	59.6	334.5	261.3	1.97	835.3
0.585	3.55	2.62	35.9	207.9	138.9	1.49	585.2
0.585	3.55	2.62	36.5	200.1	138.9	1.49	585.2
0.585	3.55	2.62	37.5	197.2	138.9	1.49	585.2
0.585	3.55	2.62	34.9	201.6	138.9	1.49	585.2
0.585	3.57	2.62	49.0	254.8	172.8	1.85	588.2
0.585	3.57	2.62	51.3	265.7	172.8	1.85	588.2
0.585	3.57	2.62	43.5	242.3	172.8	1.85	588.2
0.585	3.57	2.62	46.6	237.1	172.8	1.85	588.2
0.585	3.55	2.62	53.9	288.6	205.4	2.20	585.6
0.585	3.55	2.62	56.5	284.5	205.4	2.20	585.6
0.585	3.55	2.62	57.8	267.8	205.4	2.20	585.6
0.585	3.55	2.62	54.7	300.1	205.4	2.20	585.6
0.585	3.54	2.62	54.4	298.5	235.3	2.53	584.1
0.585	3.54	2.62	57.8	307.4	235.3	2.53	584.1
0.585	3.54	2.62	59.9	314.2	235.3	2.53	584.1
0.585	3.54	2.62	57.3	315.2	235.3	2.53	584.1
0.585	3.55	2.62	64.6	350.6	274.6	2.94	585.9
0.585	3.55	2.62	66.0	347.0	274.6	2.94	585.9
0.585	3.54	2.62	77.4	414.7	316.9	3.41	583.6
0.585	3.54	2.62	77.9	400.6	316.9	3.41	583.6
0.585	3.57	2.62	92.5	429.8	335.8	3.59	588.2
0.585	3.57	2.62	86.0	429.8	335.8	3.59	588.2
0.585	3.56	2.62	94.6	457.4	382.1	4.09	586.2
0.585	3.56	2.62	87.0	464.2	382.1	4.09	586.2
0.585	3.56	2.62	113.3	563.2	382.1	4.09	586.2
0.585	3.56	2.62	102.1	498.1	382.1	4.09	586.2
0.585	3.54	2.62	31.0	267.8	413.5	4.45	584.1
0.585	3.54	2.62	90.1	427.7	413.5	4.45	584.1
0.585	3.54	2.62	89.4	527.8	413.5	4.45	584.1
0.585	3.54	2.62	96.6	485.1	413.5	4.45	584.1

TABLE 1. (CONTINUED)

D_g MM.	l SEC.	s	η/D_g	λ/D_g	a/n_g	$U_m \sqrt{(s-1)g/\lambda_g}$	$T \sqrt{(s-1)g/D_g}$
0.585	3.54	2.62	100.0	491.3	413.5	4.45	584.1
0.585	3.53	2.62	81.8	405.9	423.3	4.57	581.9
0.585	3.53	2.62	72.7	463.7	423.3	4.57	581.9
0.585	3.53	2.62	85.4	462.6	423.3	4.57	581.9
0.585	3.53	2.62	93.5	473.1	423.3	4.57	581.9
0.585	3.53	2.62	94.6	495.5	455.4	4.91	582.3
0.585	3.53	2.62	94.3	519.4	455.4	4.91	582.3
0.585	3.53	2.62	100.6	533.0	455.4	4.91	582.3
0.585	3.53	2.62	94.0	499.6	455.4	4.91	582.3
0.585	3.55	2.62	111.2	483.0	497.1	5.34	584.7
0.585	3.55	2.62	103.2	553.8	497.1	5.34	584.7
0.585	3.55	2.62	49.5	338.7	497.1	5.34	584.7
0.585	3.55	2.62	65.1	266.8	497.1	5.34	584.7
0.585	3.55	2.62	100.6	599.2	497.1	5.34	584.7
0.585	3.56	2.62	72.4	397.0	526.4	5.64	586.9
0.585	3.56	2.62	103.2	524.6	526.4	5.64	586.9
0.585	3.56	2.62	112.3	547.6	526.4	5.64	586.9
0.585	3.56	2.62	113.3	556.4	526.4	5.64	586.9
0.585	3.56	2.62	108.9	569.5	526.4	5.64	586.9
0.585	3.55	2.62	107.8	616.9	558.6	5.99	585.9
0.585	3.55	2.62	93.3	719.5	558.6	5.99	585.9
0.585	3.53	2.62	115.9	667.9	601.3	6.49	582.1
0.585	3.53	2.62	119.3	624.2	601.3	6.49	582.1
0.585	3.55	2.62	119.6	742.4	639.7	6.88	584.4
0.585	3.55	2.62	103.4	572.1	639.7	6.88	584.4
0.585	3.55	2.62	93.8	517.9	639.7	6.88	584.4
0.585	3.47	2.62	103.9	790.9	670.4	7.35	572.7
0.585	3.47	2.62	133.1	750.2	670.4	7.35	572.7
0.585	3.47	2.62	115.1	833.6	670.4	7.35	572.7
0.585	3.55	2.62	119.6	804.9	724.0	7.76	586.1
0.585	3.55	2.62	117.2	703.4	724.0	7.76	586.1
0.585	3.56	2.62	51.1	317.8	211.1	2.26	586.9
0.585	3.56	2.62	61.9	287.1	211.1	2.26	586.9
0.585	3.56	2.62	47.1	290.2	211.1	2.26	586.9
0.585	3.56	2.62	53.7	291.8	211.1	2.26	586.9

NOTICE

This document is not to be used by anyone.

Quarterly Report 7
Project A-798

Prior to 11-20 1969
without permission of the Research Sponsor
and the Experiment Station Security Office.

AN ANALYTICAL AND EXPERIMENTAL STUDY OF BED RIPPLES UNDER
WATER WAVES (EVOLUTION OF A DUNED BED UNDER OSCILLATORY FLOW)

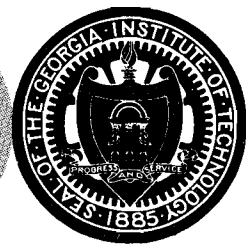
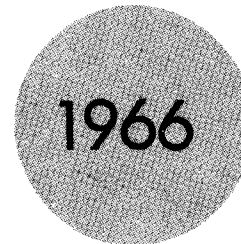
M. R. Carstens and F. M. Neilson

Contract No. DA-49-055 CIVENG-65-1

Prepared for
Department of the Army
Coastal Engineering Research Center
Washington, D. C.

1 January thru 31 March 1966

Engineering Experiment Station
GEORGIA INSTITUTE OF TECHNOLOGY
Atlanta, Georgia



Quarterly Report 7
Project A-798

AN ANALYTICAL AND EXPERIMENTAL STUDY OF BED RIPPLES UNDER
WATER WAVES (EVOLUTION OF A DUNED BED UNDER OSCILLATORY FLOW)

M. R. Carstens and F. M. Neilson

Contract No. DA-49-055 CIVENG-65-1

Prepared for
Department of the Army
Coastal Engineering Research Center
Washington, D. C.

1 January thru 31 March 1966

EVOLUTION OF A DUNED BED UNDER
OSCILLATORY FLOW

Marion R. Carstens and Frank M. Neilson

Georgia Institute of Technology, Atlanta, Georgia

Abstract

The evolution of a duned bed from an initially flat bed was observed in a large water tunnel in which water moved over a sand bed with simple harmonic motion. Bed forms were observed to be of two types, (a) rolling-grain and (b) vortex which are called ripples and dunes, respectively. Ripples are the initial transient bed form which are replaced by dunes. Ripples would form spontaneously if the water-motion amplitude were sufficiently large. Ripples can be induced to form at lesser water-motion amplitudes by placing an obstruction on the otherwise flat bed. The history of a duned bed was observed and is presented from birth to equilibrium.

Introduction

Some experimental results about the development of the bed configurations which result from oscillatory flow over a sand bed are presented herein. The water motion was simple harmonic parallel to the bed. The period of the oscillation was constant. The amplitude of the oscillation was a controlled variable. The experiments were performed with a medium sand and with a coarse sand.

As a result of observations the bed features are classified as follows:

A. Ripples

1. Spontaneous (rolling-grain ripples)
2. Induced (leading ripple is rolling-grain and the following sand waves are vortex bed forms)

B. Dunes

1. Two-dimensional (vortex bed form in which the vortices are two-dimensional line vortices which form in the lee of each dune crest)
2. Three-dimensional (vortex bed form in which the vortices are three-dimensional vortices which form in the lee of ill-defined dune crests)

The principal classification is based upon permanence. Ripples are a temporary bed form whereas dunes are an equilibrium or permanent bed form. Ripples are temporary in that a ripple system is entirely obliterated as a dune system is developed. The above classification is entirely consistent with the observations of Bagnold [1946] who observed a rolling-grain bed form and a vortex bed form. In the rolling-grain bed form, parallel transverse bands of grains roll back and forth separated by bands in which the grains are stationary. With the vortex bed

form, visible vortices are formed in the lee of each crest. In oscillatory flow, vortices are formed twice in each cycle with the residual vortex being ejected from the trough up into the main flow slightly before flow reversal occurs. Thus a ripple in the writers' classification is a rolling-grain ripple in Bagnold's [1946] classification and a dune is characterized by a separation and vortex formation in the lee of a crest.

Ripples are further classified as being spontaneous or induced. At amplitudes of water motion greater than a minimum value, ripples form spontaneously and simultaneously all over the bed. With smaller amplitudes of water motion, ripples can be induced by placing a disturbance element on the bed. In this case a ripple will form on each side of the disturber. These ripples grow in wavelength and amplitude becoming two-dimensional dunes. A new ripple is formed when the former ripple attains sufficient amplitude to disturb the flow above the flat bed. The process is repetitive.

Dunes are further classified as being two-dimensional or three-dimensional. Two-dimensional dunes are characterized by straight and level crests which are oriented perpendicular to the direction of the water motion. As the water-motion amplitude is increased, the two-dimensional dune system begins to be destroyed. A further increase in water-motion amplitude results in a three-dimensional dune system

which is highly irregular in crest alinement and crest elevation. Continued increases in water-motion amplitude results in lower crest elevations. With some value of the water-motion amplitude the bed is again flat with the surface particles moving back and forth resembling a second fluid beneath the water.

In this paper only temporary bed forms, ripples, are discussed. In a subsequent paper the experimental results for equilibrium bed forms, dunes, will be discussed.

Because of the complexity of the physical problem involving an interface of fluid and particulate solids, very few attempts have been made to formulate a mathematical analog for the happenings at the interface under an oscillatory flow. Kennedy and Falcon [1965] have formulated a kinematical potential flow model based upon an assumed bed form which does not involve separation and vortex formation. Their model appears to be rational for the transient bed form, ripples. In their analysis, an empirical law of sediment transport was employed and a phase difference between sediment movement and water motion was assumed. As a consequence, coefficients of proportionality appear in the solution which have not been verified independently. Hunt [1961] was concerned with mud flows on the sea bed. He formulated a mathematical model using boundary layer equations in which the densities and viscosities were different on each side of the interface. The mud layer was of

uniform thickness. Inasmuch as the interface was restrained to remain plane, Hunt's [1961] analysis does not appear to be relevant to interfacial deformations such as ripples and dunes. The formulation of reasonable mathematical equations which can be solved for dunes under oscillatory flow is very difficult. An irrotational potential flow solution is precluded because of the lack of a mechanism for generating the vortices. The solution of the Navier-Stokes equation for the generation of lee vortices in one-half cycle and their ejection into the main stream is a formidable problem even if one disregards the fact that momentum transfer is undoubtedly by turbulent processes rather than by viscous processes.

The Experiments

Experimental set up. An experimental investigation about ripples has been conducted in a large U-tube. The test section is the bottom horizontal leg of the U. The test section is 3.05 m long, 0.305 m high, and 1.21 m wide. The central section of the floor is depressed in order to form a container for the erodible bed material. The erodible bed is 1.83 m long, 1.21 m wide, and 10.2 cm deep. The sidewalls and top of the test section are transparent plastic in order to permit visual observation of the phenomena occurring within the test section. The vertical legs of the U-tube are 0.305 m by 1.21 m in a horizontal cross section. The vertical legs are joined to the horizontal legs so as to form a streamlined flow passage. The free surface of the water

in one of the vertical legs serves as a piston. Air is continuously forced into the confined volume above the water. Two large, solenoid-actuated, piston-operated, exhaust valves are used to quickly relieve the excess pressure in the air above the water surface. The exhaust valves are closed for about one-quarter cycle during the time when the water surface is falling in that leg. A float gage in the other vertical leg is joined to a direction-sensing switch which is the first element in a feedback-control system used to close and to open the exhaust valves at the proper time during the cycle. This system oscillates the water in the U-tube with simple harmonic motion at resonant frequency. Equilibrium amplitude can be controlled by adjustment of the air pressure. Air pressure is controlled by means of speed regulation of the blower. Initial transients are eliminated by means of a separate air system whereby the water levels are initially unbalanced to the desired equilibrium amplitude. Upon release of the initial unbalance, the water oscillates at equilibrium amplitude.

Amplitude and period of oscillation are recorded on a direct-writing oscillograph. The float-elevation sensor system consists of an endless, small-diameter, stainless-steel cable which passes over pulleys at the top and bottom in one vertical leg of the U-tube. The endless cable is fastened to a wooden float. A three-turn potentiometer, which is connected

to the axle of the upper pulley, is one leg of a wheatstone bridge. Bridge unbalance is sensed and recorded. The recorder is also equipped with a timing marker which marks pips at one-second intervals on the record. In all runs, the float elevation system is calibrated just before and immediately following a run by making short records at several elevations of the float.

Bed material. Two different bed materials were used having the properties listed in TABLE 1.

TABLE 1. Bed-Material Properties

Property	Ottawa Sand	Glass Beads
D_g (geometric mean diameter)	0.585 mm	0.297 mm
σ_g (geometric standard deviation)	1.16	1.06
s (specific gravity)	2.62	2.47

Experimental method and observations. The following description is chronological. Prior to a run the bed was leveled by means of a wooden screed which bridged the depression in the floor (sediment container.) The U-tube was then filled with water to a reference level. Since a constant reference level was used in all runs (constant mass of oscil-

lating water), the period of oscillation for all runs was constant at 3.54 ± 0.02 sec. The blower was then started and the speed regulated to give the desired equilibrium amplitude of water motion. Next the water levels in the legs of the U-tube were unbalanced at nearly the equilibrium amplitude. As soon as the initial unbalance was released the water began oscillating in the U-tube. The data about the development of a dune system were observed through the transparent sidewalls of the test section.

If the water-motion amplitude, a , was greater than about 19 cm and after a few cycles of oscillation spontaneous ripples would simultaneously form over the flat bed. Prior to the onset of spontaneous ripples some of the surface grains would be moving back and forth practically in phase with the water velocity. At the onset of spontaneous ripples, the motion of the surface grains became restricted to transverse bands of grains moving essentially in phase with velocity. The bands of moving grains were separated by bands of stationary grains. The bands of moving grains became ripple crests and the stationary bands became ripple troughs. The ripple crests move back and forth nearly to the edges of the band of moving grains. The appreciable movement of the ripple crests in phase with the water motion might explain why no separation and vortex motion was observed in the lee of the crests. As the oscillation continues, ripple amplitude increases until separa-

tion occurs and vortices form, that is, a dune system is born. From this time until an equilibrium dune system is scoured into the bed, the bed form pattern is very irregular as the shorter wave length ripple system is being replaced by the longer wave length dune system. For example in a run with the 0.585-mm sand, the wave length of the ripples was 7.6 cm with a water-motion amplitude, a , of 19.3 cm whereas the dune wave length was 23.4 cm at the corresponding amplitude. In other words there were about five ripples in the total water-motion travel, $2a$, as compared with about two dunes.

If the water-motion amplitude, a , was less than about 18 cm ripples would not form spontaneously but could be induced. The ripples were induced by placing a half-round bar on the flat bed. The radius of the bar was 6.35 mm. The length of the bar was 1.21 m. The bar was placed on the flat bed with the plane face on the bed and with the axis perpendicular to the water motion. Upon starting the oscillation, ripples are formed on both sides of the bar. These ripples grow in amplitude and wave length becoming dunes. Then a new pair of ripples form. The process is repetitive. Since the dunes are formed with an initial wave length of the ripples, the wave length must increase as the dune system develops into the equilibrium state. The position of the ripple and dune crests was periodically measured by noting the crest positions in relation to coordinate scales which were marked on

the sidewalls of the test section. The observed crest positions are shown in Figure 1 as a function of the elapsed number of cycles, t/T , for Run 48. The stages of development of an equilibrium dune system are clearly shown in Figure 1. The scouring process in Run 48 was slow enough for the dunes to develop in an orderly manner, that is, the increasing wave length was accomplished by continuous outward movement of the more recently formed dunes. For runs in which the amplitude of oscillation was greater, the scouring process was so rapid that the older dunes overtook and absorbed some of the newer dunes resulting in a mixed and disorderly pattern as the dune system developed. In spite of this interim disorderliness, the dune system developed into a regular pattern at equilibrium.

Results

Spontaneous ripples. Since spontaneous ripples are transitory, experimental observations were limited. The simultaneous appearance of the rolling-grain ripples over the bed when the amplitude of the oscillatory water motion was greater than about 19 cm with a period of 3.54 seconds is indicative that spontaneous ripples are the result of the onset of a perturbation or of a secondary motion within the oscillatory flow. Prior to the appearance of spontaneous ripples the bed was flat--at least to the visual observer. In these experiments spontaneous ripples occurred at water-motion amplitudes at which the

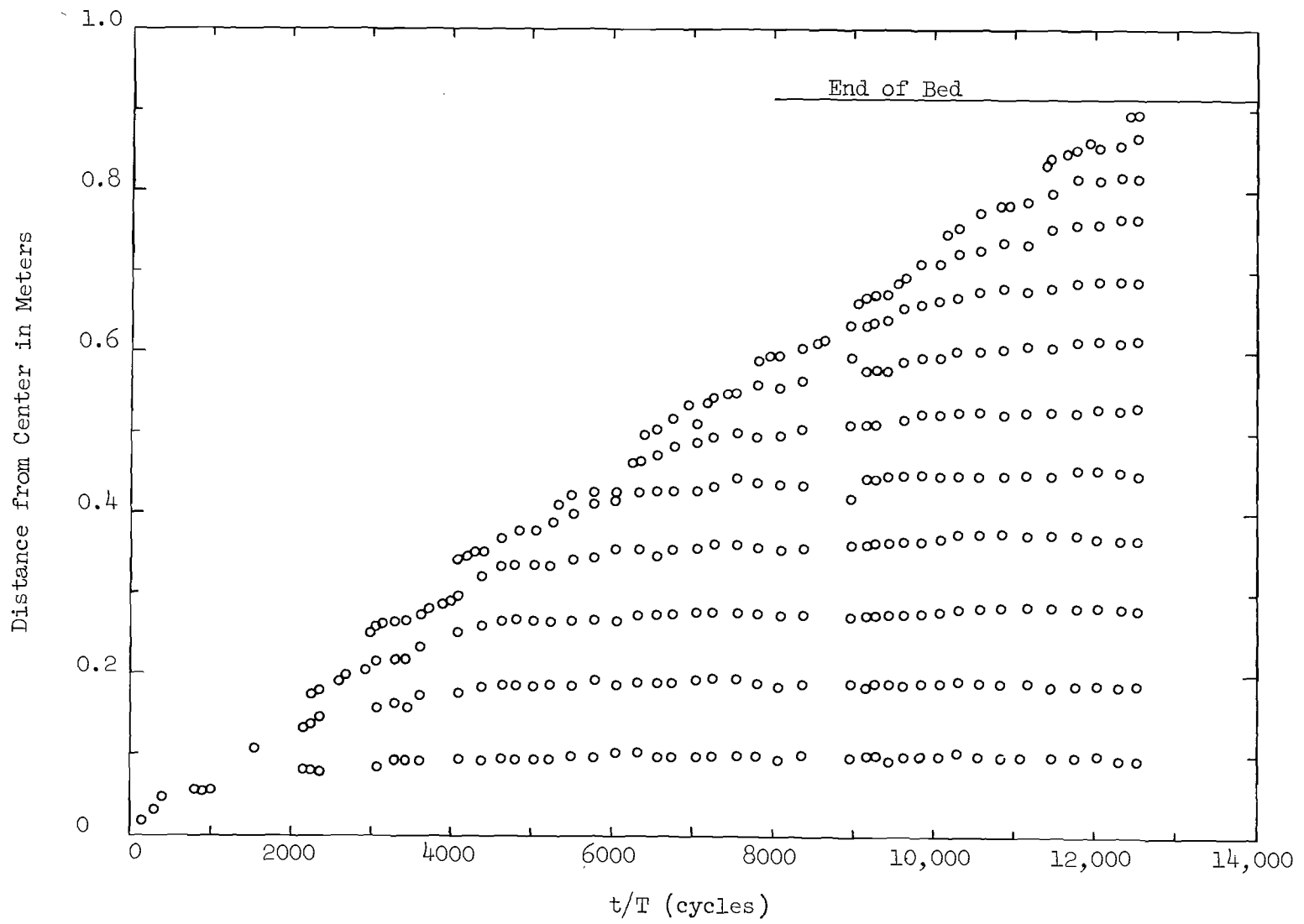


Figure 1. Dune Location as a Function of Time

boundary layer had started to become turbulent and at which some of the surface grains were in motion all over the bed. The water-motion amplitude at the beginning of boundary-layer transition, incipient motion, and the first appearance of spontaneous ripples are given in TABLE 2.

TABLE 2. Water-Motion Amplitude at Various Occurrences

Occurrence	D_g (mm)	T (sec)	Water Temp. (°C)	Water-Motion Amplitude, a, in cm
Beginning of boundary-layer transition	0.297	3.56	21.0	11.0
	smooth	3.58	22.4	14.7
Fully Turbulent Boundary Layer	smooth	3.63	22.4	23.8
Incipient Motion	0.585	3.58	22.2	16.6
	0.297	3.56	19.4	14.0
Spontaneous Appearance of Ripples	0.585	3.55	23.9	18.8
	0.297	3.55	22.8	18.3

The boundary-layer data were obtained by the observation of dye which was allowed to seep upward from the bed. The beginning of transition was deemed to occur when line vortices were first noticed to form parallel to the bed and perpendicular to the direction of the water motion. Vortices formed about at the time of flow reversal. The axes of the vortices were a small distance from the bed. This distance

was estimated to be about 5 mm. The flow was laminar both above and beneath this visual row of vortices. In the beginning the vortices persisted for a very short period in the cycle. With increasing amplitude, the vortices persisted for longer durations in the cycle. The boundary layer was deemed to be fully turbulent when the vortices persisted throughout the entire cycle. Even with the turbulent boundary layer, the main body of the flow remained laminar. The smallest amplitude for fully turbulent boundary layer could not be determined on the sand bed because of the rolling of the surface particles.

Incipient motion was visually observed and was defined when approximately ten percent of the surface particles were rolling back and forth. Some particles had been moved at lesser water-motion amplitudes than those listed in TABLE 2. The first motion was a rocking motion of some particles which were perched in an unstable position. With a slightly greater amplitude these particles rolled into more stable positions on the surface of the bed. The amplitude at incipient motion listed in TABLE 2 is not precise but is subject to the judgement of the observer.

Development of a dune system. The development of a dune system by means of a disturbance element placed on the bed under the oscillatory flow proceeded slowly enough to permit extensive visual observation.

The stages of dune development are clearly shown in Figure 1. When the leading dune became sufficiently developed, a newly induced ripple would form beyond the dune system. This induced ripple would grow and then change into a dune. A dune system could be induced to develop with flow conditions on a flat bed in which the boundary layer is laminar and all surface grains are stationary. In other words, a dune system could be induced to form at water-motion amplitudes much smaller than the incipient-motion condition shown in TABLE 2. On the other hand, a definite lower limit was found.

This lower limit for dune formation can be expressed in terms of a dimensionless parameter called the sediment number, N_s . The sediment number, N_s , is discussed more completely by one of the authors Carstens [1966] in a paper about similarity laws for localized scour. The square of the sediment number, N_s^2 , is proportional to the ratio of the forces causing particle movement to the forces resisting particle movement. By definition,

$$N_s = \frac{U}{\sqrt{(s-1)gD_g}} \quad (1)$$

in which

U = maximum velocity of the oscillatory flow;

s = ratio of sediment density to the fluid density;

g = acceleration of gravity; and

D_g = mean diameter of the particles

In these experiments the lowest value of N_s at which dunes can be induced to develop was found to be 1.3. This critical value is called the critical sediment number N_{sc} .

The velocity of propagation, V , at which a developing dune system progresses over a flat bed can be determined from data plotted as in Figure 1. The velocity of propagation was determined from graphs similar to Figure 1 for seventeen experimental runs. Eleven of the runs were with the 0.297 mm glass beads and six of the runs were with the 0.585 mm sand. The results are shown in Figure 2. The propagation velocity, V , can be represented by the function

$$\frac{V}{U} = 1.7(10^{-4})(N_s^2 - N_{sc}^2)^{3/2} \quad (2)$$

Summary of Results

Based upon experiments in which water was oscillated with simple-harmonic motion over a bed of sand, the important observations and conclusions are as follows:

- (1) Bed forms are logically classified as rolling-grain type and vortex type. The authors have called the first type ripples and the second type dunes in order to have consistent nomenclature for bed forms in unidirectional flow and oscillatory flow.

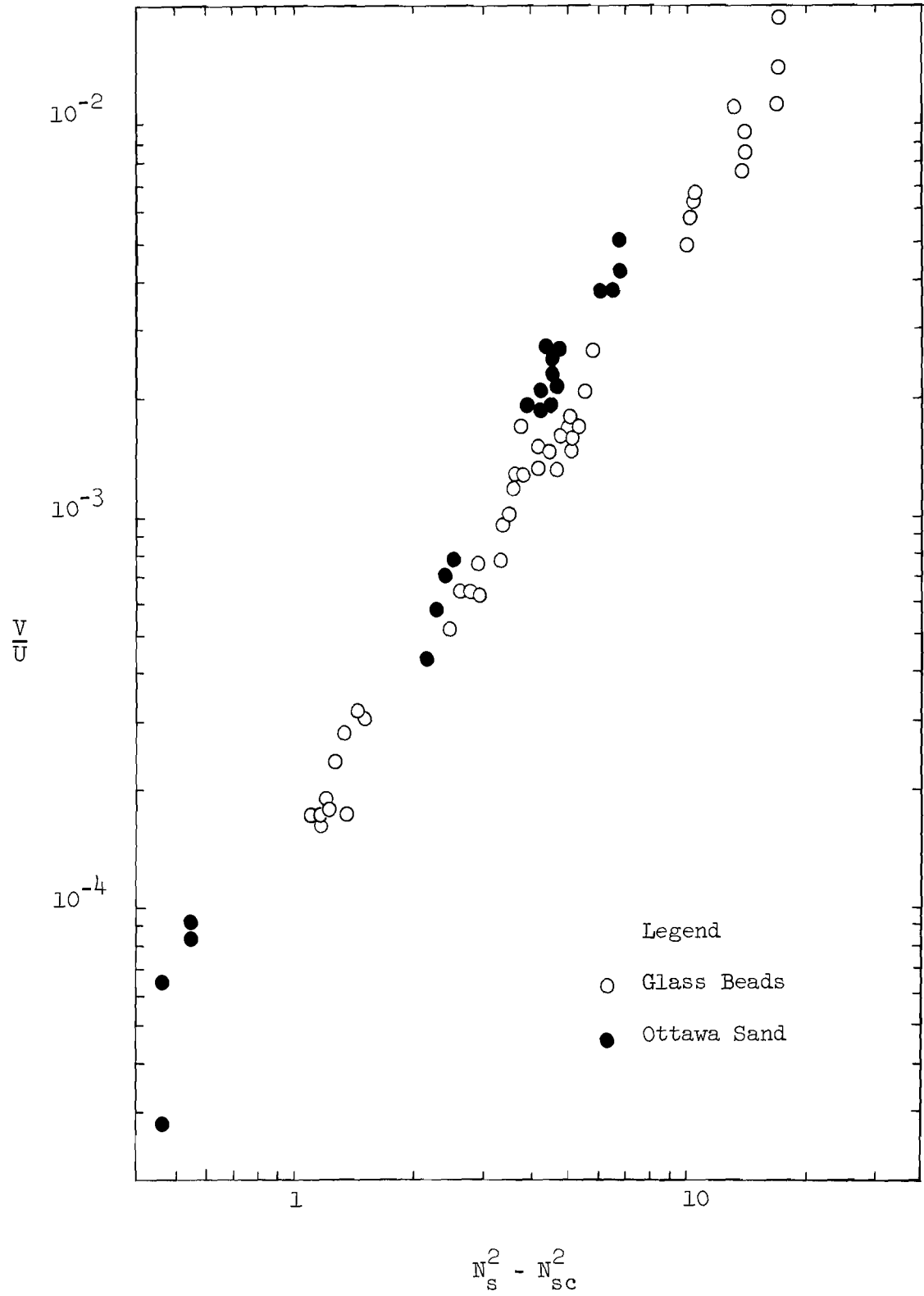


Figure 2. Rate of Ripple Propagation

- (2) Following the above classification, ripples are transient bed forms which are replaced by dunes.
- (3) Ripples occur spontaneously all over the bed if the bed is initially flat and if the water-motion amplitude exceeds a certain value.
- (4) Ripples can be induced to form at lesser water-motion amplitudes by placing an obstruction on the otherwise flat bed to cause a local flow disturbance.
- (5) Since ripples can be induced to form at flow conditions less than the widely used incipient-motion condition, the incipient-motion condition is not a comprehensive lower limit for the existence of a duned bed.
- (6) Since any natural bed is almost certain to be littered with flow obstructions, the sediment number is a more rational criterion for the lower limit for the existence of a duned bed than is the incipient-motion criterion.
- (7) In these experiments ripples could not be induced to form if the value of the sediment number N_s , was less than 1.3. Hence a sediment number of 1.3 is the lower limit for the existence of a duned bed.
- (8) The initial appearance of spontaneous ripples on an otherwise flat bed is a manifestation of a perturbation of the oscillatory

flow. On the basis of these limited experiments, the cause cannot be delineated. In any event the appearance of spontaneous ripples occur at greater amplitudes than incipient motion.

- (9) The velocity of propagation of a developing dune system which is expanding from a flow disturbance is a function of the sediment number as shown in Figure 2.

Acknowledgements

This work was supported by the Coastal Engineering Research Center, Department of the Army, under contract DA-49-055-CIVENG-65-1. Permission to publish the results is gratefully acknowledged.

References

- Bagnold, R. A., Motion of waves in shallow water -- interaction between waves and sand bottoms, Proc. Royal Society A, 187, 1-18, 1946.
- Carstens, M. R., Similarity laws for localized scour, Proc. American Society of Civil Engineers, Journal of the Hydraulics Division, 92, H Y 3, , 1966.
- Kennedy, John F. and Marco Falcon, Wave-generated sediment ripples, Massachusetts Institute of Technology, Hydrodynamics Laboratory Report No. 86, 1965.
- Hunt, J. N., Oscillations in a viscous liquid with an application to tidal motion, Tellus, 13, 79-84, 1961.